36352

National Library of Canada
Bibliothèque nationale du Canada

CANADIAN THESES ON MICROFICHE

THÈSES CANADIENNES SUR MICROFICHE

NAME OF AUTHOR/*NOM DE L'AUTEUR* Frances E Bates

TITLE OF THESIS/*TITRE DE LA THÈSE* Mid-Infrared Spectra of Ices II and IX and the Clathrate Hydrates of Cyclopropane and Ethylene Oxide

UNIVERSITY/*UNIVERSITÉ* of Alberta

DEGREE FOR WHICH THESIS WAS PRESENTED/ *GRADE POUR LEQUEL CETTE THÈSE FUT PRÉSENTÉE* Ph. D

YEAR THIS DEGREE CONFERRED/*ANNÉE D'OBTENTION DE CE GRADE* 1978

NAME OF SUPERVISOR/*NOM DU DIRECTEUR DE THÈSE* Dr. J E Bertie

Permission is hereby granted to the NATIONAL LIBRARY OF CANADA to microfilm this thesis and to lend or sell copies of the film.

The author reserves other publication rights, and neither the thesis nor extensive extracts from it may be printed or otherwise reproduced without the author's written permission.

L'autorisation est, par la présente, accordée à la BIBLIOTHÈQUE NATIONALE DU CANADA de microfilmer cette thèse et de prêter ou de vendre des exemplaires du film.

L'auteur se réserve les autres droits de publication; ni la thèse ni de longs extraits de celle-ci ne doivent être imprimés ou autrement reproduits sans l'autorisation écrite de l'auteur.

DATED/*DATÉ* Jan 24th 1978 SIGNED/*SIGNÉ* Frances E. Bates

PERMANENT ADDRESS/*RÉSIDENCE FIXÉ*
C43 - 445 S.W Marina Dr.
Vancouver, B.C V5X 2R9

NL-91 (3-74)

National Library of Canada

Cataloguing Branch
Canadian Theses Division

Ottawa, Canada
K1A 0N4

Bibliothèque nationale du Canada

Direction du catalogage
Division des thèses canadiennes

NOTICE

The quality of this microfiche is heavily dependent upon the quality of the original thesis submitted for microfilming. Every effort has been made to ensure the highest quality of reproduction possible.

If pages are missing, contact the university which granted the degree.

Some pages may have indistinct print especially if the original pages were typed with a poor typewriter ribbon or if the university sent us a poor photocopy.

Previously copyrighted materials (journal articles, published tests, etc.) are not filmed.

Reproduction in full or in part of this film is governed by the Canadian Copyright Act, R.S.C. 1970, c. C-30. Please read the authorization forms which accompany this thesis.

THIS DISSERTATION
HAS BEEN MICROFILMED
EXACTLY AS RECEIVED

AVIS

La qualité de cette microfiche dépend grandement de la qualité de la thèse soumise au microfilmage. Nous avons tout fait pour assurer une qualité supérieure de reproduction.

S'il manque des pages, veuillez communiquer avec l'université qui a conféré le grade.

La qualité d'impression de certaines pages peut laisser à désirer, surtout si les pages originales ont été dactylographiées à l'aide d'un ruban usé ou si l'université nous a fait parvenir une photocopie de mauvaise qualité.

Les documents qui font déjà l'objet d'un droit d'auteur (articles de revue, examens publiés, etc.) ne sont pas microfilmés.

La reproduction, même partielle, de ce microfilm est soumise à la Loi canadienne sur le droit d'auteur, SRC 1970, c. C-30. Veuillez prendre connaissance des formules d'autorisation qui accompagnent cette thèse.

LA THÈSE A ÉTÉ
MICROFILMÉE TELLE QUE
NOUS L'AVONS REÇUE

NL-339 (3/77)

THE UNIVERSITY OF ALBERTA

MID-INFRARED SPECTRA OF ICES II AND IX AND THE CLATHRATE HYDRATES OF CYCLOPROPANE AND ETHYLENE OXIDE

Ⓒ by

FRANCES ELIZABETH BATES

A THESIS

SUBMITTED TO THE FACULTY OF GRADUATE STUDIES AND RESEARCH
IN PARTIAL FULFILMENT OF THE REQUIREMENTS FOR THE DEGREE
OF
DOCTOR OF PHILOSOPHY

DEPARTMENT OF CHEMISTRY
EDMONTON, ALBERTA
SPRING 1978

THE UNIVERSITY OF ALBERTA

FACULTY OF GRADUATE STUDIES AND RESEARCH

The undersigned certify that they have read, and recommend to the Faculty of Graduate Studies and Research, for acceptance, a thesis entitled

'MID-INFRARED SPECTRA OF ICES II AND IX AND THE CLATHRATE HYDRATES OF CYCLOPROPANE AND ETHYLENE OXIDE'

submitted by FRANCES ELIZABETH BATES in partial fulfilment of the requirements for the degree of Doctor of Philosophy.

John E. Bertie
Supervisor

J. S. Martin

Ross W. Binn

W. F. Hyers

Stuart A. Rice
External Examiner

Date: January 18th, 1978

To Gordon

Abstract

The infrared absorption bands due to the O-D stretching vibrations of D_2O and HDO and to the rotational D_2O vibrations in ordered ices, ices II and IX, dispersed in a 3-methylpentane glass were recorded at temperatures of 100, 60 and 10 K. Calculations of the frequencies and relative infrared intensities of the $\underline{k}=0$ $\nu_{OD}(D_2O)$ vibrations in the harmonic and bond moment approximation are reported and explain the features of the $\nu_{OD}(D_2O)$ band of ice IX very well and are in reasonable agreement with those of ice II. The features are, however, less well resolved than if they were due solely to the $\underline{k}=0$ $\nu_{OD}(D_2O)$ vibrations. The breadth of the features is interpreted as due to the enhancement of the intensity of overtone and combination transitions by Fermi resonance between the fundamental ν_{OD} levels and the isoenergetic continuum of overtone and combination levels.

The mid-infrared spectra of cyclopropane structure I clathrate hydrate dispersed in mulling agents at 90 K and in potassium bromide pellets at 45 to 155 K and of ethylene oxide clathrate hydrate dispersed in potassium bromide pellets at 45 to 155 K were recorded. The water absorption bands of cyclopropane structure I hydrate are assigned by comparison with the spectra of other clathrate hydrates and ice I and the spectral similarities are discussed.

The ν_{OD}(HDO) and ν_{OH}(HDO) bands of cyclopropane structure I hydrate differ markedly from those of the structure I hydrates of ethylene oxide and oxetane. This difference is attributed to the interaction of the guest dipole moment with the water lattice.

The assignment of the guest absorption bands of cyclopropane structure I hydrate follows from that of gaseous cyclopropane. The existing assignment of the guest absorption bands of ethylene oxide hydrate has been modified. The differences between the frequencies of the encaged molecules of the structure I deuterates of ethylene oxide and cyclopropane and the corresponding frequencies in the gas phase were interpreted using the loose cage-tight cage ideas of Pimentel and Charles. The relative sizes of the guest molecules of these clathrate deuterates and of oxetane structure I deuterate are clearly reflected in the average frequency shifts on clathration and in the number of gas phase infrared inactive fundamentals observed.

The frequency shifts with temperature of the guest absorption bands of ethylene oxide hydrate and cyclopropane structure I hydrate indicate that the guest molecules generally experience a looser cage environment at lower temperatures. For ethylene oxide hydrate the dominant temperature dependent contribution to the bandwidths of the guest bands appears to be due to the reorientation of the guest molecules, while for cyclopropane structure I hydrate it appears to be due to the different potential minima occupied by the guest molecules within the cages at different temperatures.

The guest absorption bands due to $\nu_7(A_2'')$, a CH_2 rock, and $\nu_{11}(E')$, the ring deformation, of cyclopropane and to $\nu_3(A_1)$, the ring breathing vibration, of ethylene oxide are split into doublets at low temperatures and this is attributed to guest molecules occupying two nonequivalent sets of preferred orientations within the cages.

Acknowledgements

I would like to express my appreciation to Dr. John E. Bertie for his guidance and encouragement during the course of this work, and to present and former members of his group for their interest and cooperation. I would also like to thank Dr. Martin Cowie for his assistance, and members of the electronic and machine shops for their excellent workmanship.

I am grateful to Shirley Stawnychy and Diane Dowhaniuk for typing this thesis. To Gordon, I express my deepest gratitude for his patience and understanding during the course of this work.

Financial assistance from the University of Alberta, the Killam Estate and the National Research Council of Canada is gratefully acknowledged.

Table of Contents

Page

Abstract v

Acknowledgements viii

List of Tables xiii

List of Figures xv

Chapter One. Introduction 1

1.1 General 1
1.2 The Polymorphs of Ice 1
1.3 The Clathrate Hydrates 10
1.4 Vibrations in Solids 23
1.5 Vibrational Spectra of the Ice Polymorphs 30
1.6 Vibrational Spectra of the Clathrate Hydrates 44
1.7 Vibrational Spectra of Cyclopropane 51
1.8 Objectives 54

Chapter Two. Experimental Techniques 58

2.1 Introduction 58
2.2 Chemicals 58
2.3 Preparation of Cyclopropane Structure I Hydrate (Deuterate) 59
2.4 Preparation of Cyclopropane Structure II Hydrate (Deuterate) 63
2.5 Preparation of Ice II and Ice IX 64
2.6 Characterization of the Samples 67
2.7 Preparation and Handling of Infrared Samples Studied at 90 K 70

Page

2.7.1 Liquid Nitrogen Cell 70

2.7.2 Preparation of Mulls 70

2.8 Preparation and Handling of Infrared Samples Studied between 10 and 150 K.. 73

2.8.1 Liquid Helium Cryostat 73

2.8.2 Preparation of Potassium Bromide Pellets 78

2.8.3 Preparation of 3-methylpentane Glasses 81

2.9 Temperatures of the Infrared Samples.. 83

2.10 Infrared Instrumentation 86

Chapter Three. Ice II and Ice IX 88

3.1 Introduction 88

3.2 Characterization of Ice II and Ice IX Samples 88

3.3 Mid-Infrared Spectra of Ice II and Ice IX to 10 K 95

3.3.1 Results 95

3.3.2 Discussion 108

3.4 Normal Coordinate Analysis of the $\nu_{OD}(D_2O)$ Vibrations of Ice II and Ice IX 114

3.4.1 General Method 114

3.4.2 Calculations of the Relative Infrared Intensities of the $\nu_{OD}(D_2O)$ Normal Vibrations 118

3.4.3 Force Fields used in Normal Coordinate Calculations 120

3.4.4 Normal Coordinate Analysis of the $\underline{k}=0$ $\nu_{OD}(D_2O)$ Vibrations of Ice IX 124

3.4.5 Normal Coordinate Analysis of the $\underline{k}=0$ $\nu_{OD}(D_2O)$ Vibrations of Ice II 144

3.5 Origin of the $\nu_{OD}(D_2O)$ and $\nu_R(D_2O)$ Bands of Ices II and IX 164

Page

Chapter Four. Results of the Study of the Clathrate Hydrates 171

4.1 Introduction 171

4.2 Characterization of the Structure I Hydrates 172

4.3 Characterization of Cyclopropane Structure II Hydrate 178

4.4 Mid-Infrared Spectra of Cyclopropane Structure I Hydrate at 90±5 K 184

4.4.1 General 184

4.4.2 Absorption by the Water Molecules at 90±5 K 187

4.4.3 Absorption by the Cyclopropane Molecules at 90±5 K 202

4.5 Temperature Dependence of the Mid-Infrared Spectra of Cyclopropane Structure I Hydrate 206

4.5.1 General 206

4.5.2 Absorption by the Water Molecules 210

4.5.3 Absorption by the Cyclopropane Molecules 215

4.6 Temperature Dependence of the Absorption by Ethylene Oxide in Ethylene Oxide Hydrate 225

Chapter Five. Discussion of the Mid-Infrared Spectra of the Structure I Hydrates of Cyclopropane and Ethylene Oxide 242

5.1 Introduction 242

5.2 Absorption by the Water Molecules 243

5.3 Absorption by the Guest Molecules 259

5.3.1 General 259

5.3.2 Discussion of the Absorption by the Guest Molecules in the Structure I Hydrates of Ethylene Oxide and Cyclopropane 262

Page

References 276

Appendix 293

LIST OF TABLES

Table Page

1.1 Geometric Parameters of the Unit Cells and Cages of the Structure I and Structure II Clathrate Hydrates 13

1.2 Vibrational Frequencies of Cyclopropane 52

1.3 Irreducible Representations Formed by Internal Displacement Coordinates of Cyclopropane 53

2.1 Apparent and Literature Values of Deposition Temperatures of Various Gases 85

3.1 X-ray Powder Diffraction Pattern of Ice II at 100 K 90

3.2 X-ray Powder Diffraction Pattern of Ice IX at 100 K 93

3.3 Frequencies of Features in the Mid-Infrared Spectrum of Ice II 102

3.4 Frequencies of Features in the Mid-Infrared Spectrum of Ice IX 104

3.5 Internal Displacement Coordinates for Ice IX 127

3.6 Symmetry Coordinates for Ice IX 130

3.7 Non-Zero $\underset{\sim}{G}$ Matrix Elements for D_2O Ice IX 132

3.8 Non-Zero $\underset{\sim}{F}$ Matrix Elements for Ice IX 133

3.9 Force Fields Used for Ice IX 135

3.10 Comparison of the Observed and Calculated Frequencies and Relative Infrared Intensities of Ice IX 136

3.11 Symmetrized Eigenvector Elements for Ice IX 139

3.12 Internal Displacement Coordinates for Ice II 146

3.13 Symmetry Coordinates for Ice II 149

3.14 Non-Zero $\underset{\sim}{G}$ Matrix Elements for D_2O Ice II .. 152

3.15 Non-Zero $\underset{\sim}{F}$ Matrix Elements for Ice II 153

Table Page

3.16 Force Fields Used for Ice II 155

3.17 Comparison of the Observed and Calculated Frequencies and Relative Infrared Intensities of Ice II 156

3.18 Symmetrized Eigenvector Elements for Ice II 159

4.1 X-ray Powder Diffraction Patterns of Cyclopropane Structure I Hydrate and Ethylene Oxide Hydrate at 100 K 173

4.2 X-ray Powder Diffraction Pattern of Cyclopropane Structure II Hydrate at 100 K.. 179

4.3 Frequencies of the Features Observed in the Mid-Infrared Spectra of Cyclopropane Structure I Hydrate and Deuterate at 90 K... 188

4.4 Temperature Dependence of the $\nu_{OD}(D_2O)$ and $\nu_{OD}(HDO)$ Bands of Cyclopropane Structure I Deuterate and Hydrate, respectively 213

4.5 Temperature Dependence of Guest Features in the Mid-Infrared Spectra of Cyclopropane Structure I Hydrate and Deuterate to 45 K... 219

4.6 Temperature Dependence of Guest Features in the Mid-Infrared Spectra of Ethylene Oxide Hydrate and Deuterate to 45 K 227

5.1 The O···O Bond Distances and $\nu_{OD}(HDO)$ Frequencies of Ices I, II, V, VI, and IX, the Structure I Hydrates of Cyclopropane, Ethylene Oxide and Oxetane and the Structure II Hydrates of Oxetane and Tetrahydrofuran at 100±10 K 248

5.2 Comparison of the Fundamental Frequencies of Cyclopropane in the Spectra of Gaseous Cyclopropane and the Structure I Deuterate of Cyclopropane 263

5.3 Comparison of the Fundamental Frequencies of Ethylene Oxide in the Spectra of Gaseous Ethylene Oxide and the Structure I Deuterate of Ethylene Oxide 265

List of Figures

Figure		Page
1.1	Phase diagram of ice	3
1.2	Cages of the structure I (a,b) and structure II (c,d) clathrate hydrates viewed along axes of highest symmetry	12
1.3	Phase diagram of the cyclopropane-H_2O system	17
1.4	Phase diagram of the cyclopropane-D_2O system	18
1.5	Correlation diagram for ice II	28
1.6	Correlation diagrams for ice IX	31
2.1	Stainless steel manifold used to prepare cyclopropane structure I hydrate	60
2.2	Pressure apparatus	65
2.3	Liquid nitrogen cell	71
2.4	Schematic diagram of the Helitran equipment	74
2.5	Schematic diagram of the Helitran optical cell	76
3.1	Microdensitometer traces of X-ray powder diffraction photographs of ices II and IX ..	94
3.2	The ν_{OD}(HDO) band of ice II	96
3.3	The ν_{OD}(D_2O) band of ice II	97
3.4	The ν_R(D_2O) band of ice II	98
3.5	The ν_{OD}(HDO) band of ice IX	99
3.6	The ν_{OD}(D_2O) band of ice IX	100
3.7	The ν_R(D_2O) band of ice IX	101

Figure Page

3.8 The effect of emission on the $\nu_R(D_2O)$ band of ice IX 109

3.9 The configurations for the two types of intermolecular interaction force constants 122

3.10 The structure of ice IX as viewed along the c axis 125

3.11 Effect of intramolecular and intermolecular coupling on the $\nu_{OD}(D_2O)$ vibrations of ice IX 141

3.12 Comparison of the calculated and observed $\nu_{OD}(D_2O)$ band of ice IX 143

3.13 The structure of ice II as viewed along the hexagonal c axis 145

3.14 Comparison of the calculated and observed $\nu_{OD}(D_2O)$ band of ice II 161

4.1 The $\nu_{OD}(HDO)$ bands of tetrahydrofuran structure II hydrate, cyclopropane structure II hydrate and cyclopropane structure II hydrate mixed with ice Ih in propene at 90±5 K 182

4.2 Mid-infrared spectrum of cyclopropane structure I hydrate dispersed in mulling agents at 90±5 K 185

4.3 Mid-infrared spectrum of cyclopropane structure I deuterate dispersed in mulling agents at 90±5 K 186

4.4 The $\nu_{OH}(H_2O)$ band of cyclopropane structure I hydrate in a chlorotrifluoromethane mull at 90±5 K 193

4.5 The $\nu_{OD}(D_2O)$ band of cyclopropane structure I deuterate in a propene mull at 90±5 K 195

4.6 The $\nu_R(D_2O)$ band of cyclopropane structure I deuterate in a propane mull at 90±5 K 197

Figure Page

4.7 The ν_{OD}(HDO) band of cyclopropane structure I hydrate in a propene mull at 90±5 K 199

4.8 The ν_{OH}(HDO) band of cyclopropane structure I deuterate in a chlorotrifluoromethane mull at 90±5 K 201

4.9 Absorption by $\nu_7(A_2'')$, $\nu_{11}(E')$, $\nu_{10}+\nu_{11}$ and $\nu_5+\nu_{10}$ of cyclopropane structure I deuterate in mulling agents at 90±5 K 203

4.10 Absorption between 2840 and 3120 cm^{-1} by cyclopropane structure I deuterate in a chlorotrifluoromethane mull at 90±5 K 205

4.11 The $\nu_{OD}(D_2O)$ band of cyclopropane structure I deuterate (KBr pellet) at 105 and 45 K ... 212

4.12 The ν_{OD}(HDO) band of cyclopropane structure I hydrate (KBr pellet) containing 4 mole percent HDO at 45, 85, and 130 K 214

4.13 Temperature dependence of the absorption by $\nu_7(A_2'')$ and $\nu_{11}(E')$ of cyclopropane in its structure I deuterate (KBr pellet) .. 216

4.14 Temperature dependence of the absorption by $\nu_{10}(E')$ of cyclopropane in its structure I hydrate and deuterate (KBr pellet) 217

4.15 Temperature dependence of the absorption by $\nu_9(E')$, $\nu_{10}+\nu_{11}$, $\nu_5+\nu_{10}$ of cyclopropane in its structure I deuterate and $\nu_8(E')$ of cyclopropane in its structure I hydrate (KBr pellets) 218

4.16 Mid-infrared spectrum of ethylene oxide deuterate in a potassium bromide pellet at 150 K 226

4.17 Temperature dependence of the absorption by $\nu_8(A_2)$, $\nu_{15}(B_2)$, $\nu_5(A_1)$ and $\nu_{12}(B_1)$ of ethylene oxide in its deuterate (KBr pellet).236

Figure Page

4.18 Temperature dependence of the absorption by $\nu_3(A_1)$ of ethylene oxide in its hydrate and deuterate (KBr pellet) 237

4.19 Temperature dependence of the absorption by $\nu_{11}(B_1)$, $\nu_{14}(B_2)$, $\nu_4(A_1)$, $\nu_2(A_1)$ and $\nu_{10}(B_1)$ of ethylene oxide in its hydrate (KBr pellet) 239

4.20 Temperature dependence of the absorption between 2900 and 3100 cm^{-1} by ethylene oxide in ethylene oxide deuterate (KBr pellet) ... 240

5.1 Graph of $\nu_{OD}(HDO)$ versus O-O distance for ices I, II and IX and cyclopropane structure I hydrate or weighted mean O-O distance for ices V and VI, the structure I hydrates of ethylene oxide and oxetane and the structure II hydrates of tetrahydrofuran and oxetane .. 247

5.2 The $\nu_{OH}(H_2O)$ and $\nu_{OD}(D_2O)$ bands of ice Ih and the oxetane hydrates 253

5.3 The $\nu_{OH}(H_2O)$ and $\nu_{OD}(D_2O)$ bands of ethylene oxide hydrate 254

Chapter One. Introduction

1.1 General

This thesis presents two independent but closely related projects. The first project is the re-examination of the mid-infrared spectra of ices II and IX and their interpretation. The second project is concerned with the mid-infrared spectra of cyclopropane structure I clathrate hydrate, cyclopropane structure II clathrate hydrate and oxirane structure I clathrate hydrate (hereafter called cyclopropane hydrate I, cyclopropane hydrate II and ethylene oxide hydrate), and continues previous infrared studies of the clathrate hydrates in this laboratory (1,2).

General introductions to the polymorphs of ice and the clathrate hydrates are presented in Sections 1.2 and 1.3, respectively. In Section 1.4, the basic principles of vibrations in solids are discussed with particular reference to ices II and IX. Previous work on the vibrational spectra of the ices and the clathrate hydrates is discussed in Sections 1.5 and 1.6, respectively, and the previous studies of the vibrational spectra of cyclopropane are briefly discussed in Section 1.7. The objectives of this work are discussed in Section 1.8.

1.2 The Polymorphs of Ice

A brief introduction to the polymorphs of ice is presented in this section. The reader is referred to a number of review articles (3-9) for a more complete discussion.

Ice is known to exist in at least eleven different crystalline solid phases (3,5,10), and although there is great diversity in the structures of these phases (3,10,11), they are all composed of discrete, hydrogen-bonded water molecules. Each water molecule forms four hydrogen bonds which are approximately tetrahedrally directed. In two of these hydrogen bonds the water molecule donates its hydrogen atoms, and in the other two it accepts a hydrogen atom from two other water molecules. There are, thus, six possible orientations which occur with equal probability when the average coordination of the water molecules is tetrahedral, as shown by diffraction experiments. Consideration of the positions of the hydrogen atoms results in an important classification of the different ice phases. Water molecules that are in the same positions in different unit cells are translationally equivalent. If the orientations of translationally equivalent water molecules are the same in all unit cells, the ice is ordered, and if the orientations vary randomly from cell to cell, the ice is orientationally disordered. If some sets of translationally equivalent water molecules have essentially the same orientation in all unit cells whereas other sets do not, the ice is partially ordered. For all of the ice phases there is, of course, some short range correlation in the orientations of neighbouring molecules, such that there remain discrete water molecules and only one hydrogen atom between each pair of nearest neighbour oxygen atoms.

The phase diagram of ice is shown in Fig. 1.1. This

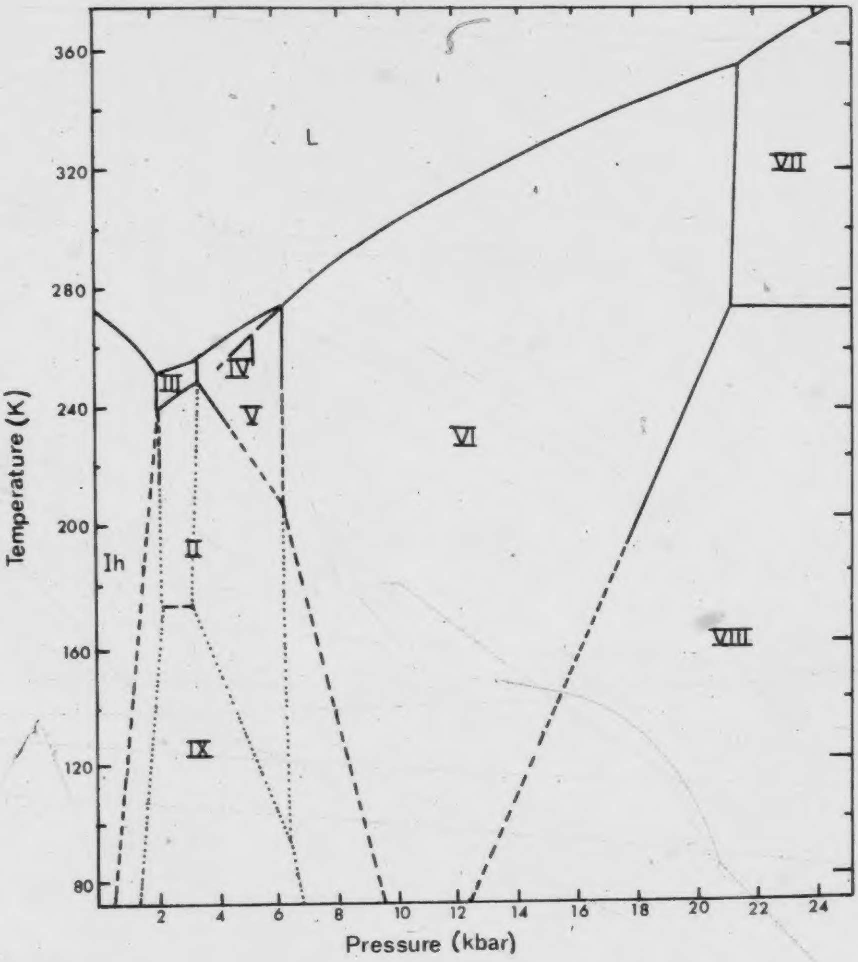

Figure 1.1. Phase diagram of ice. The solid and long-dashed lines are directly measured stable and metastable lines, respectively, and the short-dashed and dotted lines are extrapolated or estimated stable and metastable lines, respectively. Reproduced from reference 9.

has been determined by measuring the volume as a function of applied pressure at different temperatures. From such measurements it is also possible to determine the entropy changes occurring at the phase transitions (12), and these entropy changes are due mainly to changes in the configurational entropy (9) and, thus, have yielded information on the order or disorder of the hydrogen atoms.

Many other techniques have been employed to study the ice phases and the structures of most of them have been determined by X-ray diffraction (3,10,11). This technique yields information primarily on the oxygen atom positions, although constraints can be imposed by the crystallographic symmetry which allows one to deduce that the protons are disordered (10). To determine the hydrogen atom positions, neutron diffraction has been used (13-18). Dielectric measurements of the ices (19-24) provide information on the reorientational processes of the water molecules, and these measurements indicate whether or not the ice is orientationally disordered. In the presence of an applied field, molecules can only reorient if there is more than one possible orientation of similar energy, and thus dielectric relaxation or absorption is only observed for the disordered or partially ordered ice phases. The infrared and Raman spectra of the ices have also indicated which phases are ordered or disordered (Section 1.5).

Hexagonal or ordinary ice, ice Ih, is the form of ice stable at normal pressures. Two other forms of ice, a cubic form, ice Ic, and a vitreous or amorphous phase also exist metastably in the low temperature field of stability of ice Ih (3,4). Vitreous ice is not a true polymorph of ice (25), and so it is not considered further. The structures of ice Ih (26,27) and ice Ic (28) are very similar. They are both orientationally disordered (27,29) and every water molecule is tetrahedrally hydrogen bonded to its four nearest neighbours. The lattices are formed by puckered layers composed of hexagonal rings of water molecules which have the chair conformation. The lattices differ only in the stacking of these puckered layers. In ice Ic, the hexagonal rings formed by three oxygen atoms of one layer and the three oxygen atoms in an adjacent layer have the chair conformation, whereas they have the boat conformation in ice Ih.

The remaining ice phases are formed at high pressure and can be studied either in their field of stability or, if they exist metastably at low temperature, as quenched phases at atmospheric pressure and low temperature.

The presence of high pressure forms of ice was first demonstrated by Tammann in 1900 (30) who formed ices II and III. The phase diagram was later extended by Bridgman (31-33) who discovered ices IV, V, VI and VII. More recently two more phases, ice VIII (23) and ice IX (24), have been identified. The first attempts to determine the structures of the high pressure ices were by McFarlan (34,35) who reported the X-ray powder diffraction patterns of ices II and IX. His work did not, however, agree with later studies by

Bertie, Calvert and Whalley (36).

Ice II was first recognized as being ordered by its infrared spectrum (37). The structure of ice II was initially determined by a single crystal X-ray diffraction study (38), and an ordered arrangement of the hydrogen atoms was found to give the best agreement with the X-ray data. This ordered arrangement has been confirmed by neutron diffraction studies of the powdered samples of the deuterated ice by Finch et al. (17) and also of single crystal samples of the deuterated ice by Kamb et al. (16). The ordered structure was also confirmed by dielectric (20) and entropy (12) measurements. A neutron diffraction study has also shown that the crystal structure obtained for ice II in its field of stability is the same as that of the quenched form (39).

Dielectric studies of ices III, V and VI above 228 K and in their field of stability (20) have shown that these phases are orientationally disordered. Ice IV exists only metastably in the field of ice V and is difficult to study. Entropy considerations (40) have indicated that it is also probably disordered and this has been confirmed recently by a single crystal X-ray diffraction study (41).

The phase obtained by cooling ice III to 100 K was first recognized as being ordered by its infrared spectrum (37). Later, dielectric measurements indicated that a disorder to order transition occurs at about 170 K (24). This ordered phase is now designated ice IX, but prior to 1968 it was called ice III. Kamb and Datta (42) reported a preliminary structure for ice IX, and a more complete single crystal X-ray diffraction determination was later reported by Kamb and Prakash (43). They were, however, unable to distinguish between a proton ordered or disordered structure. Neutron diffraction studies of powdered samples of the deuterated ice by Rabideau *et al*. (18) and also of single crystal samples of the deuterated ice by Hamilton *et al*. (13) showed that ice IX is ordered. Later a more detailed neutron diffraction study (15) of the deuterated ice showed that the deuterium atoms occupy the two possible positions between hydrogen-bonded oxygen atoms with probabilities of 0.96±0.01 and 0.04±0.01, compared with 1.0 and 0.0 for a fully ordered structure and 0.5 and 0.5 for a fully disordered one. This partial disorder has been confirmed by Nishibata and Whalley (44) who have studied the heat of transformation of ice III to ice IX. Neutron diffraction studies of ices III and IX under pressure have also been reported (39). The space group is the same for both phases, but the transition changes the c/a ratio of the tetragonal cell from 1.044±.017 for ice III to 1.000±.003 for ice IX. Proton and deuteron nuclear magnetic resonance studies of ices II and IX have also been reported (45).

Ice VII, like ice III, has been found to undergo a disorder to order transition near 273 K to form ice VIII (23). The occurrence of this transition was first suggested by Whalley and Davidson (12) from entropy considerations. More precise entropy calculations based on a remeasurement of the phase diagram (46) and dielectric measurements (21) indicated that ice VIII is ordered and a neutron diffraction study (47) and the Raman spectrum (48) of ice VIII have confirmed this.

Kamb (5,10) has proposed the existence of two more forms of ice, ice X, a partially ordered low-temperature form of ice VI, and ice XI, a partially ordered low-temperature form of ice V. Dielectric measurements (21) have indicated that ice VI is not completely disordered at any temperature, and that there is a transition near 123 K. X-ray diffraction studies of ice VI in its field of stability (49) and X-ray and neutron diffraction studies of the quenched form (50,51) have indicated that the space groups of these two forms are different (10). The difference between the two phases is unclear at present.

The evidence for the new phase, ice XI, is not as conclusive as for ice X. Entropy (32) and dielectric (20) measurements at high temperature have shown that ice V is disordered, while the neutron diffraction study by Hamilton et al. (13) of the quenched phase at 110 K indicated that there is significant proton order. Attempts to detect an ordering transition in ice V at low temperature have been unsuccessful since it transforms to ice II below about 227 K (21).

The high pressure ices are much more compact than ices Ih and Ic. This higher density is not the result of shorter

O-H...O distances, but is due to smaller second-and higher-nearest neighbour distances. For ice Ih the O-H...O and second-nearest neighbour distances are 2.74 and 4.5 Å, respectively, while for ices II, V, VI and IX these distances are 2.75 to 2.87 Å and 3.24 to 3.51 Å, respectively (4,10). For ice VII both distances are about 2.96 Å (5). Ice VIII is quite unusual in that its O-H...O distances are 2.96 Å while the nearest non-bonded distances are 3.15 and 2.80 Å (5), so that some of the non-bonded distances are shorter than the hydrogen-bonded distances. The small second-nearest neighbour distances for the densest ices, ices VI, VII, and VIII, are the result of the interesting feature that they are composed of two identical interpenetrating, but not interconnecting lattices. Kamb has used the term self-clathrate to describe these ices (10).

In ices II, V, VI, VIII and IX, the changes in the O-O distances are accompanied by distortions from the ideal tetrahedral geometry found in ices Ih, Ic and VII. These distortions are believed to result in the proton order found in the high pressure ices at low temperature. Presumably, the water molecules orient themselves so that the H-O-H angles are most closely matched to the available O...O...O angles (10). Considerations of this type in fact led Whalley et al. (24) to predict the correct orientations of the water molecules in ice IX before they were determined from neutron diffraction studies.

1.3 The Clathrate Hydrates

A brief introduction to the clathrate hydrates is presented in this section, with particular reference to the clathrate hydrates of cyclopropane, ethylene oxide and oxetane. The reader is referred to a number of review articles for a more complete discussion (52-54) and to previous theses (1,2) for more complete accounts of the discovery and properties of ethylene oxide and the oxetane hydrates.

The clathrate hydrates are crystalline compounds in which hydrogen-bonded water molecules form a host lattice containing cage-like cavities in which small guest molecules are encaged. A large number of clathrate hydrates exist, and most of them conform to one of two structures which are termed structure I and structure II (52). The structure of the structure I hydrate has been defined by single crystal X-ray diffraction study of ethylene oxide hydrate at 248 K (55) and neutron diffraction study of ethylene oxide deuterate at 80 K (56), while that of the structure II hydrate has been defined by a single crystal X-ray diffraction study of the double hydrate of tetrahydrofuran and hydrogen sulphide at 253 K (57).

The clathrate hydrates are sometimes considered to be forms of ice (58), since each water molecule is hydrogen bonded to four nearest neighbours. Three of the hydrogen bonds formed by each water molecule form the edges of a cage, while the fourth is directed outwards from the cage.

The four types of cages found in the structure I and structure II hydrates, are shown in Fig. 1.2, as viewed along their axes of highest symmetry (59). Some of the geometric parameters associated with the structures are given in Table 1.1 (56,60).

The structure I clathrate hydrates have the space group Pm3n, O_h^3 (55,56), with 46 water molecules per unit cell. The oxygen atoms are at the vertices of 6 tetrakaidecahedra (14-hedra) and 2 pentagonal dodecahedra (12-hedra). The 12-hedra (Fig. 1.2a) are composed of pentagonal faces, are situated at the vertices and centre of the unit cell, and have a free inside diameter of about 4.9 Å (56). The 14-hedra (Fig. 1.2b) are composed of two opposite hexagonal faces and 12 pentagonal faces and have an approximately ellipsoidal free volume with free inside diameters of about 5.2 Å along the $\bar{4}$ axis in the direction perpendicular to the hexagonal rings and 6.0 to 6.3 Å in the equatorial directions (56).

The structure II clathrate hydrates have the space group Fd3m, O_h^7 (57) with 136 water molecules per face-centred unit cell. The oxygen atoms are at the vertices of 16 pentagonal dodecahedra (12-hedra) and 8 hexakaidecahedra (16-hedra). The 12-hedra (Fig. 1.2c) are very similar to those of the structure I hydrate and have a free inside diameter of about 5.0 Å. The 16-hedra (Fig. 1.2d) are composed of four tetrahedrally arranged hexagonal faces and 12 pentagonal faces and are almost spherical with free in-

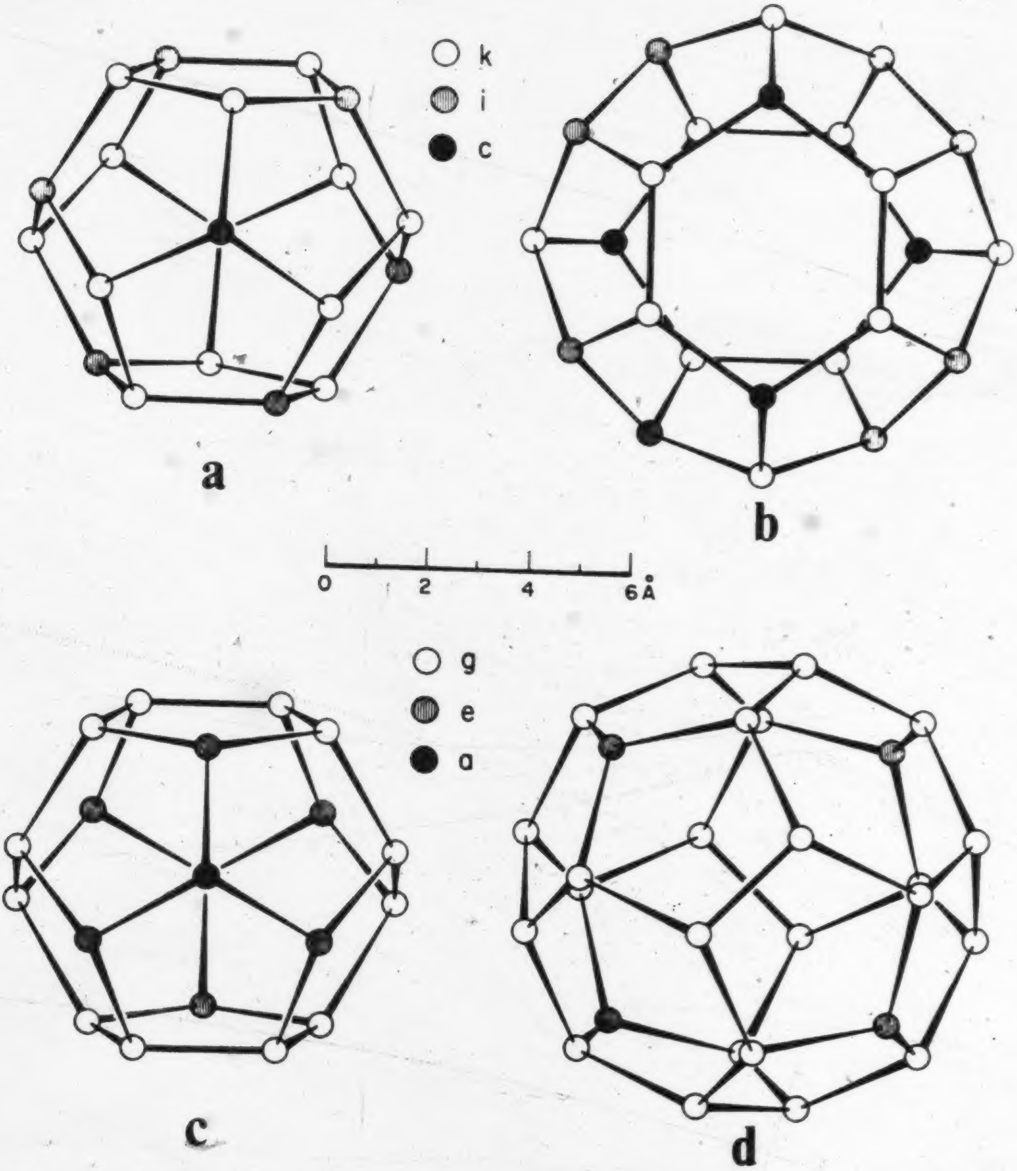

Figure 1.2. Cages of the structure I (a,b) and structure II (c,d) clathrate hydrates viewed along axes of highest symmetry. Literal identification of the sites follows the notation of The International Tables for X-ray Crystallography. Reproduced from reference 59.

TABLE 1.1

Geometric Parameters of the Unit Cells and Cages of the Structure I and Structure II Clathrate Hydrates[a,b]

	Structure I[c]				Structure II[c]		
Space group, cell parameter		Pm3n, 11.87 Å			Fd3m, 17.31 Å		
Number of H_2O molecules			46			136	
Non-equivalent O sites		6c	16i	24k	8a	32e	96g
O site symmetry		$\bar{4}2m$	3m	m	$\bar{4}3m$	3m	m
Departure of O--O--O angle from tetrahedral:							
Average at O site		0.8°	1.2°	5.3°	0°	2.1°	3.6°
Average in structure			3.3°			3.0°	
Average O--O length (Å)			2.757			2.790	
Small cages:							
Number, symmetry			2, m3			16, $\bar{3}m$	
O sites		8i		12k	2a	6e	12g
Distance to center (Å)		3.78		3.91	3.748	3.845	3.956
Average cage radius (Å)			3.86			3.902	
Large cages:							
Number, symmetry			6, $\bar{4}2m$			8, $\bar{4}3m$	
O sites	4c	8i	8k	4k	4e	12g	12g
Distance to center (Å)	4.20	4.41	3.99	4.595	4.729	4.715	4.635
Average cage radius (Å)			4.27			4.683	

continued......

TABLE 1.1 (continued)

a) Adapted from reference 60.

b) The structure I parameters are for ethylene oxide hydrate at 80 K (56), the structure II parameters are for the tetrahydrofuran-hydrogen sulphide hydrate at 253 K (57).

c) The symmetry symbols follow the notation of The International Tables for X-ray Crystallography.

side diameters of 6.6 Å (57).

The structure I and structure II clathrate hydrates are formed by a wide variety of guest molecules (52). The most important criterion for which structure is formed is the size and shape of the guest molecule. In general, those guest molecules with van der Waals diameters less than 5.5 Å form structure I hydrates and those with van der Waals diameters between 5.5 and 6.7 Å form the structure II hydrates (2). Thus, ethylene oxide has a largest van der Waals diameter of 5.2 Å (61), and forms a structure I hydrate with all of the large cages occupied but only 19 to 40 percent of the smaller cages occupied (55,62). Tetrahydrofuran has a largest van der Waals diameter of 5.9 Å (61), and forms the structure II hydrate with the 16-hedra fully occupied and the 12-hedra empty (63), or, in the double hydrate of tetrahydrofuran and hydrogen sulphide, the 12-hedra partially occupied by hydrogen sulphide (57).

Oxetane and cyclopropane are unique. Oxetane has largest van der Waals diameters of 5.5 and 6.2 Å and cyclopropane has a largest van der Waals diameter of 5.4 Å (2), and these two molecules form both structure I and structure II clathrate hydrates (2,64,65). No other compounds are known to form hydrates of both structures without the help of a second type of guest molecule (61).

The formation of cyclopropane hydrate I was first established by Miller (66) and Barduhn et al. (67). The formation of cyclopropane hydrate II was later established by Hafemann and Miller (65). The phase diagrams of the cyclopropane hydrates and deuterates are shown in Figs. 1.3 and 1.4, respectively, and were determined from the dissociation pressures of the hydrates or deuterates as a function of temperature (65,68). Cyclopropane hydrate II and deuterate II are only stable from 257.2 to 274.7 K and from 249.9 to 278.7 K, respectively (65) and at cyclopropane pressures less than the decomposition pressure of the structure I hydrate or deuterate (68). In both structures cyclopropane, like oxetane (2), occupies all of the large cages and none of the small cages (65,68).

The clathrate hydrates have been extensively studied by dielectric (69,70,71) and nuclear magnetic resonance techniques (72-74). These techniques yield information concerning the reorientational processes of the guest and water molecules.

Dielectric absorption due to molecular reorientation usually occurs at frequencies below about 30 GHz (1). For the clathrate hydrates two dielectric relaxation processes are observed, one at low frequency due to the reorientation of the water molecules and one at high frequency due to the reorientation of dipolar guest molecules. The observation of dielectric relaxation clearly shows that the molecules are orientationally disordered. The frequency of maximum dielectric absorption is usually equated with the rate of molecular reorientation (75), and its temperature dependence is usually described by an Arrhenius rate equation (70).

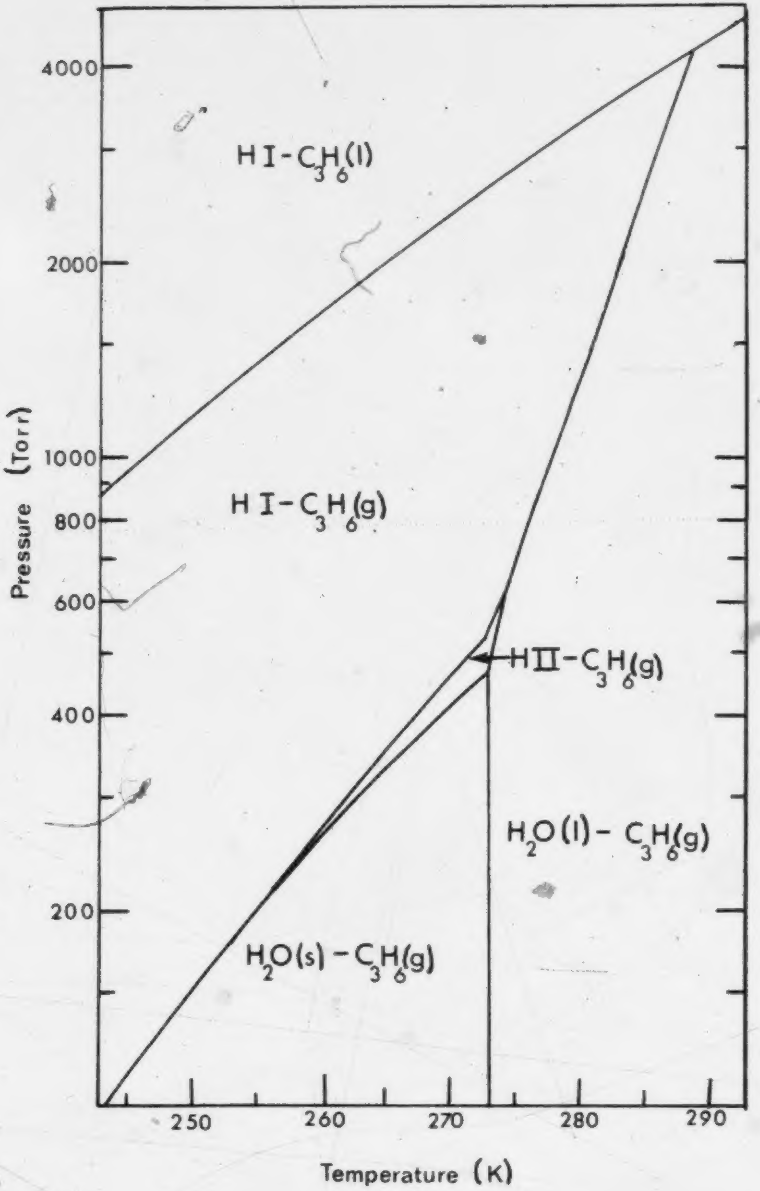

Figure 1.3. Phase diagram of the cyclopropane - H_2O system. HI and HII indicate cyclopropane structure I hydrate and cyclopropane structure II hydrate, respectively.

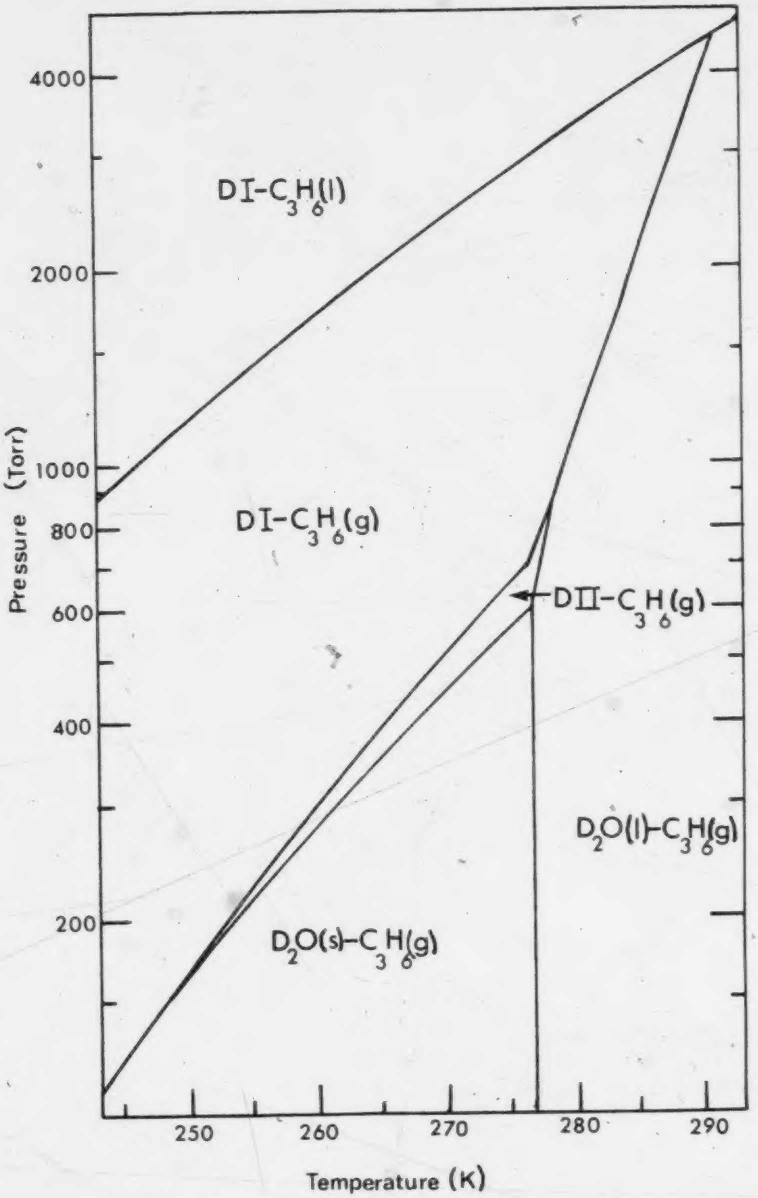

7

Figure 1.4. Phase diagram of the cyclopropane - D_2O system. DI and DII indicate cyclopropane structure I deuterate and cyclopropane structure II deuterate, respectively.

The reorientation rates of the water molecules are highly sensitive to the nature of the guest molecules and are slower for nondipolar guest molecules than for dipolar guest molecules (69,70). For example, the reorientation rates of the water molecules in the structure I hydrates of cyclopropane, ethylene oxide and oxetane at 233 K are 3.57 kHz (69), 3.03 MHz (76) and 33.3 MHz (77), and the corresponding activation energies are 10, 7.7 and 5.8 kcal/mole, respectively. This slower relaxation rate for nondipolar guest molecules has been attributed to the ability of polar guest molecules to inject defects into the water lattice (69,70). At 100 K the reorientation rates of the water molecules in the clathrate hydrates are negligible (70).

Nuclear magnetic resonance studies of the clathrate hydrates have been concerned mainly with the determination of the temperature dependence of the spin-lattice relaxation times, from which it is possible to determine the activation energy for the reorientation of the guest or water molecules, and with measurements of the second moment of the resonance line. The second moment is a measure of both linewidth and lineshape and it is sensitive to the motion of the molecules. Second moments can be calculated for a rigid lattice from the geometry of the solid, and for rapidly moving molecules by assuming certain types of motion (78). Thus, the comparison of the calculated and observed second moments can yield information concerning the reorientation of the guest or water molecules.

Proton nuclear magnetic studies of the second moment of the resonance line due to the water molecules have confirmed the results from dielectric work that the water molecules of clathrate hydrates with dipolar guest molecules reorient more rapidly than those with nondipolar guest molecules (73,79). This is shown clearly by the temperature at which narrowing of the resonance line occurs. For the structure I hydrates of cyclopropane, ethylene oxide and oxetane, these temperatures are about 250, 170 and 150 K (79).

At convenient temperatures (T>90 K), the dielectric relaxation of dipolar guest molecules occurs at very high frequencies where dielectric measurements are difficult (71). For ethylene oxide hydrate at 88 K, the reorientation rate of the guest molecules is 6.6 GHz (80), so much lower temperatures have to be employed to enable the absorption to be studied at lower frequencies (1 Hz to 1 MHz) (71). The low-temperature studies have shown that the relaxation rates decrease and the activation energies for reorientation increase with increasing guest size for both types of clathrate hydrates (69,71). For example, for the structure I hydrates of ethylene oxide and oxetane, the temperatures associated with guest reorientation rates of 1 kHz are 28 and 52 K, and the activation energies for reorientation are 1.42 and 2.43 kcal/mole, respectively (76,81).

Proton nuclear magnetic resonance studies of the guest molecules in the deuterates have shown that, in general, the guest molecules are fixed on the nuclear magnetic resonance time scale below about 4 K (72). The second moments of the proton resonance of ethylene oxide and cyclopropane in their structure I deuterates show that the guest molecules effectively undergo isotropic rotation above 230 K (76,82). Proton spin-lattice relaxation measurements of cyclopropane, between 77 and 125 K (82), and ethylene oxide, between 77 and 170 K (83), in their structure I deuterates have yielded activation energies of 0.83 and 0.9 kcal/mole, respectively. The activation energy determined for ethylene oxide in its deuterate is in good agreement with the activation energy, 0.89 kcal/mole, determined from deuterium spin-lattice relaxation times of ethylene oxide-d_4 between 100 and 170 K in its hydrate (84). These values are appreciably lower than those determined by dielectric measurements, 1.42 kcal/mole below 40 K (76) or 1.26 kcal/mole between 30 and 90 K (71). This difference is undoubtedly due to the different temperatures.

The structure I hydrate of oxetane differs from other structure I hydrates in that dielectric and nuclear magnetic resonance studies (81) have indicated that the oxetane molecules undergo an ordering transition below 105 K, in which nearest neighbour guest molecules adopt a predominantly parallel alignment along the $\bar{4}$ axis of the 14-hedral cages. No evidence for a preference for axial orientations of the guest molecules has been found from dielectric or nuclear magnetic studies of the structure I hydrates of cyclopropane or ethylene oxide (68,76,82). The presence of such preferred orientations has, however, been invoked to account for the electron density distribution determined from an X-ray diffraction study of ethylene oxide hydrate at 248 K (55). This interpretation of well defined orientations of the guest molecules is inconsistent with the small activation energies for the reorientation of the guest (76,85) and also with a recent neutron diffraction study of ethylene oxide deuterate (56). In this latter study a model involving the 24-fold disorder of the guest molecules was used to describe the neutron scattering by the ethylene oxide molecules in the 14-hedral cages (56).

Davidson (85) has tried to determine the orientations of greatest stability of ethylene oxide in the 14-hedral cage, by calculations using Lennard-Jones potentials between the oxygen atoms of the water molecules forming the cage and the atoms of the guest molecule. These calculations failed to establish any preference for axial positions. Similar calculations (76) of this type have suggested that there are a large number of orientations of similar energy within the cages which are separated by low (1 kcal/mole) potential barriers, but that it is possible that axial configurations may be favoured at very low temperatures. Nuclear magnetic resonance and dielectric relaxation measurements (76) have shown that the different orientations of the guest molecules do become appreciably nonequivalent at low temperatures.

1.4 Vibrations in Solids

A brief introduction to the vibrations in solids is presented in this section. More detailed discussions are available in the literature (86-93). The principles presented are applied to ices II and IX at the end of this section.

The property that distinguishes the crystalline state from all other states is the periodic arrangement of the atoms in crystals. Due to this periodicity the vibrations in a crystal can be regarded as displacement waves propagating through the lattice (87-90) and are characterized by a frequency, ν, and a wavelength, λ. The wavelengths can take certain values between the dimensions of the crystal and twice the unit cell length in the direction of propagation (87-90). The vibrations are usually described by a wavevector, $\underline{k}$, whose magnitude is the reciprocal of the wavelength, and whose direction is the direction of propagation (87). The relation between the frequencies and wavevectors of the vibrations is described by dispersion curves.

If there are p m-atomic molecules per unit cell, there are 3pm branches of dispersion curves. p(3m-6) of these are due to intramolecular vibrations. The frequencies of these vibrations usually depend primarily on the strong intramolecular forces and do not exhibit a strong wavevector dependence. The remaining 6p branches are due to intermolecular vibrations, the frequencies of which are determined primarily by intermolecular forces. These intermolecular forces depend on the relative displacements of the molecules, which are strongly dependent on the wavevector, so the frequencies of the intermolecular vibrations exhibit a strong wavevector dependence. 3p of these latter branches are due to the rotational vibrations of the molecules, and the remaining 3p branches are due to the translational vibrations of the molecules. At zero wavevector three of the translational branches have zero frequency and correspond to the pure translation of the crystal in three orthogonal directions, and at wavevectors close to zero these branches correspond to sound waves in the crystal. These branches are, thus, called acoustic branches. The remaining 3pm-3 branches are called the optic branches because the optically active vibrations occur in them.

The periodicity of the vibrations in an ordered solid means that the changes in dipole moment or polarizability during each vibration are also periodic. Electromagnetic radiation waves are also periodic, and the interaction between the radiation wave and the vibration wave only yields infrared absorption if the two waves have the same wavelength and propagate in the same direction (87,94,95); i.e. if $\underline{K}=\underline{k}$, where $\underline{K}$ is the wavevector of the light. Infrared radiation has a wavelength of 10^{-4} to 1 cm, much greater than the unit cell length, so that vibrations with $\underline{K}=\underline{k}$ have essentially the same frequency as those with $\underline{k}=0$ for crystals with short-range forces. The $\underline{k}=0$ vibrations are those in which the atomic displacements which occur in one unit cell are duplicated in all unit cells, so it is only necessary to consider the displacements in one unit cell to visualize the optically-active vibrations. Thus, although there are about 10^{25} vibrations per mole of molecules, the number of vibrations that need be considered for an ordered solid is only 3pm-3, where p and m are defined as above. Not all of these zero-wavevector vibrations result in a change in the dipole moment or polarizability that is required for infrared or Raman activity. To determine which ones are active a unit-cell-group symmetry analysis (92,93) is performed, the procedure for which will be illustrated for ices II and IX later in this section.

For an orientationally disordered solid there is no wavevector selection rule because the changes in the dipole moment or polarizability during the vibration are not periodic. Thus, all of the 10^{25} vibrations per mole of molecules are infrared and Raman active. The absorption by an orientationally disordered solid must be described by a density of vibrational states function multiplied by an intensity distribution function (96-98). The density of vibrational states is defined as the number of vibrations at each frequency (87) and can be determined from the dispersion curves, if they are known. The frequencies are often not greatly dependent on the wavevector for wavevectors close to zero (near the Brillouin zone centre) or close to the maximum wavevector value (near the Brillouin zone boundary). The vibrations are uniformly distributed in wavevector space, so there are far more vibrations with wavevectors close to the maximum value than with wavevectors close to zero, and the maxima in the density of vibrational states usually arise from vibrations near the zone boundary (98).

Ices II and IX are essentially ordered (Section 1.2) so their fundamental absorption should be due solely to $\underline{k}=0$ vibrations. To determine which vibrations are infrared or Raman active a unit-cell-group analysis is performed. This requires a knowledge of the symmetry properties of the solid.

The symmetry of the solid is described by the space group, which is formed by all symmetry elements in the crystal, and therefore includes all combinations of primitive translations, and proper and improper rotations. The fundamental unit of the crystal is the primitive unit cell which is defined as the smallest unit in which no atoms are equivalent by simple translations and sums and multiples thereof. The symmetry of the unit cell is described by the unit-cell group, which is defined as the finite subgroup of the space group in which translations which carry a point in one unit cell into the equivalent point in another unit cell are defined as the identity (99). The unit-cell group is isomorphous with one of the 32 point groups and can be obtained by deleting the superscript from the Schoenflies symbol for the space group. The symmetry of the sites occupied by the molecules is described by a site group, which is defined as the group of symmetry elements which leave the site invariant, and this group is a subgroup of the molecular point group and of the unit-cell group.

The method most commonly used for a unit-cell group analysis is the correlation method (92,93). To apply this method one needs to know the space group, the symmetries of the sites occupied by the molecules and the number of molecules per primitive unit cell. The method consists of three steps. First, the representations formed by the vibrations of the free molecules under their point group are obtained (100). From these the representations under the site group are obtained by the use of correlation tables (100), and then from these representations, the representations under the unit-cell group are obtained by the use of correlation tables (100). This method is illustrated below for ices II and IX.

Ice II, space group $R\bar{3}$, C_{3i}^2, has twelve molecules per unit cell which occupy two sets of sixfold equivalent sites of symmetry C_1 (16,38). The unit-cell group is isomorphous with the group $C_{3i} \equiv S_6$, so the character tables for S_6 can be used for the unit-cell group. Shown in Fig. 1.5 is the correlation diagram for ice II which relates the irreducible representations of the molecular point group, C_{2v}, to those under the site group, C_1, and the unit-cell group, S_6. The free water molecule has three intramolecular vibrations, ν_1, a symmetric O-H stretching vibration of symmetry species A_1, ν_2, the H-O-H bending vibration of symmetry species A_1, and ν_3, the antisymmetric O-H stretching vibration of symmetry species B_1. The translational degrees of

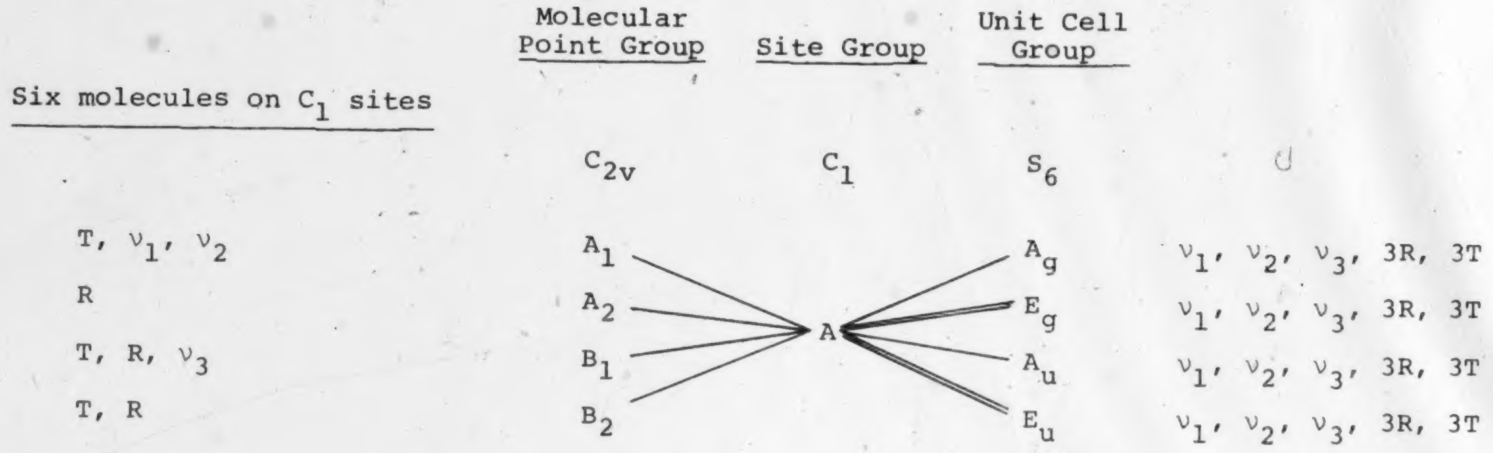
Six molecules on C_1 sites
Molecular Point Group
Site Group
Unit Cell Group
C_{2v}
C_1
S_6
T, ν_1, ν_2
R
T, R, ν_3
T, R
A_1
A_2
B_1
B_2
A
A_g
E_g
A_u
E_u
ν_1, ν_2, ν_3, 3R, 3T
ν_1, ν_2, ν_3, 3R, 3T
ν_1, ν_2, ν_3, 3R, 3T
ν_1, ν_2, ν_3, 3R, 3T

Figure 1.5 Correlation Diagram for ice II. The above diagram applies for both sets of non-equivalent water molecules.

freedom of the water molecule form the representation $A_1+B_1+B_2$ and the rotational degrees of freedom form the representation $A_2+B_1+B_2$. There are twelve molecules per unit cell so that twelve vibrations exist in the unit cell for each translational (T), rotational (R) or vibrational (ν_1,ν_2 or ν_3) degree of freedom of the free molecule. From the correlation diagram (Fig. 1.5) the following representations are obtained under the unit-cell group:

$$\Gamma_{\nu_1}=\Gamma_{\nu_2}=\Gamma_{\nu_3}=2A_g+2E_g+2A_u+2E_u$$

$$\Gamma_R=6A_g+6E_g+6A_u+6E_u$$

$$\Gamma_T=6A_g+6E_g+6A_u+6E_u.$$

Three of the translational vibrations correspond to the acoustic modes which have zero frequency and form the representation A_u+E_u. The representation formed by the translational vibrations with finite frequency is, therefore

$$\Gamma_T=6A_g+6E_g+5A_u+5E_u$$

The infrared active vibrations are of symmetry species A_u and E_u, and the Raman active vibrations are of symmetry species A_g and E_g. Thus, a unit-cell-group analysis predicts 10 infrared active and 12 Raman active translational vibrations, 12 infrared and 12 Raman active rotational vibrations and 4 infrared and 4 Raman active vibrations due to each of the intramolecular vibrations. Because the structure is centrosymmetric the Raman active vibrations are not infrared active, and vice versa.

Ice IX, space group $P4_12_12$, D_4^4, has twelve molecules per unit cell (15,43). Eight of these molecules are on sites of symmetry C_1, and four are on sites of symmetry C_2. Shown in Fig. 1.6 are the correlation diagrams for ice IX, which relate the irreducible representations of the molecular point group, C_{2v}, to those under the site group, C_1 or C_2, and the unit-cell group, D_4. From these correlation diagrams the following representations are obtained under the unit-cell group:

$$\Gamma_{\nu_1}=\Gamma_{\nu_2}=2A_1+A_2+B_1+2B_2+3E$$

$$\Gamma_{\nu_3}=A_1+2A_2+2B_1+B_2+3E$$

$$\Gamma_R=4A_1+5A_2+5B_1+4B_2+9E$$

$$\Gamma_T=4A_1+4A_2+5B_1+4B_2+8E,$$

where the three acoustic modes have been omitted from Γ_T, and C_2'' was taken to be diagonal to the a axis of the unit cell.

The infrared active vibrations are of symmetry species A_2 and E and the Raman active vibrations are of symmetry species A_1,B_1,B_2 and E. Thus, a unit-cell-group analysis predicts 12 infrared and 21 Raman active translational vibrations, 14 infrared and 22 Raman active rotational vibrations, 4 infrared and 8 Raman active H-O-H bending vibrations and 9 infrared and 15 Raman active O-H stretching vibrations.

1.5 Vibrational Spectra of the Ice Polymorphs

The studies of the vibrational spectra of the ices have been reviewed a number of times (4,7,8,101-104) and no

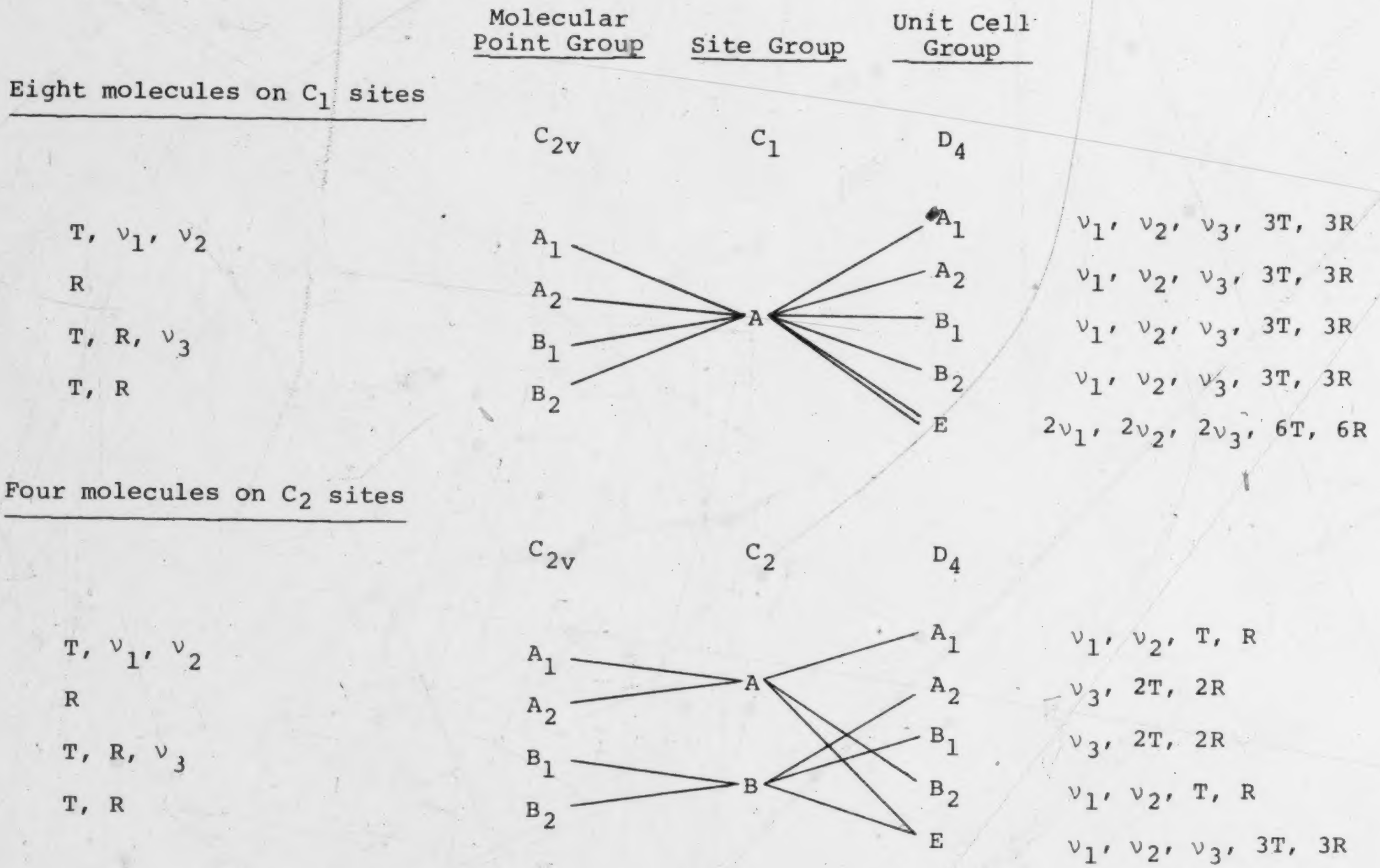
Molecular Point Group
Site Group
Unit Cell Group
Eight molecules on C_1 sites
C_{2v}
C_1
D_4
T, ν_1, ν_2
R
T, R, ν_3
T, R
A_1
A_2
B_1
B_2
A
A_1
A_2
B_1
B_2
E
ν_1, ν_2, ν_3, 3T, 3R
ν_1, ν_2, ν_3, 3T, 3R
ν_1, ν_2, ν_3, 3T, 3R
ν_1, ν_2, ν_3, 3T, 3R
$2\nu_1$, $2\nu_2$, $2\nu_3$, 6T, 6R
Four molecules on C_2 sites
C_{2v}
C_2
D_4
T, ν_1, ν_2
R
T, R, ν_3
T, R
A_1
A_2
B_1
B_2
A
B
A_1
A_2
B_1
B_2
E
ν_1, ν_2, T, R
ν_3, 2T, 2R
ν_3, 2T, 2R
ν_1, ν_2, T, R
ν_1, ν_2, ν_3, 3T, 3R

Figure 1.6. Correlation Diagrams for Ice IX.

attempt will be made to cover this subject exhaustively. Instead the purpose of this section is to briefly describe what is known about the vibrational spectra of the ices.

The infrared and Raman spectra of ices Ih and Ic have been extensively studied (105-116). No differences have been detected between the mid-infrared or Raman spectra of these two ices, but their far-infrared spectra have very recently been shown (115) to differ slightly. The first infrared spectra of the high pressure forms of ice were reported by Lippincott, Weir and van Valkenburg (117) who studied ice in a diamond anvil cell at a temperature of about 255 K and pressures of 3000 and 9000 atmospheres. More recently, the mid-infrared spectra of ices II, V and IX (37) and VI (118), the far-infrared spectra of ices II, V and IX (119) and VI (118) and the Raman spectra of ices II, V and IX (111), VI (120,121), VII (121) and VIII (48,120,121) have been reported: All of these spectra were of the ices quenched to 100 K and at atmospheric pressure, except for the Raman spectra of ices VI, VII and VIII (121) which were of the ices in their region of stability. To date the temperature dependence of the spectra have only been reported for ice Ih (98,106,109,116) and uncharacterized samples of ice Ic (122).

The infrared spectra of all of the ice phases studied contain a broad band centred at about 3200 cm^{-1} for the H_2O ices and at about 2400 cm^{-1} for the D_2O ices, which is called the $\nu_{OH}(H_2O)$ or $\nu_{OD}(D_2O)$ band and is assigned to the O-H or O-D stretching vibrations. There is also a broad absorption band at about 1600 cm^{-1} for the H_2O ices and at about 1200 cm^{-1} for the D_2O ices, which is called the $\nu_2(H_2O)$ or $\nu_2(D_2O)$ band and is assigned to the H-O-H or D-O-D bending vibrations.

The intermolecular vibrations are due to the hindered translational or hindered rotational (librational) motions of the water molecules. These two types of motion occur in separate frequency regions below about 1100 cm^{-1}. The infrared absorption bands below about 360 cm^{-1} in the H_2O and D_2O ices are assigned to the translational vibrations, and are called the $\nu_T(H_2O)$ or $\nu_T(D_2O)$ bands. Absorption due to the rotational vibrations occurs at about 1100 to 400 cm^{-1} in the H_2O ices and at about 900 to 350 cm^{-1} in the D_2O ices, and these bands are designated $\nu_R(H_2O)$ or $\nu_R(D_2O)$. There is also a broad, weak absorption band at about 2200 cm^{-1} in the H_2O ices and at about 1600 cm^{-1} in the D_2O ices which is assigned to the second overtone of the rotational vibrations, $3\nu_R$, and to the combination transitions $\nu_2+\nu_R$.

The discussion of the absorption due to the O-H or O-D stretching vibrations is best approached by introducing the results obtained from isotopic dilution studies. In the spectra of ice samples which contain a few percent of HDO in H_2O or D_2O, absorption can be seen due to O-D oscillators surrounded by H_2O molecules or O-H oscillators surrounded by D_2O molecules. These absorption bands are called the isolated O-D and O-H bands or the $\nu_{OD}(HDO)$ and

ν_{OH}(HDO) bands. Because the O-D and O-H stretching vibrations absorb at sufficiently different frequencies, the isolated O-D or O-H oscillators are virtually uninfluenced by intra- and intermolecular coupling. Thus, the absorption frequency of an isolated O-D or O-H bond reflects the environment (static field) experienced by that bond in the crystal and from these frequencies the O-D or O-H stretching force constants can be determined (104).

Differences are observed between the ν_{OD}(HDO) or ν_{OH}(HDO) bands of the ordered ices and those of the disordered ices (37,110). The ν_{OD}(HDO) bands of the ordered ices are composed of a number of sharp features, with half-widths (bandwidth at half peak absorbance) of about 5 cm^{-1} (37), that are assigned to absorption due to the different sets of diffraction-equivalent O···O bonds. The frequencies of these features have been shown to correlate well with the O···O bond lengths and to generally increase with increasing bond length (43,96). The disordered ice Ih has only one type of diffraction-equivalent O···O bond length and its ν_{OD}(HDO) band has a half-width of about 30 cm^{-1} (110). The half-widths of the ν_{OD}(HDO) or ν_{OH}(HDO) bands of ice Ih do, however, vary with the method used to prepare the infrared samples. For ice Ih mulled in isopropane or propene the half-width of the ν_{OD}(HDO) band is 30 cm^{-1} (110), while it is 18 cm^{-1} (109,110) for samples prepared by freezing a capillary film of water or by condensing water vapour onto a cold plate and then annealing the ice film. The smallest observed half-width is still, however, three to four times broader than the features of the ν_{OD}(HDO) bands of the ordered ices.

The larger half-width observed for ice Ih is believed to be the result of the orientational disorder of the water molecules, which causes the oxygen atoms to be displaced slightly from regular lattice sites, so that the diffraction-equivalent O···O bonds do not have exactly the same length (110). The frequency of the O-D oscillator depends on the length of the O-D···O bond it forms, so a broader band results from each diffraction-equivalent O···O bond in a disordered phase than in an ordered phase. In order to explain the bandwidth, a range of only a few hundredths of an angstrom in O···O bond length is required, which is much smaller than the root mean square vibrational amplitude of the oxygen atom (110) and thus these differences in O···O bond length are not detected by X-ray or neutron diffraction methods. This explanation is supported by the ratio of about $\sqrt{2}$ for the half-widths of the ν_{OH}(HDO) (50 cm^{-1}) and the ν_{OD}(HDO) (30 cm^{-1}) bands (110).

The ν_{OD}(HDO) bands of ices V and VI show no fine structure (37,118) and, thus, show no evidence of the partial order of the hydrogen atoms at 100 K (Section 1.2). The half-widths of these bands are consistent with those predicted for a disordered ice. If the half-width of the ν_{OD}(HDO) band of ice Ih is taken as characteristic of that due to a single diffraction-equivalent O···O bond length, then the ν_{OD}(HDO) bands of a disordered ice should be composed of features with half-widths of about 18 cm^{-1}, frequencies related to the bond lengths, and intensities proportional to the multiplicities of the different sets of diffraction-equivalent O···O bonds. In ice V there are seven sets of diffraction-equivalent O···O bonds and in ice VI there are five sets. No features due to these different sets are resolved in the ν_{OD}(HDO) bands but the half-widths of these bands are roughly consistent with the weighted mean deviations from the weighted mean O···O bond lengths (96). The frequencies of the ν_{OD}(HDO) bands of ices V, VI and I correlate well with the weighted mean O···O bond lengths in these phases, but the correlation differs from that for the ordered ice phases (96).

The ν_{OD}(HDO) and ν_{OH}(HDO) bands have also yielded information about the intermolecular interaction constants. At sufficiently high HDO concentrations in H_2O, the ν_{OD}(HDO) bands have weak side bands which are assigned to coupled O-D···O-D vibrations. From the frequencies of the side bands the intermolecular interaction constant for ice Ih has been determined to be -0.123 mdyne/Å (107), and those for ices V, VI and IX (37,118) are clearly approximately the same.

The infrared and Raman spectra of the ice phases show that the coupled O-H or O-D stretching vibrations extend over a wide frequency range. The $\nu_{OH}(H_2O)$ and $\nu_{OD}(D_2O)$ bands of ice Ih extend from 3000 to 3600 cm^{-1} and 2200 to 2700 cm^{-1}, respectively with a total of five features observed in the Raman spectrum (112) and six in the infrared spectrum (110). The reasons for the breadth of these bands have been discussed by Whalley (101). The ν_1 and ν_3 vibrations of the isolated molecules have different frequencies due to intramolecular coupling and are perturbed in the crystal by two main effects: First, the static field of the crystal lowers their frequencies by about 400 cm^{-1} and may change their separation (123,124); second, the intermolecular coupling should cause a broad band of vibrational frequencies to result from the ν_1 and ν_3 vibrations. Further, since there is no symmetry, the crystal vibrations derived from ν_1 and ν_3 can interact to produce mixed vibrations, and all vibrations are infrared and Raman active. The infrared and Raman spectra must therefore be described as a density of vibrational states function multiplied by an intensity distribution function (96-98). The intensity distribution functions need not be smooth functions, so that frequencies of maximum absorption or Raman scattering may correspond to maxima in the density of vibrational states or in the intensity distribution function, or a combination of both. Further, the most intense Raman band of ice Ih (112) is at a frequency well below the frequency of maximum infrared absorption (110), so the infrared and Raman intensity distribution functions differ markedly.

Wong and Whalley (112) have discussed the origin of the features on the $\nu_{OH}(H_2O)$ and $\nu_{OD}(D_2O)$ bands. They have assigned the strong, polarized Raman band at 3083 cm^{-1} to coupled ν_1 vibrations in which the molecules move nearly in phase, and have speculated that the Raman band at 3209 cm^{-1} and the infrared band at 3220 cm^{-1} are due mainly to coupled ν_3 vibrations. The corresponding assignments were made for the $\nu_{OD}(D_2O)$ band. A detailed interpretation of these bands, however, requires a detailed knowledge of the density of vibrational states and intensity distribution functions. Attempts have been made recently by Rice and coworkers (125) to calculate the density of vibrational states for ice Ih and from this, using a bond polarizability theory, to calculate the Raman spectrum. Their agreement between the observed and calculated spectra was poor and this is undoubtedly due, in part, to their neglect of off-diagonal elements of the $\underset{\sim}{G}$ matrix which are the primary source of the intramolecular coupling between ν_1 and ν_3.

Significant differences are expected between the $\nu_{OD}(D_2O)$ or $\nu_{OH}(H_2O)$ bands of the ordered and disordered ices. Only a small number of vibrations of the ordered ices should be infrared or Raman active (Section 1.4), so only a small number of sharp features are predicted in the infrared or Raman spectra. In contrast to the predictions, the $\nu_{OH}(H_2O)$ and $\nu_{OD}(D_2O)$ infrared absorption bands of ices II and IX are just as broad as those of ices Ih and Ic, although the $\nu_{OD}(D_2O)$ bands show (37) more peaks than is the case for ice Ih or Ic. For ice II, five peaks or moderately sharp features are resolved (37) and a total of eight unit-cell-group allowed vibrations are predicted (Section 1.4); for ice IX, four sharp features are resolved (37) and a total of nine unit-cell-group allowed vibrations are predicted (Section 1.4). Thus, the sharper features may be due to the allowed fundamentals, but the broad absorption is unexpected and of unknown origin; contributions from difference-combination, sum-combination, hot and overtone transitions (126) have been proposed to explain it (37).

The $\nu_{OD}(D_2O)$ and $\nu_{OH}(H_2O)$ bands of ices V and VI (37,118) are even more poorly resolved than those of ice Ih and Ic. This is presumably due to the nonequivalent O···O bonds which occur in ices V and VI but not in ice I. A more detailed interpretation is not possible at present.

The $\nu_{OD}(D_2O)$ and $\nu_{OH}(H_2O)$ Raman bands are very similar for all of the ice phases that have been studied (48,111,120, 121). They all have a very strong peak about 100 cm^{-1} below the frequency of maximum infrared absorption and one or more weaker features at higher frequencies. For the ordered phase ice VIII, the bands have been fully assigned by Whalley and Wong (48) to the $\underline{k}=0$ vibrations allowed under the D_{4h} unit-cell group of the crystal. For the other phases, ices Ih, Ic, V, IX (111) and VI (120), the only assignment that seems settled is that of the strong low-frequency peak to the most symmetric O-H or O-D stretching vibrations in the crystal (111,120).

The $\nu_2(H_2O)$ and $\nu_2(D_2O)$ infrared absorption bands of the ice phases are broad and relatively featureless (37,110, 118). These bands have yielded no useful information, and it is not even known to what extent they are due to ν_2 and to what extent they are due to the first overtones of the rotational vibrations which absorb quite strongly above 1000 cm^{-1} (37). The $\nu_2(H_2O)$ and $\nu_2(D_2O)$ Raman bands have only been detected for ice Ih (112) and ice VIII (48). For ice Ih these bands are broad and very weak (112), while for ice VIII, an ordered ice, two weak but moderately sharp bands at 1677 and 1346 cm^{-1} for the H_2O ice and at 1229 and 1008 cm^{-1} for the D_2O ice have been assigned to unit-cell-group allowed vibrations (48).

The infrared and Raman bands due to the intermolecular vibrations are significantly different in the spectra of the ordered and disordered ices. In the infrared spectra of the ordered ices, ices II and IX, the $\nu_R(H_2O)$ and $\nu_R(D_2O)$ bands consist of sharp features superimposed on a broad absorption (37). For ice II, ten sharp features were observed on the $\nu_R(D_2O)$ band (37) and a unit-cell-group analysis predicts twelve infrared active fundamentals (Section 1.4), while for ice IX, eight sharp features were observed (37) and fourteen infrared active fundamentals are predicted (Section 1.4). It was concluded (37) that these sharp features are due to unit-cell-group allowed fundamentals. This was supported by isotopic dilution studies. The sharp features weakened and broadened with the addition of isotopic impurities, which is the expected effect of the disorder introduced into the system. The

Raman bands due to the rotational vibrations of ice VIII, unlike the corresponding infrared bands of ices II and IX, consist only of three sharp features which have been assigned to the unit-cell-group allowed vibrations (48).

The $\nu_R(H_2O)$ and $\nu_R(D_2O)$ infrared absorption bands of the disordered ices, ices Ih, Ic, V and VI (37,110,118) are broad and show no sharp features. The $\nu_R(H_2O)$ vibrations of ice Ih (110) extend from 1050 to 400 cm^{-1} and heat capacity data indicate that the mean frequency of these vibrations is near 650 cm^{-1} (127). The Raman intensity is distributed roughly symmetrically across the band for ice Ih (112) while the maximum infrared intensity is at about 840 cm^{-1} (110). Thus, the intense infrared absorption occurs only in the high frequency region of this band and the reasons for this are unclear. Whalley has proposed (104) that the observed infrared intensity distribution can be explained using a model in which the rotational vibrations are considered to be mechanically regular, or periodic, and the dipole moment derivative with respect to the rotation of a molecule to be composed of two parts. The first part is due to the reorientation of the molecular dipole and the second part is a dipole moment induced by the relative reorientation of neighbouring molecules. The details of this explanation have not, however, been published and clearly the assumption of mechanically regular rotational vibrations is questionable. The infrared intensity of the $\nu_R(H_2O)$ bands of ices II and IX is centred at about 800 cm^{-1}

and for ices V and VI at about 700 cm^{-1}. No heat capacity data are available for these ices so the mean rotational vibrational frequency is unknown, and the intensity distribution of the $\nu_R(H_2O)$ or $\nu_R(D_2O)$ Raman bands is unknown. It is, however, probable that the infrared intensity of these bands, as in ice I, is asymmetric.

The absorption by the translational vibrations is reasonably well understood (102). Only sharp features due to these vibrations are observed in the infrared spectra of ices II and IX (119) and the Raman spectrum of ice VIII (48), and these are undoubtedly due to the unit-cell-group allowed vibrations (48,102).

The absorption by the translational vibrations of ices Ih and Ic is broad and extends from about 320 to 0 cm^{-1} (105,113,115). The absorption below 240 cm^{-1} has been interpreted by Bertie and Whalley (98) using a theory for the translational vibrations of orientationally disordered crystals which they developed (97). They considered these vibrations to be mechanically regular or periodic and so characterized by a wavevector. This assumption is justified in the case of translational vibrations since the molecules are situated near regular lattice sites and thus the potential field opposing small translational displacements of the water molecules has approximate translational symmetry. The electrical properties of the vibrations are, however, strongly dependent on the orientations of the water molecules and thus the dipole moment changes that accompany the vibrations are not periodic. Bertie and Whalley (98) assumed that the orientations of neighbouring molecules are uncorrelated and showed that the absorption is approximately proportional to the density of vibrational states multiplied by the square of the frequency under the simplest possible approximations. The density of vibrational states deduced from the far-infrared spectrum of ice Ih using this method (98) agrees qualitatively with that deduced from inelastic neutron scattering (128) below about 240 cm^{-1}. Differences between the far-infrared spectra of ices Ih and Ic have only recently been detected and these differences have been attributed (115) to differences between the densities of vibrational states.

Calculations using the periodic forces implied by Bertie and Whalley's theory can only explain the existence of translational vibrations of the water molecules below about 240 cm^{-1} (98) and hence can only explain the absorption below this frequency. Wong and Whalley (113) have considered the effect of the dynamic forces between the dipole moment derivatives with respect to O···O bond distance. These forces are not periodic, because the directions of the dipole moment derivatives depend on the orientations of the water molecules which are not periodic. Wong and Whalley (113) showed that these forces are of the correct magnitude to explain the existence of translational vibrations above 240 cm^{-1}. In an ordered crystal these forces are the ones which cause the longitudinal and transverse vibrations which are based on the same k=0 vibration to have different frequencies.

The absorption by the translational vibrations of ices V and VI is broad (118,119), but three reasonably sharp features are observed for ice V below 150 cm^{-1} (119). This may be spectroscopic evidence of the partial orientational order (129) of the water molecules in ice V; if so it is the only such evidence. No spectroscopic evidence of the partial orientational order in ice VI exists.

1.6 Vibrational Spectra of the Clathrate Hydrates

There has been a limited number of studies of the vibrations in the clathrate hydrates, not all of which have been of well characterized samples.

Naumann and Safford (130) have studied the inelastic neutron scattering by ice Ih and the structure I hydrate of sulphur dioxide, both at 248 K. No details of sample preparation were reported. This study showed that the density of vibrational states of the clathrate hydrate is similar to that of ice Ih. For both compounds there is a strong peak at about 560 cm^{-1} due to the rotational vibrations of the water molecules, a broad maximum between 300 and 100 cm^{-1} and a second broad maximum below 100 cm^{-1} due to the translational vibrations of the water molecules. The shape and relative intensity of this latter feature, however, differs for the two compounds and for the hydrate it is about 20 cm^{-1} to high frequency of that of ice Ih.

Harvey, McCourt and Shurvell (131) have reported the infrared spectra of the structure I hydrates of sulphur dioxide, hydrogen sulphide and krypton. The samples were prepared by codepositing the water and guest onto a cesium iodide window at 78 K and then annealing the deposit at 110 K. These samples were not characterized and Hardin and Harvey(132) later reported that the most probable phases studied were amorphous mixtures of ice and guest.

Luck and Ditter (133) have reported the first overtone of the O-H stretching bands of uncharacterized sulphur dioxide hydrate, and found the absorption maximum to be 70 cm^{-1} to high frequency of that of ice Ih.

Anthonsen (134) has studied the Raman spectra below 600 cm^{-1} of uncharacterized hydrates of bromine, chlorine and bromine chloride. He reported the halogen-halogen stretching frequencies, and frequencies below 200 cm^{-1} which he assigned to lattice vibrations. In this study Anthonsen incorrectly assumed that all of the guest molecules form the structure I hydrate: bromine does not and is the only guest molecule known to form a clathrate hydrate in which the guest molecules occupy undistorted 15-hedral cages (135).

The far-infrared spectra between 20 and 100 cm^{-1} of uncharacterized samples of the mixed structure II hydrates of hydrogen sulphide with carbon tetrachloride, chloroform or methylene chloride have been reported (136).

The mid-infrared spectra of characterized samples of ethylene oxide hydrate (1,96), the structure I and structure II hydrates of oxetane (hereafter called oxetane hydrate I and oxetane hydrate II) (2), and hexamethylenetetramine hexahydrate (137) have been reported at about 100 K. The far-infrared spectra of characterized samples of cyclopropane hydrate I (138,139), ethylene oxide hydrate (139,140), oxetane hydrate I (139), the structure II hydrate of tetrahydrofuran (141) and hexamethylenetetramine hexahydrate (129) have also been reported. This latter hydrate is classed as a semiclathrate (52), since the guest molecules are hydrogen bonded to the host lattice, and it will not be discussed further in this section. Most of these previous mid-infrared and far-infrared studies of the clathrate hydrates have been reviewed recently (2), so only a brief introduction is presented here.

The mid-infrared absorption by H_2O and D_2O in the hydrates and deuterates of ethylene oxide and oxetane is very similar to the absorption by ices Ih and Ic (2,96). As Bertie and Othen (96) and Wright (2) have pointed out, this similarity means that the structural differences do not markedly affect either the density of vibrational states or the intensity distribution function. The features of the $\nu_{OH}(H_2O)$ and $\nu_{OD}(D_2O)$ bands of the hydrates and deuterates are, however, generally broader than those of ice I, and this has been attributed to the fact that there are four different O···O bond lengths in the clathrate hydrates but only one in ice I (96). The $\nu_{OH}(H_2O)$ and $\nu_{OD}(D_2O)$ bands are not understood in detail. There is, however, an approximate correlation between the frequencies of maximum absorption of the $\nu_{OH}(H_2O)$ or $\nu_{OD}(D_2O)$ bands and the weighted mean O···O bond lengths for the clathrate hydrates and the disordered or partially ordered ices, ices Ih, Ic, V and VI (2).

The $\nu_{OD}(HDO)$ and $\nu_{OH}(HDO)$ bands of ethylene oxide and the oxetane hydrates and deuterates, respectively, are consistent with those of disordered ices (2,96). No features due to the different sets of diffraction-equivalent O···O bond lengths are resolved but the frequencies of the $\nu_{OD}(HDO)$ bands and weighted mean O···O bond lengths correlate well with those of ices Ih, Ic, V and VI (2,96). The half-widths of the $\nu_{OD}(HDO)$ bands and the weighted mean deviations from the weighted mean O···O bond lengths of the clathrate hydrates are roughly consistent with those of ices Ih, Ic, V and VI (2).

The $\nu_2(H_2O)$ and $3\nu_R(H_2O)$ or $\nu_2(H_2O)+\nu_R(H_2O)$ of the hydrates and the corresponding bands of the deuterates are not understood at all and have yielded no information. The $\nu_R(H_2O)$ band is distorted by guest absorption for all of the hydrates studied. There is, however, an approximate correlation between the frequencies of maximum absorption of the $\nu_R(D_2O)$ bands and the weighted mean O···O bond lengths for the clathrate hydrates and the disordered or partially ordered ices, ices Ih, Ic, V and VI (2).

The mid-infrared absorption by the guest molecules in ethylene oxide and the oxetane hydrates has been assigned by comparison with the spectra of the gaseous, liquid and solid phases (2,96). The differences between the frequencies of the encaged molecules and the corresponding frequencies in the gas phase have been related via a qualitative theory of Pimentel and Charles (142) to the relative sizes of the guest molecules and the cages they occupy (2). Pimentel and Charles' ideas are basically that the vibrational frequencies of a molecule in a tight cage environment are higher than those of the gas, whereas the vibrational frequencies of a molecule in a loose cage environment are lower than those of the gas. The average frequency shifts on clathration for ethylene oxide and oxetane have indicated (2) that oxetane is in a looser cage environment in its structure II hydrate than in its structure I hydrate, and that ethylene oxide is in a looser cage environment than oxetane in their structure I hydrates (2). These indications are consistent with the known sizes of the guest molecules and the cages they occupy (Section 1.3). For oxetane hydrate I (2), this interpretation was extended by considering separately the frequency shifts on clathration of the αCH_2 and βCH_2 vibrations of oxetane. The frequency shifts at 95 K indicated that the βCH_2 vibrations experience a tighter cage environment than the αCH_2 vibrations which is consistent with the proposed preferred orientation of oxetane within the 14-hedral cages (81).

All of the mid-infrared guest absorption bands of ethylene oxide hydrate and the oxetane hydrates are fairly sharp (2,96), and only one absorption band, that due to the ring breathing vibration of ethylene oxide, shows fine structure (96). This band at 100 K is split into a doublet, the components of which are separated by about 2 cm^{-1} (96). Bertie and Othen (96) have stated that the possible causes of the doublet are intermolecular coupling between neighbouring ethylene oxide molecules, the presence of two preferred orientations for the guest molecules in the 14-hedral cages, and a difference between the frequencies of the ring breathing vibrations of ethylene oxide molecules in the 12- and 14-hedral cages. They argued that the most probable cause is the presence of two preferred orientations within the 14-hedral cages. Two very weak satellite bands were also observed at about 13 cm^{-1} to either side of this doublet. Bertie and Othen (96) assigned the low frequency satellite band to the ring breathing vibration of $C^{12}C^{13}H_4O$ but they did not assign the high frequency satellite band which is, thus, of unknown origin.

The only study of the temperature dependence of the mid-infrared spectrum of a clathrate hydrate is that of oxetane hydrate I (2). In this study the absorption by the guest or water molecules showed no obvious effect of the ordering of the guest molecules below 100 K that was proposed (81) to explain the anomaly in the dielectric and nuclear magnetic resonance measurements.

The far-infrared absorption by the clathrate hydrates is due to the translational vibrations of the water molecules and the intermolecular vibrations of the guest molecules. The absorption due to the water molecules can be readily identified from the frequency shifts observed on deuteration. Above 100 cm^{-1} the water absorption is similar to that of ice I and extends to about 340 cm^{-1} with a fairly sharp peak at about 230 cm^{-1} (138-140). Bertie and Othen (140) have noted that there is an empirical correlation between the frequencies of maximum absorption and the number and length of the hydrogen bonds for the disordered and partially ordered ices, ices Ih, Ic, V and VI and ethylene oxide hydrate.

The absorption by the water molecules should be the same in all of the structure I hydrates, if the vibrations of the water molecules do not couple with those of the guest (139). For cyclopropane hydrate I (138,139) the absorption above 100 cm^{-1} is essentially the same as that of ethylene oxide hydrate (139,140) except that it is shifted to low frequency by about two percent. This shift has been attributed to the larger lattice parameter and hence longer hydrogen bonds in cyclopropane hydrate I (138). For oxetane hydrate I the absorption above 100 cm^{-1} is essentially the same as that of cyclopropane hydrate I, except between 160 and 180 cm^{-1}. The reasons for this difference are at present unknown (139).

The far-infrared spectra of the structure I hydrates differ below 100 cm^{-1}. For cyclopropane hydrate I, the absorption decreases rapidly with decreasing frequency (138,139), while for ethylene oxide hydrate and oxetane hydrate I (138,140) two absorption bands are observed between 70 and 35 cm^{-1}, and are assigned to the rotational oscillations of the guest molecule about the axes perpendicular to the dipolar axis. Similar guest absorption bands have also been observed in the far-infrared spectrum of the structure II hydrate of tetrahydrofuran (141).

1.7 Vibrational Spectra of Cyclopropane

The assignment of the guest absorption bands of the cyclopropane hydrates given in Chapters 4 and 5 is based on that of gaseous cyclopropane, so a brief introduction to the vibrational spectra of cyclopropane is presented in this section.

Cyclopropane belongs to the point group D_{3h} and the normal vibrations of the free molecule form the representation,

$$\Gamma_{vib}=3A_1'+A_1''+A_2'+2A_2''+4E'+3E''$$

There have been a number of infrared (143-151) and Raman (152-156) studies of gaseous cyclopropane and a number of infrared and Raman studies of the liquid (143,146,153, 157,158) and solid (146,157-161) phases. The studies of the gas and solid phases have resulted in an unambiguous assignment of all of the fundamental vibrations (146,162). The fundamental frequencies in the gas, liquid and solid Phases are given in Table 1.2.

The representations formed by the internal displacement coordinates of cyclopropane are given in Table 1.3. The descriptions of the normal vibrations in terms of the

TABLE 1.2

Vibrational Frequencies[a] of Cyclopropane

	Gas[b]	Liquid[c]	Solid[d]
$\nu_1(A_1')$	3038.0	3010	3010
$\nu_2(A_1')$	1479.0[e]	1454	1455
$\nu_3(A_1')$	1188.0	1188	1185
$\nu_4(A_1'')$	1126.0	1129	1127
$\nu_5(A_2')$	1070.0	-	1076
$\nu_6(A_2'')$	3101.7	3086	3086
$\nu_7(A_2'')$	854.0	-	853
$\nu_8(E')$	3024.4	3028	3008
$\nu_9(E')$	1437.7	1434	1431
$\nu_{10}(E')$	1028.4	1025	1025
$\nu_{11}(E')$	868.5	866	863
$\nu_{12}(E'')$	3082.0	3077	3070
$\nu_{13}(E'')$	1188.0	1178	1191
$\nu_{14}(E'')$	739.0	742	750

a) units are cm^{-1}.

b) The frequencies of the vibrations of symmetry species A_1' and E" are from reference 153, those of symmetry species A_2'' and E' are from reference 145 and those of symmetry species A_1'' and A_2' from reference 146.

c) The frequencies are the average frequencies from references 143, 145, 153, 157 and 158. The agreement between the sets of frequencies is ±3 cm^{-1}.

d) The frequencies, except for those of ν_1, ν_4, ν_5, ν_8, and ν_{12}, are for isotopically dilute solid solutions of C_3H_6 in C_3D_6 and are from references 146, 158 and 159. The agreement between the sets of frequencies is ±3 cm^{-1}. The frequencies of ν_1 and ν_{12} are from reference 156, those of ν_4, ν_5 and ν_8 are from reference 146, and these five frequencies are for pure C_3H_6 solid.

e) ν_2 is in Fermi resonance with $2\nu_{14}$ and the unperturbed frequency is given.

TABLE 1.3

Irreducible Representations Formed by Internal Displacement Coordinates of Cyclopropane

C-H stretch	$A_1' + A_2'' + E' + E''$
CH_2 deformation	$A_1' + E'$
ring vibration	$A_1' + E'$
CH_2 twist	$A_1'' + E''$
CH_2 rock	$A_2'' + E''$
CH_2 wag	$A_2' + E'$

internal displacement coordinates are usually provided by normal coordinate calculations. There have been three such calculations for cyclopropane recently (162-164). One of these calculations (164) yielded a very poor fit between the observed and calculated frequencies and it is not considered further.

The major difference between the remaining two normal coordinate calculations, by Duncan and Burns (162) and Hirokawa *et al*. (163) is in the description of ν_{13} and ν_{14}. Duncan and Burns determined ν_{13} and ν_{14} to be mixtures of CH_2 rocking and CH_2 twisting coordinates, whereas, Hirokawa *et al*. (163) determined them to be almost pure CH_2 rocking and CH_2 twisting vibrations, respectively. The description of the normal vibrations determined by Duncan and Burns (162) is preferred for a number of reasons: Their agreement between the observed and calculated frequencies is better than that of Hirokawa *et al*. (163); Coriolis zeta constants were calculated by both groups and the experimental values (145, 150-152,156) are in much better agreement with those of Duncan and Burns (162) than with those of Hirokawa *et al*. (163); from their force field Duncan and Burns were also able to obtain good agreement between the observed and calculated frequencies of C_3D_5H. Thus, the descriptions of the normal vibrations of cyclopropane presented later in Chapters 4 and 5 are those of Duncan and Burns (162).

1.8 Objectives

The first project of this thesis, described in Chapter

3, is concerned with the re-examination of the mid-infrared spectra of ices II and IX. These ices are essentially fully ordered (Section 1.2) and thus their fundamental infrared absorption should yield sharp features (Section 1.4). The absorption by the translational vibrations is sharp and some of the absorption due to the rotational vibrations is sharp. However, in contrast to the predictions, the sharp rotational absorption is superimposed on a broad absorption, and the absorption due to the O-H or O-D stretching vibrations of the H_2O or D_2O ices is broad with only moderately sharp features superimposed. The objectives of this study were to investigate the origin of the broad absorption and, with the aid of normal coordinate calculations, to determine if the moderately sharp features superimposed on the $\nu_{OD}(D_2O)$ band are due to the unit-cell-group allowed vibrations.

Evans and Lo (165) have found that the absorption by the HBr stretching vibrations of HBr_2^- in its tetrabutyl ammonium salt sharpens markedly between 100 and 20 K. Thus, the infrared spectra of ices II and IX were studied below 100 K to see if their absorption bands sharpen significantly. At low temperatures (~10 K), the only transitions that should contribute to the infrared spectra are the unit-cell-group allowed transitions and overtone and sum-combination transitions that originate from the ground state. The frequencies of the unit-cell-group allowed O-D stretching vibrations can be calculated if the O-D stretching and

OD-OD intramolecular and intermolecular interaction force constants are known. The ν_{OD}(HDO) bands have provided information concerning the O-D stretching and OD-OD intermolecular interaction constants (Section 1.5) and studies of the salt hydrates (123,124) have provided information concerning the intramolecular OD-OD interaction constants for hydrogen-bonded water molecules. Thus, the frequencies of the unit-cell-group allowed O-D stretching vibrations were calculated and compared with the spectra observed at low temperature to obtain information concerning the origin of the ν_{OD}(D_2O) bands of ices II and IX.

The second project, described in Chapters 4 and 5, is concerned with the mid-infrared absorption due to the guest and water molecules of the cyclopropane hydrates and the guest molecules of ethylene oxide hydrate. This continues the series of studies of the infrared spectra of the clathrate hydrates in this laboratory (1,2,96).

Cyclopropane was chosen as a guest molecule because it is nondipolar. Dielectric and nuclear magnetic resonance studies (Section 1.3) have shown that the rate of reorientation of the water molecules in the clathrate hydrates at relatively high temperatures is affected by the dipole moment of the guest molecule. Although at 100 K the water molecules do not reorient (70), it is possible that the dipole moment of the guest molecule does perturb the water lattice. One objective of this study was to compare the water absorption bands of cyclopropane hydrate I with those of ethylene oxide hydrate and oxetane hydrate I to see if the dipole moment of the guest does affect the water absorption bands.

In the previous study of oxetane hydrate I (2), the temperature dependence of the water and guest absorption bands showed no effect that could be attributed to the proposed ordering of the guest molecules below 100 K. Thus, a second objective was to compare the temperature dependence of the guest and water absorption bands of cyclopropane hydrate I, which has no known ordering transition, with that of oxetane hydrate I, to confirm that the ordering transition does not affect the infrared spectrum of oxetane hydrate I.

A third objective was to seek further evidence of the origin of the fine structure seen for the ring breathing vibration of ethylene oxide in ethylene oxide hydrate (96). To this end, the temperature dependence of the cyclopropane and ethylene oxide absorption in their structure I hydrates was studied.

Chapter Two. Experimental Techniques

2.1 Introduction

In this thesis the mid-infrared spectra of five different but related compounds in various isotopic forms are reported; cyclopropane hydrate I, cyclopropane hydrate II, ethylene oxide hydrate, ice II and ice IX. Three low temperature techniques were used to prepare infrared samples. A low temperature mulling technique, initially developed by Bertie and Whalley (166), was used for the cyclopropane hydrates at 90±5 K. A low temperature potassium bromide pelleting technique, developed by P.G. Wright (2) and S.M. Jacobs of this laboratory, was used for cyclopropane hydrate I and ethylene oxide hydrate between 45 and 150 K. This technique could not be used for the low temperature study of ice II or ice IX because these ices revert to ice I under the conditions required to make the pellets (36). Instead the ices were dispersed in a 3-methylpentane glass at low temperature for study between 10 and 100 K.

The preparation of ethylene oxide hydrate is not described in this chapter, because the samples used were made by D. Othen by methods described elsewhere (1,140).

2.2 Chemicals

Cyclopropane, obtained from Linde, was condensed at 77 K and degassed twice using standard vacuum techniques.

It was then distilled from a dry ice/methanol bath into the cold finger of a gas storage bulb. The infrared and Raman spectra of the gas were compared with published spectra (143,146,153) and showed no absorption due to impurities.

Triply distilled water was obtained from the laboratory of Dr. H.B. Dunford. Deuterium oxide, obtained from Columbia Organic Chemicals Company, was checked for isotopic purity by studying the p.m.r. spectrum of a solution of known composition of anhydrous dimethylsulpnoxide in D_2O. The relative integrated intensities of the signals from the dimethylsulphoxide and from the residual H in the D_2O sample corresponded to an isotopic purity of 99.88±.05% conforming to the manufacturers minimum purity specification of 99.77%.

Commercial propene (>99.99%), propane (>99.5%), chlorotrifluoromethane (>99%) and 3-methylpentane (>99%) were not further purified. Infrared quality potassium bromide (Harshaw Chemical Company) was used as received.

2.3 Preparation of Cyclopropane Structure I Hydrate (Deuterate)

Cyclopropane hydrate I was prepared in the stainless steel manifold shown in Fig. 2.1. A steel rod and about 1 ml of water were placed into the detachable finger, the water was degassed twice and valve A was closed.

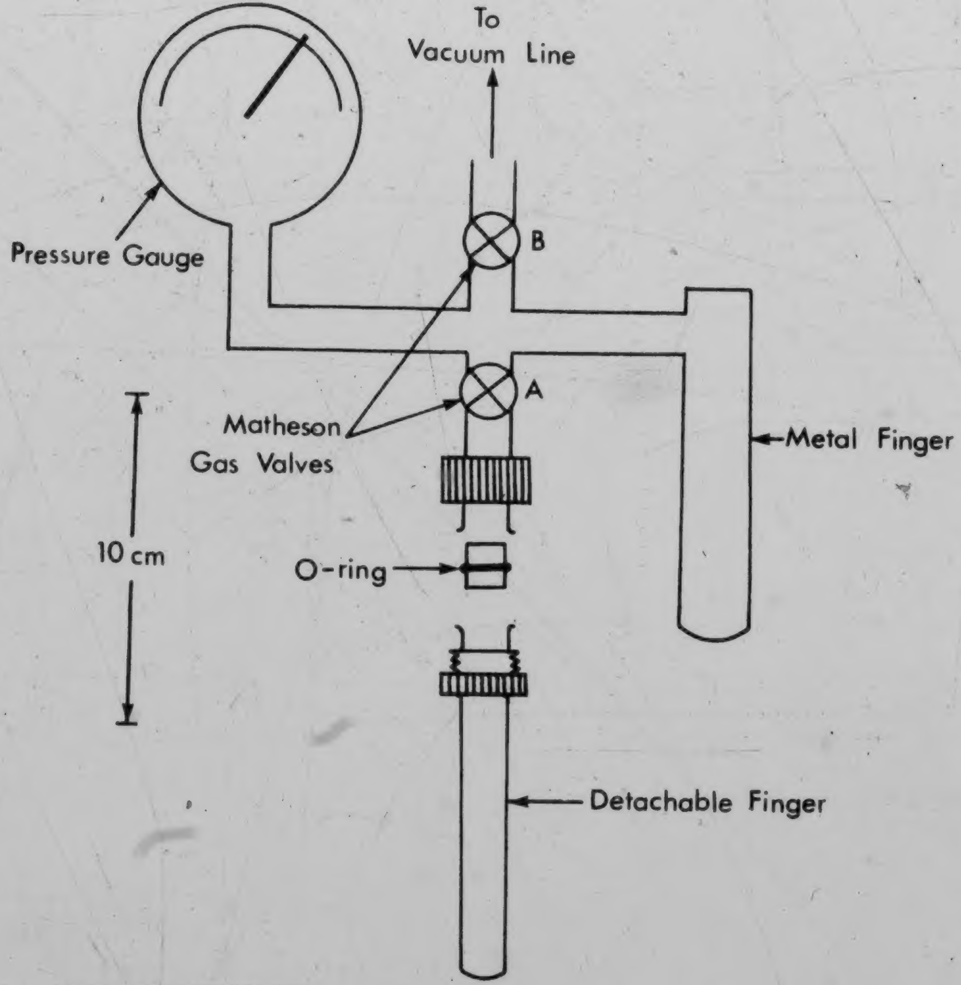
To
Vacuum Line
Pressure Gauge
B
A
Matheson
Gas Valves
Metal Finger
10 cm
O-ring
Detachable Finger

Figure 2.1. Stainless steel manifold used to prepare cyclopropane structure I hydrate.

An excess (about 2 ml) of cyclopropane was condensed into the second metal finger which was cooled in a dry ice/ methanol bath, valve B was closed and the apparatus was transferred to a refrigerator maintained at 278 K. After 20 minutes valve A was opened, and the apparatus was shaken vigorously until the steel rod could no longer be heard to rattle (about 5 to 10 minutes). The apparatus was left for 48 hours at 278 K. The detachable finger was then cooled to 195 K and the apparatus was connected to a vacuum line. The pressure of cyclopropane was reduced to 2 Torr with the sample at 195 K, valve A was closed, and the detachable finger was cooled to 77 K. The stainless steel manifold was evacuated, valve B was closed and the apparatus was detached from the vacuum line.

All subsequent handling of the hydrates was done in a cold can. This low temperature technique was originally described by Bertie and Whalley (166) and is a convenient method of handling samples that are not stable at room temperature and pressure. A cold can is an uninsulated metal can into which liquid nitrogen is poured, either directly or through a side arm. A metal table in the cold can provides a working surface within a cold (80-100 K), dry atmosphere provided by the rapidly boiling liquid nitrogen. Plexiglass covers were usually used to cover about half of the top of the cold can, to provide a more confined atmosphere. Long-handled tweezers and spatulae were used to manipulate the samples and apparatus. All utensils and apparatus were pre-cooled to 77 K before use. Rubber gloves were always worn.

The stainless steel manifold containing the cyclopropane hydrate was filled with dry nitrogen gas in the cold can. The detachable finger was removed and placed in a container on the table. The polycrystalline hydrate was removed and ground for 20 minutes in a stainless steel mortar containing clean liquid nitrogen, using a stainless steel long-handled pestle. The powdered hydrate was transferred to a small screw-top vial containing clean liquid nitrogen, which was placed inside a larger screw-top vial also containing liquid nitrogen. A long piece of piano wire was attached to the top of this vial, so that the sample could be stored suspended in a 5 litre dewar containing liquid nitrogen. Prior to the preparation of infrared samples the hydrates were reground for another 20 minutes.

Cyclopropane deuterate I was prepared and handled in the same way, except that the vacuum line and stainless steel manifold were exposed overnight to D_2O vapour prior to use.

2.4 Preparation of Cyclopropane Structure II Hydrate (Deuterate)

Cyclopropane hydrate II and deuterate II are only stable from 257.2 to 274.7 K and from 249.9 to 278.7 K, respectively (65), and at cyclopropane pressures less than the decomposition pressure of the structure I hydrate or deuterate (68), see Figs. 1.3 and 1.4. Attempts to make the structure II hydrate from water or ice and cyclopropane always gave a product heavily contaminated with ice Ih. The method found to be the most successful was to carefully decompose the structure I hydrate.

A finely ground sample of the structure I hydrate was placed in a glass tube, which was then connected via a stopcock to the vacuum line and evacuated at 77 K. The sample was then maintained at 263 to 268 K and the pressure of cyclopropane gas was set approximately to the decomposition pressure of the structure II hydrate. The pressure in the vacuum line gradually increased to the decomposition pressure of the structure I hydrate. The sample was then isolated, cooled to 77 K, removed from the vacuum line and reground. This procedure was repeated until the pressure no longer reached the decomposition pressure of the structure I hydrate. The sample was then cooled to 195 K, the excess cyclopropane pumped off and the sample ground as described in Section 2.3.

Cyclopropane deuterate II was prepared and handled in the same manner, except that the vacuum line was exposed overnight to D_2O vapour prior to use.

2.5 Preparation of Ice II and Ice IX

Ices II and IX were prepared in the pressure apparatus shown in Fig. 2.2. The apparatus consisted of two 19 mm diameter pistons, A and B, and a cylinder C which contained the sample. Brass back-up rings D, located in grooves in the piston, prevented extrusion of the sample between the cylinder and pistons. The pistons and cylinder rested on the retaining block E and pressure-distributing block F inside a stainless steel jacket G. The lid of the jacket had a circular hole through which spacer H protruded. Pressure was applied to this spacer via block J. The apparatus, except for parts D and G, was made of Vascomax 350, 18% nickel maraging steel, which had been heat treated to a hardness of 54 Rockwell C.

The temperature of the sample was monitored by a thermocouple placed in a hole drilled into the top piston and ending 1 mm from the face of the piston. A drop of oil provided thermal contact between the piston and thermocouple. The apparatus was cooled by a stream of cold nitrogen gas. The entrance port K was connected to a 50 litre liquid nitrogen dewar, in which a 200 watt

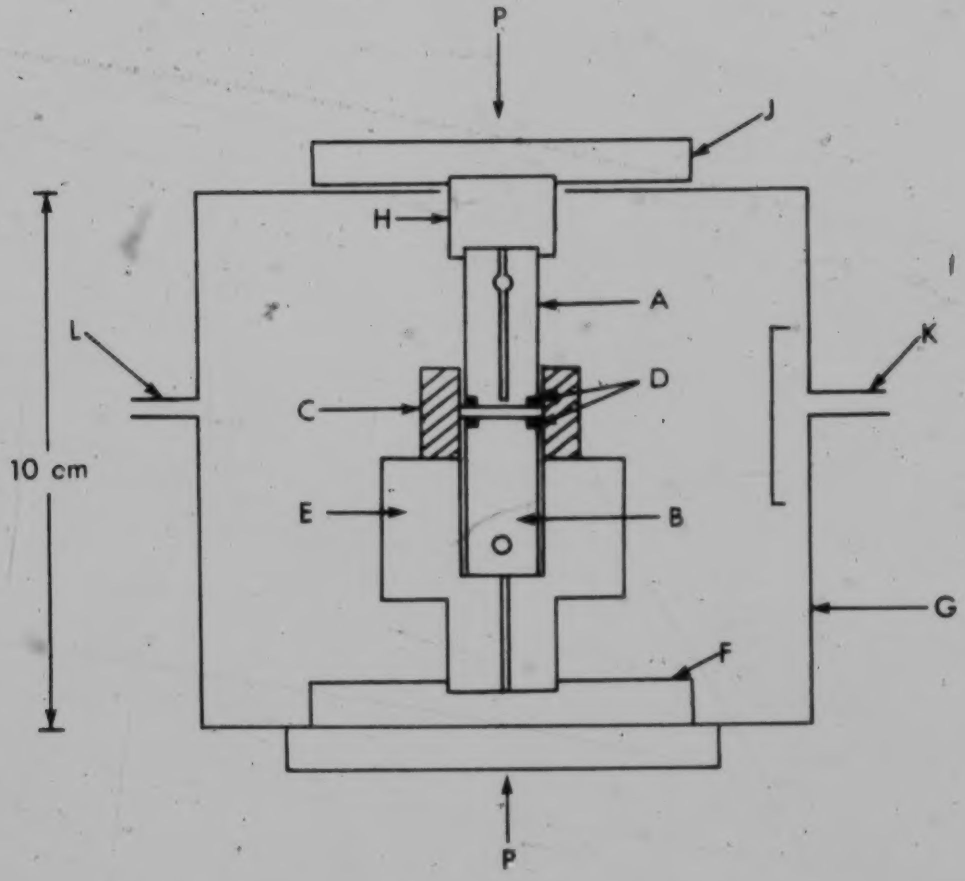

Figure 2.2. Pressure apparatus: A, top piston; B, bottom piston; C, cylinder; D, backup rings; E, retaining block; F, pressure distributing block; G, outer jacket; H, spacer; J, pressure distributing block; K, entrance port; L, exit port.

pencil heater was immersed. The temperature of the sample could be varied by changing the voltage applied to the heater and thus varying the boiling rate of the liquid nitrogen. At the end of the preparation the apparatus was cooled rapidly to 77 K by pouring liquid nitrogen through the exit port L via a funnel and tubing.

The apparatus was assembled in the jacket G without the top piston A, spacers H and J, and the lid of the jacket. Liquid nitrogen was poured into the jacket and about 2 ml of water of the correct isotopic composition was syringed into the cylinder. After the water had frozen, the remainder of the pressure apparatus was assembled, placed on the insulated platen of a 100 ton press and the cold gas was connected to the entrance port K.

The conditions used to prepare the ices were those of Bertie, Calvert and Whalley (36). For the preparation of ice II, the apparatus was maintained at 196±2 K and atmospheric pressure for about 30 minutes, a pressure of 2.1 kbar was applied for about 20 minutes, then the pressure was increased to 3 kbar. This pressure was maintained for about 1.5 hours while the temperature of the sample was allowed to increase to 225 K.

To prepare ice IX, the apparatus was maintained at 245±2 K and atmospheric pressure for 30 minutes, a pressure of 2.1 kbar was applied for 15 minutes and the pressure was then increased to 3 kbar for a further 40 minutes. The temperature was maintained at 245±2 K throughout.

The samples of ice II or IX were cooled to 77 K at a pressure of 3 kbar before the pressure was released. The piston-cylinder assembly was transferred to the table in the cold can (Section 2.3). The ice sample was removed from the cylinder and ground with a stainless steel mortar and pestle. Samples were originally ground using a Spex Freezer/Mill (Spex Industries Inc.), but this procedure always converted some of the ice II or IX to ice Ic. The samples were stored as described in Section 2.3.

2.6 Characterization of the Samples

Ground samples of the clathrate hydrates (deuterates) and ices were characterized by X-ray powder photographs. The sample was transferred from the storage dewar into a small cold can. On the working table in the cold can was a brass block with a tapered hole drilled into it. A Lindeman glass capillary (0.5 mm i.d.), which had a wide neck for easy filling, was placed in the hole. Some of the sample was placed in the capillary, lightly packed by gently tapping the neck of the capillary, then compacted with a very fine glass rod. A warm Bakelite support containing a trace of oil was placed over the capillary.

After approximately 10 seconds the oil solidified to secure the capillary tube to the support. The support and capillary tube were then quickly immersed in liquid nitrogen and transported to the X-ray camera in a metal scoop containing liquid nitrogen, and were then lifted quickly into a cold gas stream and fastened to the goniometer head. The cold gas stream which cooled the sample while it was mounted on the camera was controlled by the voltage applied to a pencil heater in a 50 litre can of liquid nitrogen, and was directed onto the sample by a silvered dewar tube; a coaxial stream of warm nitrogen gas outside the cold gas stream reduced the condensation of ice onto the sample.

A Jarrell-Ash precession camera was used as a flat plate powder camera. An Enraf Nonius Diffractis 601 X-ray generator supplied the Ni-filtered CuK_α radiation that was used. Typical exposure times were 3 to 4 hours.

The composition of the samples was determined by comparing the observed interplanar spacings (d-spacings) with literature values (36,55,56,57). The photographs were analysed to determine the d-spacings and lattice parameters by measuring the inside and outside diameters of each diffraction circle (with an accuracy of 0.10 mm). These values, the wavelength of the radiation, and the crystal-to-film distance (~60 mm) were input to a computer program, POWDER, written by S. Sunder of this laboratory. This program calculates the mean diameter of each diffraction circle and the corresponding d-spacing and value of the diffraction angle (2θ). The Miller indices of the observed diffraction circles, their 2θ values and approximate lattice parameters were input to the program DREFINE (167). This program refines the lattice parameters by a least-squares fit of the $\sin\theta$ data.

The crystal-to-film distance was calibrated from time to time using X-ray powder photographs of ice Ih. The photographs were analysed as described above, and the crystal-to-film distance was varied to give the closest fit between the lattice parameters obtained and those reported by Brill and Tippe (168). The temperature of the sample was measured by inserting a fine iron-constantan thermocouple through a hole in the Bakelite support into the sample. The temperature of the sample was only recorded during these calibration runs and was found to be 100±5 K. The voltage setting for the pencil heater, and thus the gas flow, was the same for all samples and it is assumed that all samples were at 100±5 K.

The relative intensities of the diffraction circles were obtained from the relative peak heights on a microdensitometer trace. The microdensitometer used was a Joyce, Loebl and Co. Ltd. Model MK III c.

2.7 Preparation and Handling of Infrared Samples Studied at 90 K

2.7.1 Liquid Nitrogen Cell

Fig. 2.3. shows the liquid nitrogen cell used to hold the infrared mull samples. It was made of stainless steel with a copper sample holder by the Chemistry Department Machine Shop. Two copper-constantan thermocouples were located in holes drilled into the top and bottom of the sample holder. On the sides of the sample holder were two 25 watt heaters. The sample was placed between two cesium iodide windows which were held inside the sample holder by a spring compressed by the faceplate which was tightened against the sample holder by four screws. The assembled cell was evacuated to 1×10^{-2} Torr and the sample was cooled by liquid nitrogen in the reservoir. The temperature of the sample could be varied by applying a voltage (<12 volts) to the two heaters.

2.7.2 Preparation of Mulls

All manipulations were performed in a cold can fitted with a side arm designed to contain the outer jacket of the cell. The inner part of the cell was placed in the cold can with its flange about 3 cm above the plexiglass covers (Section 2.3), which contained a slot to accommodate the cell. Heating tape was wrapped around the cell above

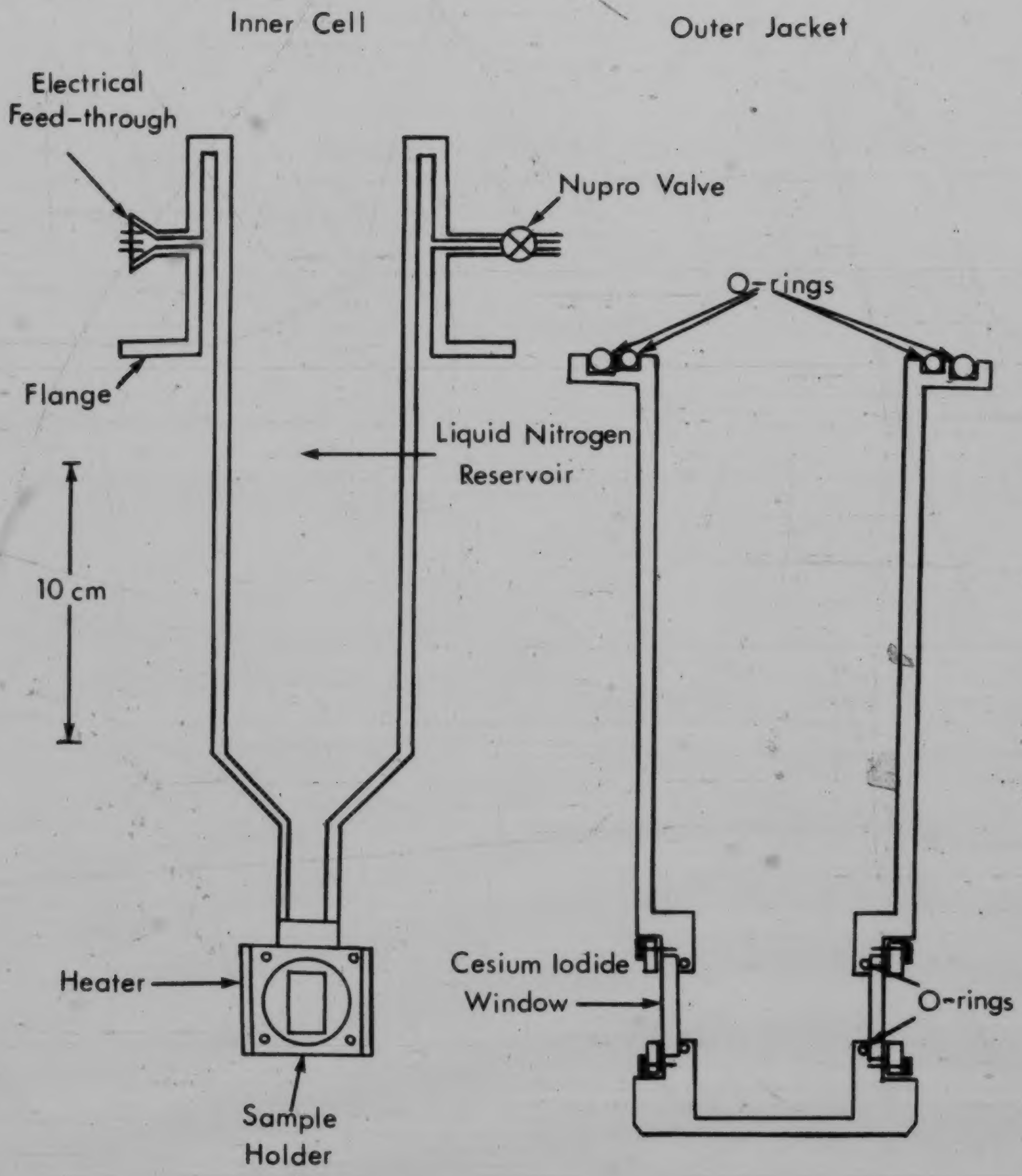
Inner Cell
Outer Jacket
Electrical Feed-through
Nupro Valve
O-rings
Flange
Liquid Nitrogen Reservoir
10 cm
Cesium Iodide Window
O-rings
Heater
Sample Holder

Figure 2.3. Liquid nitrogen cell.

the plexiglass covers and below the flange to prevent ice from condensing on the cell while it was in the cold can. Typically 15 volts was applied to this tape. The cell was connected to a vacuum line by rubber tubing, which was evacuated with the nupro valve (Fig. 2.3) closed.

The faceplate, spring, two cesium iodide windows and a vial containing the sample were placed on the table in the cold can. One window was placed on a small platform. After about 20 minutes, a small amount of finely ground hydrate was placed on this window. The mulling agent (chlorotrifluoromethane, propane or propene) was condensed directly from a gas cylinder into a disposable pipette cooled to about 100 K. The pipette was tapped against the window to place a few drops of the mulling agent onto it and the second window, in the centre of which was a small indentation, was placed on top. One point of a pair of tweezers was placed in the indentation and the other point at the edge of the window, to hold the window firmly to rotate it against the bottom window and uniformly disperse the hydrate in the mulling agent. The windows were transferred to the sample holder, followed by the spring and faceplate which was then screwed to the sample holder using a long-handled Allen key inserted through a hole in the side of the cold can. The outer jacket of the cell was purged with dry nitrogen or argon and placed in the side arm of the cold can. The heating tape was removed from the inner part of the cell and the two halves of the cell were coupled while still in the dry atmosphere of the cold can. The cell was then evacuated and the reservoir filled with liquid nitrogen. When the cell had been evacuated to $1x10^{-2}$ Torr, it was transferred to the sample compartment of the infrared spectrophotometer, and reattached to a vacuum line.

2.8 Preparation and Handling of Infrared Samples Studied between 10 and 150 K

2.8.1 Liquid Helium Cryostat

An LT-3-110 Helitran liquid helium transfer refrigerator (Air Products and Chemicals Inc.) was used for the variable temperature studies. The Helitran consists of an optical cell and a flexible transfer line which connects the cell to a storage dewar. A schematic diagram of the Helitran and its accessory equipment is shown in Fig. 2.4.

The pickup tube of the transfer line was supported in a liquid helium dewar (Supairco Model HV-25 or HV-50) by a dewar adapter which was sealed to the dewar by rubber tubing enabling pressure to build up within the dewar. Two safety vent valves (5 psig and 2.5 psig) on the adapter prevented over-pressurization. The dewar

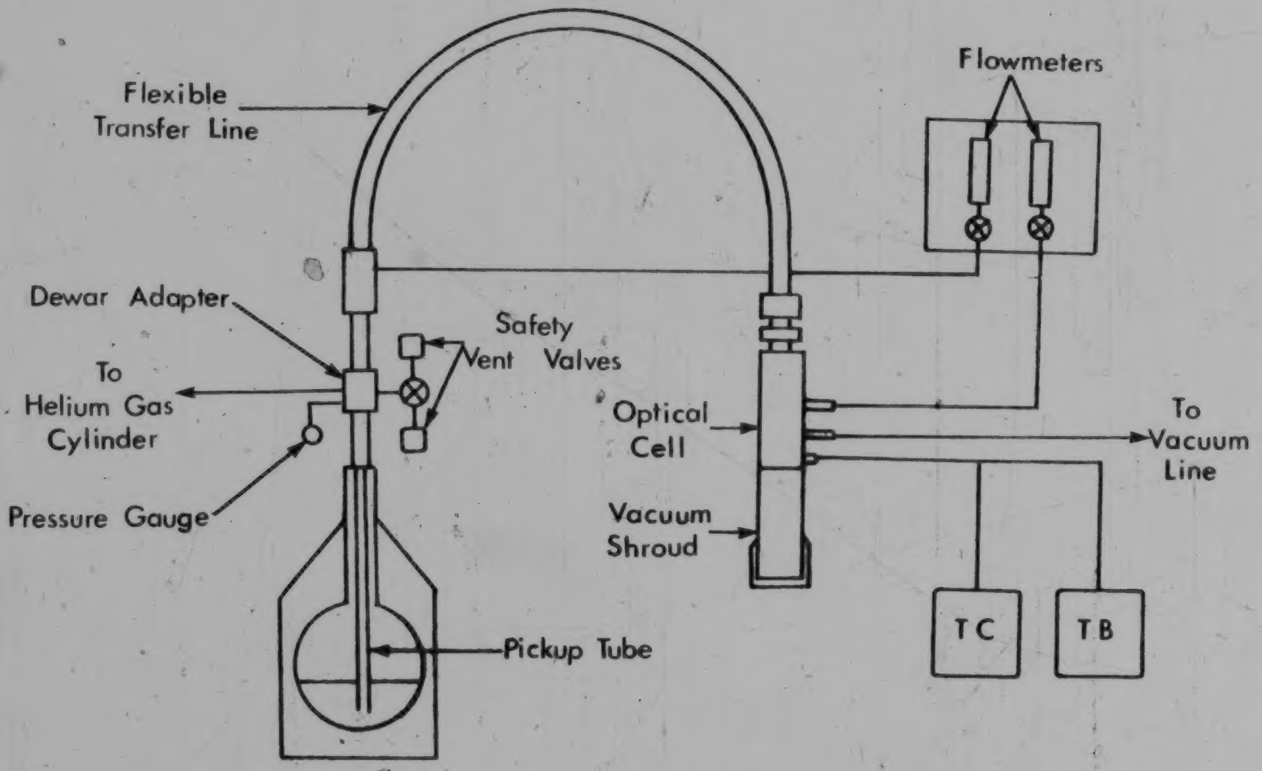
Flexible
Transfer Line
Flowmeters
Dewar Adapter
Safety
Vent Valves
To
Helium Gas
Cylinder
Optical
Cell
To
Vacuum
Line
Pressure Gauge
Vacuum
Shroud
TC
TB
Pickup Tube

Figure 2.4. Schematic diagram of the Helitran equipment: TC, Artronix Model 5301 Temperature Controller; TB, Metlabs Model CTB-1 Temperature Bridge.

was pressurized by the evaporation of the liquid helium. Additional pressure could be supplied by a helium gas cylinder. Two types of liquid helium flow occurred within the transfer line. The cryotip flow passed through the cryotip to cool the sample and was then heated and vented through a flowmeter. The heat shield flow cooled the heat shield and, after reaching the optical cell, flowed back along the transfer line to provide further cooling and was then vented through a flowmeter.

A schematic diagram of the cold end of the optical cell is shown in Fig. 2.5. The sample holder (not shown) was screwed into the lower end of the cryotip, compressing an indium gasket to provide good thermal contact. The temperature sensors were germanium resistance and platinum resistance thermometers. A chromel vs gold with 0.07 atomic % Fe thermocouple was used with a strip chart recorder to monitor the temperature when the system was left overnight. The other two thermometers were attached to an Artronix Model 5301 Temperature Controller, which would automatically maintain a preset temperature to ±0.01 K by varying the voltage applied to the control heater. For the range of temperatures studied, the platinum thermometer was found to be the most useful. A platinum thermometer, which was attached to a Metlabs

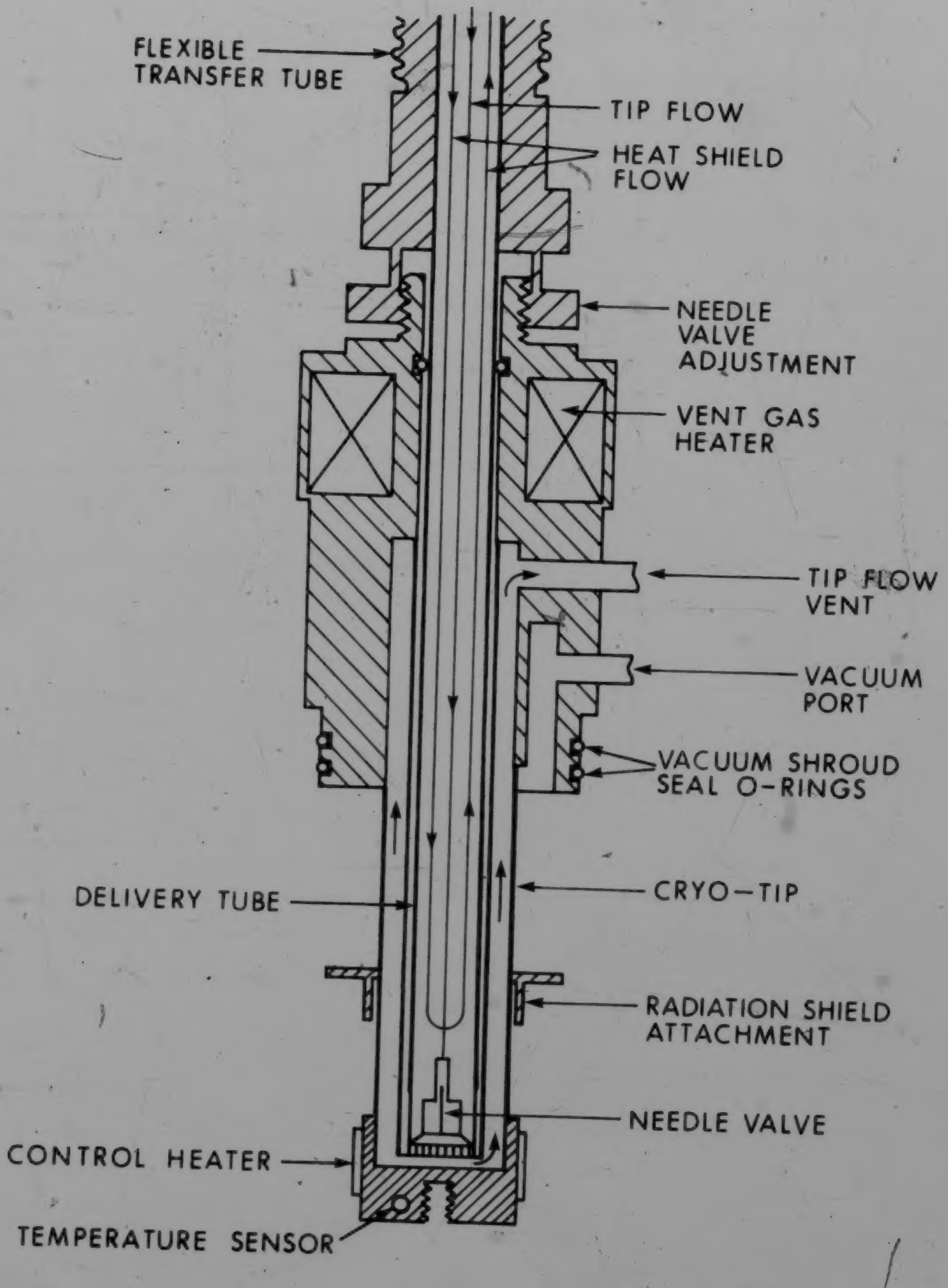
FLEXIBLE TRANSFER TUBE
TIP FLOW
HEAT SHIELD FLOW
NEEDLE VALVE ADJUSTMENT
VENT GAS HEATER
TIP FLOW VENT
VACUUM PORT
VACUUM SHROUD SEAL O-RINGS
DELIVERY TUBE
CRYO-TIP
RADIATION SHIELD ATTACHMENT
NEEDLE VALVE
CONTROL HEATER
TEMPERATURE SENSOR

Figure 2.5. Schematic diagram of the Helitran optical cell.

Model CTB-1 Temperature Bridge, was located in a hole in the sample holder. Under operating conditions a radiation shield and vacuum shroud were attached to the cold end and the cell was evacuated to 1×10^{-3} to 1×10^{-4} Torr. The flexible transfer line was re-evacuated to 1×10^{-5} Torr every three weeks.

The optical cell was precooled by pouring liquid nitrogen into the aperture which receives the transfer line (Section 2.8.2 and 2.8.3). The transfer line took 40 to 50 minutes to cool so the following procedure was used to cool the transfer line, and to insert it into the cell without freezing the liquid nitrogen. The dewar adapter was attached to the liquid helium storage dewar and the pickup tube was slowly inserted through the adapter into the dewar. The pressure within the dewar was allowed to increase to 5 psig. A thermocouple was inserted into the tip of the transfer line to monitor the temperature of the gas emerging from the line. The transfer line tip was then placed inside a graduated cylinder to create a confined helium atmosphere around the tip, to prevent the condensation of atmospheric components. The heat shield flowmeter showed the gas flow to be quite erratic initially, but after about 40 minutes the flow stabilized and the temperature of the emerging gas began to decrease. Meanwhile, liquid nitrogen was added to the optical cell from time to time to maintain its temperature at 85 to 100 K, thus ensuring that no liquid nitrogen remained in the cell. When the temperature of the gas emerging from the transfer line reached 240-250 K, the thermocouple was removed and the transfer line was quickly inserted into the optical cell. The maximum temperature that the sample reached after inserting the transfer line into the cell was 120 K. As the sample cooled the heat shield flow was reduced until it was just sufficient to maintain the desired temperature. The cryotip flow was then similarly reduced. The dewar pressure was allowed to decrease to 2.5 psig. This pressure was maintained by connecting the dewar to a helium gas cylinder.

2.8.2 Preparation of Potassium Bromide Pellets

The apparatus used to prepare the potassium bromide pellets was that used to prepare ice II and ice IX (Fig. 2.2), except that the cylinder C was machined from OFHC (oxygen-free, high-conductivity) copper and had a threaded tip so that it could be screwed into the lower end of the cryotip and thus be the sample holder. The pellets were prepared from 0.36 to 0.40 gm of potassium bromide, that had been dried at 450 K and a pressure of 1×10^{-5} Torr for at least 3 days prior to use.

The retaining block E, bottom piston B and sample holder C (Fig. 2.2) were assembled and placed in a cold can together with the top piston A, a vial containing the powdered sample and a stainless steel mortar. Clean liquid nitrogen was poured into the mortar. A tube containing the anhydrous potassium bromide was removed from the vacuum line and opened in the cold nitrogen atmosphere of the cold can. The potassium bromide was poured into the mortar and a small amount of sample was added and mixed. The mixture was ground for two minutes to disperse the sample in the potassium bromide. The liquid nitrogen was allowed to evaporate from the mortar and the mixture was transferred to the cylinder. The top piston was inserted and rotated a few times to distribute the powder evenly. The remaining pressure apparatus was placed in the side arm of the cold can, and liquid nitrogen was poured into the jacket, G. The apparatus was assembled and transferred to the insulated platen of a 100 ton press and connected to the nitrogen gas coolant as described in Section 2.5. The apparatus was maintained at 225±3 K and 230±3 K, for pellets containing cyclopropane hydrate I and ethylene oxide hydrates, respectively. The sample was pressurized to 300 bar. After 30 minutes the pressure was released for 5 minutes and then increased to 2.5 kbar for a total of 4 hours. Once an hour the pressure was released for 5 minutes. After 4 hours the sample was cooled under pressure to 170 K by increasing the gas flow, and was then cooled with liquid nitrogen to 77 K and the pressure was released.

The pressure apparatus was transferred from the press to the side arm of the cold can where it was partially dismantled. The retaining block E, holding the still assembled pistons and cylinder, was placed in the cold can, which contained two cylindrical brass holders fixed to the table. The radiation shield of the Helitran optical cell was secured in one of the brass holders by a polyethylene screw. The other brass holder was designed to hold the cylinder. The cold end of the optical cell was suspended inside the cold can with the plexiglass covers of the cold can situated just below the vacuum shroud seal O-rings (Fig. 2.5), which were wrapped with heating tape. A long metal rod was screwed onto the threaded tip of the cylinder to hold it while the two pistons were removed. The cylinder was then placed inside its brass holder and the metal rod was removed. An indium gasket was placed over the treaded tip and the cylinder was screwed onto the cryotip by rotating the cold end. The cold end was then raised sufficiently to allow an attached platinum resistance thermometer to be inserted into a hole in the cylinder. The radiation shield was then screwed onto the cold end, again by rotating the cold end. The cold end was connected to a vacuum line and the rubber tubing was evacuated with the valve on the cold end closed. The vacuum shroud was purged with dry nitrogen or argon, placed inside the side arm and coupled with the cold end to complete the assembly of the optical cell. The cell was then evacuated, and cooled by pouring liquid nitrogen into the aperture which takes the transfer line. When the cell was evacuated to $1x10^{-2}$ Torr, it was transferred to the infrared spectrophotometer and further evacuated. The transfer line was cooled as described previously and inserted into the optical cell which was left overnight at 125 to 150 K. The following day spectra were recorded with the sample temperature between 45 and 150 K with $1x10^{-1}$ to $2x10^{-1}$ Torr of helium in the cell as an exchange gas.

2.8.3 Preparation of 3-methylpentane Glasses

The optical cell described in Section 2.8.1 was also used to study samples dispersed in 3-methylpentane. The sample holder was made of OFHC copper. It consisted of the main body, which screwed into the cryotip, and a faceplate, both pieces contained circular grooves to hold indium O-rings. These O-rings were compressed against two cesium iodide windows when the sample holder was assembled, thus securing the windows to the faceplate and sample holder and providing good thermal contact. A platinum resistance thermometer was located in a hole at the bottom of the main body of the sample holder.

The radiation shield clamped in its brass holder (Section 2.8.2), a vial containing the finely ground sample and a stainless steel mortar containing the tip of a thermocouple, were placed in the cold can. The cold end of the Helitran optical cell, with the sample holder attached was suspended inside the cold can as described in Section 2.8.2 and heating tape was wrapped around the vacuum shroud seal O-rings (Fig. 2.5) just above the plexiglass covers. Three of the four screws which attach the faceplate to the sample holder were removed and the faceplate swung aside with a window attached. Approximately 0.1 ml of 3-methylpentane was syringed into the mortar. When the 3-methylpentane had cooled to 140 K a small amount of sample was added and thoroughly mixed. If the mixture cooled below 120 K it became too viscous to mix, so the mortar was raised from the table surface until the mixture was sufficiently mobile to be worked. When the sample was sufficiently dispersed, a small amount was spread on the window of the sample holder with a spatula. The faceplate was swung back into position and screwed down so that the glass formed as a thin film between the two windows. The optical cell was assembled, evacuated and cooled as described in Section 2.8.2.

2.9 Temperatures of the Infrared Samples

The actual temperature of low temperature infrared samples is usually uncertain if the sample is not in direct contact with the coolant. The temperature of the mull samples was estimated from the melting points of the mulling agents, which are for propane, propene and chlorotrifluormethane, 85, 88 and 92 K, respectively (166). Heat had to be applied very rarely to propane mulls, occasionally to propene mulls and always to chlorotrifluoromethane mulls to keep the mulling agents in the liquid state. The samples were therefore in the temperature range 85-95 K.

For the pellet and glassing techniques, a platinum resistance thermometer was located in a hole in the bottom of the sample holder. To determine the accuracy of the apparent temperatures given by this thermometer, various gases were deposited onto a pellet or the window of the sample holder, and the conditions under which the resultant solids sublimed were determined.

The procedure for calibrating the apparent temperature of the pellet sample holder was as follows. A clear potassium bromide pellet was prepared in the sample holder. The Helitran optical cell was assembled at room temperature, evacuated and cooled. From the pressure within the cell ($1x10^{-3}$ to $1x10^{-4}$ Torr), the highest temperature at which a particular gas would deposit was determined from the literature (169). These temperatures are given in Table 2.1. The sample holder was cooled below this temperature and the gas deposited. The sample holder was then warmed slowly (heating rate less than 0.2°/minute) and the apparent temperature at which the deposit first started to sublime from the pellet, as observed visually, and the apparent temperature and pressure at which the deposit had completely disappeared, were determined. The procedure was repeated, depositing the gas at slightly higher apparent temperatures until the gas condensed and sublimed within 1 K. The apparent temperatures so determined are given in Table 2.1 and are seen to be within 5 K of the literature values; the pellet (literature) temperature being warmer than the sensor (apparent) temperature. The temperatures reported for pellet samples in Chapters 4 and 5 have been adjusted by adding 5 K to the apparent temperatures.

For the calibration of the apparent temperatures of the glass samples, the procedure was that described above except that two clear cesium iodide windows were assembeld in the sample holder, and the gases were deposited onto the window attached to the faceplate. The results are given in Table 2.1. The apparent temperatures differ by no more than 4 K from the literature values except at

TABLE 2.1

Apparent and Literature Values of Deposition Temperatures of Various Gases

	Gas	Apparent Temperature (K)	Literature (169) Temperature (K)	Pressure (Torr)
Pellet Samples				
	CO_2	103	106.0	1×10^{-3}
	Xe	72	74.4	1×10^{-3}
	Kr	50	53.9	1×10^{-3}
	CH_4	45	46.3	5×10^{-4}
	Ar	34	39.2	1×10^{-3}
	N_2	29	34.1	1×10^{-3}
Glass Samples				
	CO_2	117	119.0	3×10^{-2}
	Xe	83	82.0	1×10^{-2}
	Kr	70	66.7	1.2×10^{-2}
	Ar	45	43.3	1×10^{-2}
	N_2	37	33.3	5×10^{-4}
	Ne	21	9.5	1×10^{-5}

the lowest temperature where the sensitivity of the platinum resistance thermometer is very low. Further, the apparent temperatures are usually higher than the literature values, so the temperatures reported for the glass samples are unadjusted apparent temperatures except at 10 K.

Three main sources of error in this calibration exist. First, the calibration of the gas pressure gauges varies with the gas and no correction was made. This should cause little error. Second, the thermal contact between the pellet and its holder probably varied from pellet to pellet. To counter this problem 0.1 to 0.2 Torr of helium gas was used as an exchange gas. Third, the actual infrared samples absorbed radiation but the samples used for calibration did not. The error due to this is hard to estimate, but the actual sample temperatures are believed to have been within 10 K of those cited.

2.10 Infrared Instrumentation

A Beckman IR-12 spectrophotometer was used in the studies presented in this thesis. It was equipped with a fiducial marker which marked every 25 cm^{-1} below 2000 cm^{-1} and every 50 cm^{-1} above 2000 cm^{-1}. These marks were calibrated against the spectra of gaseous ammonia, methane, water, hydrogen chloride, deuterium chloride, carbon dioxide, hydrogen bromide, hydrogen cyanide and deuterium cyanide (170,171). The accuracy of these marks is believed to be at least 0.5 cm^{-1} below 2000 cm^{-1} and 1 cm^{-1} above 2000 cm^{-1} and all frequencies were measured relative to these marks. Routine scans were done using a slit program that gave a resolution of about 4 cm^{-1} between 300 and 650 cm^{-1} and 2 cm^{-1} at higher frequencies, and at scan speeds of 20 or 40 cm^{-1}/min with a time constant of 2 seconds. Sharp features were scanned at slower speeds and normally under higher resolution.

The instrument had a variable scale expansion facility which was used to compensate for low baseline transmission. For some of the spectra of pellets and glasses an iris was used in the reference beam either instead of, or in conjunction with, the variable scale expansion. An airtight seal between the low temperature cells and sample compartment was provided by using plexiglass covers and plasticine. The instrument was purged with dry nitrogen gas, provided by boiling liquid nitrogen, or by dry air from a Pure Gas Model HR-211-112-9 dryer.

Chapter Three. Ice II and Ice IX

3.1 Introduction

This chapter describes the studies of the mid-infrared absorption spectra of ices II and IX to 10 K that were introduced in Section 1.8.

Samples of fully deuterated ice II and ice IX, and partially deuterated ices II and IX (2 or 4 mole percent HDO in H_2O) were prepared as described in Section 2.5. The samples were characterized by X-ray powder diffraction photographs (Section 2.6), and the X-ray powder diffraction data are summarized in Section 3.2. Mid-infrared spectra showing the $\nu_{OD}(D_2O)$, $\nu_{OD}(HDO)$ and $\nu_R(D_2O)$ bands of ices II and IX at 10, 60 and 100 K are presented in Section 3.3.1. The mid-infrared spectra are discussed in Section 3.3.2. In Section 3.4, the calculations of the frequencies and relative infrared intensities of the $\underline{k}=0$ $\nu_{OD}(D_2O)$ vibrations in the harmonic and bond moment approximations are discussed. The origin of the $\nu_{OD}(D_2O)$ and $\nu_R(D_2O)$ bands is discussed in Section 3.5.

3.2 Characterization of Ice II and Ice IX Samples

In this study it was important to have well characterized samples. Likely impurities were ice Ih, if sufficient time was not allowed for the transformation to the high pressure phases, and also ice Ic, if the samples warmed above ~150 K (36) during removal from the pressure apparatus.

These impurities are readily detected in X-ray powder diffraction photographs (36) which were used to characterize all samples of ice II and ice IX.

The X-ray data for ices II and IX at 100 K are summarized in Tables 3.1 and 3.2, respectively. The d-spacings and 2θ values are the averages of four sets of values (two sets of values determined from each of two photographs) for ice II, and six sets of values (two sets of values determined from each of three photographs) for ice IX. The crystal-tc-film distance was 59.8 mm (Section 2.6). Typical microdensitometer traces (Section 2.6) for ices II and IX are given in Fig. 3.1. The observed intensities, given in Tables 3.1 and 3.2, are the averages of the relative peak optical densities measured from eight microdensitometer traces (four traces from each of two photographs) for ice II, and six microdensitometer traces (two traces from each of three photographs) for ice IX.

The X-ray diffraction pattern of ice II was indexed on the hexagonal unit cell of the space group $R\bar{3}$ and yielded the lattice parameters a=12.91±0.01 Å and c=6.24±0.01 Å, in good agreement with previous studies (36,38). Ice IX was indexed on the space group $P4_12_12$ and yielded the lattice parameters a=6.74±0.01 Å and c= 6.77±0.02 Å, also in good agreement with previous studies (36,43). No impurities were detected in any of the samples. The observed intensities of the diffraction circles were compared with the cal-

TABLE 3.1

X-ray Powder Diffraction Pattern[a] of Ice II at 100 K

$(\text{Index})_{hex}$	$(\text{Index})_{rh}$	Calculated Intensity[b]	2θ[c]	$d(\text{Å})$[c]	Observed Intensity[d]
110	$0\bar{1}1$	73	13.72(5)	6.45(2)	87
101	001	1			
021	$1\bar{1}1$	1			
300	$1\bar{2}1$	33	23.85(6)	3.73(1)	40
211	$0\bar{1}2$	8	25.45(5)	3.50(1)	15
220	$0\bar{2}2$	48	27.62(4)	3.229(6)	57
012	011	75	29.74(5)	3.004(7)	79
131 202	$1\bar{2}2$ 002	79 6	32.20(5)	2.780(5)	88
401 122	$1\bar{3}1$ $1\bar{1}2$	1 75	35.76(7)	2.511(6)	92
410	$1\bar{3}2$	100	36.84(7)	2.440(6)	100
321	$0\bar{2}3$	31	37.91(4)	2.374(4)	42
312	$0\bar{1}3$	6	41.03(1)	2.200(2)	8

(continued.....)

TABLE 3.1 (continued)

(Index)$_{hex}$	(Index)$_{rh}$	Calculated Intensity[b]	2θ[c]	d(Å)[c]	Observed Intensity[d]
330	$0\bar{3}3$	6	42.01(1)	2.151(5)	7
501	$2\bar{3}2$	1			
402	$2\bar{2}2$	11	43.49(4)	2.081(2)	13
003	111	1			
241	$1\bar{3}3$	9	45.30(2)	1.975(3)	10
232	$1\bar{2}3$	2			
113	012	6			
511	$1\bar{4}2$	12	47.57(2)	1.911(1)	10
600	$2\bar{4}2$	0.2			
502	$1\bar{4}1$	9	50.23(5)	1.818(2)	8
303	003	0.2			
033	$2\bar{1}2$	0.1			

---

a) Cu K_α radiation, wavelength 1.5418 Å.

b) Crystals of ice II have been found to exist in two twin configurations (16, 38), so that reflections from the hkl and khl planes of the twin configurations are combined, and consequently the structure factors given in reference 38 are expressed as $G(hkl) = [\frac{1}{2}F^2(hkl)+\frac{1}{2}F^2(khl)]^{\frac{1}{2}}$. This assumes equal volume fractions of the twin configurations.

(continued......)

TABLE 3.1 (continued)

c) Average of four sets of values. The figure in parenthesis is the standard deviation of the last figure.

d) Average of eight measurements. Estimated accuracy is 20% or 30% of the value for values greater than or less than 20, respectively.

TABLE 3.2

X-ray Powder Diffraction Pattern[a] of Ice IX at 100 K

Index	Calculated Intensity	2θ[b]	d(Å)[b]	Observed[c] Intensity
110	1	18.56(5)	4.78(3)	-
111	7	22.80(5)	3.90(1)	9
200	4	26.51(8)	3.36(1)	6
102	48	29.57(5)	3.021(5)	100
201	52			
210	0.1			
112	11	32.51(7)	2.754(6)	33
211	30			
202	2	37.70(8)	2.386(5)	4
220	0.6			
212	8	40.09(2)	2.249(4)	12
221	3			
103	5	42.40(5)	2.132(3)	15
310	0.6			
301	12			
113	2	44.61(5)	2.031(2)	4
311	4			
222	12	46.64(4)	1.947(3)	11
203	5	48.74(5)	1.868(3)	8
320	9			

a) Cu K_α radiation, wavelength 1.5418 Å.

b) The average of six sets of values. The figure in parenthesis is the standard deviation in the last figure.

c) The average of six measurements. Estimated accuracy is 20% or 30% of the value for values greater than or less than 20, respectively.

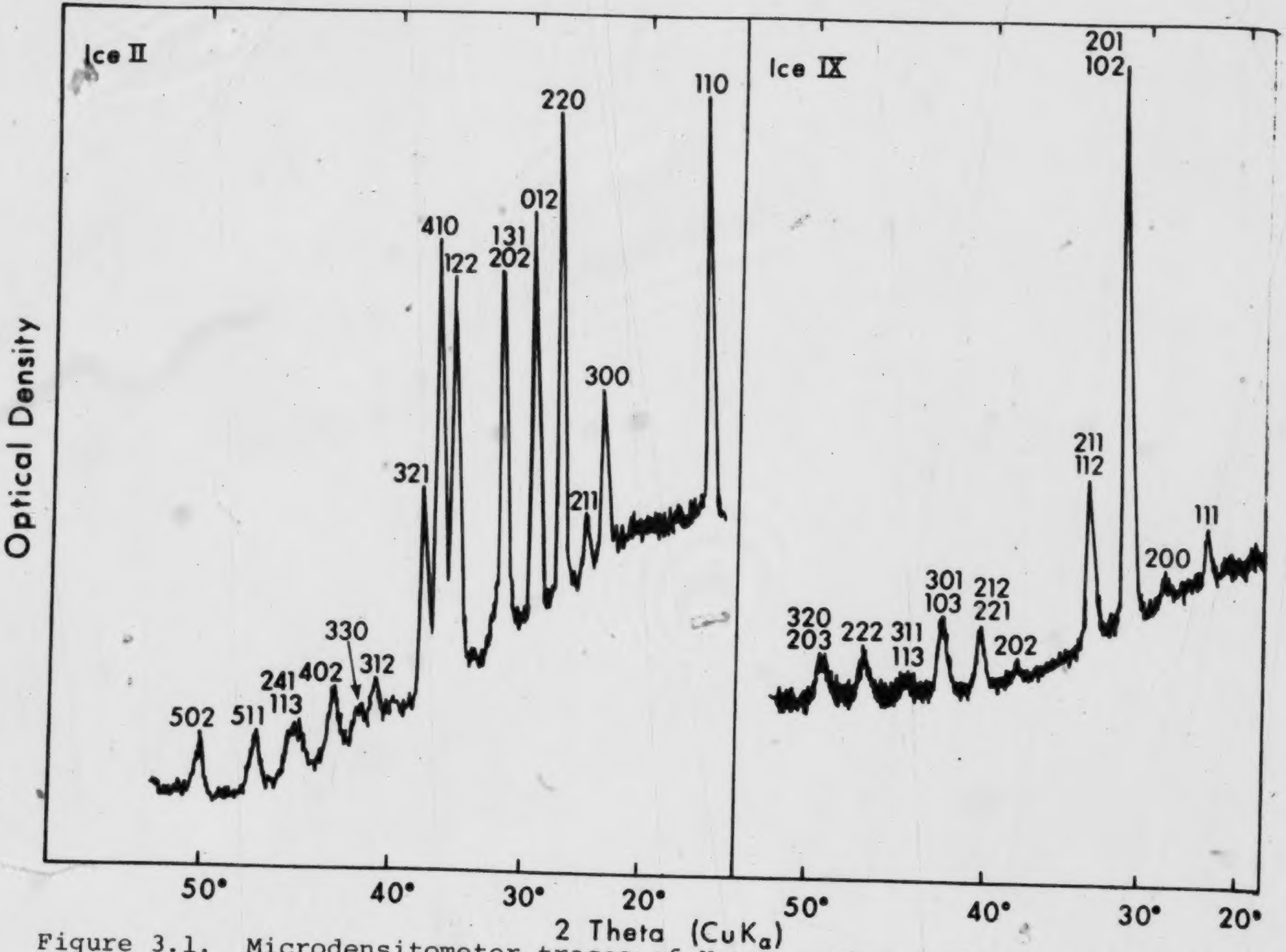

Figure 3.1. Microdensitometer traces of X-ray powder diffraction photographs of ices II and IX.

culated values of the integrated intensities (Tables 3.1 and 3.2), which are given (172) for a flatplate camera by

$$I \propto [(1+\cos^2 2\theta)/\sin^2\theta\cos\theta]\,(\cos 2\theta)pF^2 \qquad (1)$$

where p is the multiplicity factor and F is the experimental structure factor obtained from single crystal X-ray diffraction studies (38,43). The observed intensities generally agree with the calculated values within experimental error.

3.3 Mid-Infrared Spectra of Ice II and Ice IX to 10 K

3.3.1 Results

The mid-infrared samples were prepared by mixing the finely ground ice samples into 3-methylpentane as described in Section 2.8.3.

The $\nu_{OD}(HDO)$, $\nu_{OD}(D_2O)$ and $\nu_R(D_2O)$ bands of ice II and ice IX are shown in Figs. 3.2 to 3.4 and Figs. 3.5 to 3.7, respectively. The weak absorption by the 3-methylpentane has been subtracted, and the spectra have been offset for clarity. The frequencies of the spectral features for ices II and IX are given in Tables 3.3 and 3.4, respectively. The spectral features and their frequencies agree with those reported previously (37). The features of the $\nu_{OD}(D_2O)$ and $\nu_R(D_2O)$ bands are, however, more resolved than in the previous study (37) because of the improved sampling methods.

The $\nu_{OD}(HDO)$ bands are shown in Fig. 3.2 for ice II (4 mole percent HDO in H_2O) and in Fig. 3.5 for ice IX

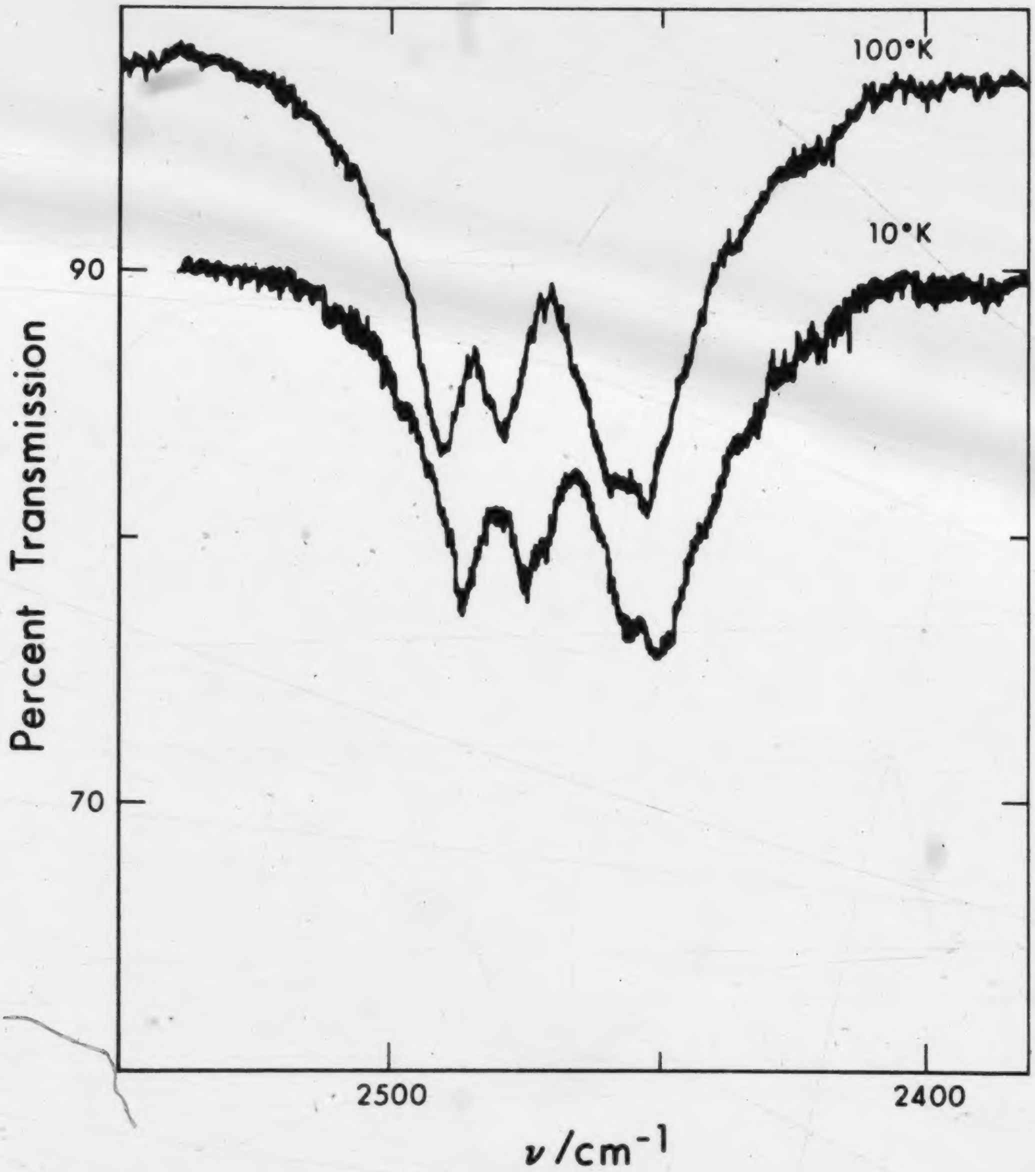

Figure 3.2. The ν_{OD}(HDO) band of ice II; resolution 2 cm^{-1}. The 10 K spectrum has been lowered by 5 percent for clarity.

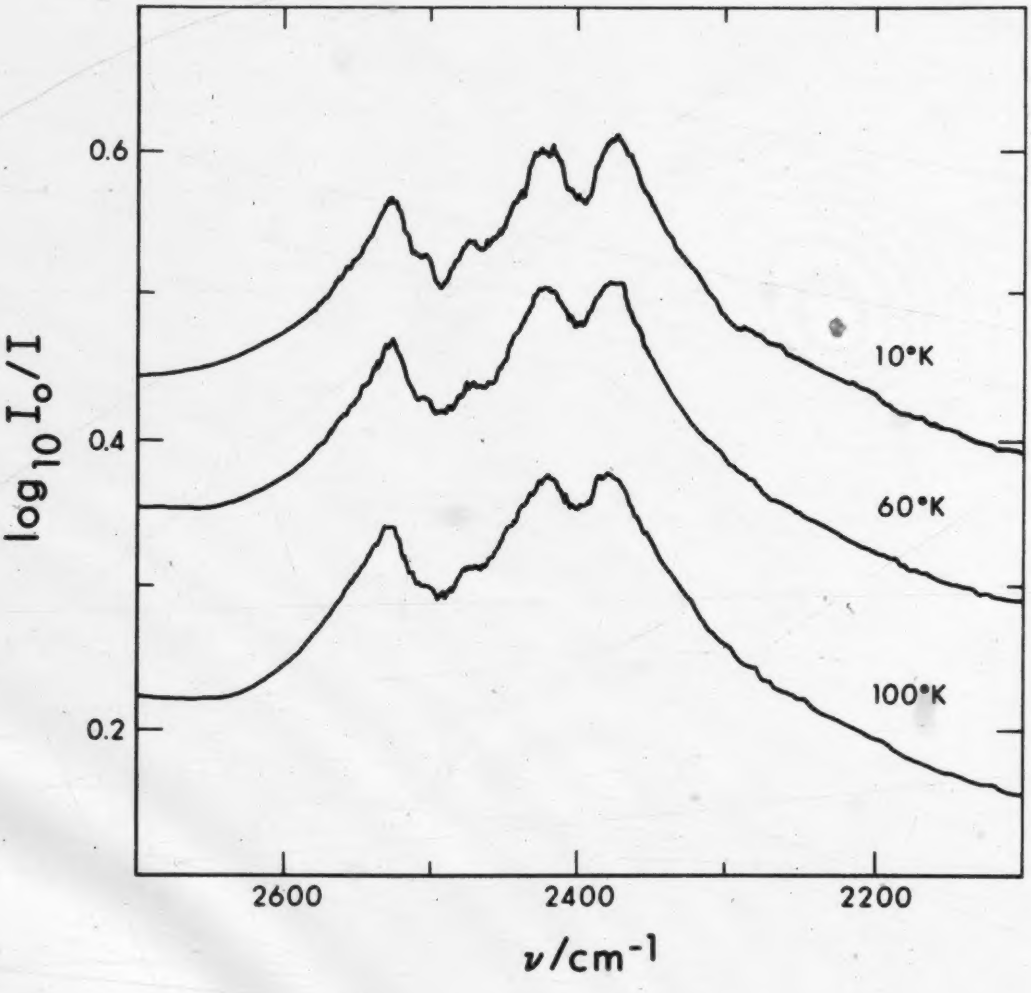

Figure 3.3. The $\nu_{OD}(D_2O)$ band of ice II; resolution 2 cm^{-1}. The 10 and 100 K spectra have been displaced up and down by 0.1 unit, respectively.

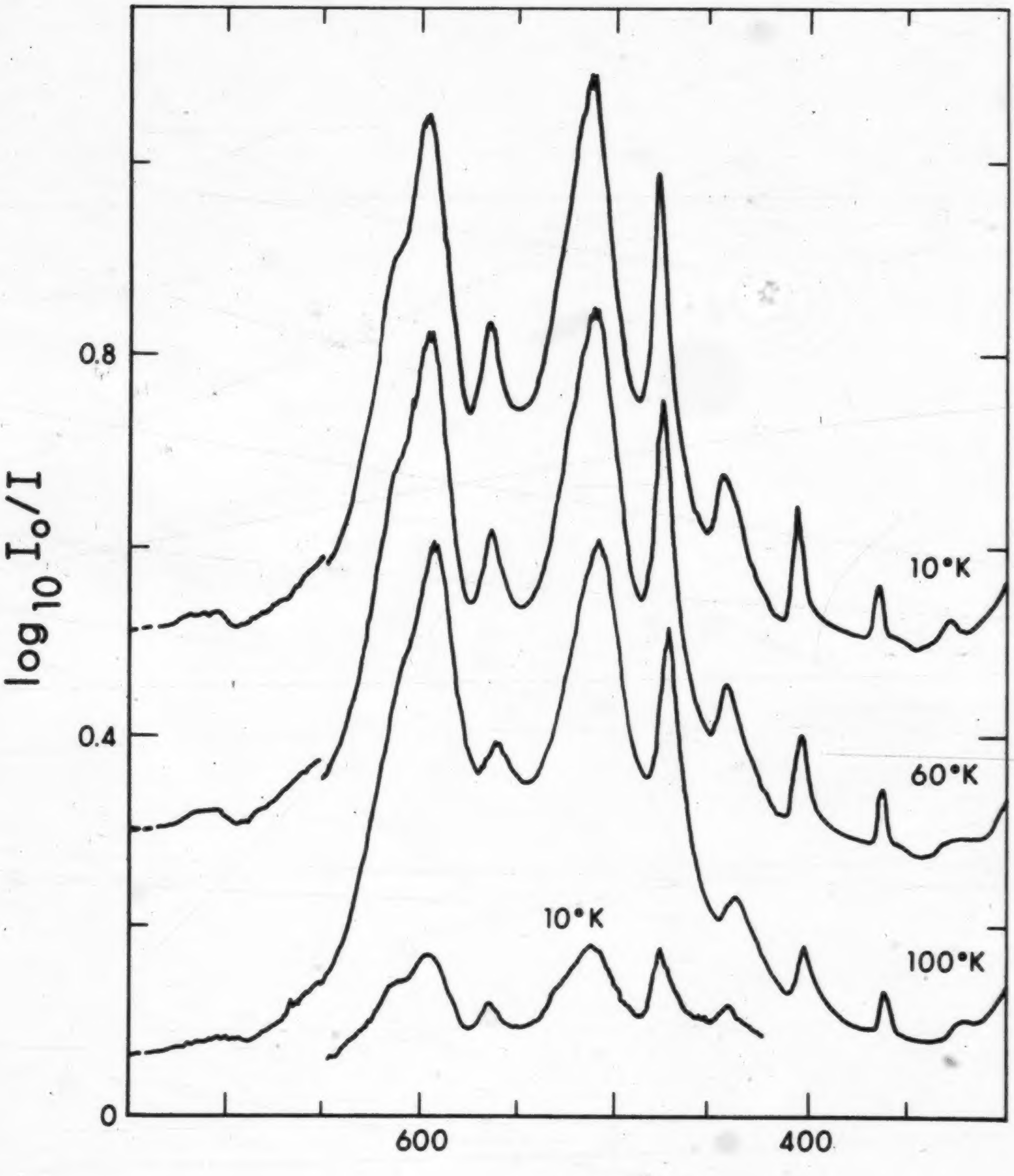

Figure 3.4. The $\nu_R(D_2O)$ band of ice II; resolution 2 to 4 cm^{-1}. The more intense bands at 10 and 100 K have been displaced up and down by 0.2 units, respectively. The weak 10 K band has been displaced down by 0.2 units and is from the same sample as the bands in Figure 3.3.

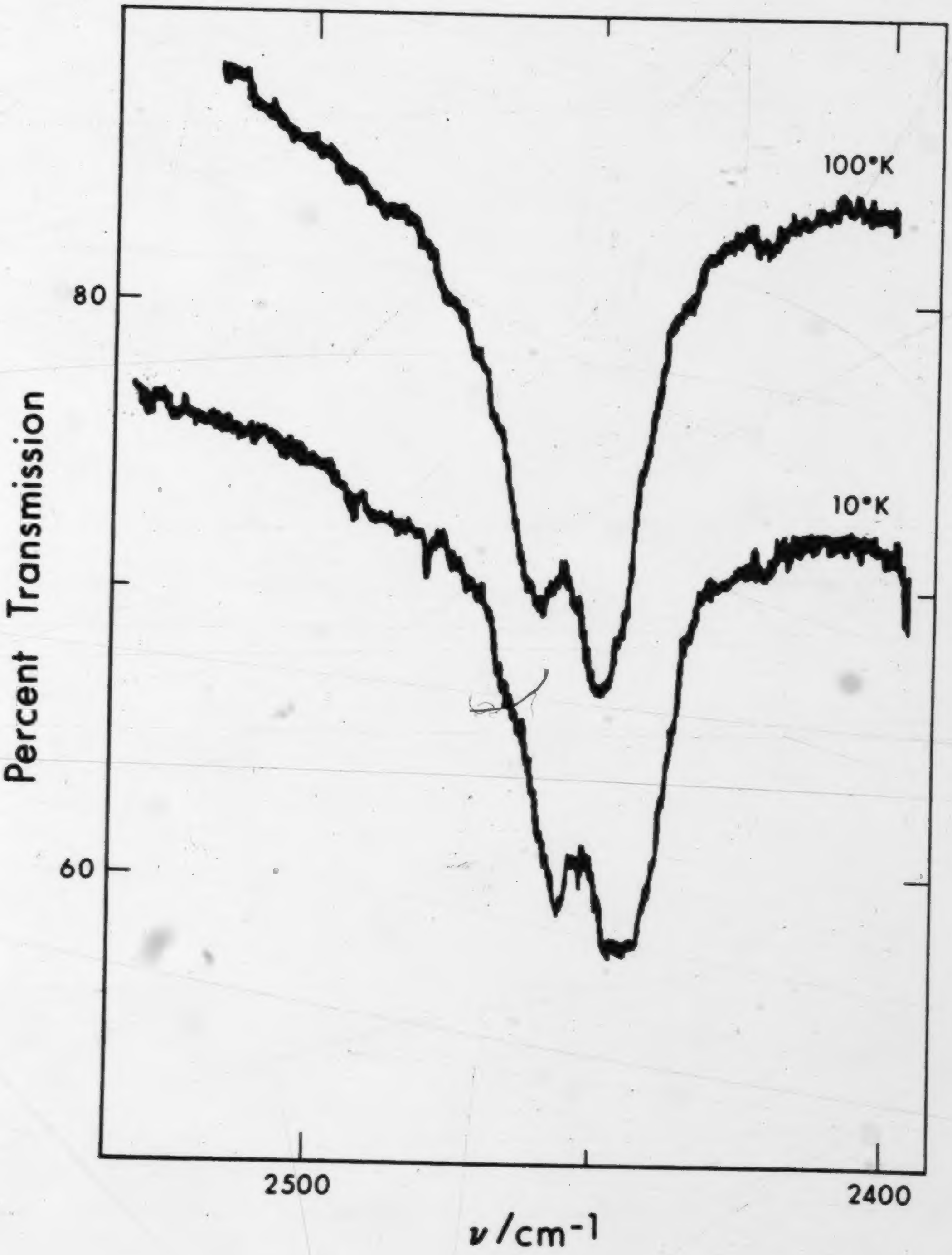

Figure 3.5. The ν_{OD}(HDO) band of ice IX; resolution 2 cm^{-1}. The 10 K spectrum has been lowered by 20 percent.

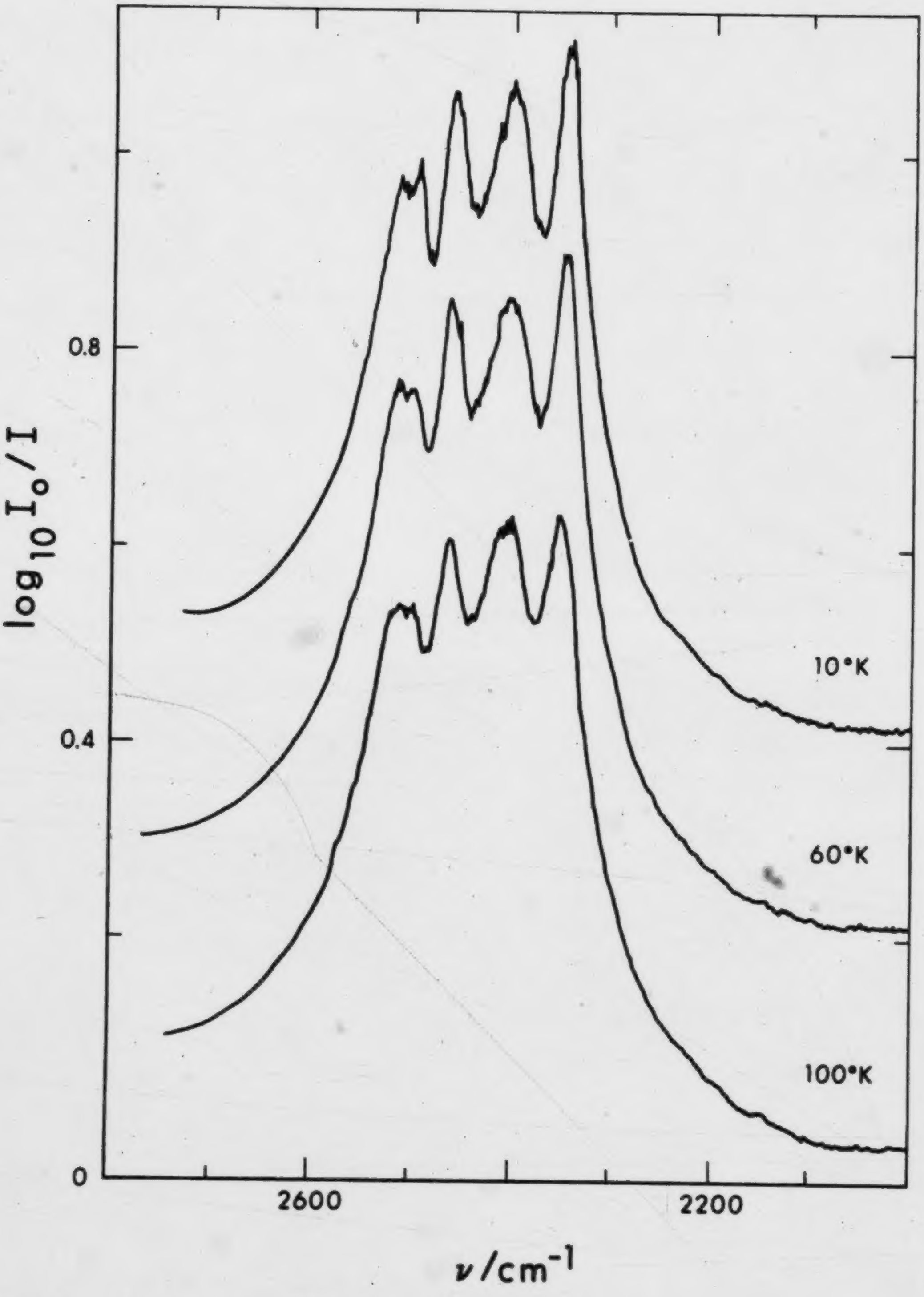

Figure 3.6. The $\nu_{OD}(D_2O)$ band of ice IX; resolution 2 cm^{-1}. The 10 and 100 K spectra have been displaced up and down by 0.2 units, respectively.

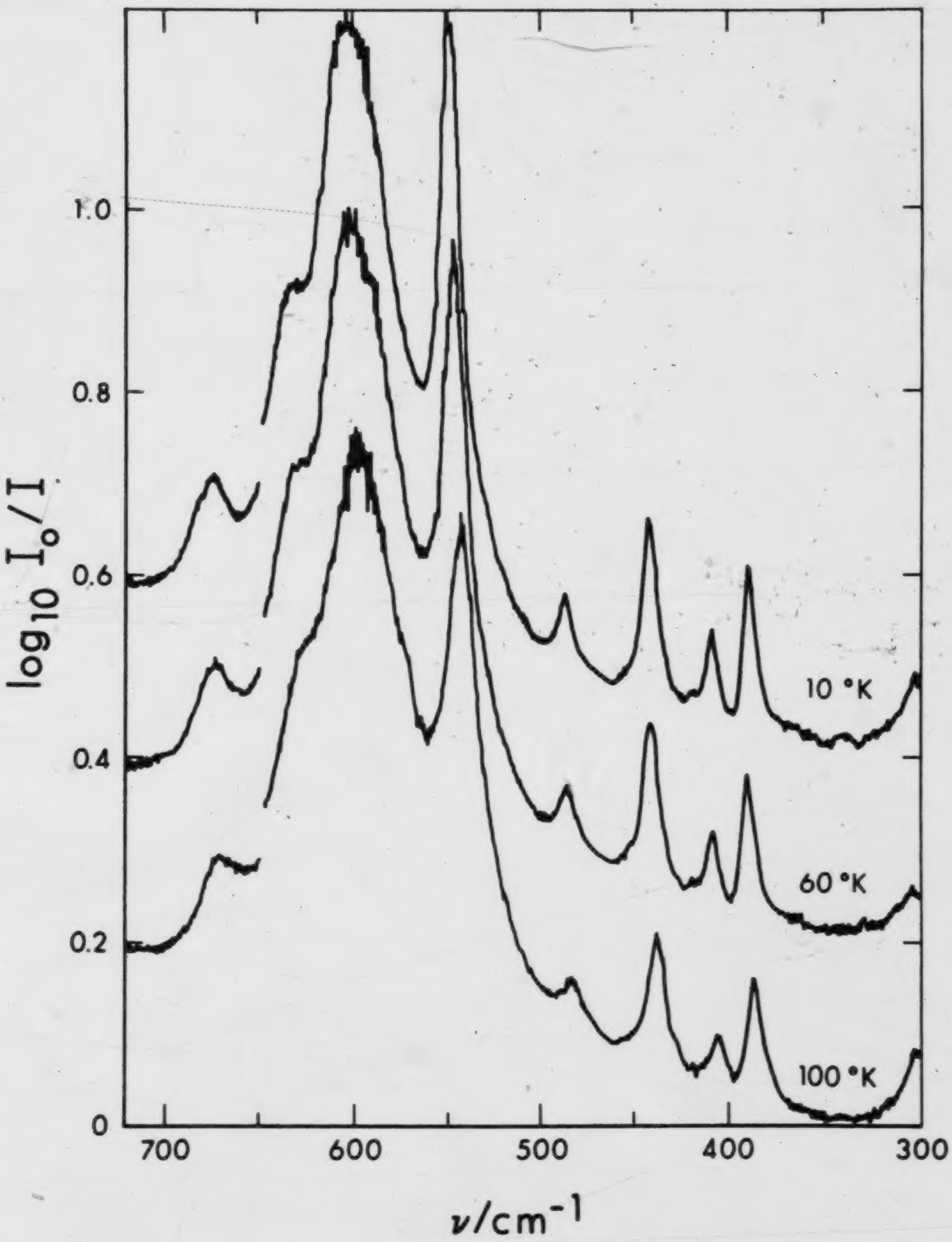

Figure 3.7. The $\nu_R(D_2O)$ band of ice IX; resolution 2 to 4 cm^{-1}. The 10 and 100 K spectra have been displaced up and down by 0.2 units, respectively.

TABLE 3.3

Frequencies of Features in the Mid-Infrared Spectrum of Ice II

	Frequency[a]/cm^{-1}			Intensity[b]
	100 K	60 K	10 K	
ν_{OD}(HDO)	2490	2488	2487	m
	2479	2476	2475	m
	2459	2457	2455	m
	2454	2451	2450	m
ν_{OD}(D_2O)			~2550	sh
	2528	2525	2524	vs
		2502 ± 4	2501 ± 4	sh
	2473 ± 4	2470 ± 4	2470 ± 4	sh
	2420	2420	2418	vs
	2378	2372	2370	vs
ν_R(D_2O)	705 ± 5	711 ± 5	713 ± 5	w,br
	606	608	610	sh
	592	594	595	vs
	559	562	563	m
	528 ± 3	528 ± 3	528 ± 3	sh
	507	509	511	vs
	471	475	476	s
	439	442	444	m

(continued......)

TABLE 3.3 (continued)

Frequency[a]/cm^{-1} 100 K	60 K	10 K	Intensity[b]
402 ± 3	403 ± 3	407 ± 3	m
361 ± 3	363 ± 3	365 ± 3	w
	359 ± 3	360 ± 3	sh
324 ± 3	327 ± 3	328 ± 3	vw

a) The accuracy is ± 2 cm^{-1} for ν_{OD}(HDO) and $\nu_R(D_2O)$ and ± 3 cm^{-1} for $\nu_{OD}(D_2O)$, except where indicated.

b) s = strong, m = medium, w = weak, v = very, sh = shoulder, br = broad.

TABLE [illegible].4

Frequencies of Features in the Mid-Infrared Spectrum of Ice IX

	Frequency[a]/cm^{-1}			Intensity[b]
	100 K	60 K	10 K	
ν_{OD}(HDO)	2460	2457	2455	m
	2449	2447	2446	m
			2444	m
	2434	2432	2429	sh
ν_{OD}(D_2O)	2513 ± 6	2518	2517	vs
		2502	2499	vs
	2466	2465	2462	vs
	2407	2404	2403	vs
	2354	2350	2348	vs
ν_R(D_2O)	674 ± 3	677 ± 3	678 ± 3	m,br
	627 ± 4	631 ± 4	633 ± 4	sh
	602 ± 3	606 ± 3	607 ± 3	vs
		592	595 ± 3	sh
	545	547	549	vs
	485	487	489	w
	441	443	445	m
		419	421	sh
	408	410	412	w
	389	391	393	m

(continued......)

TABLE 3.4 (continued)

a) The accuracy is ± 2 cm^{-1} for ν_{OD}(HDO) and $\nu_R(D_2O)$ and ± 3 cm^{-1} for $\nu_{OD}(D_2O)$, except where indicated.

b) vs = very strong, m = medium, w = weak, sh = shoulder, br = broad.

(2 mole percent HDO in H_2O). These bands are composed of several features which appear to have half-widths of about 5 cm^{-1}. The ν_{OD}(HDO) band of ice II consists of four features which have approximately equal intensities, while the ν_{OD}(HDO) band of ice IX at 100 K consists of two features which have an intensity ratio of about 2:1. The more intense, low frequency feature is nearly resolved into two components for ice IX at 10 K. The ν_{OD}(HDO) band of the ice IX sample containing 4 mole percent HDO in H_2O was the same as that shown in Fig. 3.5 except that a shoulder due to coupled vibrations of neighbouring O-D groups (37) was observed at 2429 cm^{-1} .

The $\nu_{OD}(D_2O)$ bands of ices II and IX (Figs. 3.3 and 3.6, respectively) are quite broad, extending from 2200 to 2600 cm^{-1}. Features reported previously (37) at 2360 and 2300 cm^{-1} for ice II were not observed, but this may have been due to the weakly absorbing samples used in this study. Cooling the samples resulted in more structure being resolved. For ice II at 10 K, shoulders were observed at 2501 and 2550 cm^{-1}. For ice IX, the peak observed at 2513 cm^{-1} at 100 K resolved into two peaks at 2517 and 2499 cm^{-1} at 10 K.

The $\nu_R(D_2O)$ bands of ices II and IX (Figs. 3.4 and 3.7, respectively) are comparatively rich in detail. The bands are composed of moderately sharp features superimposed on a broad background absorption. This broad absorption is, however, not as intense relative to the sharp features as reported previously (37). Cooling the samples resulted in more structure being resolved. Thus, for ice II at 10 K a shoulder was observed at 360 cm^{-1}, and for ice IX at 10 K shoulders were observed at 421 and 595 cm^{-1}.

In infrared transmission studies, the temperature dependence of the frequencies and bandwidths of the spectral features is usually associated with changes in the absorption by the sample. This is, however, not necessarily the case. Infrared transmission spectra are not simply absorption spectra. Superimposed on the absorption spectra are reflection and, sometimes, emission spectra. The infrared spectrophotometers used in this and the previous (37) study, chop the radiation between the source and the sample and also between the sample and the detector. Radiation is emitted by the sample and the detector. The chopper between the sample and the detector modulates this emitted radiation, so that superimposed on the transmission spectrum is the spectrum of the net emission between the sample and the detector. This net emission is a function of the temperature difference between the sample and the detector, and thus could contribute to the observed temperature effects. The detector used was a room temperature thermocouple, and so for low temperature samples the net emission is from the detector to the sample. If the thermocouple behaves as a blackbody source its emission should be greatest near 600 cm^{-1}, and therefore the $\nu_R(D_2O)$ bands should be most affected. To check for distortion of the spectra by emission, the $\nu_R(D_2O)$ band of ice IX was recorded with the chopper between the sample and the detector connected, and then with this chopper stopped. The spectra so obtained are presented in Fig. 3.8 for two sample temperatures, 10 and 100 K. The lower two curves of Fig. 3.8 were recorded with the chopper between the sample and the detector stopped. Comparison of the spectra for the two sets of conditions shows that when the emission is eliminated the broad background absorption is more intense and the relative intensities of the features change. This is most noticeable for the intensities of the two features at 633 and 549 cm^{-1} relative to the peak at 607 cm^{-1}. It may also be noted that the discontinuity at the grating change at 650 cm^{-1} was not observed when the emission was eliminated. Comparison of the 10 and 100 K spectra for the two sets of conditions shows that the sharpening of the features as the sample is cooled is due to changes in the absorption by the sample. Although the spectra are distorted by emission this does not effect the interpretation of the spectra given later.

3.3.2 Discussion

Trends observed with decreasing temperature were, first, the $\nu_{OD}(HDO)$ and $\nu_{OD}(D_2O)$ bands shifted to lower frequencies, while the $\nu_R(D_2O)$ bands shifted to higher frequencies and, second, the features sharpened, so that more structure was resolved. The first trend is usually attributed to an

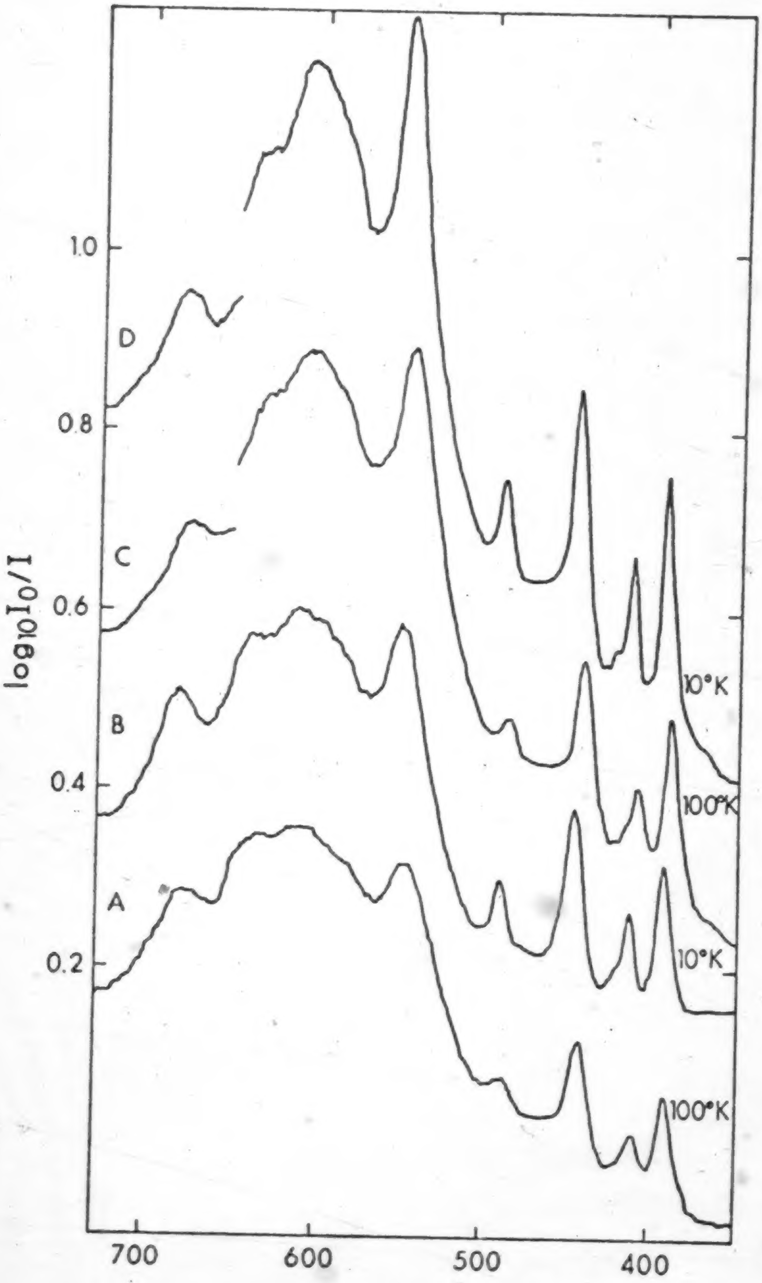

Figure 3.8. The effect of emission on the $\nu_R(D_2O)$ band of ice IX. Curves A and B were recorded with the chopper between the sample and the detector stopped.

anharmonic intermolecular potential. This results in stronger effective harmonic intermolecular forces and a decrease in unit cell size with decreasing temperature, so that the intermolecular vibrations shift to higher frequencies while the intramolecular vibrations shift to lower frequencies. The second trend is usually attributed to a decrease in the number of transitions arising from thermally excited states (89) with decreasing temperature. Anharmonicity causes the hot transitions ($v_i=1$, $v_j=0$ to $v_i=2$, $v_j=0$ or $v_i=0$, $v_j=1$ to $v_i=1$, $v_j=1$) to occur at different frequencies than the fundamental transitions ($v_i=0$, $v_j=0$ to $v_i=1$, $v_j=0$), so such transitions contribute to the temperature dependent breadth of a fundamental band.

Anharmonicity can also result in the occurrence of overtone, sum and difference transitions. These transitions are subject to the wavevector (conservation of momentum) selection rule that $\sum_i \underline{k}_i = 0$. However, they are not limited to $\underline{k}_i=0$, and hence the transitions can occur at different frequencies depending on the particular values of $\underline{k}_i$. The significance of this is that sharp spectral features are predicted for fundamental $\underline{k}=0$ transitions, and broader spectral features are predicted for overtone and combination transitions.

Difference transitions, like hot transitions, arise from thermally excited states and, thus, provide a temperature dependent contribution to the infrared spectrum, while the contribution of sum and overtone transitions is temperature independent. Thus for samples of ices II and IX at 10 K, the only transitions that should contribute significantly to the infrared spectra are fundamental transitions and overtone and sum-combination transitions originating from the ground state.

The ν_{OD}(HDO) bands are due to O-D oscillators that are not coupled to the surrounding O-H oscillators and, thus, reflect the different environments of these isolated O-D oscillators. Various correlations between the ν_{OD}(HDO) frequencies and O···O distances have been made (173,174). These correlations are only approximate, presumably because other factors, such as the non-linearity of the O-D···O bonds, also affect the frequencies. Generally though the ν_{OD}(HDO) frequencies increase with O···O distance. The ν_{OD}(HDO) frequencies of ices II and IX at 100 K have been assigned previously (15,43,96) and the assignment at 10 K follows from this and is given below using the atom description of Kamb _et_ _al_. for ice II (16) and of LaPlaca _et_ _al_. for ice IX (15).

The ν_{OD}(HDO) features of ice II at 10 K at 2487, 2475, 2455 and 2450 cm^{-1} are assigned to the stretching of O-D bonds of the type O(II)-D(3)···O(I), O(I)-D(2)···O(I), O(II)-D(1)···O(II) and O(I)-D(4)···O(II), which have O···O distances of 2.844, 2.803, 2.781 and 2.768 Å, respectively at 110 K (16). Similarly for ice IX at 10 K, the ν_{OD}(HDO) features observed at 2455, 2446 and 2444 cm^{-1} are assigned to the stretching of O-D bonds of the type O(2)-D(7)···O(1), O(1)-D(6)···O(2) and O(1)-D(5)···O(1), which have O···O distances 2.793, 2.763 and 2.750 Å, respectively at 110 K (15). The assignment of the ν_{OD}(HDO) band of ice IX at 10 K differs from that at 100 K (43,96) only in that the ν_{OD}(HDO) features due to bonds of length 2.763 and 2.750 Å are nearly resolved at the lower temperature. Comparison of the ν_{OD}(HDO) bands of ice IX at 10 and 100 K (Fig. 3.5) indicates that the resolution of the 2445 cm^{-1} peak is not the result of a decrease in bandwidth as the sample is cooled, but is due to an increase in separation of the two features, probably resulting from an increase in the difference of the two O···O bond lengths as the temperature is lowered.

Kamb and Prakash (43) have noted that although the ν_{OD}(HDO) bands due to O···O distances that differ by only 0.013 Å are resolved in ice II at 100 K, they are not in ice IX at 100 K. There are several possible explanations for this difference. The ν_{OD}(HDO) bands of ice IX may be inherently broader than those of ice II (43) because of the small amount of proton disorder found in ice IX (15,44). Experimental error in O···O distances could also explain the difference, since the estimated standard deviations (±0.015 and ±0.011 Å) of the O···O distances are quite large for ice II (16,38). Finally, the correlation of ν_{OD}(HDO) frequencies versus O···O distance is not exact.

A unit-cell group analysis of ice II and ice IX (Section 1.4) predicts twelve infrared active ν_R vibrations for ice II and fourteen for ice IX. A total of twelve fairly sharp features were observed in the $\nu_R(D_2O)$ band of ice II, and ten features were observed in the $\nu_R(D_2O)$ band of ice IX. Presumably these sharp features are due to the unit-cell-group allowed vibrations (37). However, some of the features are broader than those observed for the ν_T bands (119), and there is clearly an underlying broad absorption even at 10 K. Thus, the bands are not due solely to unit-cell-group allowed vibrations.

A unit-cell-group analysis of ice II (Section 1.4) predicts eight infrared active O-D stretching vibrations and a total of six features were observed in the $\nu_{OD}(D_2O)$ band of ice II at 10 K. For ice IX, nine infrared active O-D stretching vibrations are predicted and a total of five features were observed in the $\nu_{OD}(D_2O)$ band. The $\nu_{OD}(HDO)$ bands of ices II and IX are sharp indicating that the bands due to O-D stretching vibrations are not intrinsically broad (37). However, the $\nu_{OD}(D_2O)$ bands are extremely broad, even at 10 K, with moderately sharp features superimposed, and clearly the bands are not due solely to unit-cell-group allowed vibrations. Sum-combination and overtone bands arising from the lower frequency vibrations can contribute to this absorption since there is virtually a continuum of combination and overtone levels (such as

$2\nu_2$, $\nu_2+2\nu_R$, $4\nu_R$ and various combinations with ν_T) that are isoenergetic with the $\nu_{OD}(D_2O)$ fundamental levels. Normal coordinate calculations of the frequencies of the $\underline{k}=0$ $\nu_{OD}(D_2O)$ vibrations were, thus, attempted to see whether the observed infrared features can be assigned to fundamental transitions.

3.4 Normal Coordinate Analysis of the $\nu_{OD}(D_2O)$ Vibrations of Ice II and Ice IX

3.4.1 General Method

The O-D stretching vibrations in ices II and IX have frequencies sufficiently different from those of other intra- or intermolecular vibrations that a normal coordinate analysis of the $\nu_{OD}(D_2O)$ vibrations can be usefully made while neglecting all other displacements of the molecules. Such normal coordinate calculations were done using the Wilson GF matrix method (100,175,176) which will be briefly described to introduce the terminology.

The normal coordinates, Q, are defined such that the potential, V, and kinetic, T, energies can be expressed by

$$2V = \underset{\sim}{Q}^t \, \underset{\sim}{\Lambda} \, \underset{\sim}{Q} \qquad (2)$$

and

$$2T = \underset{\sim}{\dot{Q}}^t \, \underset{\sim}{E} \, \underset{\sim}{\dot{Q}} \qquad (3)$$

where $\underset{\sim}{Q}$ is the column matrix of the normal coordinates, $\underset{\sim}{\dot{Q}}$ is the column matrix of the time derivatives of the normal coordinates, $\underset{\sim}{\Lambda}$ is the diagonal matrix of the eigenvalues

$\lambda_k = 4\pi^2 c^2 \nu_k{}^2$, where ν_k is the wavenumber of the k^{th} vibration expressed in cm^{-1} and c is the velocity of light, $\underset{\sim}{E}$ is a unit matrix and the superscript t signifies the transpose of the matrix. The normal coordinates are orthogonal, so that any vibrational motion can be expressed as a linear combination of the normal coordinates (177). Normal coordinates can only be defined in the approximation that the kinetic and potential energies are quadratic functions of the displacement coordinates. If internal displacement coordinates, R_i, such as bond stretching or angle bending coordinates are used the potential and kinetic energies are given, in this approximation, by

$$2V = \underset{\sim}{R}^t \underset{\sim}{F} \underset{\sim}{R} \qquad (4)$$

and

$$2T = \underset{\sim}{\dot{R}}^t \underset{\sim}{G}^{-1} \underset{\sim}{\dot{R}} \qquad (5)$$

where $\underset{\sim}{F}$ is a square matrix whose elements F_{ij} are the force constants relating the internal displacement coordinates R_i and R_j, $\underset{\sim}{R}$ is the column matrix of the internal displacement coordinates and $\underset{\sim}{G}$ is called the inverse kinetic energy matrix whose elements G_{ij} are functions of the atomic masses and equilibrium geometry. To determine the normal coordinates the transformation

$$\underset{\sim}{R} = \underset{\sim}{L}\underset{\sim}{Q} \qquad (6)$$

is sought, where $\underset{\sim}{L}$ is the eigenvector matrix. $\underset{\sim}{L}$ is defined (100,175) by the matrix equations

$$\underset{\sim}{L}^{t}\,\underset{\sim}{F}\,\underset{\sim}{L} = \underset{\sim}{\Lambda} \qquad (7)$$

and

$$\underset{\sim}{L}^{t}\,\underset{\sim}{G}^{-1}\,\underset{\sim}{L} = \underset{\sim}{E} \qquad (8)$$

or

$$\underset{\sim}{G}\,\underset{\sim}{F}\,\underset{\sim}{L} = \underset{\sim}{L}\,\underset{\sim}{\Lambda}. \qquad (9)$$

The problem of determining the normal coordinates reduces to solving equations (7) and (8) or (9). When using computer methods to solve the secular equations, it is less time consuming to diagonalize two symmetric matrices, such as $\underset{\sim}{G}$ and $\underset{\sim}{F}$ than to diagonalize a nonsymmetric matrix such as $\underset{\sim}{G}\underset{\sim}{F}$. To take advantage of this, a transformation to a new set of coordinates in which $\underset{\sim}{G}$ is diagonal is made, and the corresponding transformation is applied to $\underset{\sim}{F}$. The resultant $\underset{\sim}{F}$ matrix is symmetric and it can be easily diagonalized. This method is called the method of successive diagonalization.

Symmetry can be used to factor the $\underset{\sim}{G}$ and $\underset{\sim}{F}$ matrices into block diagonal form. Symmetry coordinates can be constructed from sets of equivalent internal displacement coordinates by using projection operators (178). The symmetry coordinates, S_i, are defined by

$$\underset{\sim}{S} \; \text{[illegible]} \; \underset{\sim}{U}\underset{\sim}{R}\,, \qquad (10)$$

where $\underset{\sim}{S}$ is a column matrix of the symmetry coordinates and $\underset{\sim}{U}$ is an orthogonal transformation matrix. The $\underset{\sim}{G}$ and $\underset{\sim}{F}$ matrices can then be transformed to their symmetrized equivalents by

$$\underset{\sim}{F_s} = \underset{\sim}{U}\,\underset{\sim}{F}\,\underset{\sim}{U}^t \qquad (11)$$

and

$$\underset{\sim}{G_s} = \underset{\sim}{U}\,\underset{\sim}{G}\,\underset{\sim}{U}^t. \qquad (12)$$

Determination of the normal coordinates and their frequencies then reduces to solving

$$\underset{\sim}{G_s}\,\underset{\sim}{F_s}\,\underset{\sim}{L_s} = \underset{\sim}{L_s}\,\underset{\sim}{\Lambda} \qquad (13)$$

where

$$\underset{\sim}{S} = \underset{\sim}{L_s}\,\underset{\sim}{Q} \qquad (14)$$

and

$$\underset{\sim}{L_s} = \underset{\sim}{U}\,\underset{\sim}{L}. \qquad (15)$$

Each column of $\underset{\sim}{L_s}$ contains the symmetrized eigenvector for one vibration.

The form of a vibration can be described in terms of the eigenvectors or symmetrized eigenvectors, whose elements L_{ij} or $L_{s_{ij}}$ are $\partial R_i/\partial Q_j$ or $\partial S_i/\partial Q_j$ and so describe the contribution of the i^{th} internal displacement coordinate or symmetry coordinate to the j^{th} vibration.

Schachtschneider's computer program VSEC (179) was used to determine the frequencies and forms of the normal vibrations. The $\underset{\sim}{F}$ and $\underset{\sim}{G}$ matrices and symmetry coordinates were constructed as described later and used as input. The program then calculated the frequencies, eigenvectors and symmetrized eigenvectors. Schachtschneiders FPERT program (179) was used for ice II to refine the force constants by an iterative method to give a least-squares-fit between the observed and calculated frequencies.

Recently, Rice and coworkers (125) have reported normal coordinate calculations of the frequencies of the $\nu_{OH}(H_2O)$ vibrations in ices II and IX. They, however, neglected to include the off-diagonal elements of the $\underset{\sim}{G}$ matrix which are the primary source of the intramolecular coupling between ν_1 and ν_3. Consequently their results will not be discussed.

3.4.2 Calculation of the Relative Infrared Intensities of the $\nu_{OD}(D_2O)$ Normal Vibrations

Normal coordinate calculations determine the frequencies and forms of the normal vibrations for a given force field. They do not directly yield information about the relative infrared intensities of the fundamentals. The relative infrared intensities can, however, be estimated in the bond moment approximation with the aid of the eigenvectors obtained from the normal coordinate calculations. The assumptions (180,181) made in this approximation are, in addition to mechanical harmonicity, that a) when a bond is stretched by an amount dR a dipole moment $(\partial\mu/\partial R).dR$ is produced in the direction of the bond and b) when one bond is stretched no dipole moments are produced in the other bonds. For the present calculations on ices II and IX the further assumption was made that the dipole moment derivative $\partial\mu/\partial R$ was the same for all bonds, and that this value was equal to the value, 4.0 Debye/Å, determined for ice Ih by Ikawa and Maeda (182). The first two assumptions yield the total dipole moment change during a given vibration, $\partial\underline{\mu}/\partial Q_k$, as the vector sum of the dipole moment changes in the individual bonds, i.e.

$$\frac{\partial \mu}{\partial Q_k} = \sum_i \frac{\partial \mu}{\partial R_i} \frac{\partial R_i}{\partial Q_k} \qquad (16)$$

The third approximation yields

$$\frac{\partial \mu}{\partial Q_k} = \left|\frac{\partial \mu}{\partial R}\right| \sum_i \hat{u}_i \, l_{ik} \qquad (17)$$

where l_{ik} is the eigenvector element, $\partial R_i/\partial Q_k$, and $\hat{u}_i$ is a unit vector along O-D bond i from O to D. For Cartesian coordinates $\hat{u}_i$ is given by

$$\hat{u}_i = \frac{1}{L_i} \left[(X_{D_i} - X_{O_i}) \hat{i} + (Y_{D_i} - Y_{O_i}) \hat{j} + (Z_{D_i} - Z_{O_i}) \hat{k} \right]$$

$$= u_{ix}\hat{i} + u_{iy}\hat{j} + u_{iz}\hat{k} \qquad (18)$$

where L_i is the length of the i^{th} O-D bond and X_{D_i} Y_{D_i} Z_{D_i} and X_{O_i} Y_{O_i} Z_{O_i} are the Cartesian coordinates of the deuterium and oxygen atoms of the ith bond.

The components of $\partial\mu/\partial Q_k$ along the Cartesian axes are given by

$$\frac{\partial \mu_\alpha}{\partial Q_k} = \left|\frac{\partial \mu}{\partial R}\right| \sum_i u_{i\alpha} \, l_{ik} \qquad (19)$$

where α is x, y or z and the intensity of the vibration is proportional to

$$\left(\frac{\partial \mu}{\partial Q_k}\right)^2 = \left(\frac{\partial \mu_x}{\partial Q_k}\right)^2 + \left(\frac{\partial \mu_y}{\partial Q_k}\right)^2 + \left(\frac{\partial \mu_z}{\partial Q_k}\right)^2 \qquad (20)$$

The eigenvectors calculated by VSEC (179), Cartesian coordinates of the atoms (15,16) and the dipole moment derivative, $\partial\mu/\partial R = 4.0$ D/Å, were used in the program DMUDQ written by J.E. Bertie to calculate, by this method, the relative infrared intensities as $d_k(\partial\mu/\partial Q_k)^2$ where d_k is the degeneracy of the k^{th} vibration.

3.4.3 Force Fields used in the Normal Coordinate Calculations

The force fields used for ices II and IX were constructed using four types of force constants, O-D stretching force constants, intramolecular OD-OD interaction constants and two types of intermolecular OD-OD interaction constants.

The O-D stretching force constants were determined from the frequencies of the corresponding ν_{OD}(HDO) bands at 10 K, assuming that the O-D and O-H oscillators are not coupled and thus the observed frequencies corresponded to those of diatomic O-D vibrators. The assignment of the ν_{OD}(HDO) frequencies given in Section 3.3.2 was used.

The intramolecular OD-OD interaction constants were initially estimated from the work of Schiffer and Fifer on salt hydrates (123) to be about +0.08 mdyne/Å. Schiffer _et al_. have also presented two correlations (124) which allow the frequencies of the symmetric and antisymmetric O-D stretching vibrations of isolated D_2O molecules to be estimated from the ν_{OD}(HDO) frequencies. The D_2O frequencies were estimated from both correlations given in reference 124 and were then used to determine alternative intramolecular interaction constants. For ice II, both correlations yield values of 0.04 and -0.02 mdyne/Å for molecules D(1)-O(II)-D(3) and D(2)-O(I)-D(4), respectively, while for ice IX values of 0.03 and 0.01 or 0.01 and -0.01 mdyne/Å were determined for molecules D(5)-O(1)-D(6) and D(7)-O(2)-D(7), respectively.

The remaining force constants consist of two types of intermolecular interaction constants. The first type is for the configuration shown in Fig. 3.9a and describes the coupling of one O-D oscillator with another to which it is hydrogen bonded. This interaction constant has been determined for ice Ih (107) to be -0.123 mdyne/Å and for ice VIII (48) to be -0.01448 mdyne/Å. In ice Ih the O···O distance is 2.74 Å (10) whereas in ice VIII it is 2.965 Å (5). In ices II and IX the mean O···O distances are 2.80 and 2.77 Å, respectively, so values for this interaction constant in ices II and IX are expected to be close to that of ice Ih, -0.123 mdyne/Å. This value was adopted in some of the force fields in this work. Alternatively, values were calculated from the local geometry (see below). The second type of intermolecular interaction constant is for the configuration shown in Fig. 3.9b and describes the coupling of two O-D oscillators that are hydrogen bonded to the same oxygen atom. This coupling constant was assigned the value of 0.09 mdyne/Å or was calculated from the local geometry.

When an O-D bond is displaced, a dipole moment $(\partial\mu/\partial r)dr$ is produced, and the interaction energy between

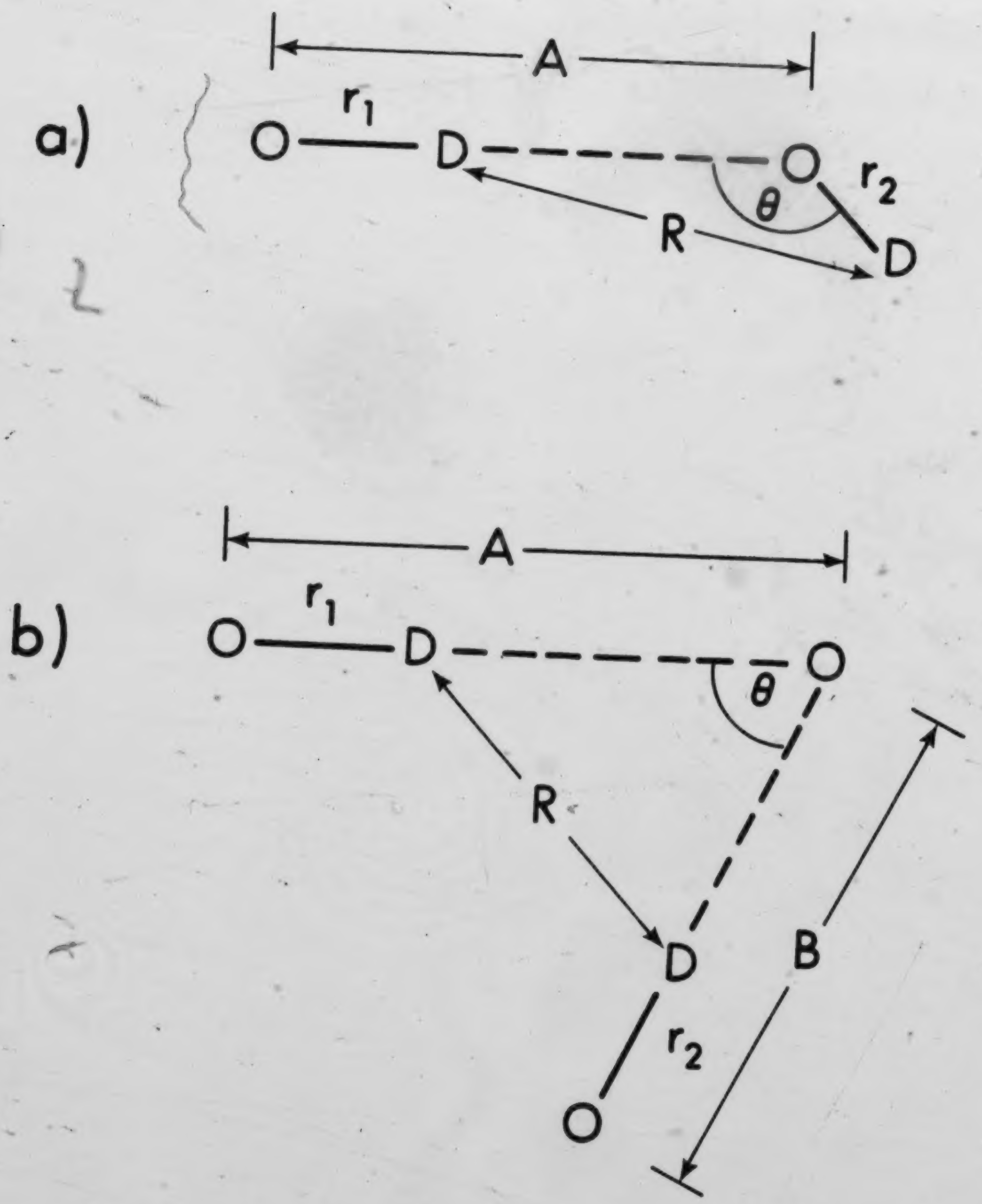
a)
A
O
r_1
D
O
r_2
θ
R
D
b)
A
O
r_1
D
O
θ
R
D
B
r_2
O

Figure 3.9. The configurations for the two types of intermolecular interaction force constants.

dipole moments produced in neighbouring bonds contribute to the potential energy. For ice Ih the dipole moment derivative with respect to the stretching of an O-D bond, $(\partial\mu/\partial r)$, is 4.0 D/Å (182). This can be regarded as equivalent to an effective charge, e^*, of 4.0×10^{-10} esu on the deuterium atom. The electrostatic contribution to the potential energy due to this effective charge on neighbouring deuterium atoms is given by

$$V(R) = \frac{e^{*2}}{R}\,, \qquad (21)$$

where R is the distance between two deuterium atoms. This distance is a function of the two O-D bond lengths. For the configuration shown in Fig. 3.9a this contribution to the potential energy is given by

$$V(R) = e^{*2}\left\{(A-r_1)^2 + r_2^{\,2} - 2\,(A-r_1)r_2\cos\theta\right\}^{-\frac{1}{2}} \qquad (22)$$

and for the configuration shown in Figure 3.9b by

$$V(R) = e^{*2}\left\{(A-r_1)^2 + (B-r_2)^2 - 2(A-r_1)(B-r_2)\cos\theta\right\}^{-\frac{1}{2}} \qquad (23)$$

The intermolecular interaction constant between r_1 and r_2 is given by

$$F_{12} = \frac{\partial^2 V(R)}{\partial r_1 \partial r_2} \qquad (24)$$

so that for the configuration shown in Fig. 3.9a

$$F_{12} = e^{*2}\,[3(r_1-A+r_2\cos\theta)(r_2-(A-r_1)\cos\theta)/R^5-\cos\theta/R^3]0.594 \tag{25}$$

and for the configuration shown in Fig. 3.9b

$$F'_{12} = e^{*2}\,[3(r_1-A+(B-r_2)\cos\theta)\,(r_2-B+(A-r_1)\cos\theta)/R^5+\cos\theta/R^3] \times 0.594 \tag{26}$$

The scaling factor 0.594 is the ratio of the experimental value of F_{12} for ice Ih (107) to the value calculated for ice Ih using equation (25) without the scaling factor. The configurations shown in Fig. 3.9 assume that the O-D···O bonds are linear. In ices II and IX the bonds do differ from linearity by as much as 9° (15,16). However, when the force constants are calculated using $\theta = \mathrm{D}\hat{\mathrm{O}}\mathrm{D}$ and $\theta = \mathrm{O}\hat{\mathrm{O}}\mathrm{O}$ very similar results are obtained. The force constants determined for ices II and IX using equations 25 and 26 are given in Sections 3.4.5 and 3.4.4, respectively.

3.4.4 Normal Coordinate Analysis of the $\underline{k}=0$ $\nu_{OD}(D_2O)$ Vibrations of Ice IX

The structure of ice IX, space group $P4_12_12$ (D_4^4), as viewed along the c axis is shown in Fig. 3.10. This figure shows the twelve molecules of one unit cell and sufficient molecules in the adjoining unit cells to clearly show the hydrogen bonded arrangement of the water molecules. The oxygen atoms are identified by the numbers in square

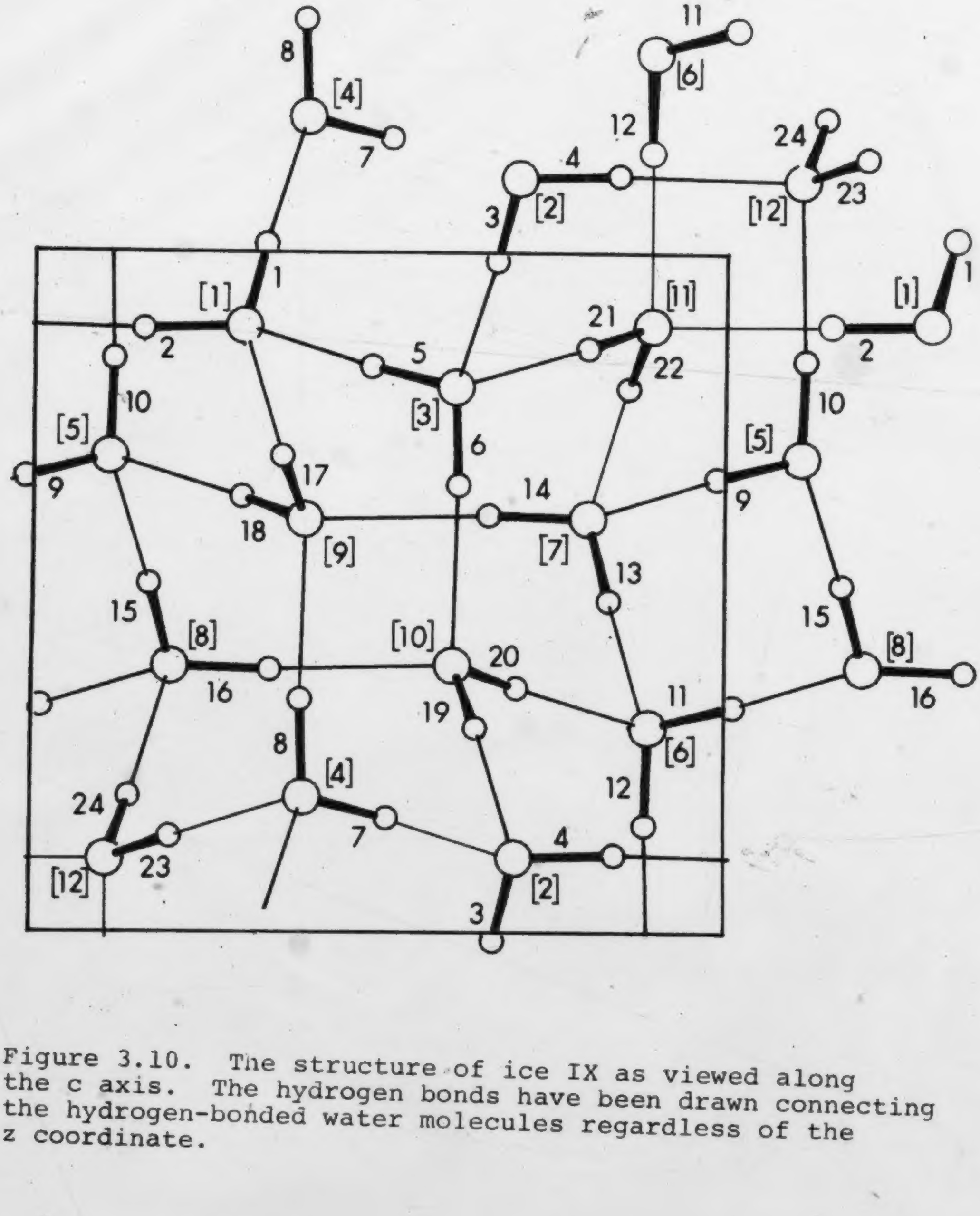
8
[4]
7
11
[6]
12
24
4
23
[12]
3
[2]
1
[1]
1
[1]
[11]
21
2
5
2
22
10
10
[3]
[5]
[5]
6
9
17
14
9
18
[9]
[7]
13
15
15
[8]
[10]
20
[8]
16
11
16
19
8
[4]
[6]
12
24
7
4
[12]
23
[2]
3

Figure 3.10. The structure of ice IX as viewed along the c axis. The hydrogen bonds have been drawn connecting the hydrogen-bonded water molecules regardless of the z coordinate.

brackets. Oxygen atoms [1] to [8] are on sites of C_1 symmetry and correspond to oxygen atoms O(1) in reference 15. Oxygen atoms [9] to [12] are on sites of C_2 symmetry and correspond to oxygen atoms O(2) in reference 15. The C_2' axes of the D_4 unit cell group are taken to be the two-fold screw axis of the space group (183) parallel to the a or b axes, and the C_2'' axes of the unit cell group are taken to be the two-fold axes through oxygen atoms [9] and [10] or [11] and [12]. The internal displacement coordinates are numbered in Fig. 3.10 and are listed and described in Table 3.5.

In order to describe the normal vibrations in terms of the symmetric and antisymmetric O-D stretching displacements of each type of water molecule, sets of equivalent symmetric and antisymmetric O-D stretching displacement coordinates were constructed from the internal displacement coordinates. For the water molecules of type D(5)-O(1)-D(6), the symmetric, s_1, and antisymmetric, as_1, O-D stretching displacements each form the representation $A_1+A_2+B_1+B_2+2E$ under the D_4 unit-cell group. For water molecules of the type D(7)-O(2)-D(7), the symmetric, s_2, O-D stretching displacements form the representation A_1+B_2+E and the antisymmetric, as_2, O-D stretching displacements form the representation A_2+B_1+E under the D_4 unit-cell group. These new sets of displacement coordinates were then used as bases for the construction of the symmetry coordinates (178). The Ea symmetry coordinates were constructed to be symmetric

TABLE 3.5

Internal Displacement Coordinates for Ice IX

Number	Designation	Description[a]	Type[b]
1	R_1	O_1-D_1	A
2	R_2	O_1-D_9	B
3	R_3	O_2-D_2	A
4	R_4	O_2-D_{10}	B
5	R_5	O_3-D_3	A
6	R_6	O_3-D_{11}	B
7	R_7	O_4-D_4	A
8	R_8	O_4-D_{12}	B
9	R_9	O_5-D_5	A
10	R_{10}	O_5-D_{13}	B
11	R_{11}	O_6-D_6	A
12	R_{12}	O_6-D_{14}	B
13	R_{13}	O_7-D_7	A
14	R_{14}	O_7-D_{15}	B
15	R_{15}	O_8-D_8	A
16	R_{16}	O_8-D_{16}	B
17	R_{17}	O_9-D_{17}	C
18	R_{18}	O_9-D_{21}	C
19	R_{19}	$O_{10}-D_{18}$	C
20	R_{20}	$O_{10}-D_{22}$	C
21	R_{21}	$O_{11}-D_{19}$	C

(continued......)

TABLE 3.5 (continued)

Number	Designation	Description[a]	Type[b]
22	R_{22}	$O_{11}-D_{23}$	C
23	R_{23}	$O_{12}-D_{20}$	C
24	R_{24}	$O_{12}-D_{24}$	C

a) The internal coordinates correspond to displacements of the specified bonds from their equilibrium length. The D atoms are not numbered in Figure 3.10, but D_1 to D_8 are of La Placa et al. (15) type D(5), D_9 to D_{16} are of type D(6) and D_{17} to D_{24} are of type D(7). The D atoms are numbered within each type in the order of the positions given in the International Tables of X-ray Crystallography (183).

b) Coordinate types A, B and C are displacements from equilibrium lengths of La Placa et al. (15) bond types O(1)-D(5), O(1)-D(6) and O(2)-D($\overline{7}$), respectively.

and the Eb symmetry coordinates to be antisymmetric to the C_2'' axis through oxygen atoms [9] and [10]. The symmetry coordinates are listed in Table 3.6, with the bases used for their construction.

The non-zero G matrix elements were calculated from the molecular geometries (15) using standard methods (100) and are given in Table 3.7.

The F matrix was constructed using the thirteen force constants listed in Table 3.8, with their description and the equivalent F matrix elements to which they correspond. The thirteen force constants were given various values in the calculations to yield different force fields. Fifteen force fields were used, four of which are given in Table 3.9.

For force field I, the intramolecular interaction constants were estimated from the work of Schiffer and Fifer (123), and for the remaining force fields values were determined from the correlations of Schiffer _et al_. (124). For force fields I to III, intermolecular interaction constants of the same type were given the same value (Section 3.4.3), while values were calculated for force field IV from equations 25 and 26 and the bond lengths and DOD angles given in reference 15.

The frequencies and relative infrared intensities calculated from these force fields and the experimental frequencies and relative infrared intensities are given in

TABLE 3.6

Symmetry Coordinates for Ice IX

Coordinate Number	Symmetry Coordinate	Basis
$S_1(A_1)$	$4^{-1}(R_1+R_2+R_3+R_4+R_5+R_6+R_7+R_8+R_9+R_{10}+R_{11}+R_{12}+R_{13}+R_{14}+R_{15}+R_{16})$	s_1
$S_2(A_1)$	$4^{-1}(R_1-R_2+R_3-R_4+R_5-R_6+R_7-R_8+R_9-R_{10}+R_{11}-R_{12}+R_{13}-R_{14}+R_{15}-R_{16})$	as_1
$S_3(A_1)$	$8^{-1/2}(R_{17}+R_{18}+R_{19}+R_{20}+R_{21}+R_{22}+R_{23}+R_{24})$	s_2
$S_4(A_2)$	$4^{-1}(R_1+R_2+R_3+R_4+R_5+R_6+R_7+R_8-R_9-R_{10}-R_{11}-R_{12}-R_{13}-R_{14}-R_{15}-R_{16})$	s_1
$S_5(A_2)$	$4^{-1}(R_1-R_2+R_3-R_4+R_5-R_6+R_7-R_8-R_9+R_{10}-R_{11}+R_{12}-R_{13}+R_{14}-R_{15}+R_{16})$	as_1
$S_6(A_2)$	$8^{-1/2}(R_{17}-R_{18}+R_{19}-R_{20}+R_{21}-R_{22}+R_{23}-R_{24})$	as_2
$S_7(B_1)$	$4^{-1}(R_1+R_2+R_3+R_4-R_5-R_6-R_7-R_8-R_9-R_{10}-R_{11}-R_{12}+R_{13}+R_{14}+R_{15}+R_{16})$	s_1
$S_8(B_1)$	$4^{-1}(R_1-R_2+R_3-R_4-R_5+R_6-R_7+R_8-R_9+R_{10}-R_{11}+R_{12}+R_{13}-R_{14}+R_{15}-R_{16})$	as_1
$S_9(B_1)$	$8^{-1/2}(R_{17}-R_{18}+R_{19}-R_{20}-R_{21}+R_{22}-R_{23}+R_{24})$	as_2
$S_{10}(B_2)$	$4^{-1}(R_1+R_2+R_3+R_4-R_5-R_6-R_7-R_8+R_9+R_{10}+R_{11}+R_{12}-R_{13}-R_{14}-R_{15}-R_{16})$	s_1
$S_{11}(B_2)$	$4^{-1}(R_1-R_2+R_3-R_4-R_5+R_6-R_7+R_8+R_9-R_{10}+R_{11}-R_{12}-R_{13}+R_{14}-R_{15}+R_{16})$	as_1
$S_{12}(B_2)$	$8^{-1/2}(R_{17}+R_{18}+R_{19}+R_{20}-R_{21}-R_{22}-R_{23}-R_{24})$	s_2
$S_{13}(Ea)$	$2^{-1}(R_{17}+R_{18}-R_{19}-R_{20})$	s_2

(continued......)

TABLE 3.6 (continued)

Coordinate Number	Symmetry Coordinate	Basis
S_{14}(Ea)	$2^{-1}(R_{21}-R_{22}-R_{23}+R_{24})$	as_2
S_{15}(Ea)	$4^{-1}(R_1+R_2-R_3-R_4+R_5+R_6-R_7-R_8+R_9+R_{10}-R_{11}-R_{12}-R_{13}-R_{14}+R_{15}+R_{16})$	s_1
S_{16}(Ea)	$4^{-1}(R_1+R_2-R_3-R_4-R_5-R_6+R_7+R_8+R_9+R_{10}-R_{11}-R_{12}+R_{13}+R_{14}-R_{15}-R_{16})$	s_1
S_{17}(Ea)	$4^{-1}(R_1-R_2-R_3+R_4+R_5-R_6-R_7+R_8+R_9-R_{10}-R_{11}+R_{12}-R_{13}+R_{14}+R_{15}-R_{16})$	as_1
S_{18}(Ea)	$4^{-1}(-R_1+R_2+R_3-R_4+R_5-R_6-R_7+R_8-R_9+R_{10}+R_{11}-R_{12}-R_{13}+R_{14}+R_{15}-R_{16})$	as_1
S_{19}(Eb)	$2^{-1}(-R_{21}-R_{22}+R_{23}+R_{24})$	s_2
S_{20}(Eb)	$2^{-1}(R_{17}-R_{18}-R_{19}+R_{20})$	as_2
S_{21}(Eb)	$4^{-1}(R_1+R_2-R_3-R_4-R_5-R_6+R_7+R_8-R_9-R_{10}+R_{11}+R_{12}-R_{13}-R_{14}+R_{15}+R_{16})$	s_1
S_{22}(Eb)	$4^{-1}(-R_1-R_2+R_3+R_4-R_5-R_6+R_7+R_8+R_9+R_{10}-R_{11}-R_{12}-R_{13}-R_{14}+R_{15}+R_{16})$	s_1
S_{23}(Eb)	$4^{-1}(R_1-R_2-R_3+R_4-R_5+R_6+R_7-R_8-R_9+R_{10}+R_{11}-R_{12}-R_{13}+R_{14}+R_{15}-R_{16})$	as_1
S_{24}(Eb)	$4^{-1}(R_1-R_2-R_3+R_4+R_5-R_6-R_7+R_8-R_9+R_{10}+R_{11}-R_{12}+R_{13}-R_{14}-R_{15}+R_{16})$	as_1

TABLE 3.7

Non-Zero $\underset{\sim}{G}$ Matrix Elements for D_2O Ice IX

Description	Equivalent Elements	Value[a]
G_{ii}	i = 1 to 24	0.559020
$G_{ij}(1)$	1,2; 3,4; 5,6; 7,8; 9,10; 11,12; 13,14; 15,16.	-0.017233
$G_{ij}(2)$	17,18; 19,20; 21,22; 23,24.	-0.015865

a) Units are in amu^{-1}.

TABLE 3.8

Non-Zero $\underset{\sim}{F}$ Matrix Elements for Ice IX

Force Constant	Type of Bond	Equivalent Elements[a]
F_1	O(1)-D(5)	1,1; 3,3; 5,5; 7,7; 9,9; 11,11; 13,13; 15,15.
F_2	O(1)-D(6)	2,2; 4,4; 6,6; 8,8; 10,10; 12,12; 14,14; 16,16.
F_3	O(2)-D(7)	17,17; 18,18; 19,19; 20,20; 21,21; 22,22; 23,23; 24,24.
F_4	D(5)-O(1)-D(6)	1,2; 3,4; 5,6; 7,8; 9,10; 11,12; 13,14; 15,16.
F_5	D(7)-O(2)-D(7)	17,18; 19,20; 21,22; 23,24.
F_6	O(1)-D(5)...O(1)-D(5)	1,5; 1,7; 3,5; 3,7; 9,13; 9,15; 11,13; 11,15.
F_7	O(1)-D(5)...O(1)-D(6)	1,8; 2,5; 3,6; 4,7; 9,14; 10,15; 11,16; 12,13.
F_8	O(2)-D(7)...O(1)-D(5)	1,17; 3,19; 5,21; 7,23; 9,18; 11,20; 13,22; 15,24.

(continued......)

TABLE 3.8 (continued)

Force Constant	Type of Bond	Equivalent Elements[a]
F_9	O(2)-D(7)...O(1)-D(6)	2,17; 4,19; 6,21; 8,23; 10,18; 12,20; 14,22; 16,24.
F_{10}	O(1)-D(6)...O(2)-D(7)'	2,21; 4,23; 6,19; 8,17; 10,24; 12,22; 14,18; 16,20.
F_{11}	O(1)-D(6)...O(2)-D(7)	2,22; 4,24; 6,20; 8,18; 10,23; 12,21; 14,17; 16,19.
F_{12}	O(1)-D(5)...O(1)...D(7)-O(2)	1,23; 3,21; 5,17; 7,19; 9,22; 11,24, 13,20; 15,18.
F_{13}	O(1)-D(6)...O(2)...D(6)-O(1)	2,12; 4,10; 6,16; 8,14.

---

a) The $\underset{\sim}{F}$ matrix is symmetric, so that its elements F_{ij} are only given for $i \leqslant j$.

TABLE 3.9

Force Fields Used for Ice IX

Force Constant[a]	Force Field I	II	III	IV
F_1	6.2950	6.2950	6.2950	6.2950
F_2	6.3053	6.3053	6.3053	6.3053
F_3	6.3518	6.3518	6.3518	6.3518
F_4	0.08	0.03	0.01	0.03
F_5	0.08	0.01	-0.01	0.01
F_6	-0.123	-0.123	-0.123	-0.118
F_7	-0.123	-0.123	-0.123	-0.106
F_8	-0.123	-0.123	-0.123	-0.122
F_9	-0.123	-0.123	-0.123	-0.120
F_{10}	-0.123	-0.123	-0.123	-0.110
F_{11}	-0.123	-0.123	-0.123	-0.118
F_{12}	0.09	0.09	0.09	0.074
F_{13}	0.09	0.09	0.09	0.080

a) Units are mdyne/Å.

TABLE 3.10

Comparison of the Observed and Calculated Frequencies[a] and Relative Infrared Intensities[b] of Ice IX

	Force Field				
Mode	I	II	III	IV	Experimental
$\nu_1(A_1)$	2529	2529	2530	2522	
$\nu_2(A_1)$	2416	2413	2412	2417	
$\nu_3(A_1)$	2349	2338	2334	2341	
$\nu_4(A_2)$	2487(17)	2499(19)	2503(19)	2496(24)	2499(51)
$\nu_5(A_2)$	2451(38)	2462(35)	2466(35)	2464(31)	2462(59)
$\nu_6(A_2)$	2361(4)	2352(4)	2348(4)	2357(4)	2348(67)
$\nu_7(B_1)$	2526	2531	2533	2527	
$\nu_8(B_1)$	2452	2463	2467	2468	
$\nu_9(B_1)$	2414	2412	2411	2412	
$\nu_{10}(B_2)$	2514	2516	2518	2513	
$\nu_{11}(B_2)$	2469	2462	2459	2457	
$\nu_{12}(B_2)$	2405	2398	2395	2401	

(continued......)

TABLE 3.10 (continued)

Mode	Force Field I	 II	 III	 IV	Experimental
ν_{13}(E)	2516(8)	2520(11)	2522(12)	2516(12)	2517(49)
ν_{14}(E)	2484(14)	2493(22)	2497(24)	2492(24)	2499(51)
ν_{15}(E)	2472(4)	2466(8)	2467(2)	2464(0.3)	2462(59)
ν_{16}(E)	2451(0.02)	2462(0.9)	2462(6)	2462(9)	
ν_{17}(E)	2397(56)	2391(51)	2389(49)	2395(48)	2403(61)
ν_{18}(E)	2367(67)	2356(64)	2353(63)	2360(65)	2348(67)

a) Units are cm^{-1}.

b) The relative infrared intensities are denoted by the number in brackets following the frequencies.

Table 3.10. The directions calculated for the dipole moment derivative with respect to normal coordinate $(\partial\mu/\partial Q_k)$ were, correctly, along the c axis for the A_2 vibrations and in the ab plane for the E vibrations.

From Tables 3.9 and 3.10 it can be seen that the calculated frequencies and intensities are insensitive to small changes in the intermolecular interaction constants (c.f. Force Fields II and IV) and in the intramolecular interaction constants (c.f. Force Fields II and III). Further, when the intramolecular interaction constants were varied from 0.08 to -0.08 mdyne/Å, the relative frequencies, intensities and description of the normal vibrations remained essentially unchanged, except between 2440 and 2480 cm^{-1}.

The description of the normal vibrations of the unit cell in terms of the symmetric and antisymmetric O-D stretching displacements of the individual water molecules is provided by the symmetrized eigenvectors. The symmetrized eigenvectors calculated for Force Field III are given in the Appendix and the assignment is summarized in Table 3.11. From Table 3.11 it can be seen that there is extensive mixing of the symmetric and antisymmetric stretching displacements of the individual molecules in the normal vibrations of the unit cell, and that only three normal vibrations can be described as either purely symmetric or purely antisymmetric stretching vibrations. These are $\nu_3(A_1)$ which is

TABLE 3.11

Symmetrized Eigenvector Elements for Ice IX

Mode	Frequency (cm^{-1})	Assignment[a]
$\nu_1(A_1)$	2530	$0.2s_1 - 0.4s_2 - 0.6as_1$
$\nu_2(A_1)$	2412	$0.3s_1 - 0.5s_2 + 0.4as_1$
$\nu_3(A_1)$	2334	$0.6s_1 + 0.4s_2$
$\nu_4(A_2)$	2503	$0.1s_1 - 0.3as_1 - 0.7as_2$
$\nu_5(A_2)$	2466	$0.7as_1 - 0.4as_2$
$\nu_6(A_2)$	2348	$0.7s_1 + 0.1as_1 + 0.1as_2$
$\nu_7(B_1)$	2533	$0.4s_1 + 0.3as_1 - 0.6as_2$
$\nu_8(B_1)$	2467	$0.6as_1 + 0.4as_2$
$\nu_9(B_1)$	2411	$0.6s_1 - 0.3as_1 + 0.3as_2$
$\nu_{10}(B_2)$	2518	$0.2s_1 - 0.3s_2 + 0.6as_1$
$\nu_{11}(B_2)$	2459	$-0.7s_1 + 0.2as_1$
$\nu_{12}(B_2)$	2395	$0.7s_2 + 0.3as_1$
$\nu_{13}(E)$	2522	$0.5s_1 + 0.2s_2 - 0.4as_1 - 0.5as_2$
$\nu_{14}(E)$	2497	$0.1s_1 + 0.1s_2 - 0.9as_1 + 0.3as_2$
$\nu_{15}(E)$	2467	$0.2s_1 - 0.2s_2 - 0.8as_1 - 0.4as_2$
$\nu_{16}(E)$	2462	$-0.5s_1 + 0.5s_2 + 0.5as_1$
$\nu_{17}(E)$	2389	$-0.7s_1 - 0.2as_1 - 0.2as_2$
$\nu_{18}(E)$	2353	$0.5s_1 + 0.5s_2 + 0.2as_1$

a) Symmetrized eigenvector elements, $\partial S_i/\partial Q_k$, where S_i is the symmetry coordinate and is denoted by the basis used for its construction. Only those symmetrized eigenvector elements that exceed 0.06 have been included. For each E mode, there are two symmetry coordinates constructed from each of the s_1 and as_1 bases, and the magnitude of the corresponding symmetrized eigenvector elements from the same basis have been added.

a symmetric stretching vibration and $\nu_5(A_2)$ and $\nu_8(B_1)$ which are antisymmetric stretching vibrations.

The separate effects of intra- and intermolecular coupling on the $\nu_{OD}(D_2O)$ vibrations cannot be investigated experimentally. They can, however, be investigated quite simply in the present normal coordinate calculations, by the successive introduction of the different types of interaction constants into the force fields. The results of such an analysis for force field III are shown diagramatically in Fig. 3.11. Line spectrum 1 depicts the ν_{OD}(HDO) frequencies, that is the absorption frequencies by the three types of O-D oscillators uninfluenced by intra - or intermolecular coupling. Line spectrum 2 was calculated using force constants F_1 to F_5 (Table 3.9) of force field III and shows the absorption frequencies of intramolecularly coupled but intermolecularly uncoupled O-D oscillators. Line spectrum 3 was calculated using force constants F_1 to F_{11} of force field III and shows the absorption frequencies of O-D vibrators that are intramolecularly coupled and also intermolecularly coupled to the O-D oscillators to which they are hydrogen bonded. Line spectrum 4 shows the absorption frequencies calculated from force field III.

When no intermolecular coupling is present the normal vibrations of one unit cell can be described in terms of the purely symmetric or antisymmetric stretching vibrations of the water molecules, however, when intermolecular coupling is present there is extensive mixing of the

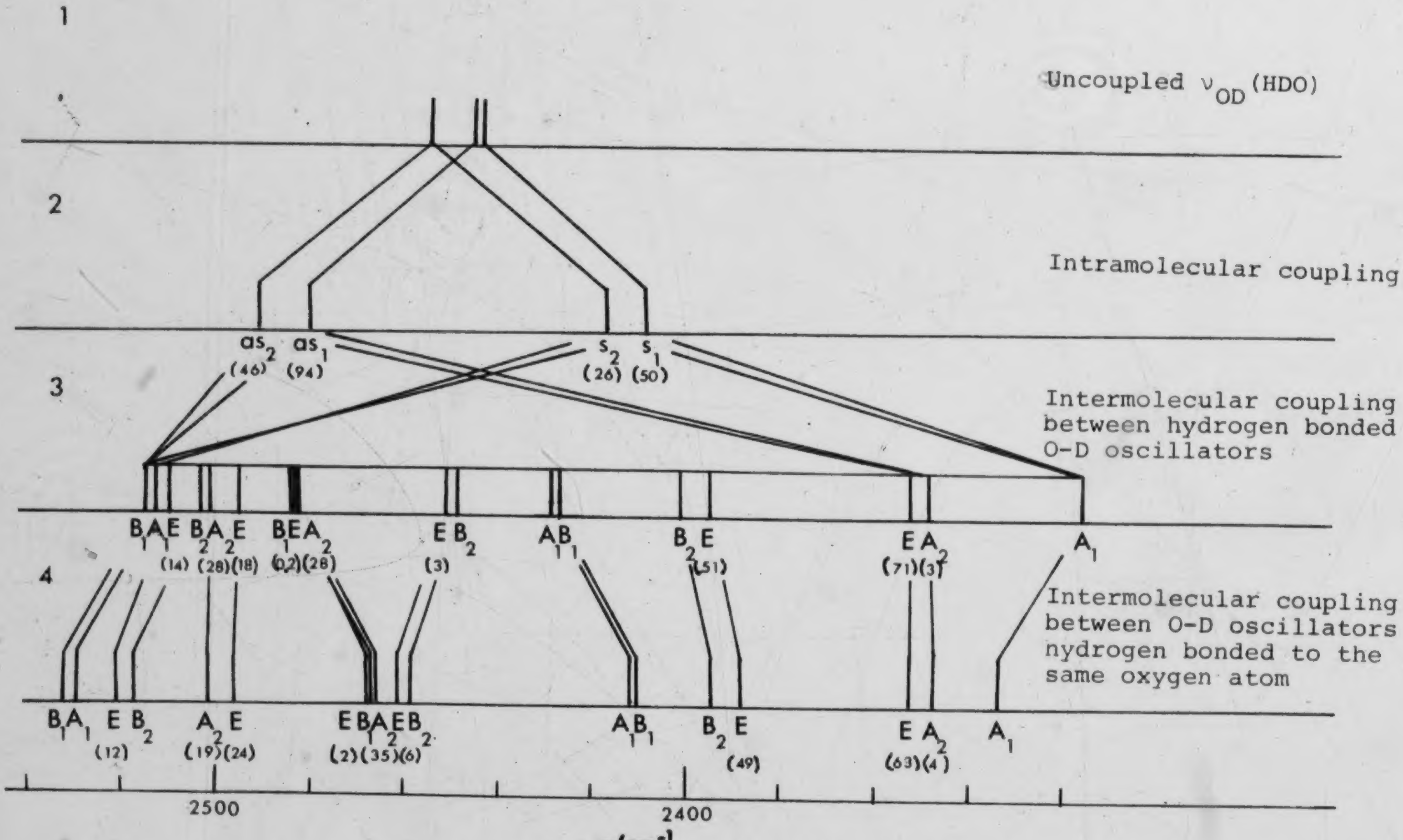
1
2
3
4
Uncoupled ν_{OD}(HDO)
Intramolecular coupling
Intermolecular coupling between hydrogen bonded O-D oscillators
Intermolecular coupling between O-D oscillators hydrogen bonded to the same oxygen atom
as_2 as_1 s_2 s_1
(46) (94) (26) (50)
B_1A_1E B_2A_2E B_1EA_2 EB_2 A_1B_1 B_2E EA_2 A_1
(14) (28)(18) (0.2)(28) (3) (51) (71)(3)
B_1A_1 E B_2 A_2E $EB_1A_2EB_2$ A_1B_1 B_2E EA_2 A_1
(12) (19)(24) (2)(35)(6) (49) (63)(4)
2500
2400
ν/cm^{-1}

Figure 3.11. Effect of intramolecular and intermolecular coupling on the ν_{OD}(D_2O) vibrations of ice IX.

symmetric and antisymmetric O-D stretching vibrations of the different water molecules. The extent of the contributions of the symmetric and antisymmetric stretching vibrations of the water molecules to the normal vibrations is shown in Figure 3.11 by the lines drawn from line spectrum 2 to line spectrum 3. The description of the normal vibrations in ice IX, in terms of either symmetric or antisymmetric O-D stretching vibrations of the water molecules, can be seen to be not that useful due to the effects of intermolecular coupling.

The results of force fields II to IV are in excellent agreement with the observed spectrum. This is shown clearly in Table 3.10 and in Fig. 3.12 which compares the observed spectrum with the results calculated from force field IV which are drawn as a line spectrum under the assumption that transitions separated by less than 5 cm^{-1} are unresolved. All of the observed features can be assigned to the $\underline{k}=0$ fundamental transitions and the calculated relative infrared intensities agree with the observed intensity distribution of the $\nu_{OD}(D_2O)$ band. The calculated results are also in good agreement with the Raman spectrum of ice IX at 100 K (111), in which the strongest peak is at 2327 cm^{-1} and can be assigned to $\nu_3(A_1)$ which is the only vibration that involves only the symmetric stretching of the water molecules (Table 3.11). A weaker peak is also observed at 2457 cm^{-1} for which several assignments are possible.

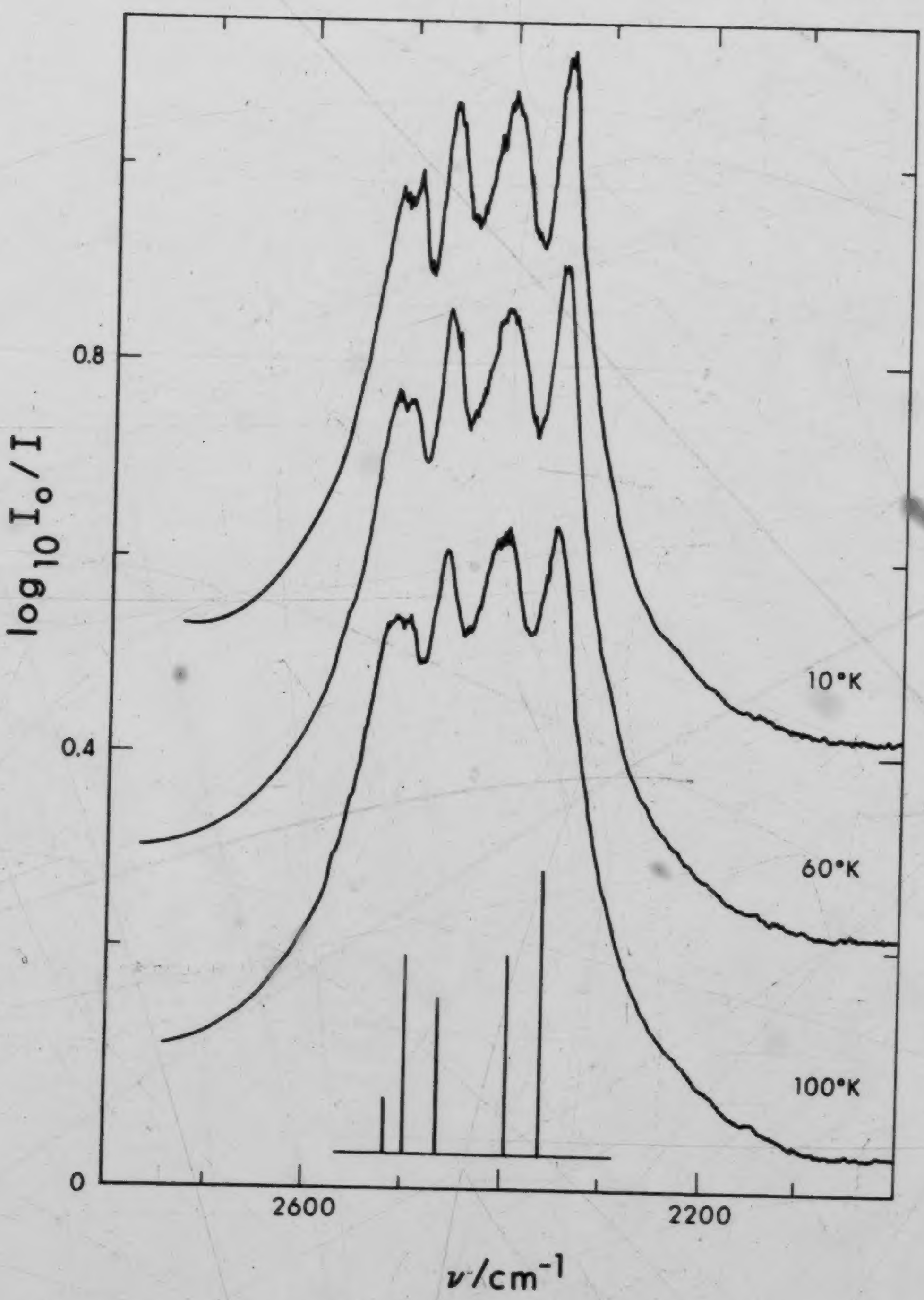

Figure 3.12. Comparison of the calculated and observed $\nu_{OD}(D_2O)$ band of ice IX.

3.4.5 Normal Coordinate Analysis of the $\underline{\underline{k}}=0$ $\nu_{OD}(D_2O)$ Vibrations of Ice II

The structure of ice II, space group $R\bar{3}$ (C_{3i}^{2}), viewed along the hexagonal c axis is shown in Fig. 3.13. There are twelve molecules in the rhombohedral unit cell and the rhomohedral axes are shown. Fig. 3.13 shows sufficient molecules to clearly define the hydrogen bonded arrangement of the water molecules. The oxygen atoms are identified by the numbers in square brackets and all oxygen atoms are on sites of C_1 symmetry. Oxygen atoms O[1] to O[6] form hexagonal rings around the corners of the rhombohedral unit cell and correspond to oxygen atoms O(I) in reference 16. Oxygen atoms O[7] to O[12] form hexagonal rings around the unit cell centre and correspond to oxygen atoms O(II) in reference 16. The internal displacement coordinates are numbered in Fig. 3.13 and are listed, and described in Table 3.12.

As described above for ice IX, sets of equivalent symmetric and antisymmetric O-D stretching displacement coordinates were constructed for the two types of molecule from the internal displacement coordinates. For each type of molecule, D(2)-O(I)-D(4) or D(1)-O(II)-D(3), the symmetric, s_1 or s_2, and antisymmetric, as_1 or as_2, O-D stretching displacements each form the representation $A_g+A_u+E_g+E_u$ under the S_6 unit-cell-group. The symmetry coordinates, constructed from the new sets of displacement coordinates (178), are listed with the bases used for their

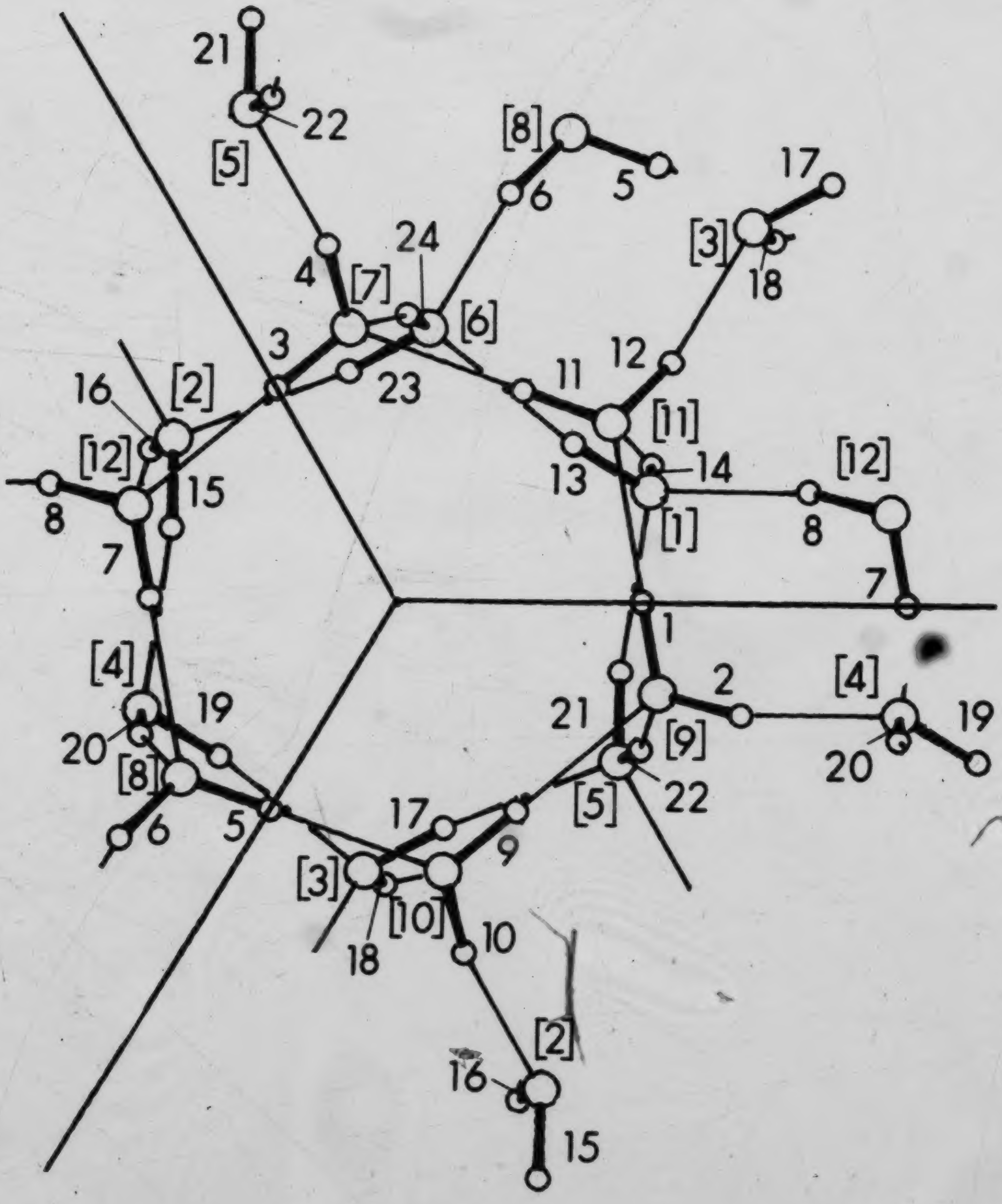
21
22
[5]
[8]
6
5
17
[3]
18
24
4
[7]
[6]
3
12
11
23
16
[2]
[11]
14
[12]
15
13
[1]
8
[12]
8
7
7
1
[4]
2
[4]
19
21
[9]
20
19
20
[8]
[5]
22
6
5
17
9
[3]
[10]
10
18
[2]
16
15

Figure 3.13. The structure of ice II as viewed along the hexagonal c axis.

TABLE 3.12

Internal Displacement Coordinates for Ice II

Number	Designation	Description[a]	Type[b]
1	R_1	O_9-D_1	A
2	R_2	O_9-D_{13}	B
3	R_3	O_7-D_2	A
4	R_4	O_7-D_{14}	B
5	R_5	O_8-D_3	A
6	R_6	O_8-D_{15}	B
7	R_7	O_{12}-D_4	A
8	R_8	O_{12}-D_{16}	B
9	R_9	O_{10}-D_5	A
10	R_{10}	O_{10}-D_{17}	B
11	R_{11}	O_{11}-D_6	A
12	R_{12}	O_{11}-D_{18}	B
13	R_{13}	O_1-D_7	C
14	R_{14}	O_1-D_{19}	D
15	R_{15}	O_2-D_8	C
16	R_{16}	O_2-D_{20}	D
17	R_{17}	O_3-D_9	C
18	R_{18}	O_3-D_{21}	D
19	R_{19}	O_4-D_{10}	C
20	R_{20}	O_4-D_{22}	D
21	R_{21}	O_5-D_{11}	C
22	R_{22}	O_5-D_{23}	D

(continued......)

TABLE 3.12 (continued)

Number	Designation	Description[a]	Type[b]
23	R_{23}	O_6-D_{12}	C
24	R_{24}	O_6-D_{24}	D

---

a) The internal coordinates correspond to displacements of the specified bonds from their equilibrium length. The D atoms are not numbered in Figure 3.13, but D_1 to D_6 are of Kamb et al. (16) type D(1), D_7 to D_{12} are of type D(2), D_{13} to D_{18} are of type D(3) and D_{19} to D_{24} are of type D(4). The D atoms are numbered within each type in the order of the positions given in the International Tables of X-ray Crystallography (183).

b) Coordinate types A, B, C and D are displacements from equilibrium lengths of Kamb et al. (16) bond types O(II)-D(1), O(II)-D(3), O(I)-D(2) and O(I)-D(4), respectively.

construction in Table 3.13.

S_6 is a cyclic group, so that each of the symbols E_g and E_u indicates two one-dimensional representations, whose characters for a given symmetry operation are the complex conjugates of each other, rather than indicating a two dimensional representation (178). To construct eight E_g and eight E_u symmetry coordinates real characters, c_1 and c_2, were obtained for each symmetry operation for each representation E_g and E_u, by taking $c_1 = (c+c^*)$ and $c_2 = \frac{1}{i}(c-c^*)$, where $i = \sqrt{-1}$ and c and c^* are the complex characters (178) for the given symmetry operation.

For noncyclic groups, such as the group D_4 of ice IX, Ea and Eb symmetry coordinates can be constructed, such that they behave differently with respect to some symmetry operation whose character for the E representation is zero. As a consequence the $\underset{\sim}{G}_s$ and $\underset{\sim}{F}_s$ matrices (Section 3.4.1) factor into two identical blocks, corresponding to Ea and Eb symmetry coordinates. Identical answers are obtained from the diagonalization of the two corresponding $\underset{\sim}{G}_s\underset{\sim}{F}_s$ matrix blocks, and only Ea or Eb symmetry coordinates contribute to each E normal coordinate. For cyclic groups, there is no symmetry operation which distinguishes Ea from E_b coordinates. Thus for ice II, although eight E_u or E_g symmetry coordinates can be constructed using the c_1 and c_2 characters, the $\underset{\sim}{G}_s$ and $\underset{\sim}{F}_s$ matrices are not factored into identical 4x4 blocks corresponding to Ea or Eb

TABLE 3.13

Symmetry Coordinates for Ice II

Coordinate Number	Symmetry Coordinate	Basis
$S_1(A_g)$	$12^{-1/2}(R_1+R_2+R_3+R_4+R_5+R_6+R_7+R_8+R_9+R_{10}+R_{11}+R_{12})$	s_2
$S_2(A_g)$	$12^{-1/2}(R_1-R_2+R_3-R_4+R_5-R_6+R_7-R_8+R_9-R_{10}+R_{11}-R_{12})$	as_2
$S_3(A_g)$	$12^{-1/2}(R_{13}+R_{14}+R_{15}+R_{16}+R_{17}+R_{18}+R_{19}+R_{20}+R_{21}+R_{22}+R_{23}+R_{24})$	s_1
$S_4(A_g)$	$12^{-1/2}(R_{13}-R_{14}+R_{15}-R_{16}+R_{17}-R_{18}+R_{19}-R_{20}+R_{21}-R_{22}+R_{23}-R_{24})$	as_2
$S_5(A_u)$	$12^{-1/2}(R_1+R_2+R_3+R_4+R_5+R_6-R_7-R_8-R_9-R_{10}-R_{11}-R_{12})$	s_2
$S_6(A_u)$	$12^{-1/2}(R_1-R_2+R_3-R_4+R_5-R_6-R_7+R_8-R_9+R_{10}-R_{11}+R_{12})$	as_2
$S_7(A_u)$	$12^{-1/2}(R_{13}+R_{14}+R_{15}+R_{16}+R_{17}+R_{18}-R_{19}-R_{20}-R_{21}-R_{22}-R_{23}-R_{24})$	s_1
$S_8(A_u)$	$12^{-1/2}(R_{13}-R_{14}+R_{15}-R_{16}+R_{17}-R_{18}-R_{19}+R_{20}-R_{21}+R_{22}-R_{23}+R_{24})$	as_1
$S_9(E_g)$	$24^{-1/2}(2R_1+2R_2-R_3-R_4-R_5-R_6+2R_7+2R_8-R_9-R_{10}-R_{11}-R_{12})$	s_2
$S_{10}(E_g)$	$8^{-1/2}(R_3-R_4-R_5+R_6+R_9-R_{10}-R_{11}+R_{12})$	as_2
$S_{11}(E_g)$	$24^{-1/2}(2R_{13}+2R_{14}-R_{15}-R_{16}-R_{17}-R_{18}+2R_{19}+2R_{20}-R_{21}-R_{22}-R_{23}-R_{24})$	s_1
$S_{12}(E_g)$	$8^{-1/2}(R_{15}-R_{16}-R_{17}+R_{18}+R_{21}-R_{22}-R_{23}+R_{24})$	as_1
$S_{13}(E_g)$	$8^{-1/2}(R_3+R_4-R_5-R_6+R_9+R_{10}-R_{11}-R_{12})$	s_2

(continued......)

TABLE 3.13 (continued)

Coordinate Number	Symmetry Coordinate	Basis
$S_{14}(E_g)$	$24^{-\frac{1}{2}}(2R_1-2R_2-R_3+R_4-R_5+R_6+2R_7-2R_8-R_9+R_{10}-R_{11}+R_{12})$	as_2
$S_{15}(E_g)$	$8^{-\frac{1}{2}}(R_{15}+R_{16}-R_{17}-R_{18}+R_{21}+R_{22}-R_{23}-R_{24})$	s_1
$S_{16}(E_g)$	$24^{-\frac{1}{2}}(2R_{13}-2R_{14}-R_{15}+R_{16}-R_{17}+R_{18}+2R_{19}-2R_{20}-R_{21}+R_{22}-R_{23}+R_{24})$	as_1
$S_{17}(E_u)$	$24^{-\frac{1}{2}}(2R_1+2R_2-R_3-R_4-R_5-R_6-2R_7-2R_8+R_9+R_{10}+R_{11}+R_{12})$	s_2
$S_{18}(E_u)$	$8^{-\frac{1}{2}}(R_3-R_4-R_5+R_6-R_9+R_{10}+R_{11}-R_{12})$	as_2
$S_{19}(E_u)$	$24^{-\frac{1}{2}}(2R_{13}+2R_{14}-R_{15}-R_{16}-R_{17}-R_{18}-2R_{19}-2R_{20}+R_{21}+R_{22}+R_{23}+R_{24})$	s_1
$S_{20}(E_u)$	$8^{-\frac{1}{2}}(R_{15}-R_{16}-R_{17}+R_{18}-R_{21}+R_{22}+R_{23}-R_{24})$	as_1
$S_{21}(E_u)$	$8^{-\frac{1}{2}}(R_3+R_4-R_5-R_6-R_9-R_{10}+R_{11}+R_{12})$	s_2
$S_{22}(E_u)$	$24^{-\frac{1}{2}}(2R_1-2R_2-R_3+R_4-R_5+R_6-2R_7+2R_8+R_9-R_{10}+R_{11}-R_{12})$	as_2
$S_{23}(E_u)$	$8^{-\frac{1}{2}}(R_{15}+R_{16}-R_{17}-R_{18}-R_{21}-R_{22}+R_{23}+R_{24})$	s_1
$S_{24}(E_u)$	$24^{-\frac{1}{2}}(2R_{13}-2R_{14}-R_{15}+R_{16}-R_{17}+R_{18}-2R_{19}+2R_{20}+R_{21}-R_{22}+R_{23}-R_{24})$	as_1

symmetry coordinates, but contain 8x8 blocks. When the $\underset{\sim}{G}_s\underset{\sim}{F}_s$ matrix is diagonalized, four pairs of identical frequencies are obtained, and all eight symmetry coordinates contribute to each normal coordinate.

The non-zero G matrix elements were calculated from the molecular geometries (16), using standard methods (100) and are given in Table 3.14.

The $\underset{\sim}{F}$ matrix was constructed using the sixteen force constants, which are listed in Table 3.15 with their descriptions and the equivalent F matrix elements, to which they correspond. The sixteen force constants were given various values in the calculations to yield different force fields. Fifteen force fields were used, four of which are given in Table 3.16. The frequencies and relative infrared intensities, calculated from these force fields, are given in Table 3.17, together with the experimentally observed frequencies and infrared intensities. The directions calculated for the dipole moment derivative with respect to normal coordinates ($\partial\mu/\partial Q_k$) were, correctly, along the c axis of the hexagonal unit cell for the A_u vibrations and perpendicular to the c axis for the E_u vibrations.

The intramolecular force constants F_5 and F_6 were initially set to 0.08 mdyne/Å. However, the agreement between the observed and calculated frequencies was much improved when values of F_5 and F_6 that were calculated from the correlations of Schiffer et al. (124) were used, so the initial force field is not reproduced. For force field

TABLE 3.14

Non-Zero $\underset{\sim}{G}$ matrix elements for D_2O Ice II

Description	Equivalent Elements	Value[a]
G_{ii}	i = 1 to 24	0.559020
$G_{ij}(1)$	1,2; 3,4; 5,6; 7,8; 9,10; 11,12	-0.018904
$G_{ij}(2)$	13,14; 15,16; 17,18; 19,20; 21,22; 23,24	-0.014276

a) Units are in amu^{-1}.

TABLE 3.15

Non-Zero $\underset{\sim}{F}$ Matrix Elements for Ice II

Force Constant	Type of Bond	Equivalent Elements[a]
F_1	O(II)-D(1)	1,1; 3,3; 5,5; 7,7; 9,9; 11,11.
F_2	O(II)-D(3)	2,2; 4,4; 6,6; 8,8; 10,10; 12,12.
F_3	O(I)-D(2)	13,13; 15,15; 17,17; 19,19; 21,21; 23,23.
F_4	O(I)-D(4)	14,14; 16,16; 18,18; 20,20; 22,22; 24,24.
F_5	D(1)-O(II)-D(3)	1,2; 3,4; 5,6; 7,8; 9,10; 11,12.
F_6	D(2)-O(I)-D(4)	13,14; 15,16; 17,18; 19,20; 21,22; 23,24.
F_7	O(II)-D(1)...O(II)-D(1)	1,9; 1,11; 3,7; 3,11; 5,7; 5,9.
F_8	O(II)-D(1)...O(II)-D(3)	1,12; 2,9; 3,8; 4,11; 5,10; 6,7.
F_9	O(I)-D(4)...O(II)-D(1)	1,22; 3,24; 5,20; 7,16; 9,18; 11,14.
F_{10}	O(II)-D(3)...O(I)-D(2)	2,19; 4,21; 6,23; 8,13; 10,15; 12,17.
F_{11}	O(II)-D(3)...O(I)-D(4)	2,20; 4,22; 6,24; 8,14; 10,16; 12,18.
F_{12}	O(I)-D(4)...O(II)-D(3)	2,22; 4,24; 6,20; 8,16; 10,18; 12,14.
F_{13}	O(I)-D(2)...O(I)-D(4)	13,24; 14,21; 15,20; 16,23; 17,22; 18,19.

(continued......)

TABLE 3.15 (continued)

Force Constant	Type of Bond	Equivalent Elements[a]
F_{14}	O(I)-D(2)...O(I)-D(2)	13,21; 13,23; 15,19; 15,23; 17,19; 17,21.
F_{15}	O(I)-D(4)...O(II)...D(1)-O(II)	1,14; 3,16; 15,18; 7,20; 9,22; 11,24.
F_{16}	O(II)-D(3)...O(I)...D(2)-O(I)	2,15; 4,17; 6,13; 8,21; 10,23; 12,19.

---

a) The $\underset{\sim}{F}$ matrix is symmetric, so that its elements F_{ij} are only given for $i \leq j$.

TABLE 3.16

Force Fields Used for Ice II

Force Constant[a]	Force Field I	II	III	IV
F_1	6.3518	6.3518	6.3518	6.3518
F_2	6.5184	6.5184	6.5184	6.5184
F_3	6.4557	6.4557	6.4557	6.4557
F_4	6.3259	6.3259	6.3259	6.3259
F_5	0.04	0.04	0.11	0.056
F_6	-0.02	-0.02	0.013	-0.010
F_7	-0.123	-0.108	-0.100	-0.116
F_8	-0.123	-0.105	-0.100	-0.116
F_9	-0.123	-0.127	-0.160	-0.116
F_{10}	-0.123	-0.112	-0.100	-0.116
F_{11}	-0.123	-0.106	-0.100	-0.116
F_{12}	-0.123	-0.110	-0.100	-0.116
F_{13}	-0.123	-0.116	-0.180	-0.116
F_{14}	-0.123	-0.118	-0.180	-0.116
F_{15}	0.090	0.090	0.040	0.046
F_{16}	0.090	0.076	0.120	0.046

a) Units are mdyne/Å.

TABLE 3.17

Comparison of the Observed and Calculated Frequencies[a] and Relative Infrared Intensities[b] of Ice II

Mode	Force Field I	II	III	IV	Experimental
$\nu_1(A_g)$	2541	2534	2527	2532	
$\nu_2(A_g)$	2584	2487	2483	2490	
$\nu_3(A_g)$	2394	2398	2399	2403	
$\nu_4(A_g)$	2354	2360	2350	2353	
$\nu_5(A_u)$	2550(10)	2544(15)	2568(8)	2539(10)	~2550(sh)
$\nu_6(A_u)$	2527(12)	2522(9)	2517(11)	2518(10)	2524(55)
$\nu_7(A_u)$	2486(4)	2487(2)	2474(0.2)	2492(3)	2470(sh)
$\nu_8(A_u)$	2395(48)	2397(48)	2410(55)	2404(51)	2418(72)
$\nu_9(E_g)$	2552	2546	2554	2540	
$\nu_{10}(E_g)$	2503	2504	2494	2502	
$\nu_{11}(E_g)$	2442	2445	2454	2447	
$\nu_{12}(E_g)$	2416	2415	2416	2422	

(continued......)

TABLE 3.17 (continued)

Mode	Force Field				Experimental
	I	II	III	IV	
$\nu_{13}(E_u)$	2522(33)	2520(31)	2518(46)	2518(24)	2524(55)
$\nu_{14}(E_u)$	2503(21)	2502(26)	2494(6)	2501(31)	2501(sh)
$\nu_{15}(E_u)$	2426(28)	2428(26)	2431(20)	2427(21)	2418(72)
$\nu_{16}(E_u)$	2370(61)	2374(59)	2370(70)	2376(67)	2370(79)

a) Units are cm^{-1}.

b) The relative infrared intensities are denoted by the number in brackets following the frequencies. sh = shoulder.

I, intermolecular force constants of the same type were set equal and for force field II they were calculated from equations 25 and 26 and the bond lengths and DOD angles given in reference 16.

The symmetrized eigenvectors, calculated from force field II, are given in the Appendix and the assignment is summarized in Table 3.18. The water molecules of ice II are asymmetric and, unlike the situation in ice IX, the two O-D···O bond lengths of each water molecule differ significantly. Consequently, the vibrations of the individual water molecules, in the absence of intermolecular coupling, are not purely symmetric or antisymmetric O-D stretching vibrations, and the normal vibrations are a mixture of symmetric and antisymmetric O-D stretching displacements. Specifically, the normal vibrations of the water molecules D(2)-O(I)-D(4) are described by $0.7s_1+0.1as_1$ and $0.1s_1+0.7as_1$ and those of water molecules D(1)-O(II)-D(3) by $0.7s_2+0.2as_2$ and $0.1s_2-0.7as_2$, using the same description for the vibrations as given in Table 3.18. From Table 3.18 it can be seen that in the presence of intermolecular coupling the normal vibrations of the unit cell are generally more mixed than this and that only two vibrations can be described as either symmetric or antisymmetric stretching vibrations. These are $\nu_2(A_g)$ which is an antisymmetric stretching vibration and $\nu_4(A_g)$ which is a symmetric stretching vibration.

TABLE 3.18

Symmetrized Eigenvector Elements for Ice II

Mode	Frequency (cm^{-1})	Assignment[a]
$\nu_1(A_g)$	2534	$-0.1s_1 + 0.2s_2 + 0.4as_1 - 0.6as_2$
$\nu_2(A_g)$	2487	$0.6as_1 + 0.4as_2$
$\nu_3(A_g)$	2398	$0.5s_1 - 0.5s_2 + 0.1as_1 - 0.3as_2$
$\nu_4(A_g)$	2360	$0.6s_1 + 0.5s_2$
$\nu_5(A_u)$	2544	$0.5s_1 + 0.2s_2 + 0.4as_1 - 0.4as_2$
$\nu_6(A_u)$	2522	$0.2s_1 + 0.5s_2 - 0.4as_1 + 0.3as_2$
$\nu_7(A_u)$	2487	$0.1s_1 + 0.5as_1 + 0.6as_2$
$\nu_8(A_u)$	2397	$-0.5s_1 + 0.5s_2 + 0.3as_1$
$\nu_9(E_g)$	2546	$0.4s_1 + 0.4s_2 - 0.4as_1 + 0.5as_2$
$\nu_{10}(E_g)$	2504	$0.2s_1 + 0.2s_2 + 0.5as_1 + 0.5as_2$
$\nu_{11}(E_g)$	2445	$0.5s_1 + 0.6s_2 + 0.2as_1 + 0.3as_2$
$\nu_{12}(E_g)$	2415	$-0.7s_1 + 0.4s_2 - 0.5as_1 + 0.2as_2$
$\nu_{13}(E_u)$	2520	$0.1s_1 + 0.3s_2 + 0.4as_1 - 0.8as_2$
$\nu_{14}(E_u)$	2502	$0.2s_1 - 0.3s_2 + 0.7as_1 + 0.3as_2$
$\nu_{15}(E_u)$	2428	$0.6s_1 + 0.7s_2 + 0.2as_1 + 0.4as_2$
$\nu_{16}(E_u)$	2374	$0.6s_1 - 0.6s_2 + 0.2as_1 - 0.1as_2$

---

a) Symmetrized eigenvector elements, $\partial S_i/\partial Q_j$, where S_i is the symmetry coordinate and is denoted by the basis used for its construction. Only those symmetrized eigenvector elements that exceed 0.06 have been included. For the E_g and E_u normal coordinates, two symmetry coordinates, constructed from each basis, s_1, s_2, as_1 or as_2, contribute to each normal cordinate and the magnitude of these two contributions have been added to give the values given in the table.

The results calculated from force fields I and II are in reasonable agreement with the observed spectrum. This is shown in Table 3.17 and in Figure 3.14, which compares the observed spectrum with the results calculated from force field II, which are shown as line spectrum A, drawn under the assumption that transitions separated by less than 5 cm^{-1} are unresolved. The most serious discrepancy is the frequency of $\nu_8(A_u)$ which is calculated to be near the minimum at about 2400 cm^{-1} instead of contributing to the observed peak at 2418 cm^{-1}. Another discrepancy is that no vibration was calculated to be near the shoulder at 2470 cm^{-1}. The calculated results are in good agreement with the Raman spectrum of ice II at 100 K (111), in which the strongest peak is at 2353 cm^{-1} and can be assigned to $\nu_4(A_g)$ which is the only vibration that involves only the symmetric O-D stretching vibrations of the water molecules (Table 3.18). A weaker peak is also observed at 2489 cm^{-1} and can be assigned to $\nu_2(A_g)$ which is the only vibration that involves only the antisymmetric O-D stretching vibrations of the water molecules.

The program FPERT (179) was used in an attempt to force $\nu_8(A_u)$ to 2418 cm^{-1} and also to fit the shoulder observed at 2470 cm^{-1}. The number of force constants was reduced by setting F_7, F_8, F_{10}, F_{11} and F_{12} equal to each other and F_{13} equal to F_{14}. Observed frequencies were assigned to the following vibrations: $\nu_2(A_g)=2489$ cm^{-1},

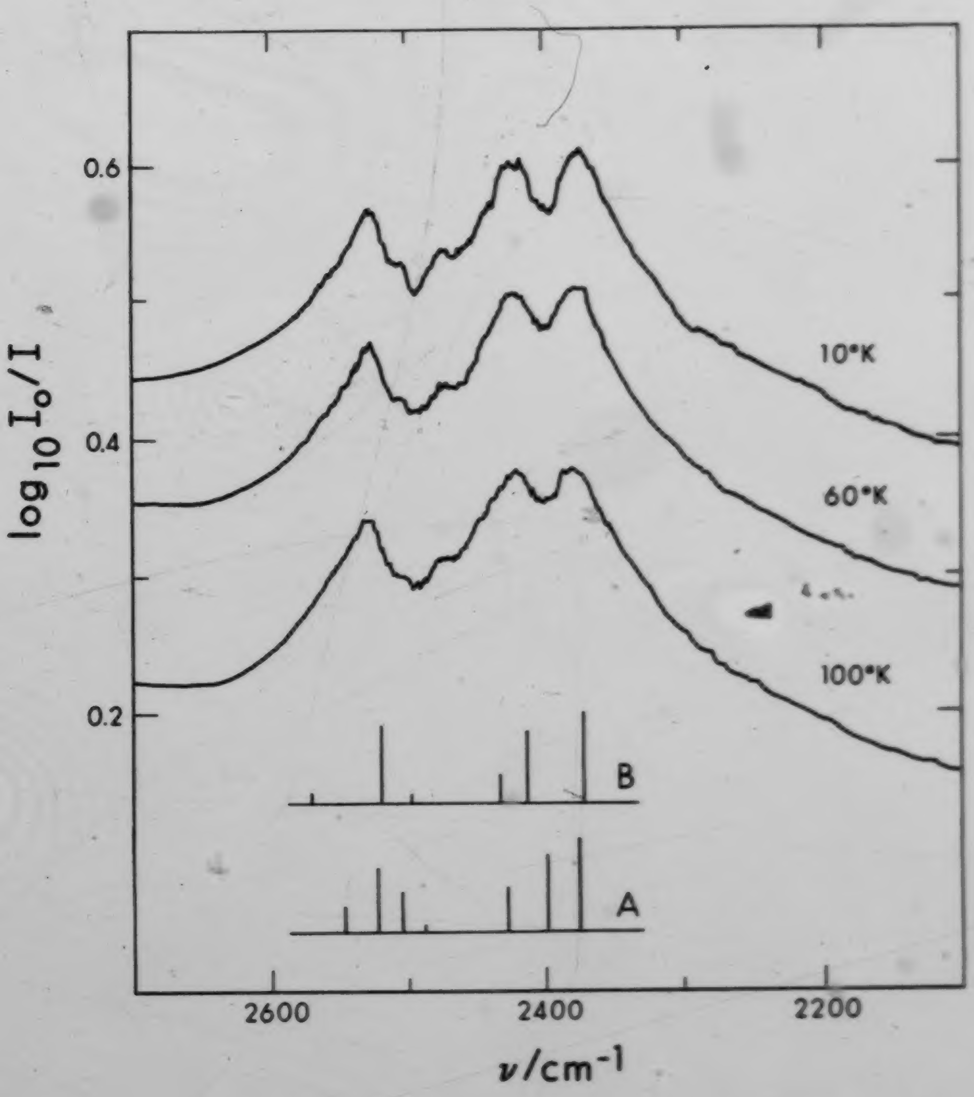

Figure 3.14. Comparison of the calculated and observed $\nu_{OD}(D_2O)$ band of ice II.

$\nu_4(A_g)=2353$ cm^{-1}, $\nu_6(A_u)=2524$ cm^{-1}, $\nu_7(A_u)=2470$, $\nu_8(A_u)=2418$ cm^{-1}, $\nu_{13}(E_u)=2524$ cm^{-1} and $\nu_{14}(E_u)=2501$ cm^{-1}. FPERT was then used to refine the intra- and intermolecular interaction constants with force field I as the initial force field.

A number of constraints were placed on the force constants. These constraints were, first, the intermolecular interaction constants F_5 and F_6 should have values between 0.1 and -0.04 mdyne/Å. Second, the intermolecular interaction constants F_7 to F_{14} should all be negative and greater than -0.2 mdyne/Å. Third, the intermolecular interaction constants F_{15} and F_{16} should be positive and less than 0.15 mdyne/Å. These constraints were satisfied by force field III given in Table 3.16. The results calculated from this force field are given in Table 3.17 and are also shown as line spectrum B in Fig. 3.15. The agreement between the observed and calculated frequencies and intensities is better than those for force fields I and II. Force field III did calculate $\nu_8(A_u)$ to be close to the strong peak at 2418 cm^{-1} and also $\nu_7(A_u)$ to be near to the observed shoulder at 2470 cm^{-1}, but the intensity of $\nu_7(A_u)$ was calculated to be essentially zero. There are, however, some discrepancies in force field III and it must remain suspect. The intramolecular interaction constant F_5 is considerably bigger than F_6, and it is also bigger than the largest value estimated from the work of Schiffer and Fifer on salt hydrates (123, Section 3.4.3), 0.08 mdyne/Å. Also, the intermolecular interaction constants of the same type (ie. F_7 and F_{13} or F_{15} and F_{16}) differ significantly (c.f. force fields II and III, Table 3.16).

Additional FPERT calculations were done with only eight force constants, by assigning F_7 through F_{14} the same value and setting F_{15} equal to F_{16}. Observed frequencies were assigned to the following vibrations: $\nu_2(A_g)=2489$ cm^{-1}, $\nu_4(A_g)=2353$ cm^{-1}, $\nu_6(A_u)=2524$ cm^{-1}, $\nu_8(A_u)=2418$ cm^{-1}, $\nu_{13}(E_u)=2524$ cm^{-1}, $\nu_{14}(E_u)=2501$ cm^{-1} and $\nu_{16}(E_u)=2370$ cm^{-1}. FPERT was then used to refine the intra- and intermolecular interaction constants with force field I as the initial force field. The force field obtained was force field IV of Table 3.16. The results calculated from this force field are given in Table 3.17 and are quite similar to those of force field II, except that $\nu_{14}(E_u)$ was calculated to be more intense than $\nu_{13}(E_u)$.

Although none of the force fields provided an ideal fit, the main features of the spectrum can be assigned. The strong peak at 2370 cm^{-1} is clearly due to $\nu_{16}(E_u)$, while the peak at 2418 cm^{-1} is probably mainly due to $\nu_8(A_u)$ with some contribution from $\nu_{15}(E_u)$. The peak at 2524 cm^{-1} is due to $\nu_6(A_u)$ and $\nu_{13}(E_u)$, the high frequency shoulder at 2550 cm^{-1} is due to $\nu_5(A_u)$ and the shoulder at 2501 cm^{-1} is due to $\nu_{14}(E_u)$. The only feature still to be assigned is the shoulder at 2470 cm^{-1} and the remaining vibration is $\nu_7(A_u)$. When this assignment is made (force field III), the intensity of $\nu_7(A_u)$ is essentially zero, so that either the intensity calculations are inaccurate, which is quite possible, or this feature cannot be assigned.

3.5 The Origin of the $\nu_{OD}(D_2O)$ and $\nu_R(D_2O)$ Bands of Ices II and IX

The $\nu_{OD}(D_2O)$ bands of ices II and IX at 10 K are broad with moderately sharp features superimposed (Section 3.3.1). The normal coordinate and intensity calculations show that these features are due to unit-cell-group allowed O-D stretching vibrations which have a wide range of frequencies, 2300 to 2550 cm^{-1}, due to the combined effects of nonequivalent sites and intra- and intermolecular coupling. The fundamental transitions of these vibrations should yield sharp absorption features and they have sufficiently different frequencies that the $\nu_{OD}(D_2O)$ bands would be much better resolved than is observed if they were due solely to fundamental transitions. Thus, the absorption by the fundamental transitions must be broadened by some mechanism.

Figs. 3.12 and 3.14 show that the features on the $\nu_{OD}(D_2O)$ bands are approximately symmetrical and, judging from the highest and lowest frequency features, the absorption extends to about 100 cm^{-1} away from each feature. Further, the breadth of each feature increases slightly and symmetrically with increasing temperature.

One possible broadening mechanism is the anharmonic interaction between the ν_{OD} vibrations and low frequency ν_L vibrations to give combination transitions of the type $\nu_{OD}+\nu_L$. An example of this broadening mechanism is found in the studies by Evans and Lo (165) of the dibromide ion, HBr_2^-. For ices II and IX the low frequency vibrations involved in the combination transitions must be the translational vibrations if the combination transitions are to absorb within 300 cm^{-1} of the $\nu_{OD}(D_2O)$ fundamentals (119). The combination transitions absorb to high frequency of the fundamental transitions, so the fundamental absorptions at 10 K should be broadened only on their high frequency sides by this mechanism. Further, the absorption due to the combination transitions should show features corresponding to the density of translational vibrational states (184) which could extend to about 250 cm^{-1} (119) from each fundamental absorption. At higher temperatures the fundamental absorption might also broaden on the low frequency side due to corresponding difference transitions, although this need not be the case (185). Clearly, this mechanism does not account for the broadening of the fundamental $\nu_{OD}(D_2O)$ absorption in the spectra of ices II and IX.

The broadening of the fundamental absorption can be explained by the enhancement of the intensity of transitions to overtone and combination levels of lower frequency vibrations by Fermi resonance (177) with the $\nu_{OD}(D_2O)$ fundamental levels. This mechanism requires that the overtone and combination levels are nearly degenerate with, and have the same symmetry as the fundamental levels. These requirements are easily met, since the overtone and combination levels of the low frequency vibrations must form a continuum of overtone and combination levels isoenergetic with the fundamentals because the fundamental $\nu_R(D_2O)$, $\nu_T(D_2O)$ and, probably, $\nu_2(D_2O)$ levels extend over a wide energy range themselves (37). The intensity of an overtone or combination transition is usually much weaker than that of a fundamental transition. However, Fermi resonance distributes the intensity of the fundamental transition over overtone and combination transitions to levels close to the fundamental level. Thus, Fermi resonance can readily explain the broadening of the fundamental absorption.

The same interpretation has been used to explain the broadening of the $\nu_{OD}(D_2O)$ and $\nu_{OH}(H_2O)$ features of hexamethylenetetramine hexahydrate (137). As noted for that system an obvious objection to this interpretation is that the fundamental ν_{OD}(HDO) absorption is sharp (Figs. 3.2 and 3.5) and, presumably, such a broadening mechanism should also apply to it. However, if the interaction which causes the Fermi resonance has a short range, the ν_{OD} fundamental level of a particular HDO molecule can only interact with combination and overtone levels due to vibrations of the same HDO molecule. There will not be a continuum of these overtone and combination levels if the vibrations of the HDO molecules do not couple with the continuum of vibrations of the surrounding H_2O molecules.

If the vibrations of the HDO molecules are localized or uncoupled from those of the surrounding H_2O or D_2O molecules, absorption by the HDO molecules must be observable superimposed on that by the H_2O or D_2O molecules. No differences are detectable in the far-infrared spectra of fully hydrated and partially deuterated samples of ices II and IX (119,186). Thus, the translational vibrations of the HDO molecules appear to couple with the translation vibrations of the H_2O molecules. On the other hand, the ν_R bands of partially deuterated samples of ices II and IX have additional features at 464 and 445 cm^{-1} for ice II and at 473 cm^{-1} for ice IX which are not observed for the fully hydrated samples (37). Thus, at least some of the $\nu_R(HDO)$ vibrations in ices II and IX do not couple with the $\nu_R(H_2O)$ vibrations. The ν_2 bands of ices II and IX are broad and relatively featureless and no differences have been detected in these bands for fully hydrated and partially deuterated samples (37). The ν_2 band of partially deuterated ice Ih does, however, have an additional feature at 1490 cm^{-1} which is not observed for fully hydrated samples (107). Thus at least some of the $\nu_2(HDO)$ vibrations in ice Ih do not couple with the $\nu_2(H_2O)$ vibrations. It is also probable that some of the ν_2(HDO) vibrations in ices II and IX do not couple with the $\nu_2(H_2O)$ vibrations. Therefore, in order to explain the broadening of $\nu_{OD}(D_2O)$ but not ν_{OD}(HDO) by the Fermi resonance mechanism, it is also necessary to postulate that the overtone and combination levels are due to ν_R and ν_2, but not ν_T.

Fermi resonance can also result in a phenomenon known as the Evans effect to create 'Evans' holes' or 'Fermi resonance minima' (187-189). This results from essentially the reverse of the Fermi resonance process described above. Suppose there is a single energy level, e.g. a fundamental level, with the same energy as a broad distribution of levels, such as combination levels and that the transitions from the ground state to the broad distribution of levels yields a broad, moderately intense absorption band while the transition from the ground state to the single level yields a very weak absorption band, in the zeroth approximation. Fermi resonance between the single level and the distribution of levels can then cause an absorption minimum to appear at the frequency of the zeroth order transition to the single level. This loss in absorption intensity is redistributed on either side of the absorption minimum, and can lead to nearby regions of increased intensity (189). Such effects have been observed in the spectra of crystalline hydrates (190) and other hydrogen bonded solids (191,192) and the presence of these effects has been used to explain the multiple maxima observed in the ν_{OH} or ν_{OD} bands of strongly hydrogen bonded systems (193,194). A good case can be made that the minima at 2490 cm^{-1} (Fig. 3.14) in the $\nu_{OD}(D_2O)$ band of ice II at 10 K is due to the Evans effect. $\nu_7(A_u)$ was earlier (Section 3.4.5) tentatively assigned to the shoulder at 2470 cm^{-1}. However its intensity was calculated to be small for all force fields, and its frequency was calculated to be 2490±5 cm^{-1} for all force fields except force field III which yielded 2474 cm^{-1}. Thus, in view of the interpretation of the breadth of the features as due to the enhancement of the intensity of overtone and combination transitions by Fermi resonance between the fundamental ν_{OD} levels and the overtone and combination levels, a second possible assignment for $\nu_7(A_u)$ is the minimum at 2490 cm^{-1}.

There is less evidence on which to draw conclusions about the origin of the $\nu_R(D_2O)$ bands. Unit-cell-group analyses (Section 1.4) predict twelve infrared active ν_R vibrations for ice II and fourteen for ice IX, and undoubtedly these are the origin of most if not all of the twelve fairly sharp features observed for ice II and the ten fairly sharp features observed for ice IX. However, even at 10 K, some of the features are broader than those of the ν_T bands (119) and underlying the features is a broad absorption. The most probable origin of this breadth is transitions to overtone and combination levels involving the $\nu_R(D_2O)$ and $\nu_T(D_2O)$ vibrations that are enhanced in intensity by Fermi resonance between the overtone and combination states and the $\nu_R(D_2O)$ fundamental states.

Chapter Four. Results of the Study of the Clathrate Hydrates

4.1 Introduction

This chapter presents the results of the studies of the mid-infrared absorption spectra of cyclopropane hydrate I and ethylene oxide hydrate at temperatures to 45 K, which were introduced in Section 1.8. The results of a far more limited study of cyclopropane hydrate II are also reported.

The mid-infrared samples were prepared by either mixing the finely ground hydrate samples with mulling agents, as described in Section 2.7.2, or by dispersing the hydrate samples in potassium bromide pellets, as described in Section 2.8.2. A potassium bromide pellet has two main advantages over a mull as a sampling medium. Potassium bromide does not absorb in the mid-infrared spectral region, and spectra of pellets can be obtained over a wide temperature range. There can be some uncertainty, though, in the nature of these pellet samples, due to the high pressure and relatively high temperatures used to prepare the pellets (2). It is important, therefore, to compare spectra obtained from pellet samples with those obtained from samples prepared by less drastic methods, such as the mulling technique.

Cyclopropane hydrate I and hydrate II were prepared as described in Sections 2.3 and 2.4, respectively. The characterization of cyclopropane hydrate I and ethylene oxide hydrate is discussed in Section 4.2. The characterization and limited spectroscopic study of cyclopropane hydrate II is reported in Section 4.3. Spectra of cyclopropane hydrate I at 90±5 K were initially recorded using the low temperature mulling technique, and these spectra are presented in Section 4.4. In Section 4.5, the temperature dependence of the absorption by cyclopropane hydrate I in potassium bromide pellets is reported, and the validity of these results is determined by comparison of the spectra of pellets and mulls.

The temperature dependence of the absorption by the guest molecules in ethylene oxide hydrate, dispersed in potassium bromide pellets, is presented in Section 4.6. The results are compared with the spectra obtained previously using the low temperature mulling technique (2,96).

4.2 Characterization of the Structure I Hydrates

All samples of cyclopropane hydrate I were characterized by X-ray powder diffraction photographs to determine the lattice parameters and the purity of the samples. The samples of ethylene oxide hydrate were previously characterized by D. Othen (2), but the X-ray powder diffraction pattern was not reported so three of his photographs were measured and the data are reported here.

The X-ray data for cyclopropane hydrate I and ethylene oxide hydrate at 100±5 K are summarized in Table 4.1. The d-spacing and 2θ values (Section 2.6) reported for cyclopropane hydrate are the averages of twenty-three sets of values obtained from sixteen photographs. The crystal-

TABLE 4.1

X-ray Powder Diffraction Patterns[a] of Cyclopropane Structure I Hydrate and Ethylene Oxide Hydrate at 100 K

Index	Calculated Intensity	Cyclopropane Structure I Hydrate			Ethylene Oxide Hydrate		
		2θ[b]	d(Å)[b]	Intensity[c]	2θ[b]	d(Å)[b]	Intensity[c]
110	14	10.41(4)	8.50(3)	24	10.50(7)	8.42(5)	13
200	2	14.78(4)	5.99(2)	7			
210	<0.01						
211	10	18.11(6)	4.90(2)	21	18.27(6)	4.86(2)	14
220	5	20.94(7)	4.24(1)	10	21.14(10)	4.20(2)	8
310	12	23.44(8)	3.79(1)	24	23.68(6)	3.757(10)	15
222	49	25.75(6)	3.459(8)	72	25.92(11)	3.434(14)	58
320	54	26.83(7)	3.323(9)	66	27.02(9)	3.300(9)	53
321	100	27.88(6)	3.200(7)	100	28.08(8)	3.178(8)	100
400	9	29.83(7)	2.995(7)	13	30.00(9)	2.979(9)	10
410	23	30.79(7)	2.904(7)	37	30.97(9)	2.888(8)	21
330,411	11	31.75(6)	2.818(5)	16	31.97(9)	2.799(8)	11
420	0.7			2[d]			2[d]

(continued......)

TABLE 4.1 (continued)

Index	Calculated Intensity	Cyclopropane Structure I Hydrate			Ethylene Oxide Hydrate		
		$2\theta^b$	d(Å)^b	Intensity^c	$2\theta^b$	d(Å)^b	Intensity^c
421	10	34.32(5)	2.616(4)	12	34.52(12)	2.598(9)	9
332	5	35.22(5)	2.548(4)	8	35.48(11)	2.530(8)	5
422	0.7			4^d			1^d
430	2	37.58(6)	2.394(3)	5			3^d
510,431	2	38.41(5)	2.344(3)	5			2^d
520,432	9	40.62(5)	2.221(3)	12	40.87(10)	2.208(5)	7
521	1			2^d			
440	0.04						
433,530	28	44.15(4)	2.051(2)	35	44.41(10)	2.040(5)	19
531	8	44.87(4)	2.020(2)	8			5^d
600,442	6	45.55(4)	1.991(2)	9			4^d
610	2						
611,532	13	46.85(4)	1.939(2)	16	47.11(8)	1.929(4)	8
620	3	48.07(5)	1.893(2)	4			3^d
540,621	2	48.82(4)	1.865(2)	4			3^d

(continued......)

TABLE 4.1 (continued)

a) Cu K_α radiation, wavelength 1.5418 Å.

b) The 2θ and d-spacings are the averages of between 4 and 6 values and 20 and 23 values for the structure I hydrates of ethylene oxide and cyclopropane, respectively, except for those due to the 531, 600, 620 and 540 reflections of cyclopropane structure I hydrate which are the averages of 10, 15, 9 and 9 values, respectively. The figure in parenthesis is the standard deviation in the last figure.

c) The estimated accuracy is 20% or 30% of the value given for values greater than or less than 20, respectively.

d) The 2θ values for these features could not be measured reliably.

2

to-film distance was 59.7±0.1 mm (Section 2.6). Six of these photographs were of the hydrate and ten were of the deuterate, since the X-ray diffraction pattern of the deuterate is identical, within experimental error, to that of the hydrate. The d-spacing and 2θ values reported for ethylene oxide hydrate are the averages of six sets of values obtained from three photographs of the hydrate using the crystal-to-film distance determined by Othen to be 60.0 mm (Section 2.6). The d-spacings and 2θ values of the structure I hydrates were indexed on a cubic unit cell, space group Pm3n (55,56), and there can be no doubt that the correct materials were obtained. The lattice parameters determined from the different sets of 2θ values were averaged to give the values a=11.96±0.02 Å and a=11.89±0.03 Å for cyclopropane hydrate I and ethylene oxide hydrate, respectively. The lattice parameter of ethylene oxide is in good agreement with the value, a=11.87±0.01 Å, determined by a neutron diffraction study at 80 K (56).

The calculated intensities of the diffraction lines given in Table 4.1 were determined using equation 3.1 and the structure factors measured during a single crystal X-ray diffraction study of ethylene oxide hydrate at 248 K (55). The observed intensities given in Table 4.1 are the averages of the relative peak optical densities measured from microdensitometer traces of four photographs of cyclopropane hydrate I and of two photographs of ethylene oxide hydrate. The intensities observed for ethylene oxide hydrate generally agree with the calculated values within the estimated error. The intensities observed for cyclopropane hydrate I agree only qualitatively with those of ethylene oxide hydrate. This is to be expected since scattering by the encaged cyclopropane molecules must be different than that by encaged ethylene oxide molecules.

Possible impurities in the samples of cyclopropane hydrate I are ice Ih, excess cyclopropane and cyclopropane hydrate II. The X-ray diffraction pattern of cyclopropane at 85 *K* has been reported previously (159), and the X-ray diffraction pattern of ice Ih is well known (36,168) so they are not reproduced here. The X-ray diffraction pattern of cyclopropane hydrate II is presented later. Excess cyclopropane is readily detected in the X-ray photographs of the hydrate by its strong line at $2\theta=23.3°$ (CuK_α radiation), while the presence of ice Ih is indicated by strong lines at $2\theta=22.8$, 24.2 and 25.9° (CuK_α radiation). Cyclopropane hydrate II was never detected in the cyclopropane hydrate I, but it would be easy to detect by its strongest lines, at $2\theta=22.67$ and 27.06° (CuK_α radiation) (Section 4.3). Excess cyclopropane is also readily detected in the deuterate samples by a mid-infrared absorption band at 3009 cm^{-1} near to the peak due to encaged cyclopropane at 3020.5 cm^{-1}

(Section 4.4.3). The presence of ice impurity can also be detected from the shapes and frequencies of the ν_{OD}(HDO) and ν_{OH}(HDO) bands, as is discussed in Section 4.4.2. Unless otherwise stated, all spectra of the structure I hydrates reported in this thesis are of samples that were shown to be pure by X-ray diffraction and spectroscopic criteria.

4.3 Characterization of Cyclopropane Structure II Hydrate

The X-ray powder diffraction pattern of cyclopropane hydrate II at 100±5 K is given in Table 4.2. The d-spacings and 2θ values are the averages of twelve sets of values obtained from six photographs. The crystal-to-film distance was 59.8 mm (Section 2.6). Four photographs were of the hydrate and two were of the deuterate since the X-ray diffraction pattern of the deuterate is identical, within experimental error, to that of the hydrate. The d-spacings and 2θ values were indexed on a cubic unit cell, space group Fd3m (57). The lattice parameters determined for the different sets of 2θ values were averaged to give the value, a=17.07±.03 Å.

The observed intensities given in Table 4.2 are the averages of the relative peak optical densities measured from microdensitomelometer traces of six photographs. The only structure II hydrate for which structure factors have been measured is the double hydrate of hydrogen sulphide

TABLE 4.2

X-ray Powder Diffraction Pattern[a] of Cyclopropane Structure II Hydrate at 100 K

Index	Calculated Intensity	2θ[b]	d(Å)[b]	Intensity[c]
111	8	8.95(2)	9.88(2)	5
220	3			
311	3	17.17(6)	5.16(2)	35
222	15	17.99(4)	4.94(1)	66
400	24	20.75(4)	4.281(7)	60
331	17	22.67(5)	3.916(9)	87
422	46	25.59(5)	3.481(7)	75
333,511	100	27.06(4)	3.295(4)	100
440	42	29.54(4)	3.023(3)	38
531	94	30.92(4)	2.891(4)	65
442	5			
620	14	33.32(7)	2.689(5)	16
533	4	34.43(4)	2.605(3)	9
622	2			
444	2			
551,711	2	37.57(7)	2.394(4)	7
642	0.2			
553,731	6	40.17(7)	2.245(4)	20
800	0.5			
733	11	43.51(7)	2.080(3)	26
644	0.3			

(continued......)

TABLE 4.2 (continued)

Index	Calculated Intensity	$2\theta^b$	$d(\text{Å})^b$	Intensity[c]
660,822	33	45.06(7)	2.012(3)	43
555,751	13	46.07(7)	1.970(3)	15
662	0.02			
840	4	47.51(5)	1.914(2)	8
911,753	11	48.68(5)	1.871(2)	11

---

a) Cu K_α radiation, wavelength 1.5418 Å.

b) The 2θ and d-spacings are the average of between 10 and 13 values. The figure in parenthesis is the standard deviation in the last figure.

c) The estimated accuracy is 20% or 30% of the value given for values greater than or less than 20, respectively.

and tetrahydrofuran at 253 K (57). These experimental structure factors were used with equation 3.1 to yield the calculated intensities in Table 4.2. The calculated intensities can be seen to be quite different from those observed for cyclopropane hydrate II, undoubtedly due to the different guest molecules and the presence of the strongly scattering sulphur atoms in the dodecahedral cages of the double hydrate (57).

A line was observed at $2\theta \doteq 24.2°$ (CuK$_\alpha$ radiation) in all of the X-ray photographs of cyclopropane hydrate II, and was attributed to ice Ih impurity. The other two lines characteristic of ice Ih at $2\theta=22.8°$ and $25.9°$ were masked by lines due to cyclopropane hydrate II. Previous studies (137) have shown that small amounts of ice impurity can seriously affect the ν_{OD}(HDO) and ν_{OH}(HDO) bands in the infrared spectra of the clathrate hydrates. The interactions between the guest molecules and the water molecules are weak in the clathrate hydrates, so to a first approximation the shapes of the ν_{OD}(HDO) bands of all structure II hydrates should be similar. To see whether the ice impurity did influence the ν_{OD}(HDO) band of cyclopropane hydrate II, the band was compared with the corresponding band of the structure II hydrate of tetrahydrofuran which is readily prepared free from ice impurity.

The ν_{OD}(HDO) band of cyclopropane hydrate II containing 10 mole percent of HDO is shown as curve B in Fig. 4.1

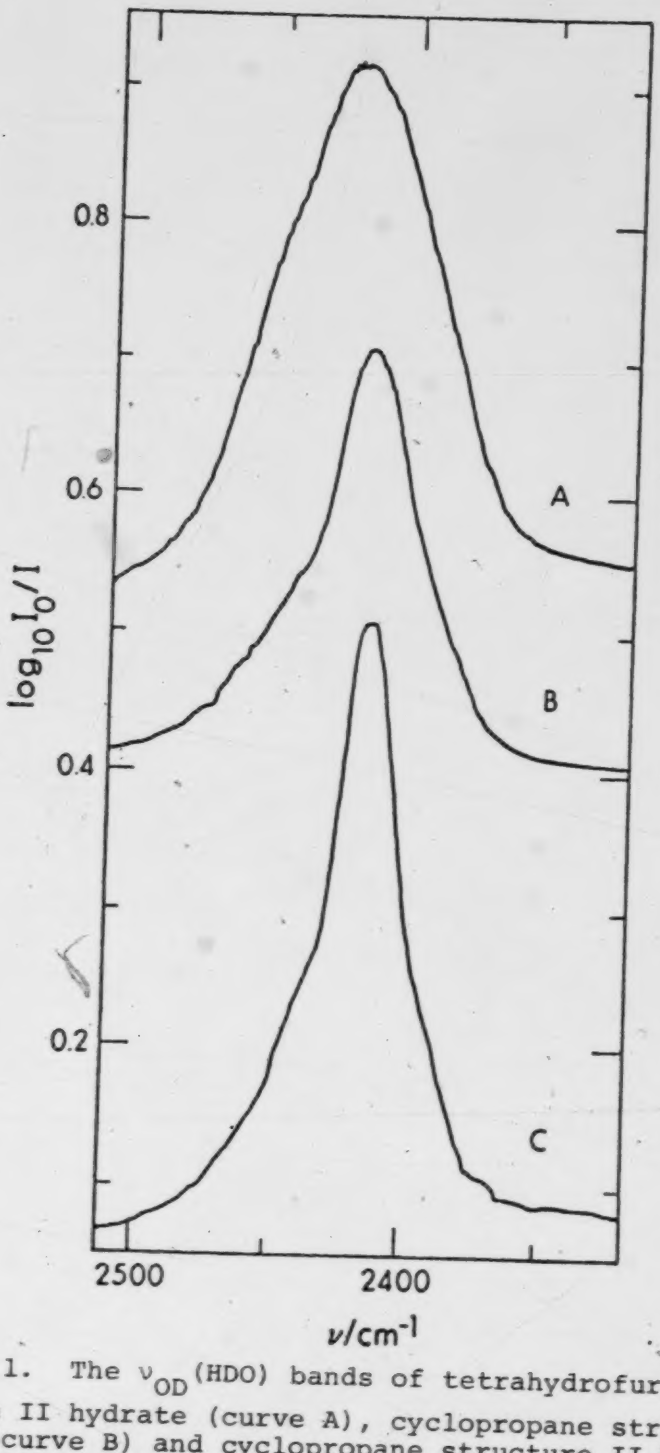

Figure 4.1. The ν_{OD}(HDO) bands of tetrahydrofuran structure II hydrate (curve A), cyclopropane structure II hydrate (curve B) and cyclopropane structure II hydrate mixed with ice Ih (curve C) in propene at 90±5 K; resolution 2 cm^{-1}.

and has a peak frequency of 2419 cm^{-1} and a half-width of 45 cm^{-1}. The ν_{OD}(HDO) band of a sample of tetrahydrofuran hydrate containing 10 mole percent of HDO, which was shown by X-ray methods to contain no ice impurity, is shown as curve A in Fig. 4.1. The peak frequency is 2425 cm^{-1} and the half-width of the band is about 70 cm^{-1}. The ν_{OD}(HDO) band of cyclopropane hydrate II is clearly much sharper than that of the tetrahydrofuran hydrate and, since the ν_{OD}(HDO) band of ice Ih has a half-width of only about 20 cm^{-1} (109), it seems clear that the ice Ih impurity severely sharpens the ν_{OD}(HDO) band of cyclopropane hydrate II. This effect was confirmed by adding some ice Ih containing 10 mole percent HDO to the cyclopropane hydrate II used for curve B of Fig. 4.1. The ν_{OD}(HDO) band of this sample is shown as curve C in Fig. 4.1 and has a peak frequency of 2418 cm^{-1} and a half-width of 30 cm^{-1}, confirming that ice Ih impurity does sharpen the ν_{OD}(HDO) band. This evidence suggests that the sample of cyclopropane hydrate II was too badly contaminated with ice Ih to warrant further study.

In these preliminary studies of cyclopropane hydrate II, only one extremely weak absorption band due to cyclopropane guest molecules was observed. This was due to ν_{10}(E') which gave the most intense guest absorption band in the spectrum of the structure I hydrate (Section 4.4.3). In order to observe the other guest absorption bands, extremely strongly absorbing samples, of which good spectra are very difficult to obtain, would have been required, so further study of this clathrate hydrate was not attempted.

4.4 Mid-Infrared Spectra of Cyclopropane Structure I Hydrate at 90±5 K

4.4.1 General

The spectra reported in this section are of samples of cyclopropane hydrate I or deuterate I dispersed in one of the mulling agents propane, propene or chlorotrifluoromethane. The hydrates are dispersed in mulling agents with a comparable refractive index to reduce reflection and scattering effects, so that the transmission spectrum is a good approximation to the absorption spectrum. This technique of preparing infrared samples at low temperature is well documented (2,96,137,166). The absorption by the mulling agent has been subtracted from the spectra presented.

The mid-infrared spectra from 4000 to 300 cm^{-1} of cyclopropane hydrate I and deuterate I at 90±5 K are presented in Figs. 4.2 and 4.3, respectively. These figures were composed from spectra obtained using each of the three mulling agents, and the intensities of the features taken from different original spectra have been scaled so that the relative intensities in Figs. 4.2 and 4.3 are approximately correct. The original spectra were recorded at a

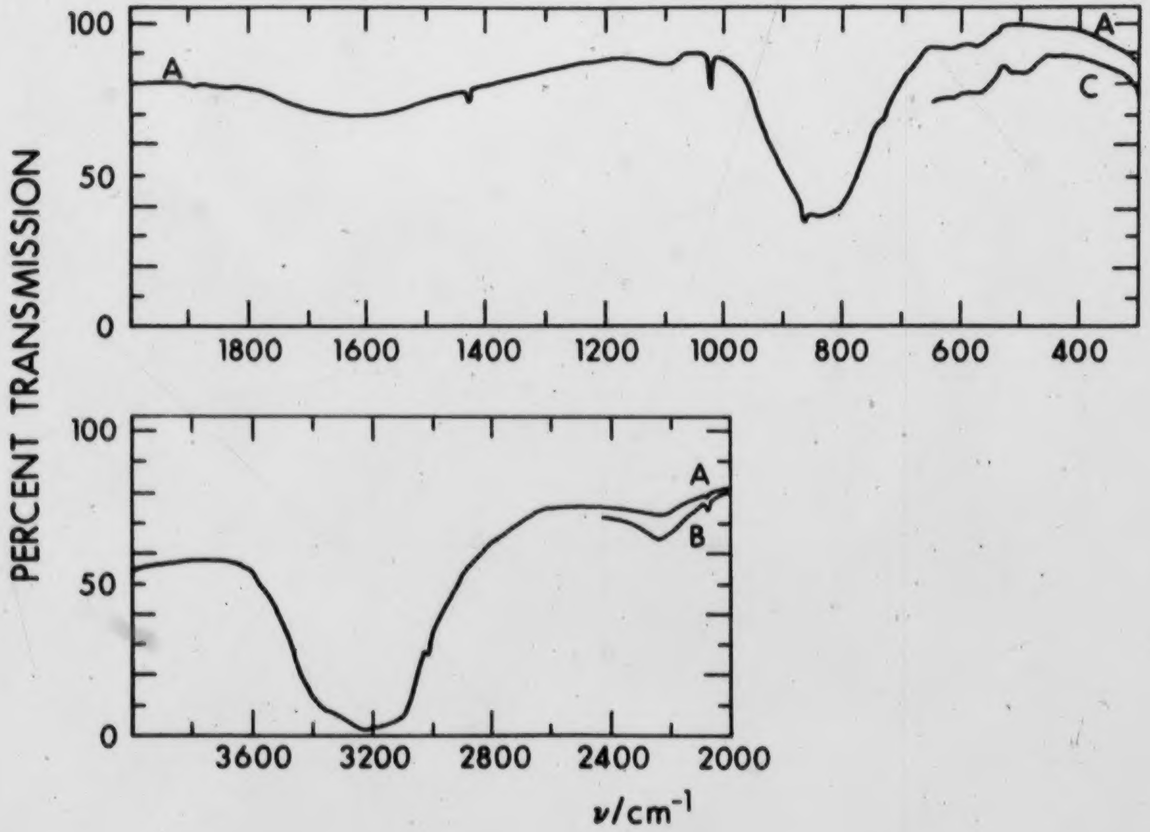

Figure 4.2. Mid-infrared spectrum of cyclopropane structure I hydrate dispersed in mulling agents at 90±5 K; resolution 4 cm^{-1} below 650 cm^{-1} and 2 cm^{-1} above 650 cm^{-1}. Curve C has been offset for clarity and is from a sample containing 10 mole percent HDO.

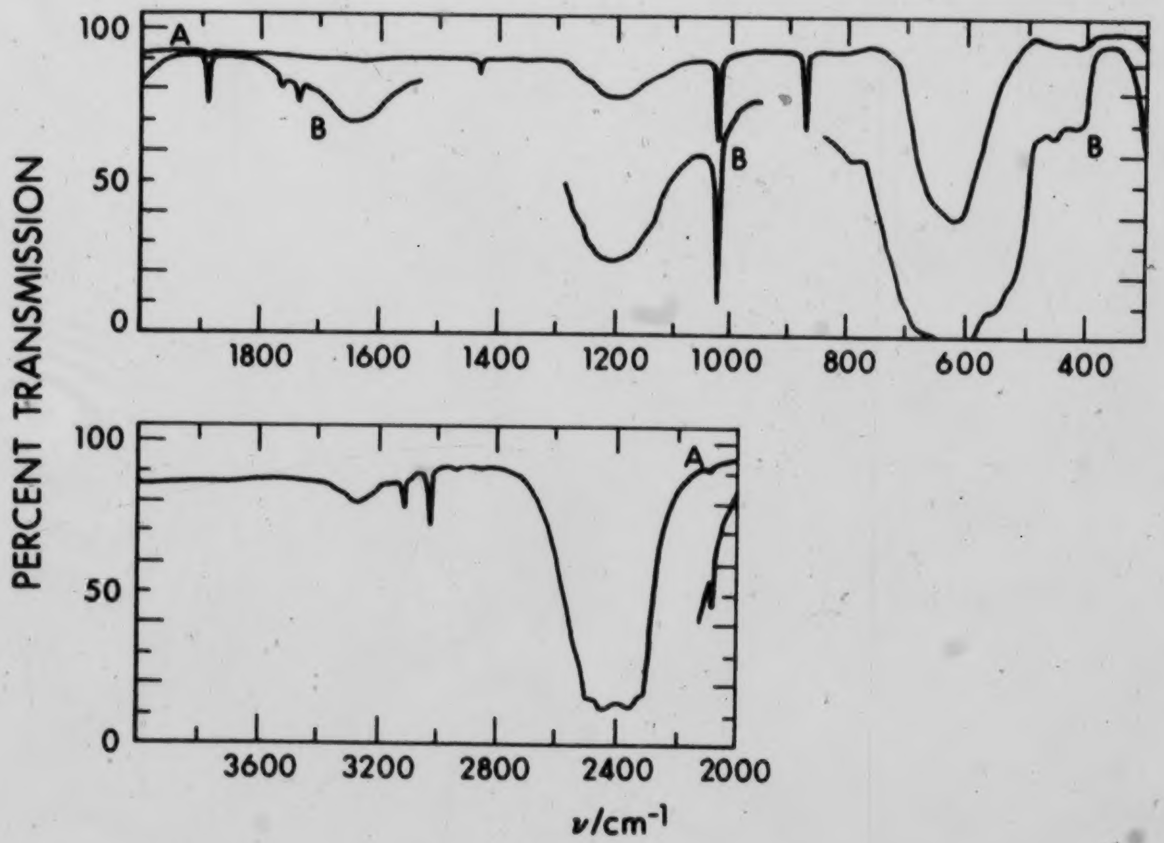

Figure 4.3. Mid-infrared spectrum of cyclopropane structure I deuterate dispersed in mulling agents at 90±5 K; resolution 4 cm^{-1} below 650 cm^{-1} and 2 cm^{-1} above 650 cm^{-1}.

resolution of about 4 cm^{-1} between 300 and 650 cm^{-1} and about 2 cm^{-1} between 650 and 4000 cm^{-1}. The frequencies of the features, their estimated accuracies, and the assignment are given in Table 4.3.

The interactions between the guest and water molecules are weak in the clathrate hydrates, so that, to a first approximation, the vibrations of the water and guest molecules can be considered separately. Absorption by the water molecules can be readily identified, since the frequencies of the intramolecular and rotational vibrations in the deuterate should be about 30 percent lower than the corresponding frequencies in the hydrate. The absorption by the water molecules is broad, and the assignment follows from the assignment of the spectra of the ices (Section 1.5) and other clathrate hydrates (Section 1.6). The absorption by the guest molecules should occur at approximately the same frequencies in the hydrate and the deuterate as in the gas. This absorption is sharp and the assignment of the features follows from the assignment of the spectrum of gaseous cyclopropane (Section 1.7).

4.4.2 Absorption by the Water Molecules at 90±5 K

The $\nu_{OH}(H_2O)$ band extends from 2800 to 3600 cm^{-1}, as shown in Fig. 4.4. The band has its maximum at 3234 cm^{-1} and a half-width of about 300 cm^{-1}. Shoulders at 3350, 3176 3113 and 3100 cm^{-1} and a weak, sharp peak at 3020 cm^{-1} are

TABLE 4.3

Frequencies of the Features Observed in the Mid-infrared Spectra of Cyclopropane Structure I Hydrate and Deuterate at 90 K

Hydrate[a]			Assignment	Deuterate[a]		
ν/cm^{-1}		$\nu_{½}^{b}$/cm^{-1}		ν/cm^{-1}		$\Delta\nu_{½}^{b}$/cm^{-1}
497±5	w,bd		ν_R(HDO)			
514±5	sh					
			ν_R(D_2O)	396±5	sh	
				412±5	w	
				452±5	w	
				530±10	sh	
				565±10	sh	
				615±5	s	105
				670±10	sh	
				795±10	sh	
536±5	sh		ν_R(H_2O)			
573±5	w,bd					
618±5	w					
740±5	sh					
833±5	s	165				
1105±10	w,bd					

(continued......)

TABLE 4.3 (continued

Hydrate[a]			Assignment	Deuterate[a]		
ν/cm^{-1}		$\Delta\nu^{b}_{1/2}/\mathrm{cm}^{-1}$		ν/cm^{-1}		$\Delta\nu^{b}_{1/2}/\mathrm{cm}^{-1}$
			$\nu_7(A_2")$	859±2	w	
865.5±1	m		$\nu_{11}(E')$	869.2±0.5	s	4
1025.2±0.5	s	4	$\nu_{10}(E')$	1022.8±0.5	s	4
			$\nu_2(D_2O)$	1110±15	cos	150
				1200±10	m,bd	
				1255±15	cos	
1432.3±0.5	w		$\nu_9(E')$	1433.3±0.5	m	2
1600±30	m,bd	270	$\nu_2(H_2O)$			
			$3\nu_R(D_2O)$, $\nu_2(D_2O) + \nu_R(D_2O)$	1644±15	w,bd	115
			$2\nu_{11}$	1734.5±1	w	
			$\nu_{10} + \nu_{14}$	1765.0±1	w	

(continued......)

TABLE 4.3 (continued)

Hydrate[a]			Assignment	Deuterate[a]		
ν/cm^{-1}		$\Delta\nu^{b}_{1/2}/cm^{-1}$		ν/cm^{-1}		$\Delta\nu^{b}_{1/2}/cm^{-1}$
1890.5±1	vw		$\nu_7 + \nu_{10}$	1867±2	vw	
			$\nu_{10} + \nu_{11}$	1887.2±1	m	3.5
2081.5±1	w		$\nu_5 + \nu_{10}$	2077.0±1	m	5
2250±15	m,bd	220	$3\nu_R(H_2O)$, $\nu_2(H_2O) + \nu_R(H_2O)$			
2415±2	m	75	$\nu_{OD}(HDO)$			
2457±2	m					
			$\nu_{OD}(D_2O$	2310±5	sh	250
				2353±4	vs	
				2415±5	sh	
				2438±3	vs	
				2494±5	sh	
				2540±10	sh	

(continued......)

TABLE 4.3 (continued)

Hydrate[a]			Assignment	Deuterate[a]		
ν/cm^{-1}		$\Delta\nu^{b}_{1/2}/cm^{-1}$		ν/cm^{-1}		$\Delta\nu^{b}_{1/2}/cm^{-1}$
			$2\nu_9$	2859.5±1	w	4
			$\nu_9 + 2\nu_{14}$	2881.5±1	w	5
			$2\nu_{10} + \nu_{11}$	2922±2	sh	
			$\nu_2 + \nu_9$	2934.0±1	w	8.5
			$2\nu_2, 4\nu_{14}$	2967±2	vw	
3020±2	w		$\nu_8(E')$	3020.5±1	s	7.5
			$\nu_1(A_1')$	3034±2	sh	
			$\nu_{12}(E'')$	3088±2	sh	
3113±3	sh		$\nu_6(A_2'')$	3104.3±1	m	8.5
			$\nu_{OH}(HDO)$	3267±2 3315±2	m sh	115
3100±10 3176±10 3234±6 3350±10	sh sh vs sh	300	$\nu_{OH}(H_2O$			

(continued......)

TABLE 4.3 (continued)

a) s = strong, m = medium, w = weak, bd = broad, v = very, sh = shoulder, cos = change of slope.

b) $\Delta\nu_{1/2}$ is the full width of the peak at half height.

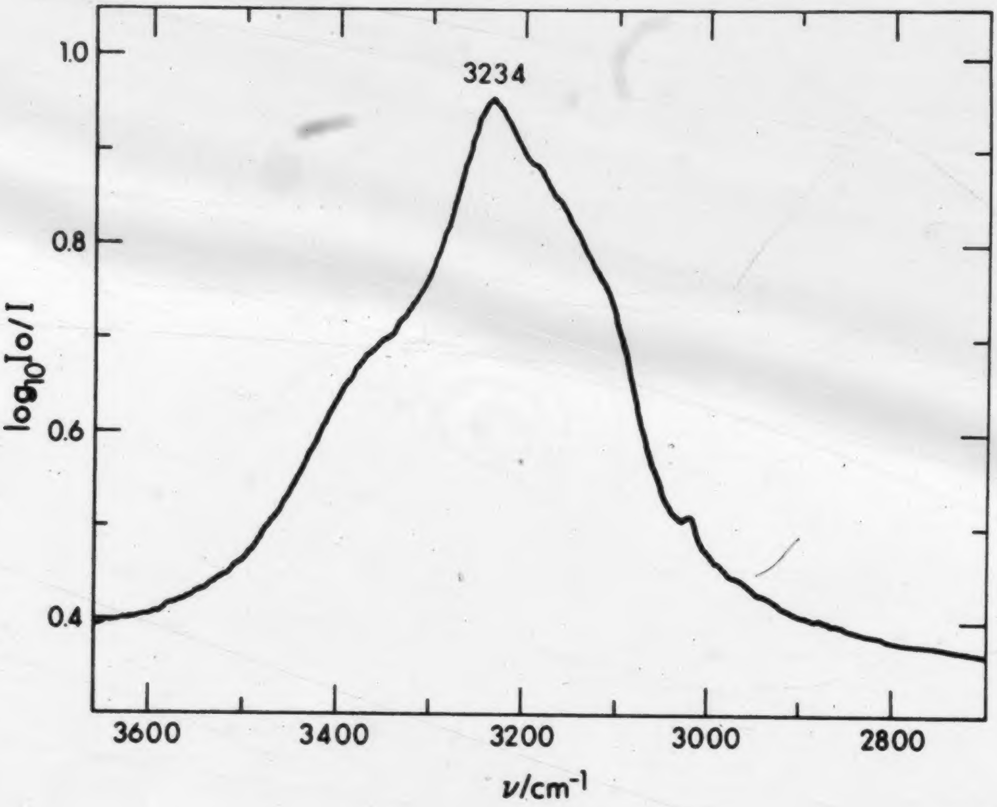

Figure 4.4. The $\nu_{OH}(H_2O)$ band of cyclopropane structure I hydrate in a chlorotrifluoromethane mull at 90±5 K; resolution 2 cm^{-1}.

observed. This latter feature is also observed in the spectrum of the deuterate at approximately the same frequency, and is assigned to cyclopropane. In the deuterate, absorption by cyclopropane also yields a sharp peak at 3104 cm^{-1} which presumably causes the sharp inflection at 3113 cm^{-1} in the hydrate. This inflection is superimposed on a much broader shoulder at about 3100 cm^{-1} which is assigned to water absorption.

The $\nu_{OD}(D_2O)$ band extends from 2200 to 2700 cm^{-1}, as shown in Fig. 4.5. The features on this band are better defined than those on the $\nu_{OH}(H_2O)$ band, with peaks at 2438 cm^{-1} and 2353 cm^{-1} and shoulders at 2540, 2494, 2415 and 2310 cm^{-1}. The band has a half-width of about 250 cm^{-1}. The ratios of the frequencies of the features on the $\nu_{OH}(H_2O)$ band, at 3350, 3234, 3176 and 3100 cm^{-1} to the frequencies of the corresponding features on the $\nu_{OD}(D_2O)$ band at 2494, 2438, 2353 and 2310 cm^{-1} are 1.343±.007, 1.326±.005, 1.350±.006 and 1.342±.010, respectively.

The $\nu_2(H_2O)$ band is poorly defined in the hydrate (Fig. 4.2) with a peak frequency of about 1600 cm^{-1}. The $\nu_2(D_2O)$ band is much better defined (Fig. 4.3), with a peak frequency of 1200 cm^{-1}. Definite changes in slope are observed in the $\nu_2(D_2O)$ band at about 1100 and 1255 cm^{-1}.

The $\nu_R(H_2O)$ band (Fig. 4.2) extends from 450 to 1100 cm^{-1}. The peak frequency is 833 cm^{-1} and the band has a half-width of about 165 cm^{-1}. The sharp features observed at 865 and

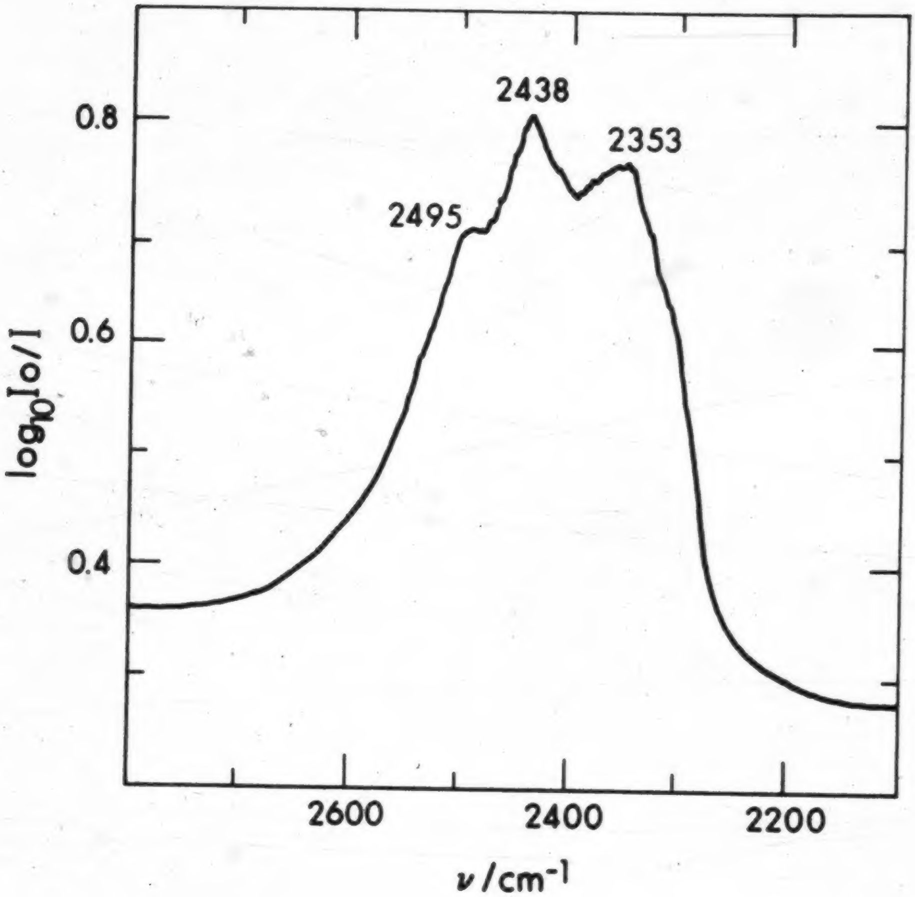

Figure 4.5. The $\nu_{OD}(D_2O)$ band of cyclopropane structure I deuterate in a propene mull at 90±5 K; resolution 2 cm^{-1}.

1025 cm^{-1} are clearly observed (Figs. 4.2 and 4.3) at approximately the same frequency in the spectrum of the deuterate, so they are due to cyclopropane. Four features are observed on the low frequency side of the $\nu_R(H_2O)$ band (Curve A, Fig. 4.2) at 740, 618, 573 and 536 cm^{-1}. There is also a broad absorption to high frequency, at about 1105 cm^{-1}.

The $\nu_R(D_2O)$ band is shown in Fig. 4.6 and extends from about 350 to 800 cm^{-1}. The peak frequency is 615 cm^{-1} and the half-width is 105 cm^{-1}. The low frequency side of $\nu_R(D_2O)$, like the $\nu_R(H_2O)$ band, shows structure, with five features observed at 565, 530, 452, 412 and 396 cm^{-1}. There is also a high frequency shoulder at 795 cm^{-1} (Fig. 4.3). The ratio of the peak frequencies of the $\nu_R(H_2O)$ and $\nu_R(D_2O)$ bands is 1.35±.02. Using this ratio the bands corresponding to the low frequency features of $\nu_R(D_2O)$ are calculated to be at about 763, 716, 610, 556 and 535±10 cm^{-1} in the hydrate spectrum, which agrees quite well with the observed features. Presumably, the two features predicted at 763 and 716 cm^{-1} are unresolved and yield the feature at 740 cm^{-1}. The ratio of the frequencies of the features at 1105 and 795 cm^{-1} in the hydrate and the deuterate, respectively, is 1.39±.03. These features are also assigned to ν_R vibrations.

The low frequency side of the $\nu_R(H_2O)$ band of a sample containing 10 mole percent HDO is shown as curve C in Fig. 4.2. Features additional to those of the pure hydrate are

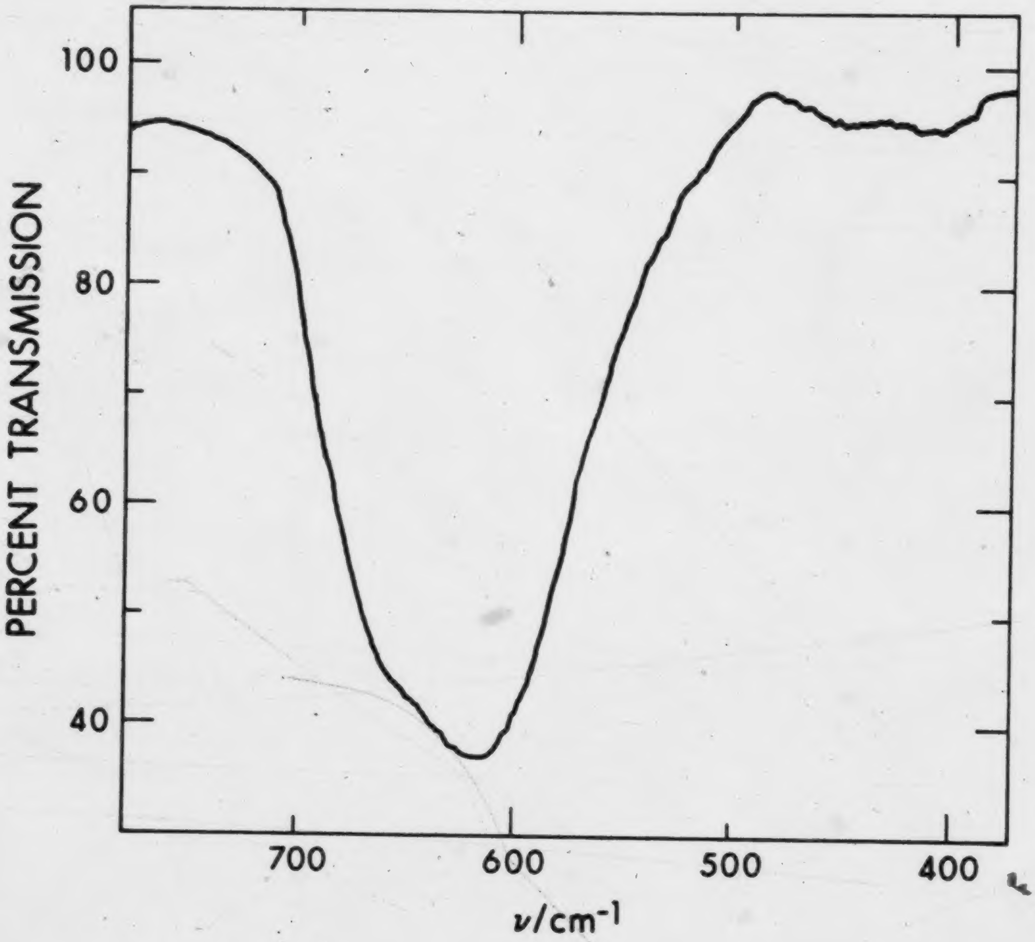

Figure 4.6. The $\nu_R(D_2O)$ band of cyclopropane structure I deuterate in a propane mull at 90±5 K; resolution 4 cm^{-1}.

seen at 514 and 497 cm^{-1} and are assigned to ν_R(HDO) vibrations.

The $3\nu_R$ or $\nu_2+\nu_R$ band is broad with peak frequencies of 2250 and 1645 cm^{-1} in the hydrate (Fig. 4.2) and deuterate (Fig. 4.3), respectively. The sharp feature at 2081 cm^{-1} in the spectrum of the hydrate is at about the same frequency in the deuterate, so it is assigned to cyclopropane.

The ν_{OD}(HDO) bands of cyclopropane hydrate I containing 4 and 10 percent HDO are shown as curves A and B, respectively, in Fig. 4.7. The band consists of two well-resolved features, at 2415 and 2457 cm^{-1}, and has a half-width of 75 cm^{-1} for samples containing 4 mole percent HDO and 85 cm^{-1} for samples containing 10 mole percent HDO. The ν_{OD}(HDO) bands of the other structure I hydrates that have been studied (2,96) were single featureless bands, so the very remote possibility that ice was contributing to the ν_{OD}(HDO) band in cyclopropane hydrate I was investigated.

A small amount of ice Ih containing 10 mole percent HDO in H_2O was ground and mixed in the approximate proportion of 1:10 with the sample used to obtain curve B of Fig. 4.7; this mixture gave the spectrum shown as curve C of Fig. 4.7. The frequency of the strongest feature is 2420 cm^{-1}, to high frequency of that of the pure sample but the overall half-width of the band is unchanged. It is concluded that the ν_{OD}(HDO) band of pure cyclopropane hydrate I has the shape shown by curves A and B of Fig. 4.7.

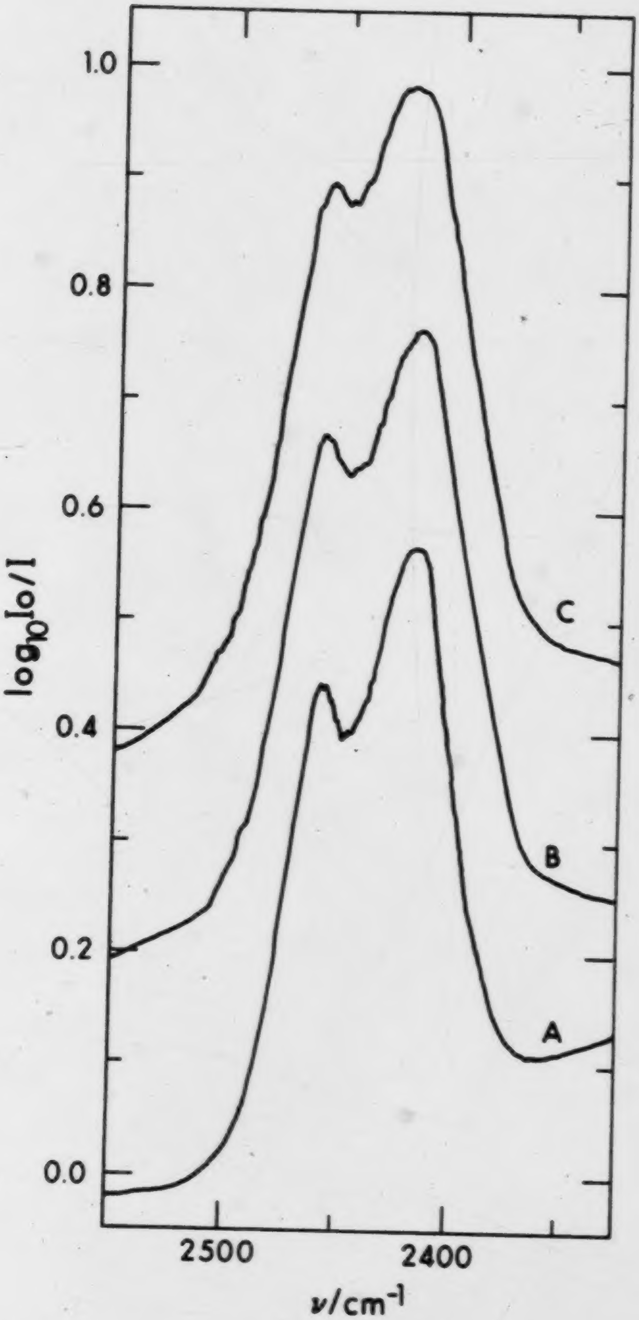

Figure 4.7. The ν_{OD}(HDO) band of cyclopropane structure I hydrate in a propane mull at 90±5 K; resolution 2 cm^{-1}. Curves A and B are from samples containing 4 and 10 mole percent HDO, respectively. Curve C is from a sample containing 10 mole percent HDO and some ice Ih of the same isotopic composition. Curves A and C have been offset for clarity.

The ν_{OH}(HDO) bands of cyclopropane deuterate I are shown in Fig. 4.8. The samples used for curves A and B were prepared from water that was a mixture of 2 and 5 mole percent, respectively, of H_2O in D_2O. It is certain that some isotopic exchange occurred between the liquid water and atmospheric moisture and the final concentrations are estimated to be about 5 and 12 mole percent HDO in D_2O. This estimate was obtained from the relative absorbances of the ν_{OH}(HDO) bands of the pure deuterate and the partially hydrated samples and assumed that the pure deuterate contained 2 mole percent HDO. Curve C of Fig. 4.8 was obtained from a sample containing 12 mole percent HDO which was found to contain a small amount of ice. This sample was later reexposed to cyclopropane, characterized again, and found to contain no ice impurity, and then used to obtain curve B.

The features on the ν_{OH}(HDO) band are not as well resolved as those in the ν_{OD}(HDO) band. The peak is at 3267 cm^{-1} but only a shoulder is seen at 3315 cm^{-1}. The half-widths of the bands for samples containing 5 and 12 mole percent HDO in D_2O are 115 and 135 cm^{-1}, respectively. The frequency of the main peak for the sample contaminated with ice (curve C) is 3272 cm^{-1}, to high frequency of that of the pure sample, the top of the band appears more pointed than that of the pure sample and the overall half-width of the band is 115 cm^{-1}. It is concluded that curves A and B

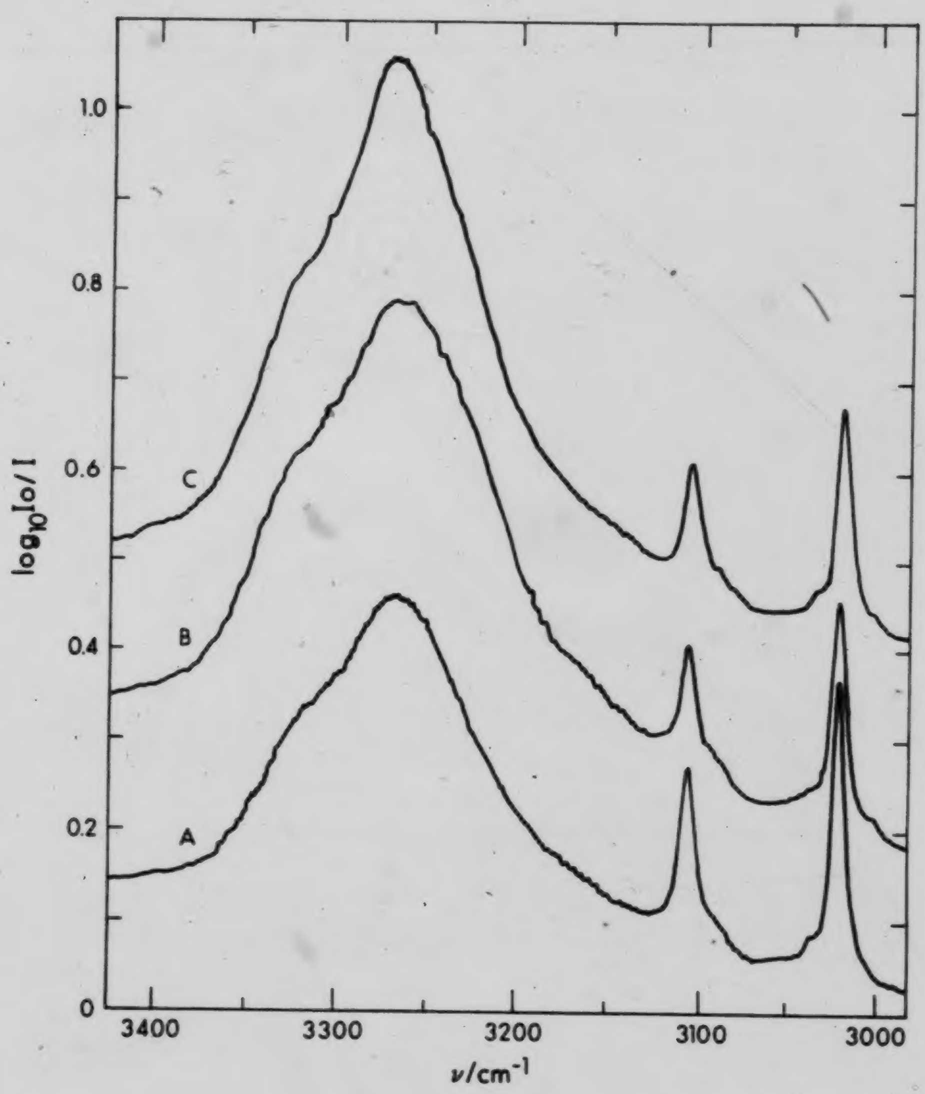

Figure 4.8. The ν_{OH}(HDO) band of cyclopropane structure I deuterate in a chlorotrifluoromethane mull at 90±5 K; resolution 2 cm^{-1}. Curves A and B are from samples containing 5 and 12 mole percent HDO, respectively. Curve C is from a sample containing 12 mole percent HDO and some ice Ih of the same isotopic composition. Curves A and C have been offset for clarity.

of Fig. 4.8 show the correct O-H stretching bands of 5 and 12 mole percent HDO in cyclopropane deuterate I.

The ratios of the frequencies of the features of the ν_{OH}(HDO) band, 3267 and 3315 cm^{-1}, to those of the corresponding features of the ν_{OD}(HDO) band are 1.353±.002 and 1.345±.002.

4.4.3 Absorption by the Cyclopropane Molecules at 90±5 K

Shown in Fig. 4.9 are the stronger guest absorption bands of cyclopropane deuterate I below 2100 cm^{-1}. In this region there are four bands assigned to fundamentals (Section 1.7). The CH_2 rocking vibration, $\nu_7(A_2")$, is seen as a very weak feature at 859 cm^{-1} (Fig. 4.9a). This band is not observed in the hydrate because it is masked by the strong $\nu_R(H_2O)$ band. The ring deformation, $\nu_{11}(E')$, yields a strong band at 869.2 cm^{-1} with a half-width of 4 cm^{-1} (Fig. 4.9a), while in the hydrate it is observed at 865.5 cm^{-1}, superimposed on the $\nu_R(H_2O)$ band (Fig. 4.2). The CH_2 wag, $\nu_{10}(E')$, yields a strong band at 1025.2 cm^{-1} (Fig. 4.9b), while in the hydrate it is observed at 1022.8 cm^{-1} (Fig. 4.2), both bands have half-widths of 4 cm^{-1}. The CH_2 deformation, $\nu_9(E')$, is seen as a band of moderate intensity at 1433.3 cm^{-1} with a half-width of 2 cm^{-1} (Fig. 4.9c), while in the hydrate it is observed at 1432.3 cm^{-1} as a weak band superimposed on the $\nu_2(H_2O)$ band (Fig. 4.2).

In the spectrum of the deuterate, five features are observed between 1700 and 2100 cm^{-1} which are assigned to

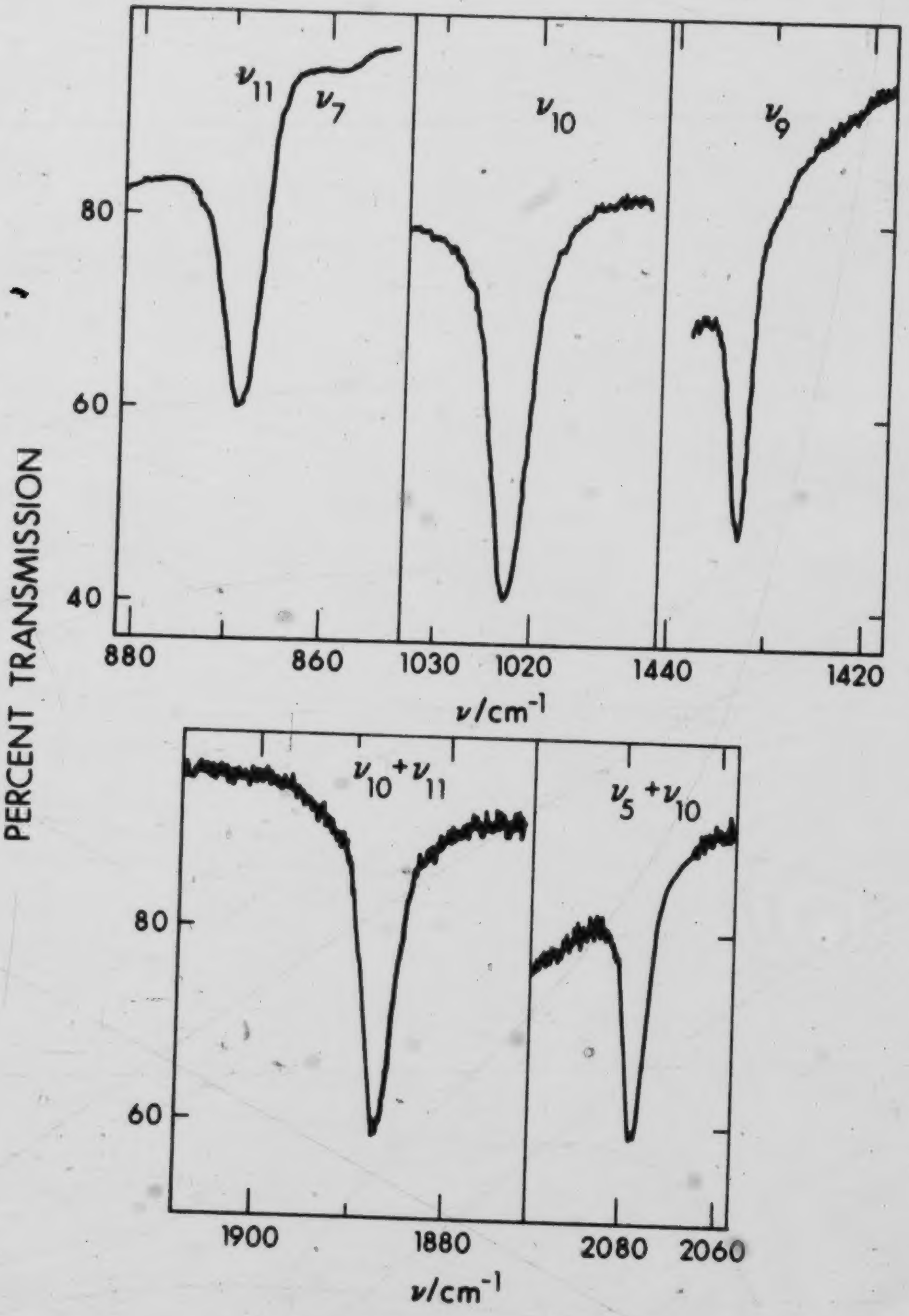

Figure 4.9. Absorption by $\nu_7(A_2'')$, $\nu_{11}(E')$, $\nu_{10}(E')$, $\nu_9(E')$, $\nu_{10}+\nu_{11}$ and $\nu_5+\nu_{10}$ of cyclopropane structure I deuterate in mulling agents at 90±5 K; resolution $\leq$ 1.4 cm^{-1}.

overtone and combination transitions. The weak peaks at 1734.5 and 1765.0 cm^{-1} (Fig. 4.3), the very weak peak at 1867 cm^{-1} (Fig. 4.3), the moderately strong band with a half-width of 3.5 cm^{-1} at 1887.2 cm^{-1} (Fig. 4.9d), and the moderately strong band with a half-width of 5 cm^{-1} at 2077.0 cm^{-1} (Fig. 4.9e) are assigned to $2\nu_{11}$, $\nu_{10}+\nu_{14}$, $\nu_7+\nu_{10}$ or $\nu_4+\nu_{14}$, $\nu_{10}+\nu_{11}$ and $\nu_5+\nu_{10}$(146), respectively. In the hydrate only $\nu_{10}+\nu_{11}$ and $\nu_5+\nu_{10}$ are seen, as weak bands at 1890.5 and 2081.5 cm^{-1}, respectively (Fig. 4.2).

Shown in Fig. 4.10 are the guest absorption bands of cyclopropane deuterate I between 2850 and 3120 cm^{-1}. The four features between 3000 and 3120 cm^{-1} are assigned to C-H stretching vibrations. The strong band, with a half-width of 7.5 cm^{-1}, at 3020.5 cm^{-1} (Fig. 4.10) is assigned to ν_8(E') which appears in the hydrate as a weak feature at 3020 cm^{-1}, superimposed on the $\nu_{OH}(H_2O)$ band. The high frequency shoulder on the ν_8 band at about 3034 cm^{-1} (Fig. 4.10) is assigned to $\nu_1(A_1')$. The strong band with a half-width of 8.5 cm^{-1} at 3104.3 cm^{-1} (Fig. 4.10) is assigned to $\nu_6(A_2")$ and its low frequency shoulder at 3088 cm^{-1} is assigned to ν_{12}(E"). In the hydrate $\nu_6(A_2")$ is seen only as a shoulder at 3113 cm^{-1}.

Five features are observed between 2850 and 2980 cm^{-1} (Fig. 4.10) that are assigned to overtone and combination transitions. The weak peaks at 2859.5 and 2881.5 cm^{-1},

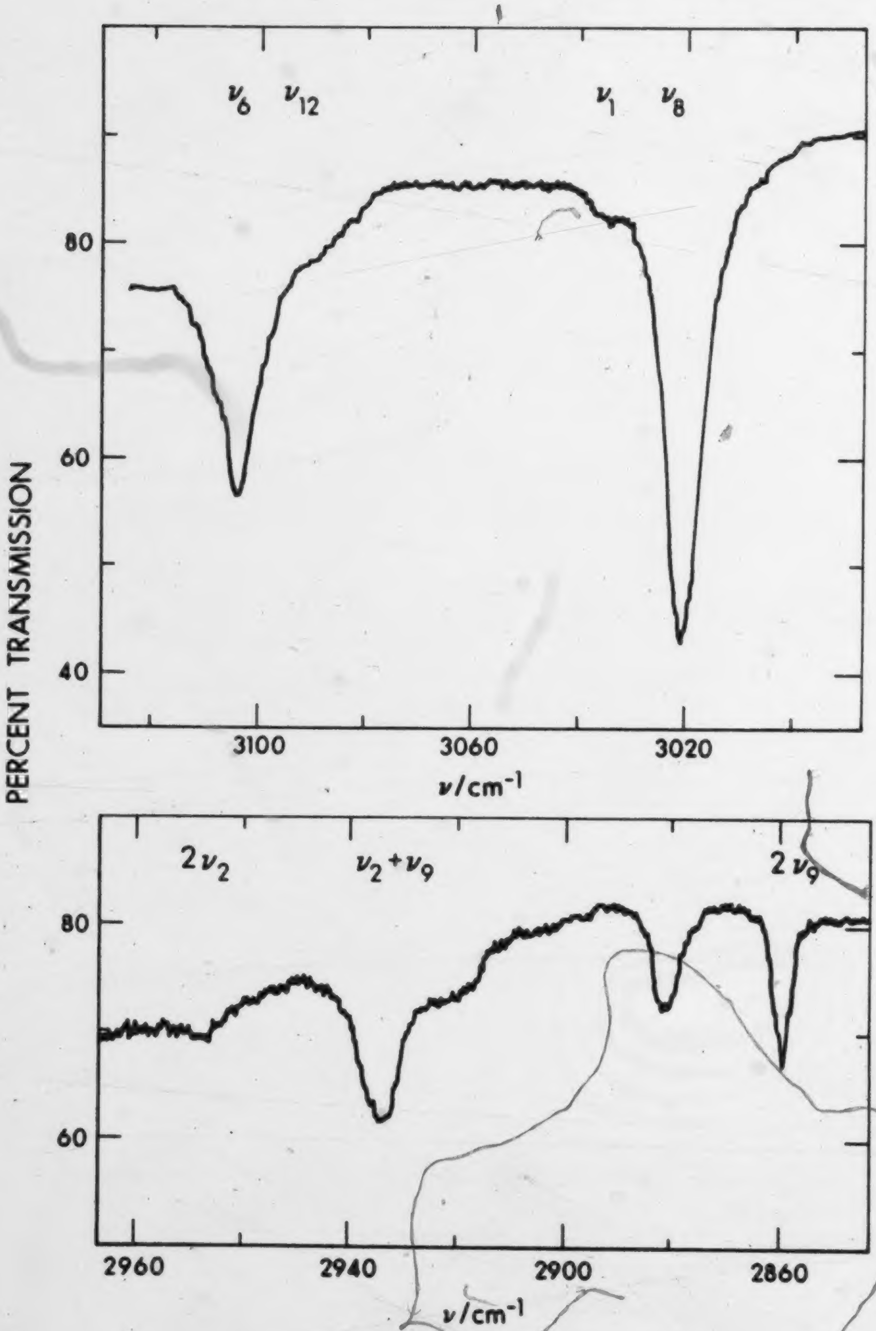

Figure 4.10. Absorption between 2840 and 3120 cm^{-1} by cyclopropane structure I deuterate in a chlorotrifluoromethane mull at 90±5 K; resolution 1.8 cm^{-1}.

the shoulder at 2922, the weak peak at 2934.0 cm^{-1} and the very weak peak at 2967 cm^{-1} are assigned to $2\nu_9$, $2\nu_{14}+\nu_9$, $2\nu_{10}+\nu_{11}$, $\nu_2+\nu_9$ and $2\nu_2$ or $4\nu_{14}$ (146,161), respectively.

4.5 Temperature Dependence of the Mid-Infrared Spectra of Cyclopropane Structure I Hydrate

4.5.1 General

The spectra presented in the remainder of this chapter are of the clathrate hydrates powdered and dispersed in potassium bromide pellets. In a previous study of the temperature dependence of the absorption by oxetane hydrate I, P. Wright used a pellet sample holder made of 2 percent beryllium-copper and, with about 0.1 Torr of air as an exchange gas, could only cool his samples to 62 K (2). To try to attain lower sample temperatures, a pellet sample holder of OFHC (oxygen-free high conductivity) copper (Section 2.8.2) was tried and found to withstand the 2.5 kbar pressure necessary to prepare the pellets. Further modifications to P. Wright's procedure made in this work were that a platinum resistance thermometer was fitted into a hole in the pellet sample holder so that its temperature could be monitored directly, and that 0.1 to 0.2 Torr of helium was used as an exchange gas.

During the calibration of the apparent temperature of the pellet sample holder (Section 2.9), it was found that when the sample holder was attached to the cryotip at room temperature and subsequently cooled, the lowest apparent temperature that was calibrated, 29 K, corresponded to an actual pellet temperature of 34 K. The lowest apparent temperature reached was 14 K, so pellet temperatures of about 20 K were achieved. However, when the pellets were prepared at low temperatures and the sample holder was attached to the cryotip at ~100 K, as was done for the infrared studies, the lowest attainable apparent temperature was only 40 K corresponding to an actual temperature of about 45 K. It was concluded that the limiting factor in attaining low temperatures was the difficulty in compressing the indium gasket which provides the thermal contact between the pellet sample holder and the cryotip when the connection was made at 100 K.

Initially pellets of oxetane deuterate I were studied to check that changes in the apparent temperatures also resulted in changes in the actual sample temperature when an absorbing sample was present. This was found to be so, because changes in the apparent temperatures resulted in changes in the guest band frequencies consistent with those reported by P. Wright (2).

Three major problems were encountered in the present study of the clathrate hydrates dispersed in pellets. The first was that significant quantities of ice condensed onto the surface of the pellet. The second was that although good spectra could be obtained when very small quantities of the hydrate were used, larger amounts of hydrates were necessary for the study of the guest bands, and these pellets yielded poorer spectra, with lower baseline transmission above 3000 cm^{-1}, than mulls. The third problem was that the absorption bands appeared to be distorted by Christiansen effects (195). The second problem was not as pronounced in the spectra of ethylene oxide hydrate, probably because the ethylene oxide bands are stronger than those of cyclopropane in cyclopropane hydrate I. The third problem was also not as serious in the spectra of ethylene oxide hydrate, the reason for which is not known.

The amount of ice condensed on the pellet remained fairly constant after the transfer line was inserted into the optical cell and the sample was cooled below 100 K. Thus since no leaks were detected in the optical cell, the ice must have originated on the upper part of the cell where it had condensed during the assembly of the cell. The ice probably condensed when the cell was raised slightly out of the cold can to insert the platinum resistance thermometer into the sample holder and to attach the radiation shield. Once the cell was assembled and evacuated, the ice could have been sublimed off the pellet by heating the sample to 200 K. However, this would have risked decomposition of the cyclopropane hydrate I, since at 200 K its decomposition pressure is 5 Torr. This technique was used for the more stable ethylene oxide hydrate, with some success, but no solution to the problem was found for cyclopropane hydrate I.

The other two problems associated with the pelleting technique are related, and depend on the relative refractive indices of the sample and the pelleting agent, and on how well the sample is ground and dispersed in the pelleting agent. To reduce reflection effects to a minimum, the size of the hydrate particles should be smaller than the wavelength of the radiation. This can be quite difficult to achieve, but this requirement can be relaxed if the refractive index of the dispersing medium is the same as that of the sample.

The refractive index of cyclopropane hydrate I can be estimated by assuming that the hydrate's molar refractivity is the weighted sum of the molar refractivities of ice and cyclopropane. From the average refractive index of ice between 1200 and 2400 cm^{-1}, 1.35 (105), and the sodium-D line refractive index of liquid cyclopropane, 1.38 (196), the refractive index of cyclopropane hydrate I is calculated to be 1.45. The sodium-D line refractive indices of potassium bromide, propane, propene and chlorotrifluoromethane are 1.56, 1.35, 1.37 and 1.30 (166,196), respectively, so the reflection effects should be of the same magnitude for cyclopropane hydrate I dispersed in any of these dispersing media. However, the refractive index of the sample is a function of frequency and changes considerably through an absorption band, such that to high frequency of the absorption band, the refractive index is less than the average value and to low frequency of the band it is greater than the average value (197). Thus, if the particle size is too large, samples of cyclopropane hydrate I dispersed in potassium bromide are expected to have higher transmission on the low frequency side of an absorption band, due to the more closely matched refractive indices of the sample and dispersing medium, and lower transmission on the high frequency side. Just the opposite effect should occur in the spectra of cyclopropane hydrate I in mulls. However, the transmission by mull samples to high frequency of broad absorption bands is usually lower than that to low frequency (Figs. 4.4 and 4.5), presumably due to the increase in the intensity of light scattered by small particles with increasing frequency. The refractive index considerations indicate that for broad bands this difference in transmission should be even more pronounced for pellet samples.

The above arguments are equally applicable to the spectrum of the deuterate since the refractive index of the deuterate parallels that of the hydrate.

4.5.2 Absorption by the Water Molecules

The temperature dependence of the water absorption bands of oxetane hydrate I has been studied previously (2). These bands changed little with temperature; consequently, only the ν_{OD}(HDO) and ν_{OD}(D_2O) bands of cyclopropane hydrate I were studied.

The $\nu_{OD}(D_2O)$ band of cyclopropane deuterate I at 105 and 45 K is shown in Fig. 4.11 and the frequencies of the features at temperatures between 155 and 45 K are given in Table 4.4. The frequencies at 85 K agree, within experimental error, with those obtained using the mulling technique (Table 4.3), except for the strongest feature at 2428 cm^{-1} and its low frequency shoulder at about 2400 cm^{-1} which are about 10 and 15 cm^{-1}, respectively to higher frequency in the spectra of mulls. The opposite change in the frequency of the peak of the $\nu_{OD}(D_2O)$ band was observed for oxetane deuterate I in mull and pellet samples (2), and both types of frequency shift must be due to reflection effects. Differences are also observed in the relative intensities of the features of the $\nu_{OD}(D_2O)$ band of cyclopropane deuterate I in mulls (Fig. 4.5) and in pellets (Fig. 4.11). These differences are in the sense expected for the reflection effects discussed in Section 4.5.1. There is little change in band shape when the sample is cooled from 155 to 45 K; the peak frequency decreased by 12 cm^{-1} and the half-width of the band decreases from 255 to 245 cm^{-1}.

The $\nu_{OD}(HDO)$ band of cyclopropane hydrate I containing 4 mole percent HDO is shown in Fig. 4.12 and the frequencies of the features at temperatures between 155 to 45 K are given in Table 4.4. This band is not as well resolved as that obtained from a mull in propene (Fig. 4.7) and resembles the $\nu_{OH}(HDO)$ band observed for mull samples

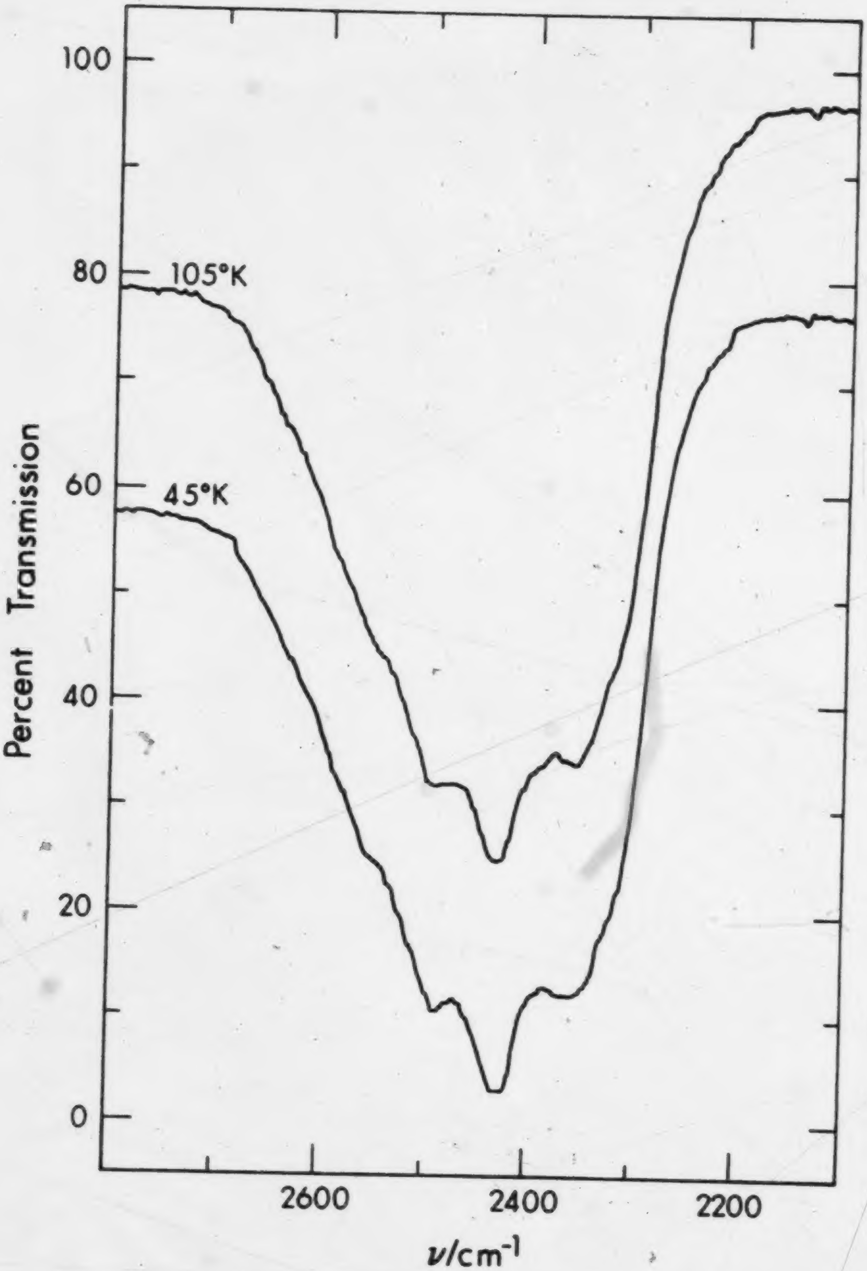

Figure 4.11. The $\nu_{OD}(D_2O)$ band of cyclopropane structure I deuterate (KBr pellet) at 105 and 45 K; resolution 2 cm^{-1}. The 45 K curve has been offset for clarity.

TABLE 4.4

Temperature Dependence of the $\nu_{OD}(D_2O)$ and $\nu_{OD}(HDO)$ Bands of Cyclopropane Structure I Deuterate and Hydrate[a], respectively.

$\nu_{OD}(D_2O)$	Temperature/K	Frequency ν/cm^{-1}		
	45-155	2316	± 5	sh
	45-155	2355	± 5	s
	45-155	2400	± 5	sh
	45	2425	± 3	vs
	65	2425		
	85	2428		
	105	2429		
	130	2431		
	155	2437		
	45-155	2488	± 5	sh
	45-155	2552	± 10	sh
$\nu_{OD}(HDO)$	45	2417	± 2	m
	55	2418		
	65	2418		
	85	2419		
	105	2420		
	130	2422		
	155	2425		
	45	2450	± 2	sh
	55	2450		
	65	2450		
	85	2452		
	105	2453		
	130	2455		
	155	2458		

a) s = strong, m = medium, sh = shoulder, v = very.

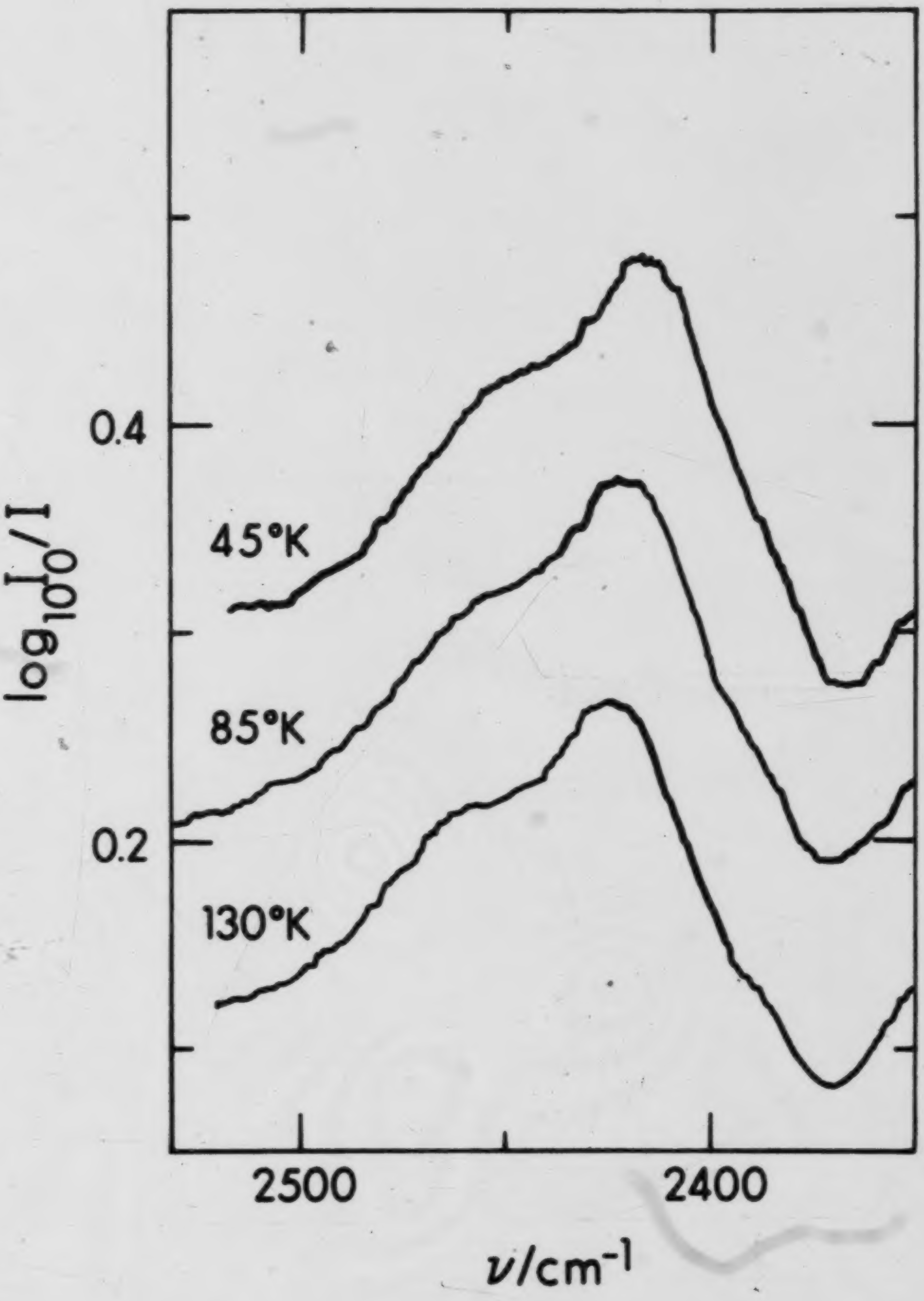

Figure 4.12. The ν_{OD}(HDO) band of cyclopropane structure I hydrate (KBr pellet) containing 4 mole percent HDO at 45, 85 and 130 K; resolution 2 cm^{-1}. The 85 and 130 K curves have been offset for clarity.

(Fig. 4.8). This is presumably due to the reflection effects discussed in Section 4.5.1. There is little change in bandshape on cooling from 155 to 45 K; the two features increase in frequency by about 8 cm^{-1} and the overall half-width of the band decreases from 74 to 66 cm^{-1}.

4.5.3 Absorption by the Cyclopropane Molecules

The cyclopropane absorption in the spectra of cyclopropane hydrate I and deuterate I at temperatures between 130 and 45 K is shown in Figs. 4.13 to 4.15. The frequencies, half-widths and peak heights are given in Table 4.5. The changes in frequencies and half-widths with temperature are small. The frequencies of the features were measured relative to fiducial marks (Section 2.10). The precision of measuring the same peak relative to the same fiducial marks was ±0.2 cm^{-1} below 2000 cm^{-1} and ±0.4 cm^{-1} above 2000 cm^{-1}, so that frequency shifts greater than thi~~s~~ are judged to be significant. Changes in half-width of the same magnitude are also judged significant for the well defined features. The peak absorbances were taken from the spectra of one hydrate and one deuterate sample, so the relative peak absorbance of the different bands are approximately correct. The estimated precision of the peak absorbances is ±0.005 units.

The shapes and frequencies of the guest absorption bands at 105 K presented in this section are essentially

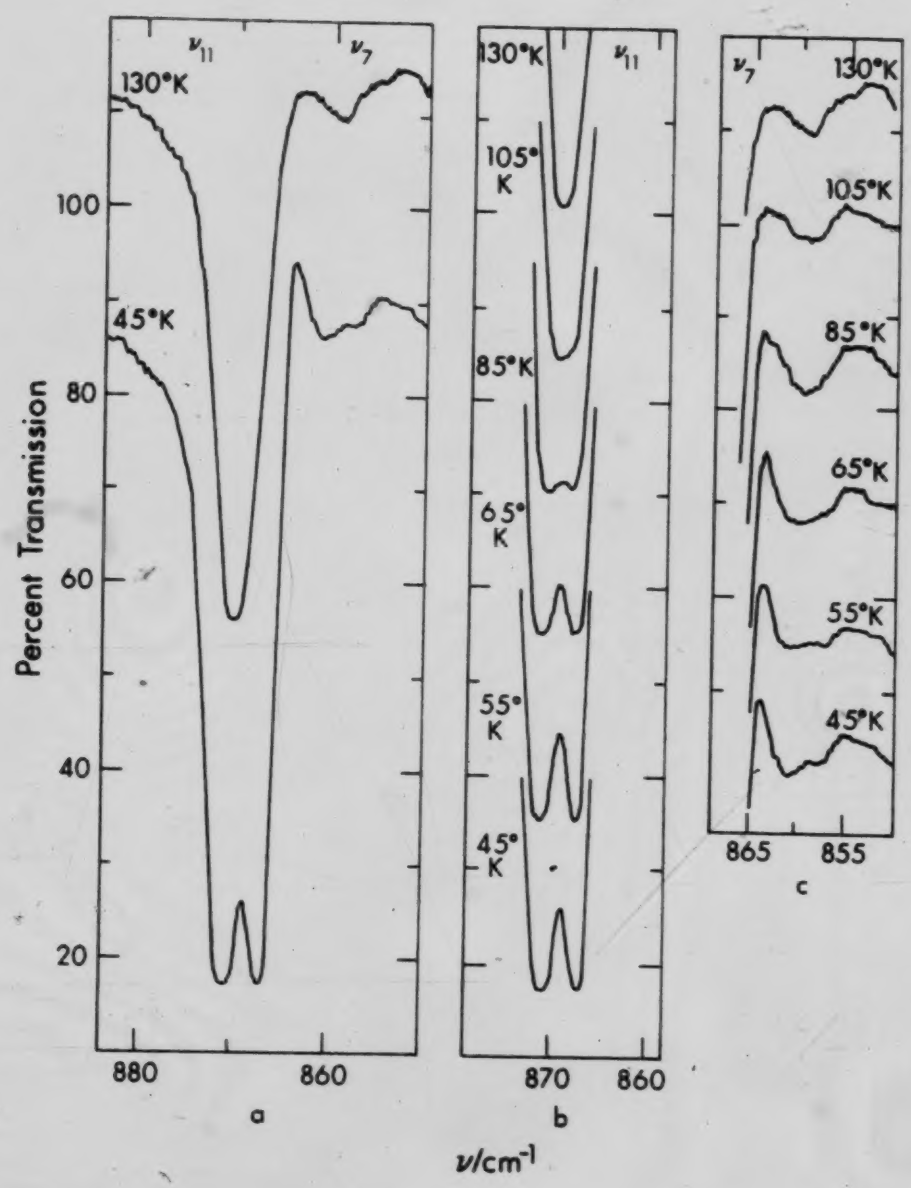

Figure 4.13. Temperature dependence of the absorption by $\nu_7(A_2'')$ and $\nu_{11}(E')$ of cyclopropane in its structure I deuterate (KBr pellet); resolution 1.4 cm^{-1}. In Figure 4.13a the 130 K curve has been offset for clarity.

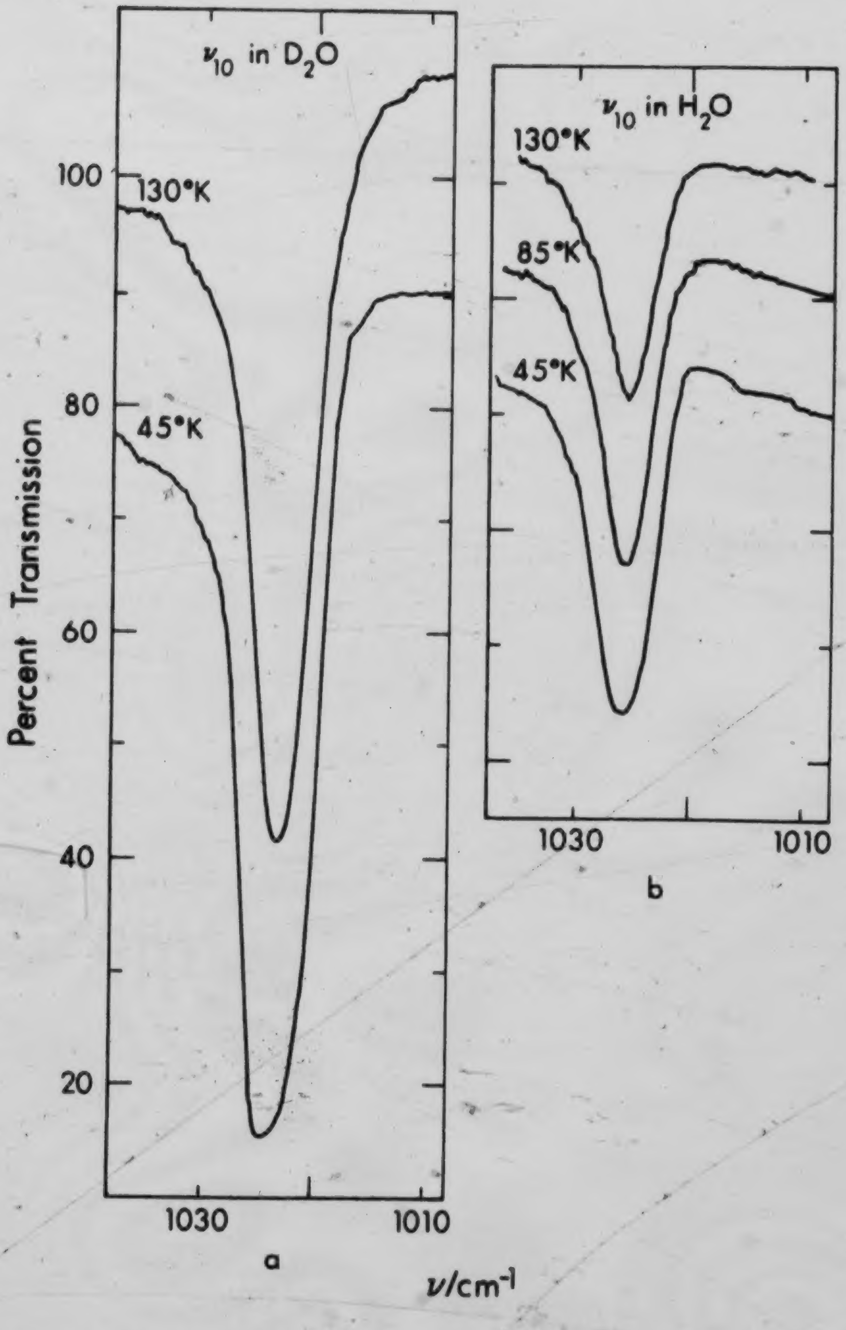

Figure 4.14. Temperature dependence of the absorption by $\nu_{10}(E')$ of cyclopropane in its structure I hydrate (b) and deuterate (a) (KBr pellet); resolution 1.4 cm^{-1}. In Figures 4.14a the 130 K curve and in Figure 4.14b the 45 and 130 K curves have been offset for clarity.

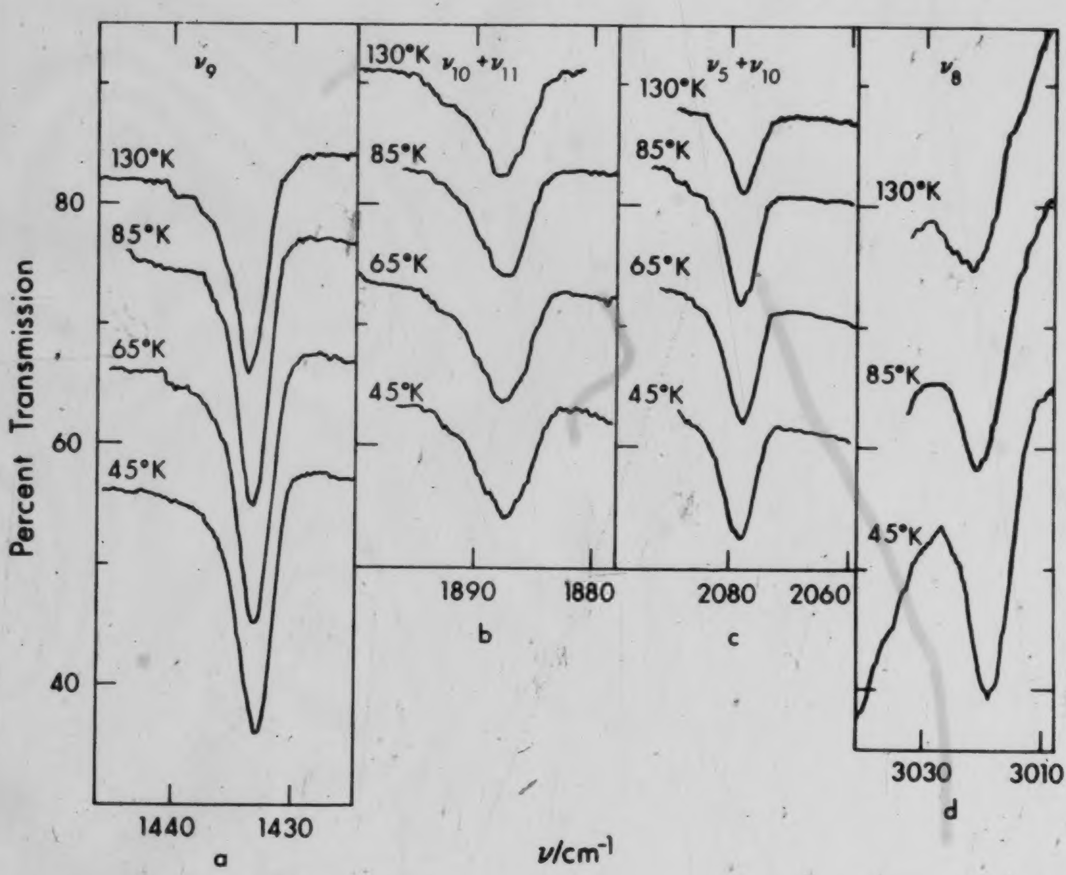

Figure 4.15. Temperature dependence of the absorption by $\nu_9(E')$, $\nu_{10}+\nu_{11}$, $\nu_5+\nu_{10}$ of cyclopropane in its structure I deuterate and $\nu_8(E')$ of cyclopropane in its structure I hydrate (KBr pellets); resolution < 1.8 cm^{-1}. In Figures 4.15a to c the 45, 65 and 85 K curves, and in Figure 4.15d the 45 and 130 K curves, have been offset for clarity.

TABLE 4.5

Temperature Dependence of Guest Features in the Mid-infrared Spectra of Cyclopropane Structure I Hydrate and Deuterate to 45 K

	Hydrate				Deuterate				
Mode	Temp	Frequency	$\Delta\nu_{1/2}^{b}$	Peak Absorbance	Mode	Temp	Frequency	$\Delta\nu_{1/2}^{b}$	Peak Absorbance
					$\nu_7(A_2'')$	45	857.5	-	-
							860.7		
						55	857.2	-	-
							860.8		
						65	859.5	6.2	.033
						85	859.4	5.2	.032
						105	859.0	4.6	.021
						130	858.8	3.8	.022
					$\nu_{11}(E')$	45	867.4	7.1	.729
							870.5		
						55	867.4	6.9	.721
							870.4		
						65	867.5	7.0	.731
							870.3		
						85	867.6	6.3	.712

(continued......)

TABLE 4.5 (continued)

		Hydrate					Deuterate		
Mode	Temp	Frequency	$\Delta\nu_{1/2}^{b}$	Peak Absorbance	Mode	Temp	Frequency	$\Delta\nu_{1/2}^{b}$	Peak Absorbance
							870.2		
						105	869.4	5.1	.709
						130	869.5	4.5	.654
						150	869.5	-	-
						180	870.1	-	-
$\nu_{10}(E')$	45	1025.7	5.6	.165	$\nu_{10}(E')$	45	1024.1	5.9	.749
	55	1025.6	5.2	.155		55	1024.0	5.7	.745
	65	1025.5	5.0	.155		65	1023.9	5.7	.746
	85	1025.3	4.9	.142		85	1023.7	5.4	.745
	105	1025.2	4.8	.130		105	1023.6	5.3	.733
	130	1025.2	4.8	.109		130	1023.5	5.0	.681
	150	1025.0	-	-		155	1023.4	6.0	-
						180	1023.4	7.0	-
$\nu_{9}(E')$	45	1431.9	3.7	.068	$\nu_{9}(E')$	45	1432.9	3.4	.121
	55	1431.9	3.6	.068		55	1432.9	3.1	.120
	65	1432.0	3.5	.054		65	1433.0	3.2	.127
	85	1432.1	3.5	.051		85	1433.4	3.1	.126

(continued......)

TABLE 4.5 (continued)

		Hydrate					Deuterate		
Mode	Temp	Frequency	$\Delta\nu_{1/2}^{b}$	Peak Absorbance	Mode	Temp	Frequency	$\Delta\nu_{1/2}^{b}$	Peak Absorbance
	105	1432.3	3.4	.045		105	1433.4	3.2	.127
	130	1432.5	3.7	.031		130	1433.4	3.1	.107
	155	1432.7	-	-		155	1433.4	-	-
						180	1434.8	-	-
					$\nu_{10}+\nu_{11}$	45	1887.5	4.9	.045
						55	1887.8	4.9	.042
						65	1887.7	5.0	.044
						85	1887.7	4.8	.043
						105	1887.7	4.8	.042
						130	1888.0	4.8	.044
					$\nu_5+\nu_{10}$	45	2078.5	6.0	.047
						55	2078.5	6.0	.047
						65	2078.5	5.7	.050
						85	2078.7	5.3	.047
						105	2078.6	5.2	.042
						130	2078.5	5.4	.032

(continued......)

TABLE 4.5 (continued)

	Hydrate					Deuterate			
Mode	Temp	Frequency	$\Delta\nu_{1/2}^{b}$	Peak Absorbance	Mode	Temp	Frequency	$\Delta\nu_{1/2}^{b}$	Peak Absorbance
						155	2078.5	-	-
						180	2079.5	-	-
$\nu_8(E')$	45	3018.5	7.2	.126					
	55	3018.9	7.0	.109					
	65	3019.1	7.2	.107					
	85	3019.9	8.4	.092					
	105	3019.9	10	.086					
	130	3020.5	-	.077					

---

a) The units are: K for temperature, cm^{-1} for ν and $\Delta\nu_{1/2}$, $\log_{10}I_o/I$ for peak absorbance.

b) $\Delta\nu_{1/2}$ is the full width of the peak at half height.

the same as those reported in Section 4.4.3 for mull samples, and it is clear that the hydrate was not changed by the pressure required to make a potassium bromide pellet.

Three guest bands showed significant changes with decreasing temperature. These are due to $\nu_7(A_2")$, a CH_2 rock, $\nu_{10}(E')$, a CH_2 wag, and $\nu_{11}(E')$, the ring deformation. The bands due to $\nu_7(A_2")$ and $\nu_{11}(E')$ in cyclopropane deuterate I are shown in Fig. 4.13 for temperatures between 45 and 130 K. The band due to $\nu_7(A_2")$ (Fig. 4.13c) at 130 K is a weak, fairly symmetrical band at 858.8 cm^{-1} with a half-width of 3.8 cm^{-1}. When the sample is cooled, this band broadens, splits into a doublet at about 55 K and becomes more resolved at 45 K. At 45 K the components of the doublet are separated by 3.2 cm^{-1}. Similar changes were observed for the band due to $\nu_{11}(E')$. At 130 K, this is a symmetric band at 869.5 cm^{-1} with a half-width of 4.5 cm^{-1}. When the sample is cooled, the band broadens, splits into a doublet at about 85 K, and becomes more resolved at lower temperatures. At 45 K the components of the doublet are separated by 3.1 cm^{-1}, and the overall half-width of the band is 7.1 cm^{-1}.

The bands due to $\nu_{10}(E')$ in cyclopropane deuterate I and hydrate I are shown in Figs. 4.14a and 4.14b, respectively. On cooling the sample the band broadens and becomes more asymmetric in both compounds but does not split.

The remaining bands studied are shown in Fig. 4.15. The band due to $\nu_9(E')$, a CH_2 deformation, at about 1433 cm^{-1}, in cyclopropane deuterate I (Fig. 4.15a) broadens marginally with decreasing temperature and behaves similarly in the spectrum of the hydrate (Table 4.5).

The bands due to $\nu_{10}+\nu_{11}$ and $\nu_5+\nu_{10}$ of cyclopropane deuterate I are shown in Figs. 4.15b and 4.15c, respectively. The frequencies decrease slightly with decreasing temperature, the half-width of $\nu_{10}+\nu_{11}$ is independent of temperature, while that of $\nu_5+\nu_{10}$ increases slightly with decreasing temperature.

The only band due to a C-H stretching vibration that was clearly defined and could be measured reliably in the spectra of the pellets was due to $\nu_8(E')$ in cyclopropane hydrate I (Fig. 4.15c). The frequency and half-width of this band decrease with decreasing temperature.

In summary, the trends observed with decreasing temperature are shifts to low frequency of the bands due to $\nu_8(E')$, $\nu_9(E')$, $\nu_{11}(E')$, $\nu_{10}+\nu_{11}$ and $\nu_5+\nu_{10}$, and shifts to high frequency of the bands due to $\nu_7(A_2")$ and $\nu_{10}(E')$. The half-widths of the bands due to $\nu_7(A_2")$, $\nu_9(E')$, $\nu_{10}(E')$, $\nu_{11}(E')$ and $\nu_5+\nu_{10}$ increase, and the half-width of the band due to $\nu_8(E')$ decrease with decreasing temperature while that of $\nu_{10}+\nu_{11}$ is independent of temperature. The peak absorbances of all the bands increase with decreasing temperature except for the band due to $\nu_{10}+\nu_{11}$ which is independent of temperature. The bands due to $\nu_7(A_2")$ and

ν_{11}(E') split into doublets below 55 and 85 K, respectively, and the band due to ν_{10}(E') broadens and becomes more asymmetric on cooling but does not split.

4.6 Temperature Dependence of the Absorption by Ethylene Oxide in Ethylene Oxide Hydrate

The mid-infrared spectra of mulls containing ethylene oxide hydrate and deuterate at 100 K have been reported (96). The present study was solely to determine the temperature dependence of the guest bands, in particular the band due to the ring breathing mode, $\nu_3(A_1)$ which was earlier found to be split into a doublet at 100 K (96).

The spectrum of ethylene oxide deuterate in a potassium bromide pellet at 150 K is shown in Fig. 4.16. The spectrum is consistent with that reported previously (96) indicating that the hydrate was not changed by the pressure required to make the pellet.

The frequencies, half-widths and relative peak absorbances of the absorption by encaged ethylene oxide at temperatures above 45 K are given in Table 4.6. The peak absorbances were measured from spectra of one hydrate and one deuterate sample, so the relative peak heights of the different guest bands are approximately correct. The shapes and frequencies of the guest absorption bands at 105 K presented in this section are essentially the same as those reported previously (96) for mull samples. The assignment of the ethylene oxide bands is taken from reference 96.

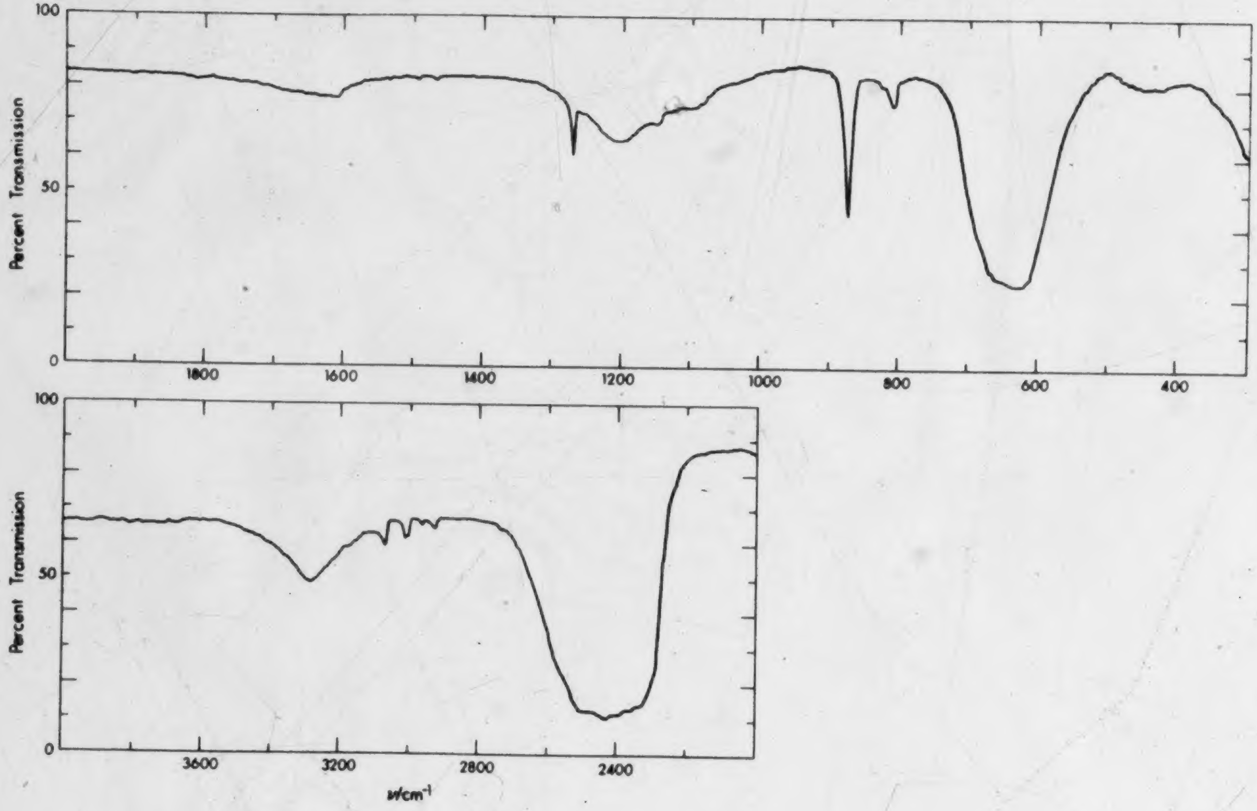

Figure 4.16. Mid-infrared spectrum of ethylene oxide deuterate in a potassium bromide pellet at 150 K; resolution $\leq$ 4 cm^{-1}.

TABLE 4.6

Temperature Dependence of Guest Features in the Mid-infrared Spectra of Ethylene Oxide Hydrate and Deuterate[a] to 45 K

Hydrate					Deuterate				
Mode	Temp	Frequency	$\Delta\nu_{1/2}$[b]	Peak Absorbance	Mode	Temp	Frequency	$\Delta\nu_{1/2}$[b]	Peak Absorbance
$\nu_8(A_2)$/ $\nu_{15}(B_2)$	45	803.7			$\nu_{15}(B_2)$	45	805.0		
	55	804.1				55	805.3		
	65	804.0				65	805.2		
	105	804.0				105	805.6		
	130	804.3				130	805.7		
	155	804.5							
					$\nu_8(A_2)$	45	807.9	7.0	.077
						55	808.1	7.0	.078
						65	808.2	6.9	.065
						105	808.5	7.6	-
						130	808.8	8.0	.044

(continued......)

TABLE 4.6 (continued)

Hydrate					Deuterate				
Mode	Temp	Frequency	$\Delta\nu_{\frac{1}{2}}^{b}$	Peak Absorbance	Mode	Temp	Frequency	$\Delta\nu_{\frac{1}{2}}^{b}$	Peak Absorbance
					$\nu_5(A_1)$	45	870.4	5.9	.524
						55	870.6	6.0	.430
						65	870.8	6.2	.389
						105	871.0	-	-
						130	871.3	7.6	.295
					$\nu_{12}(B_1)$	45	879.8		
						55	879.6		
						65	880.0		
						105	880.0		
						130	880.2		
$\nu_4(A_1)$	45	1120.2	-	-					
$\nu_{14}(B_2)$	45	1145.1	3.8	.054	$\nu_{14}(B_2)$	45	1144.8	4.0	.033
	55	1145.3	4.5	.52		55	1144.9	4.5	.033
	65	1145.2	5.0	.044		65	1144.9	5.0	.032
	85	1145.3	6.0	.044		-			

(continued......)

TABLE 4.6 (continued)

	Hydrate					Deuterate			
Mode	Temp	Frequency	$\Delta\nu_{1/2}^{b}$	Peak Absorbance	Mode	Temp	Frequency	$\Delta\nu_{1/2}^{b}$	Peak Absorbance
	105	1145.3	6.0	.041		105	1145.1	-	-
	130	1146.3	6.2	.023		130	1146.0	6.5	.010
	155	1146.9	7.8	.014					
$\nu_{11}(B_1)$	45	1148.4			$\nu_{11}(B_1)$	45	1147.3		
	55	1148.3				55	-		
	65	1148.6				-			
	85	1149.0				-			
	105	1149.3				105	1147.6		
$\nu_3(^{13}C-^{12}CH_4O)$	45	1252.0	-	.007	$\nu_3(^{13}C-^{12}CH_4O)$	45	1253.0	-	-
	55	1252.0				55	1252.4		
	65	1252.0				65	1253.6		
	85	1252.0				-			
	105	-				105	1253.5		
	130	-				130	1253.8		
$\nu_3(A_1)$	45	1265.5	4.1	.320	$\nu_3(A_1)$	45	1266.0	3.7	.171

(continued......)

TABLE 4.6 (continued)

		Hydrate					Deuterate		
Mode	Temp	Frequency	$\Delta\nu_{\frac{1}{2}}^{b}$	Peak Absorbance	Mode	Temp	Frequency	$\Delta\nu_{\frac{1}{2}}^{b}$	Peak Absorbance
		1267.9					1268.1		
	55	1265.6	4.2	.302		55	1266.1	3.5	.180
		1268.0					1268.2		
	65	1265.7	4.1	.300		65	1266.4	3.6	.157
		1268.0					1268.2		
	85	1265.8	3.7	.300		–			
		1268.1							
	105	1265.9	3.8	.302		105	1266.7	–	–
		1268.1					1268.7		
	130	1266.4	3.6	.257		130	1267.0	3.1	.147
		1268.2					1268.9		
	155	1266.9	3.6	.190					
$\nu_3(A_1)$	45	1280.0	–	.009	$\nu_3(A_1)$	45	1280.7	–	–
	55	1280.3				55	–		
	65	1280.3				65	–		
	85	1280.4				–			
	105	1280.7				105	1281.0		
	130	1280.7				130	1281.4		
	155	1282.0							

(continued......)

TABLE 4.6 (continued)

Hydrate					Deuterate				
Mode	Temp	Frequency	$\Delta\nu_{1/2}^{b}$	Peak Absorbance	Mode	Temp	Frequency	$\Delta\nu_{1/2}^{b}$	Peak Absorbance
$\nu_{10}(B_1)$	45	1463.9	3.3	.038	$\nu_{10}(B_1)$	45	1464.9	1.9	.021
	55	1464.0				55	1465.1		
	65	1464.0				65	1465.5		
	85	1464.0				–			
	105	1464.2				105	1465.3		
	130	1464.5				130	1465.7		
$\nu_2(A_1)$	45	1488.6	3.0	.026	$\nu_2(A_1)$	45	1489.8	<2	.020
	55	1488.6				55	1490.0		
	65	1488.5				65	1490.0		
	85	1488.6				–			
	105	1488.8				105	1490.0		
	130	1489.3				130	1490.2		
$2\nu_{10}$	45	2910.2			$2\nu_{10}$	45	2911.9	~3	.026
	55	2910.4				55	2911.9		
	65	2910.7				65	2911.7		
	85	2910.7				–			
	105	2911.1				105	2912.7		

(continued......)

TABLE 4.6 (continued)

	Hydrate					Deuterate			
Mode	Temp	Frequency	$\Delta\nu_{½}^{b}$	Peak Absorbance	Mode	Temp	Frequency	$\Delta\nu_{½}^{b}$	Peak Absorbance
	130	2912.1				130	2913.7		
	155	2912.9							
$\nu_2+\nu_{10}$	45	2916.6	3.6	.126	$\nu_2+\nu_{10}$	45	2918.6	3.4	.086
	55	2916.7	3.8	.119		55	2918.8	3.4	.090
	65	2917.1	-	.113		65	2919.5	3.4	.077
	85	2917.3	-	.106		-			
	105	2917.3	3.8	.098		105	2919.7	-	-
	130	2917.8	4.4	.059		130	2920.5	3.8	.051
	155	2919.1	-	.039					
$2\nu_2$	45	2954.0	4.0	.033	$2\nu_2$	45	2956.3	3.6	.032
	55	2954.2	4.0	.039		55	2956.5	3.8	.032
	65	2954.4	4.0	.035		65	2956.5	3.8	.036
	85	2954.4	4.0	.033		-			
	105	2954.9	-	.027		105	2956.9	-	-
	130	2955.8	-	-		130	2957.8	3.8	.025
	155	2956.5	-	-					

(continued......)

TABLE 4.6 (continued)

Hydrate				
Mode	Temp	Frequency	$\Delta\nu_{1/2}^{b}$	Peak Absorbance
$\nu_9(B_1)$	45	2993.7	4.6	.144
	55	2994.0	4.8	.139
	65	2994.1	4.8	.128
	85	2994.1	4.8	.127
	105	2994.3	6.0	.120
	130	2995.2	-	-
	155	2997.0	-	-
$\nu_1(A_1)$	45	3003.2	4.6	.061
	55	3003.5		
	65	3003.9		
	85	3003.7		
	105	3003.8		
	130	3004.7		
	155	3006.0		

Deuterate				
Mode	Temp	Frequency	$\Delta\nu_{1/2}^{b}$	Peak Absorbance
$\nu_9(B_1)$	45	2995.4	3.0	.164
	55	2995.7	3.8	.156
	65	2995.9	4.0	.117
	-			
	105	2996.7	-	-
	130	2997.2	6.2	.143
$\nu_1(A_1)$	45	3005.3	3.6	.074
	55	3005.4	3.8	.076
	65	3005.3	4.0	.065
	-			
	105	3006.1		
	130	3006.5	5.0	.057
$\nu_{13}(B_2)$	45	3064.5	7.0	.110
	55	3064.7	7.0	.117

(continued......)

TABLE 4.6 (continued)

		Hydrate					Deuterate		
Mode	Temp	Frequency	$\Delta\nu_{1/2}$[b]	Peak Absorbance	Mode	Temp	Frequency.	$\Delta\nu_{1/2}$[b]	Peak Absorbance
						65	3064.9	7.2	.098
						-			
						105	3066.8	-	-
						130	3068.2	-	.052

---

a) Units are: K for temperature, cm^{-1} for ν and $\Delta\nu_{1/2}$, $\log_{10}I_o/I$ for peak absorbance.

b) $\Delta\nu_{1/2}$ is the full width of the peak at half height.

The absorption by $\nu_5(A_1)$, $\nu_8(A_2)$, $\nu_{12}(B_1)$ and $\nu_{15}(B_2)$ of ethylene oxide in ethylene oxide deuterate is shown in Fig. 4.17. $\nu_8(A_2)$ and $\nu_{15}(B_2)$ yield a single broad, asymmetric peak at about 808 cm^{-1} (Fig. 4.17a) at 130 K which sharpens and splits into a doublet when the sample is cooled to 45 K. At 45 K, the overall half-width of the band is 7.0 cm^{-1} and the two features are separated by about 2.9 cm^{-1}. The strongest feature, at 808 cm^{-1}, has been assigned to $\nu_{15}(B_2)$, a CH_2 rock, while the weaker feature has been assigned to $\nu_8(A_2)$, also a CH_2 rock (96). The ring deformation, $\nu_5(A_1)$, at 870 cm^{-1} (Fig. 4.176) is the strongest guest absorption observed in the spectrum of the deuterate. At 130 K the band has a half-width of 6 cm^{-1} and a high frequency shoulder at 880.2 cm^{-1} which has been assigned to $\nu_{12}(B_1)$, also a ring deformation (96). These two features become only slightly more resolved as the sample is cooled.

The features assigned to ν_3, the ring breathing mode of ethylene oxide hydrate and deuterate are shown in Figs. 4.18a and 4.18b, respectively. The band is more clearly defined in the hydrate (Fig. 4.18a) in which it is an asymmetric band at 1266.9 cm^{-1} at 155 K. As the sample is cooled, the band develops a high frequency shoulder at 130 K which becomes a well defined peak at 105 K, and then becomes more resolved at 45 K. At 45 K, the separation of the doublet is 2.4 cm^{-1} and the overall half-width is 4.1 cm^{-1}. Two weak satellite bands are observed at about

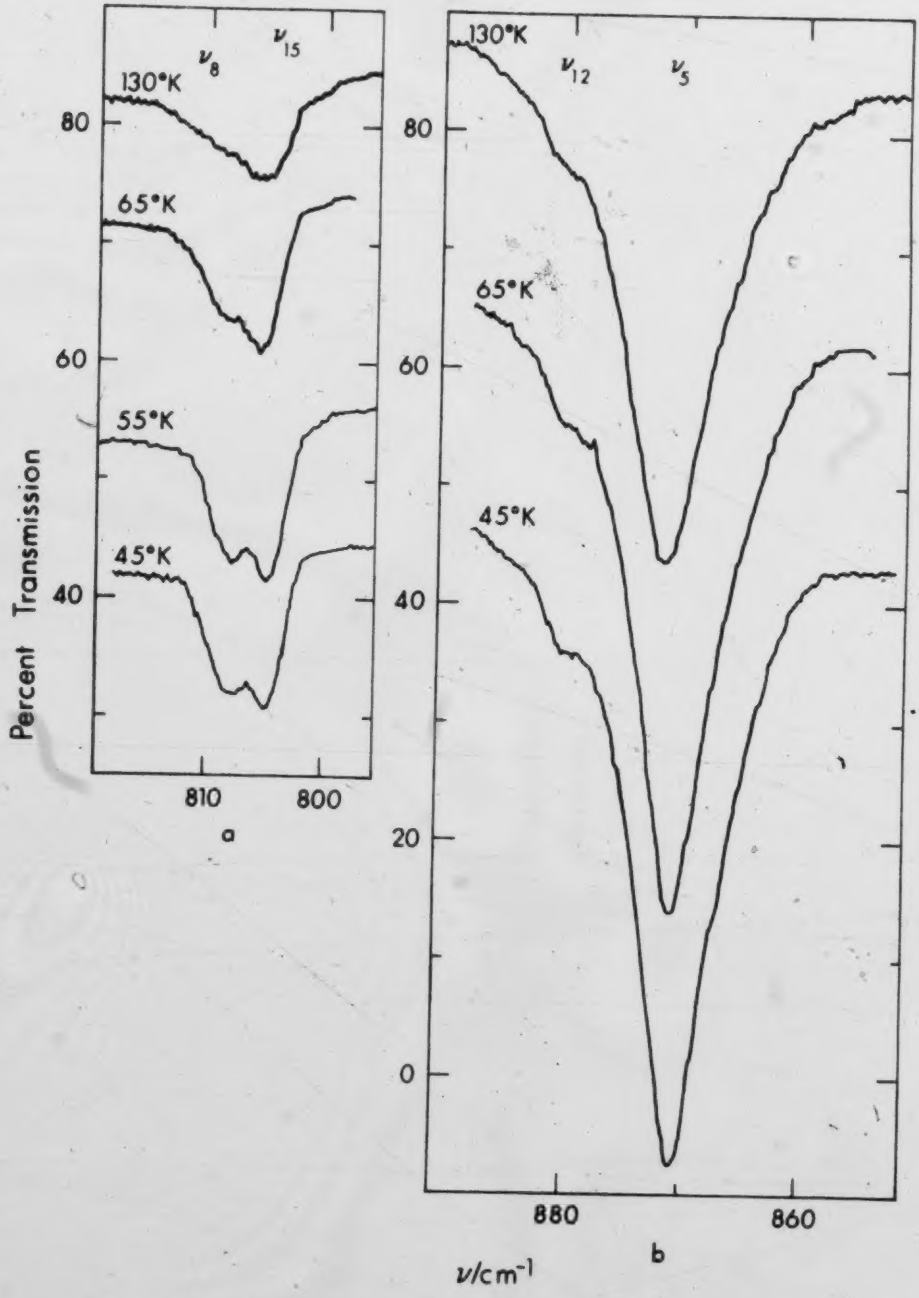

Figure 4.17. Temperature dependence of the absorption by $\nu_8(A_2)$, $\nu_{15}(B_2)$, $\nu_5(A_1)$ and $\nu_{12}(B_1)$ of ethylene oxide in its deuterate (KBr pellet); resolution 1.4 cm^{-1}. All curves except the 130 K curves have been offset for clarity.

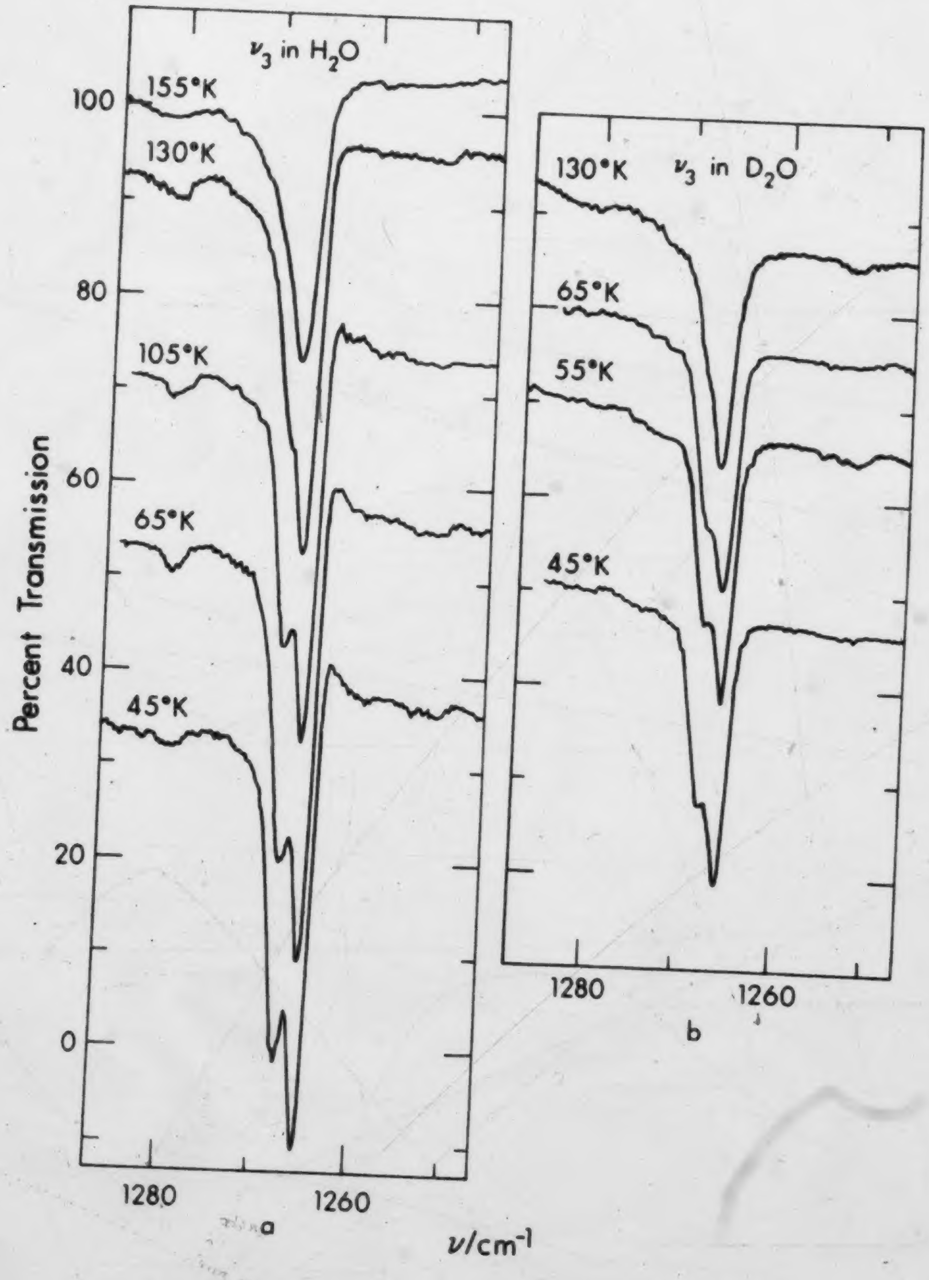

Figure 4.18. Temperature dependence of the absorption by $\nu_3(A_1)$ of ethylene oxide in its hydrate (a) and deuterate (b) (KBr pellet); resolution 1.4 cm^{-1}. All curves except the 130 K curves have been offset for clarity.

15 cm^{-1} to high and low frequency of the doublet. These are not, however, as well defined as in the previous study (96) and they appear to be essentially independent of temperature.

The absorption by $\nu_2(A_1)$, $\nu_4(A_1)$, $\nu_{10}(B_1)$, $\nu_{11}(B_1)$ and $\nu_{14}(B_2)$ of ethylene oxide in ethylene oxide hydrate is shown in Fig. 4.19. All of the features are poorly defined at 155 K. At 105 K, the peak at 1145.3 cm^{-1} due to $\nu_{14}(B_2)$, a CH_2 twist, has a clearly defined high frequency shoulder at 1149.3 cm^{-1} which is assigned to $\nu_{11}(B_1)$, a CH_2 wag. As the sample is cooled, the main peak increases in intensity and sharpens but the shoulder remains unresolved. At 45 K, the overall half-width of the band is 3.8 cm^{-1}. The band due to $\nu_4(A_1)$, a CH_2 wag, is at about 1120 cm^{-1} but was too weak to yield any useful information.

The CH_2 deformations, $\nu_2(A_1)$ and $\nu_{10}(B_1)$ are observed at about 1464 and 1489 cm^{-1}, respectively in the spectra of the hydrate (Fig. 4.18b) and deuterate (Table 4.6) with half-widths of 2 to 3 cm^{-1}. As the sample is cooled the intensity of the features increases but due to the weakness of the features little useful information is obtained.

The absorption by ethylene oxide in ethylene oxide deuterate between 2900 and 3100 cm^{-1} is shown in Fig. 4.20. $2\nu_{10}$, $\nu_2+\nu_{10}$ and $2\nu_2$ are observed at 2912, 2919 and 2956 cm^{-1} and all yield bands with half-widths of about 3 cm^{-1}. The bands due to the C-H stretching vibrations, $\nu_9(B_1)$, $\nu_1(A_1)$ and $\nu_{13}(B_2)$ are observed at 2996, 3005 and

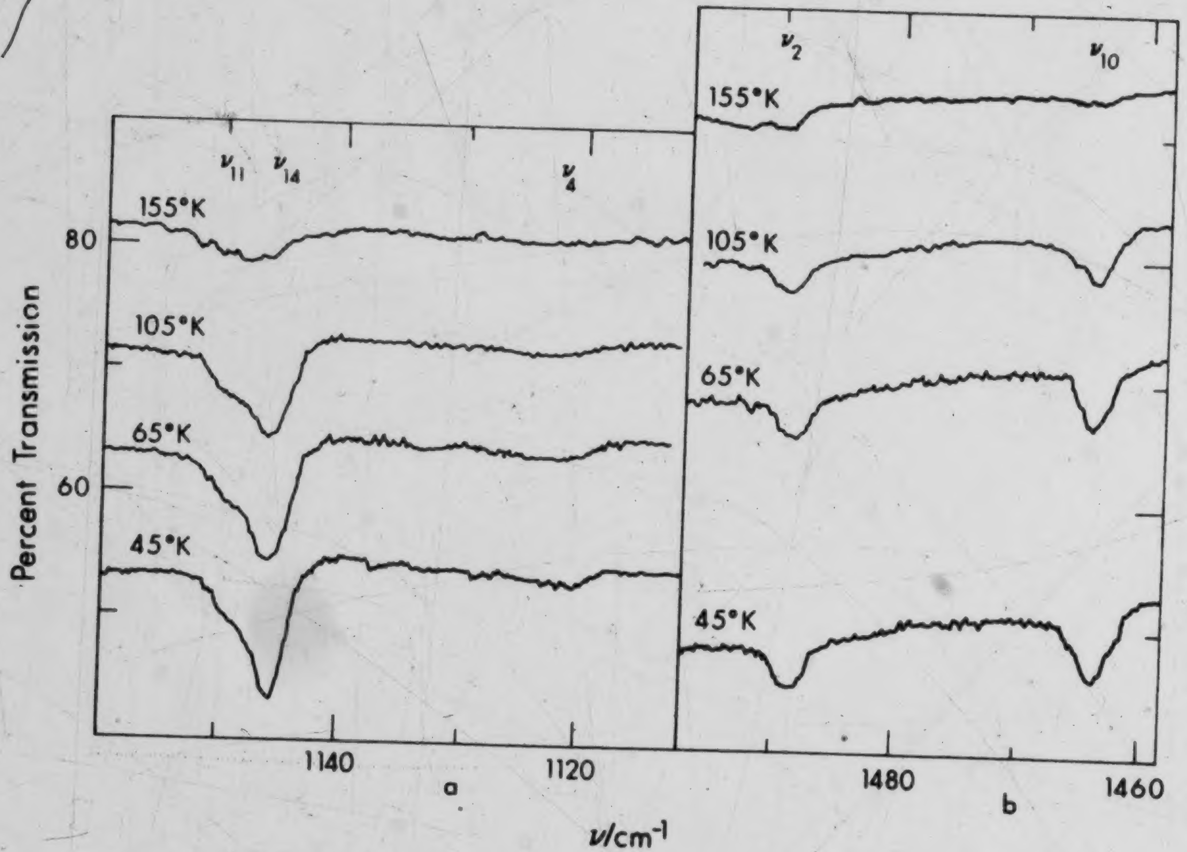

Figure 4.19. Temperature dependence of the absorption by $\nu_{11}(B_1)$, $\nu_{14}(B_2)$, $\nu_4(A_1)$, $\nu_2(A_1)$ and $\nu_{10}(B_1)$ of ethylene oxide in its hydrate (KBr pellet); resolution 1.4 cm^{-1}. All curves except the 155 K curve of Figure 4.19a and 65 K curve of Figure 4.19b have been offset for clarity.

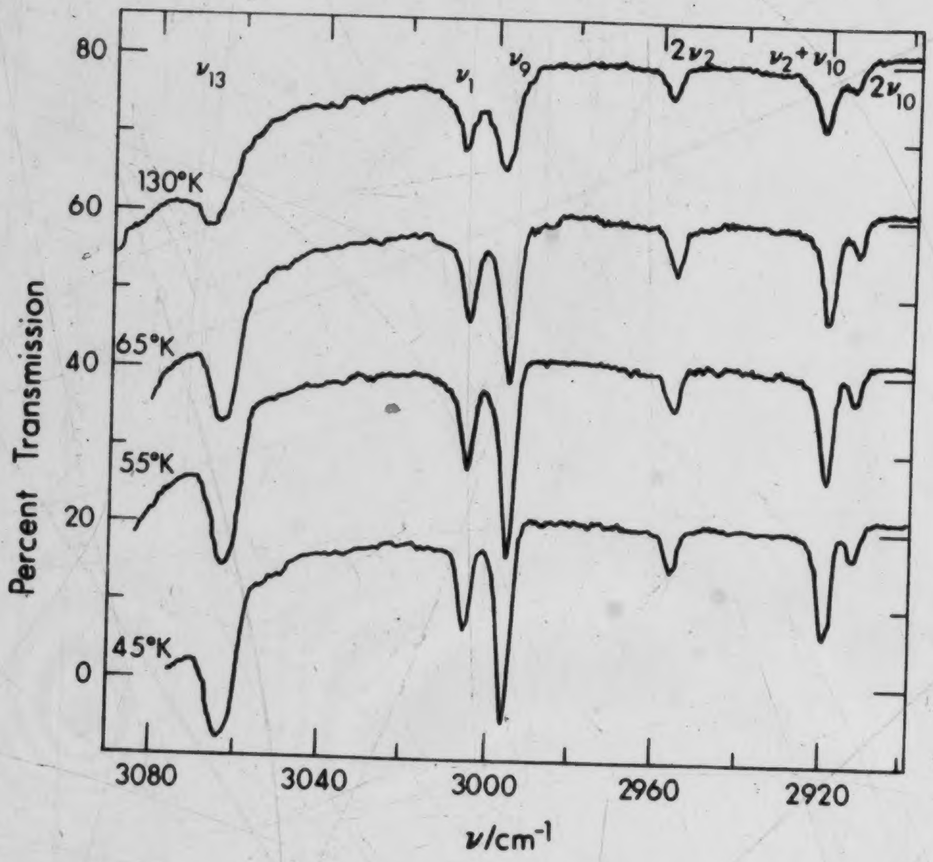

Figure 4.20. Temperature dependence of the absorption between 2900 and 3100 cm^{-1} by ethylene oxide in ethylene oxide deuterate (KBr pellet); resolution 1.8 cm^{-1}. All curves except the 130 K curve have been offset for clarity.

3065 cm^{-1}, with half-widths of 3, 4 and 7 cm^{-1}, respectively. On cooling, all of the bands increase in intensity and decrease in half-width.

In summary, the general trends observed with decreasing temperature are a small but definite shift to lower frequency of all the guest bands (Table 4.6), which for the better defined features is of the order of 1 cm^{-1}. All of the bands sharpen and increase in intensity, with decreasing temperature. The bands due to $\nu_8(A_2)$, $\nu_{14}(B_2)$ and $\nu_3(A_1)$ at 808, 1145 and 1268 cm^{-1}, respectively all develop high frequency features at or just below 130 K.

Chapter Five. Discussion of the Mid-Infrared Spectra of the Structure I Hydrates of Cyclopropane and Ethylene Oxide

5.1 Introduction

The comparison of the cyclopropane absorption frequencies and bandshapes in the spectra of cyclopropane hydrate I and deuterate I indicates that the vibrations of the cyclopropane molecules essentially do not couple with those of the water molecules, and so the absorption due to the host and guest are considered separately in Sections 5.2 and 5.3, respectively. The absorption due to the guest molecules of ethylene oxide hydrate are also discussed in Section 5.3.

The study of cyclopropane hydrate I is the third in a series of studies of the mid-infrared spectra of the clathrate hydrates (2,96). Detailed discussions of the water absorption bands of ethylene oxide hydrate, the oxetane hydrates and the disordered ices have been given elsewhere (2,96). In Section 5.2 the water absorption bands of cyclopropane hydrate I are briefly discussed and compared to those of ethylene oxide hydrate, the oxetane hydrates and ice I.

In Section 5.3.1, the various factors that can affect the guest absorption of the clathrate hydrates are introduced, and in Section 5.3.2, the absorption due to the guest molecules of ethylene oxide hydrate and cyclopropane hydrate I is discussed.

5.2 Absorption by the Water Molecules

The following discussion of the water absorption bands, except for that of their temperature dependence, will be limited to those bands observed in the spectra of mull samples, since these bands are better defined than those of the pellet samples. The discussion of the water absorption bands is best started with the ν_{OD}(HDO) band, since this band is not influenced by intra-or intermolecular coupling, and is less influenced by anharmonic effects than the ν_{OH}(HDO) band.

The ν_{OD}(HDO) bands of the disordered ice phases and clathrate hydrates are expected, like those of ices II and IX (Section 3.3.2), to reflect the different diffraction-equivalent O···O bond lengths, and generally the ν_{OD}(HDO) frequencies increase with increasing O···O bond length (2,96). However, due to the orientational disorder, there are variations in length within a set of diffraction equivalent O···O bonds and thus the ν_{OD}(HDO) absorption by each set of bonds of the disordered ices and clathrate hydrates is broader than that of the ordered ices. The half-width of the ν_{OD}(HDO) band of ice Ih is about 18 cm^{-1} (109) and can be taken as characteristic of that due to a single diffraction-equivalent O···O bond length in the disordered ices and clathrate hydrates and corresponds to a range of about 0.02 Å (110) in O···O bond length.

There are four sets of diffraction-equivalent O···O bond lengths in the structure I hydrates (55,56). The

O···O bond lengths of cyclopropane hydrate I can be calculated from those determined (56) for ethylene oxide hydrate from single crystal diffraction data, by multiplying them by the ratio of the lattice parameter of cyclopropane hydrate I, 11.96 Å, to that of ethylene oxide hydrate, 11.87 Å (56). The O···O bond lengths so determined are 2.745, 2.771, 2.789 and 2.803 Å and have the percentage occurrence of 9, 52, 26 and 13, respectively. The ν_{OD}(HDO) band of cyclopropane hydrate I is composed of two partially resolved features at 2415 and 2457 cm^{-1} in the approximate intensity ratio of 2:1 (Fig. 4.7). From the percentage occurrence of the O···O bond lengths, the absorption of the ν_{OD}(HDO) band should be mainly due to bonds of length 2.771 and 2.789 Å. The absorption due to bonds of length 2.771 Å is expected to occur at a lower frequency (96) and to be more intense than that due to the bonds of length 2.789 Å, and from this follows the assignment of the peaks at 2415 and 2457 cm^{-1} to the bonds of length 2.771 and 2.789 Å, respectively.

The ν_{OD}(HDO) band of cyclopropane hydrate I, however, differs markedly from the corresponding bands of ethylene oxide hydrate (96) and oxetane hydrate I (2) which are single, featureless bands at 2427 and 2439 cm^{-1}, respectively, with half-widths comparable to that of cyclopropane hydrate I. Thus, it is clear that different guest molecules do affect the water absorption bands.

The obvious difference between cyclopropane and ethylene oxide or oxetane is that cyclopropane does not have a permanent dipole moment. P. Wright (2) has shown, by a simple calculation, that the interaction energy between the permanent dipoles of oxetane and a water molecule of the 14-hedral cage, treated as point dipoles, is sufficient to cause a change of 0.02 Å in O···O bond length. The dipole moment of ethylene oxide, 1.88 D (198), is smaller than that of oxetane, 1.93 D (199), but the radius of the 14-hedral cage of ethylene oxide hydrate is smaller than that of oxetane hydrate I and this results in the same calculated value for the change in O···O bond length for ethylene oxide hydrate as for oxetane hydrate I. The same value can also be calculated by considering the interaction energy due to the electric field produced at an O···O bond of the 14-hedral cage by the guest dipole and the dipole moment derivative with respect to O···O distance (2,200). These calculations include many approximations, but do give the order of magnitude for the change in O···O bond length, which does of course depend on the relative orientations of the guest and water dipoles. The effect of the guest dipole on the water lattice of oxetane hydrate I and ethylene oxide hydrate is, therefore, expected to broaden the range of actual lengths of a set of diffraction-equivalent O···O bond lengths by about 0.04 Å over that range, 0.02 Å (110), that already occurs due to the proton disorder. The two features of the ν_{OD}(HDO) band of cyclopropane hydrate I are due to diffraction-equivalent O···O bonds that differ by only about 0.02 Å. Clearly, if a range of ±.02 Å is placed on these two sets of diffraction-equivalent O···O bond lengths, a continuous range of O···O bond lengths will result, which can explain why the ν_{OD}(HDO) bands of ethylene oxide hydrate and oxetane hydrate I are not resolved.

The frequencies of the ν_{OD}(HDO) bands of the ice phases and clathrate hydrates have been found to correlate well with the O-D···O bond lengths (2,96). Shown in Fig. 5.1 is a plot of the ν_{OD}(HDO) frequencies of ices I, II, IX and cyclopropane hydrate I (CP) versus O···O bond length, and of the ν_{OD}(HDO) frequencies of ices V and VI, ethylene oxide (EO), the oxetane hydrates (TMO I and TMO II) and tetrahydrofuran hydrate (THF) versus weighted mean O···O bond length. This figure is adapted from references 2 and 96 with minor changes required by more recent data (15,56). The data are summarized in Table 5.1. All of the points due to the ordered ices lie close to a straight line of slope 485 cm^{-1}/Å, and those of the other ice phases and clathrate hydrates lie close to a straight line of slope 760 cm^{-1}/Å. These correlations are only approximate since factors other than O···O bond length must influence the ν_{OD}(HDO) frequencies. However, from Fig. 5.1, it can be seen that the point due to the ν_{OD}(HDO) feature at 2415 cm^{-1} of cyclopropane hydrate I does not correlate well with the other points. This may be because the O···O bond lengths of cyclopropane hydrate I were determined from the corres-

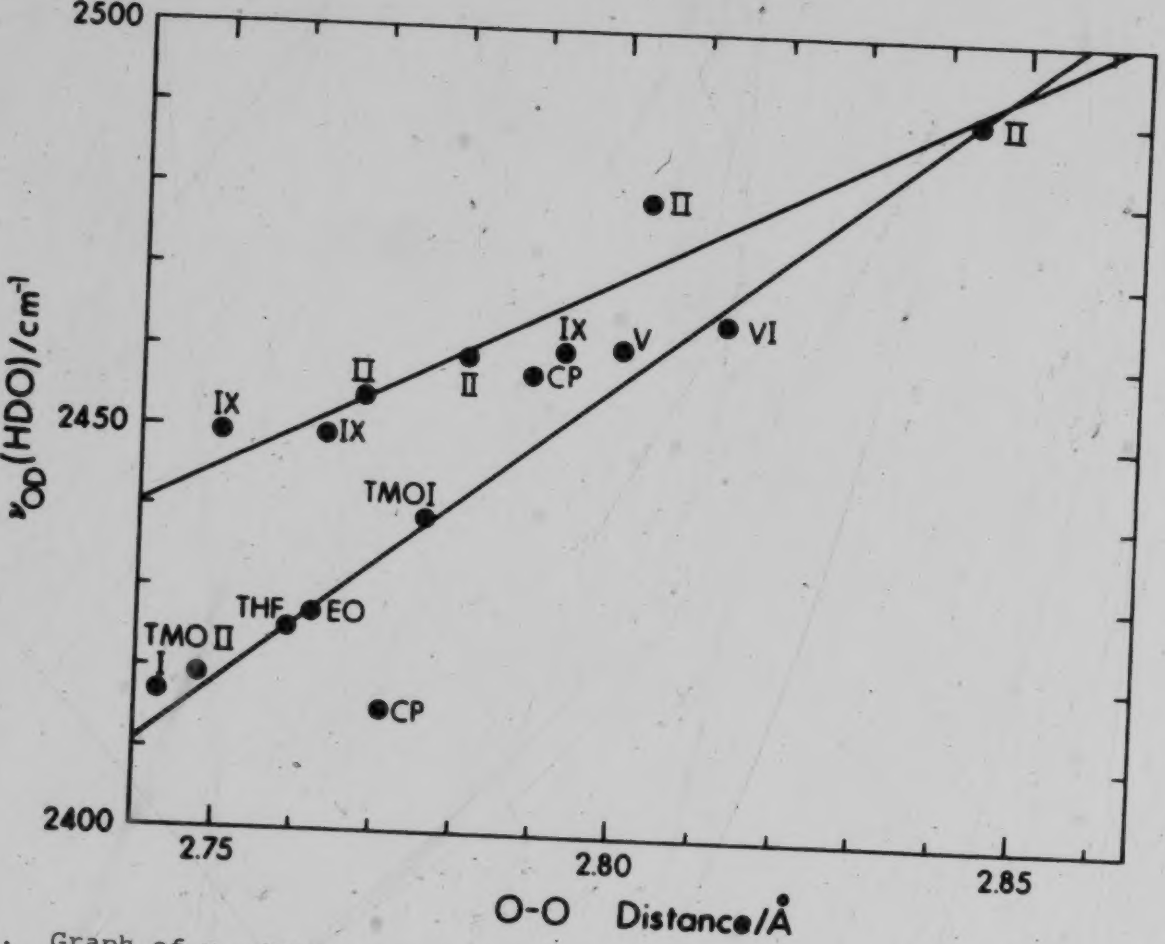

Figure 5.1. Graph of ν_{OD}(HDO) versus O-O distance for ices I, II, IX and cyclopropane structure I hydrate or weighted mean O-O distance for ices V and VI, the structure I hydrates of ethylene oxide and oxetane and the structure II hydrates of tetrahydrofuran and oxetane.

TABLE 5.1

The O...O Bond Distances and ν_{OD}(HDO) Frequencies of Ices I, II, V, VI and IX, the Structure I Hydrates[a] of Cyclopropane, Ethylene Oxide and Oxetane and the Structure II Hydrates[b] of Oxetane and Tetrahydrofuran at 100 ± 10 K

Compound	O...O Bond Distance Å	Percentage Occurrence	Weighted Mean O...O Bond Distance/Å	ν_{OD}(HDO) /cm^{-1}	Reference
Ice Ih	2.743	100	2.743	2418	10,109
Ice Ic	2.743	100	2.743	2418	10,110
Ice II	2.844			2490	16
	2.803			2479	
	2.781			2459	
	2.768			2454	
Ice V	2.766	21.45	2.800	2461	37,205
	2.781	14.3			
	2.782	14.3			
	2.798	14.3			
	2.819	14.3			
	2.820	14.3			
	2.867	7.15			
Ice VI	2.773	10	2.813	2464	51,118
	2.786	10			
	2.801	20			
	2.803	20			
	2.840	40			

(continued......)

TABLE 5.1 (continued)

Compound	O...O Bond Distance Å	Percentage Occurrence	Weighted Mean O...O Bond Distance/Å	ν_{OD}(HDO) /cm^{-1}	Reference
Ice IX	2.793			2460	
	2.763			2449	15
	2.750			2449	
Cyclopropane Hydrate I (a = 11.96Å)	2.745	9			
	2.771	52			
	2.789	26	2.778	2427	
	2.805	13			
Ethylene Oxide Hydrate (a = 11.89Å)	2.729	9			
	2.755	52			
	2.773	26	2.762	2427	96
	2.789	13			
Oxetane Hydrate I (a = 11.95Å)	2.742	9			
	2.769	52			
	2.787	26	2.776	2439	2
	2.803	13			
Oxetane Hydrate II (a = 17.06Å)	2.727	12			
	2.736	35			
	2.756	35	2.748	2419	2
	2.771	18			
Tetrahydrofuran Hydrate (a = 17.13Å)	2.738	12			
	2.747	35			
	2.767	35	2.759	2425	63
	2.783	18			

(continued......)

TABLE 5.1 (continued)

a) The O...O bond distances were calculated from those determined for ethylene oxide hydrate at 80 K (56) by multiplying by the ratio of the lattice parameter of the hydrate at about 100 K divided by 11.87Å.

b) The O...O bond distances were calculated from those determined for the double hydrate of tetrahydrofuran and hydrogen sulphide at 253 K (57) by multiplying by the ratio of the lattice parameter of the hydrate at about 100 K divided by 17.31Å.

c) In the present study Sargent and Calvert's (63) value for the lattice parameter of tetrahydrofuran hydrate was confirmed.

ponding lengths of ethylene oxide hydrate, and if the guest dipole is sufficient to broaden the range of O···O bond lengths in a set of diffraction-equivalent O···O bonds, it may also affect the average value of the bond lengths. Clearly, a single crystal diffraction study of cyclopropane hydrate I would clarify this point.

The remaining water absorption bands of cyclopropane hydrate I are broad and similar to the corresponding bands of ethylene oxide hydrate (96), the oxetane hydrates (2) and ice I (110). For ices II and IX, it was shown that the breadth of the $\nu_{OD}(D_2O)$ bands is due to the combined effects of nonequivalent sites, and intra- and intermolecular coupling (Section 3.4). Undoubtedly; these same factors determine the breadth of the water absorption bands of the clathrate hydrates and disordered ices. Ices II and IX are ordered, and so it is possible to assign the features on the $\nu_{OD}(D_2O)$ bands to unit-cell-group allowed vibrations (Section 3.4). For these ices the breadth of the features must be explained by second order effects, namely anharmonicity. For the disordered ices and clathrate hydrates, the orientational disorder relaxes the $\underline{k}=0$ selection rule and all vibrations are infrared and Raman active. Thus the breadth of the features is readily explained as due to fundamental absorption. The absorption by the disordered ices and clathrate hydrates should be related through an intensity distribution function to the density of vibrational states and, clearly, a detailed assignment of the features is impossible without a knowledge of the density of vibrational states.

Shown in Fig. 5.2 are the $\nu_{OH}(H_2O)$ and $\nu_{OD}(D_2O)$ bands of ice I (110), oxetane hydrate I and oxetane hydrate II (2) and in Fig. 5.3 are the $\nu_{OH}(H_2O)$ and $\nu_{OD}(D_2O)$ bands of ethylene oxide hydrate (96). The $\nu_{OH}(H_2O)$ bands of these hydrates, cyclopropane hydrate I (Fig. 4.4) and ice I (110), have their frequency of maximum absorption between 3220 and 3235 cm^{-1}, a high frequency shoulder at 3335 to 3400 cm^{-1} and a low frequency shoulder at 3100 to 3150 cm^{-1}. Cyclopropane hydrate I also has a clearly defined sharp shoulder at 3176 cm^{-1} (Fig. 4.4). The corresponding $\nu_{OD}(D_2O)$ bands of all these phases have their frequencies of maximum absorption between 2425 and 2440 cm^{-1}, a high frequency shoulder at 2485 to 2500 cm^{-1}, which is more pronounced in the spectra of the clathrate deuterates (Fig. 5.2), a low frequency feature at 2330 to 2370 cm^{-1} which is resolved as a well defined peak in cyclopropane deuterate I (Fig. 4.5), oxetane deuterate II and ice I (Fig. 5.2), and also a low frequency shoulder at 2240 to 2310 cm^{-1}. The $\nu_{OD}(D_2O)$ bands of cyclopropane deuterate I and ice I also have a shoulder at 2415 and 2395 cm^{-1}, respectively.

From the comparison of the $\nu_{OH}(H_2O)$ and $\nu_{OD}(D_2O)$ bands of the clathrate hydrates and ice I (Figs. 4.4, 4.5, 5.2 and 5.3) several conclusions are reached. These are that the $\nu_{OH}(H_2O)$ bands are all similar, and the presence of a dipolar (oxetane hydrate I) or nondipolar guest (cyclopropane hydrate I) or even the presence of no guest at all (ice I)

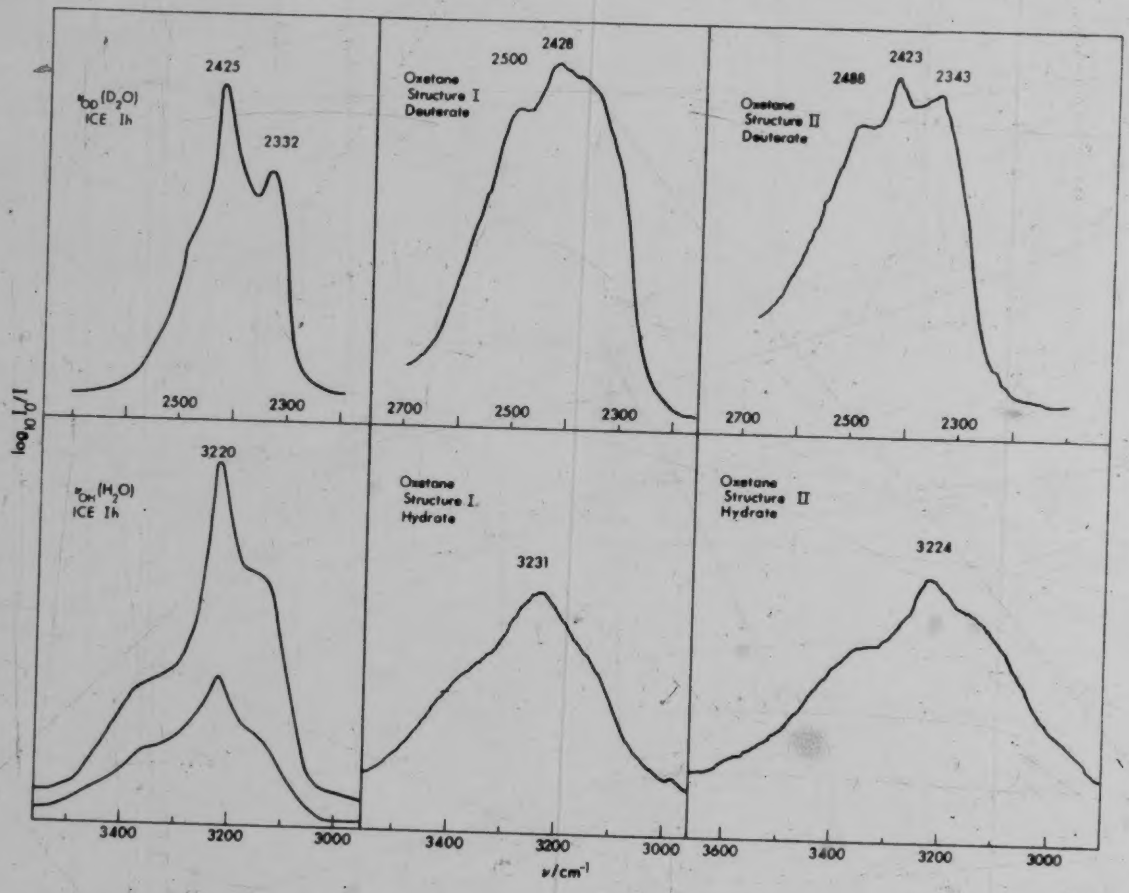

Figure 5.2. The $\nu_{OH}(H_2O)$ and $\nu_{OD}(D_2O)$ bands of ice Ih and the oxetane hydrates.

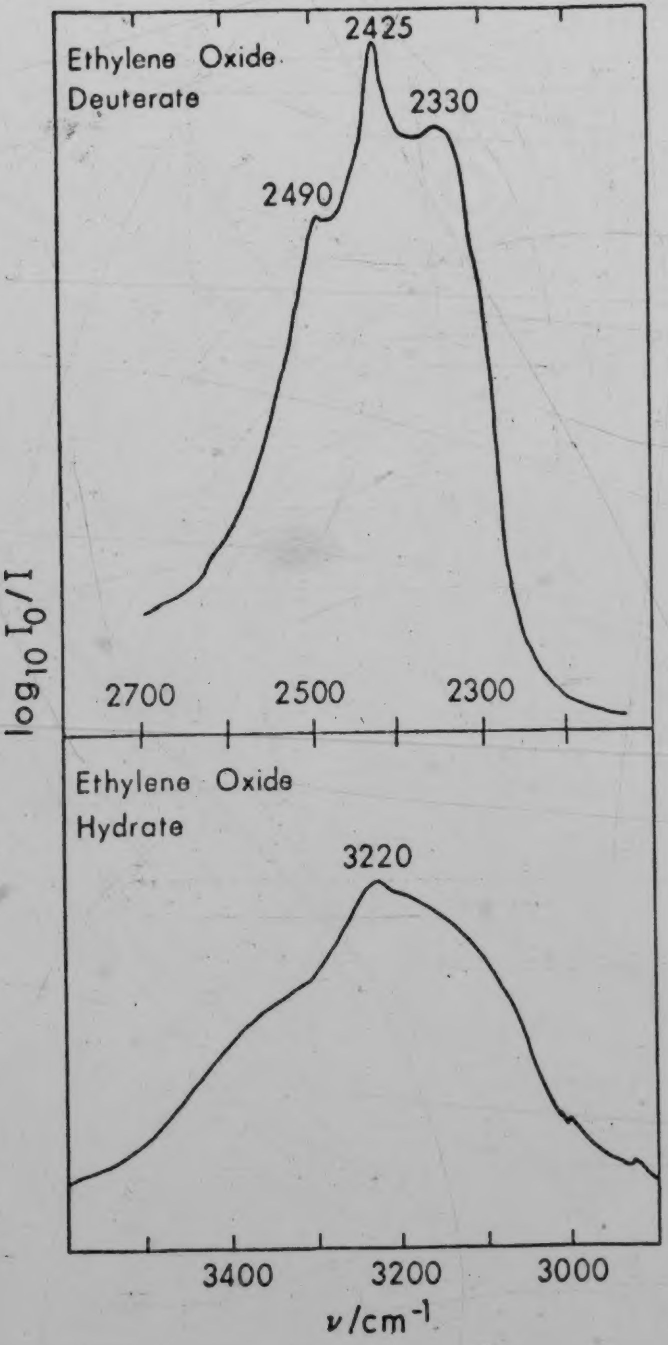

Figure 5.3. The $\nu_{OH}(H_2O)$ and $\nu_{OD}(D_2O)$ bands of ethylene oxide hydrate.

has little effect, except to change the apparent relative intensities of the features. The $\nu_{OD}(D_2O)$ bands of the clathrate deuterates and ice I do however show more structure than the $\nu_{OH}(H_2O)$ bands and the differences in band structure for the different compounds are more marked than for the $\nu_{OH}(H_2O)$ bands.

The poorer definition of the $\nu_{OH}(H_2O)$ band compared to that of the $\nu_{OD}(D_2O)$ band must arise from the greater anharmonicity of the O-H compared with the O-D stretching vibrations. This is because features with half-widths $\Delta\nu_{\frac{1}{2}}$ separated by $\Delta\nu$ in the $\nu_{OD}(D_2O)$ band should, except for anharmonicity, yield features of half-width about $\sqrt{2}\Delta\nu_{\frac{1}{2}}$ separated by about $\sqrt{2}\Delta\nu$ in the $\nu_{OH}(H_2O)$ band, so that the $\nu_{OH}(H_2O)$ band has the same appearance as the $\nu_{OD}(D_2O)$ band but extends over a wider frequency range. The effect of anharmonicity of the type discussed for ices II and IX (Section 3.3.2) is to broaden the features without changing their separation significantly, and thus, since the O-H vibrations are more anharmonic than the O-D vibrations, this results in the poorer definition of the $\nu_{OH}(H_2O)$ band than the $\nu_{OD}(D_2O)$ bands.

Significant differences are observed between the $\nu_{OD}(D_2O)$ bands of the clathrate deuterates and ice I. The $\nu_{OD}(D_2O)$ band of oxetane deuterate I is not as well resolved as that of cyclopropane deuterate I or ethylene oxide deuterate. Further, the shape of the $\nu_{OD}(D_2O)$ band of cyclopropane deuterate I (Fig. 4.5) is almost identical to that of oxetane deuterate II. This strongly suggests that the differences between the $\nu_{OD}(D_2O)$ bands of the clathrate deuterates depend on the guest molecule rather than on the structure of the water lattice. The differences between the $\nu_{OD}(D_2O)$ bands of the structure I deuterates, presumably, depend on the polarity and size of the guest molecule, and the band of the deuterate of the nondipolar guest cyclopropane is believed to approximate that of the empty deuterate water lattice.

There is a strong correspondence between the features observed for ice I and cyclopropane deuterate I; however, the relative intensities of the features do differ. These differences clearly contain useful information. In order to extract this information, calculations similar to those done for ices II and IX (Section 3.4) would have to be done for ice I and the empty clathrate hydrate water lattices and these calculations are by no means trivial. The proton disorder necessitates using in these calculations a large number of molecules oriented at random but complying with the Bernal-Fowler rules (3,201). The calculations would have to be repeated using different orientations of the water molecules to check for reproducibility. If the calculated and observed spectra agreed, a detailed interpretation of the bands would then be possible. The calculations are very time consuming, and form a project within themselves, and are out of the scope of this thesis. Recently calculations of this type have been done for ice Ih (125), but the agreement between the observed and calculated spectra was not very good, and clearly calculations of this type for the clathrate hydrates would be more difficult due to their more complex structure.

The $\nu_R(D_2O)$ bands of ice I (110), the oxetane deuterates (2), ethylene oxide deuterate (96) and cyclopropane deuterate I are very similar. The corresponding $\nu_R(H_2O)$ bands are also very similar except for their high frequency sides which are partially obscured in some of the clathrate hydrates due to guest absorption. All of the clathrate deuterates and ice I have their frequency of maximum absorption between 610 and 640 cm^{-1} and a high frequency shoulder at 675 cm^{-1}. The low frequency side of the $\nu_R(D_2O)$ band shows some weak structure below 480 cm^{-1}, which does appear to vary for the different compounds. It has been noted (110) that the $\nu_R(H_2O)$ vibrations of ice Ih extend from about 1050 to 400 cm^{-1}, and the frequency of maximum infrared absorption is at 840 cm^{-1}, while the specific heat data (127) can be represented by assuming a single ν_R frequency of 650 cm^{-1}. Thus, the intense infrared ν_R absorption occurs only in the high frequency region of this band, and it is likely the same situation that occurs for the clathrate hydrates.

Little can be said concerning the remaining water absorption bands. For all of the clathrate hydrates and ice I, the $\nu_2(H_2O)$ and $3\nu_R(H_2O)$ or $\nu_2(H_2O)+\nu_R(H_2O)$ bands are broad and have frequencies of maximum absorption at about 1600 and 2250 cm^{-1}, respectively, and the corresponding frequencies for all of the deuterates and D_2O ice I are about 1200 and 1625 cm^{-1}, respectively.

In summary, the absorption by the water molecules in ice I, the structure I hydrates and the structure II hydrate is remarkably independent of the quite different structures of these compounds. The $\nu_{OD}(D_2O)$ bands show the greatest variation from compound to compound, but for the clathrate deuterates the variation depends more on the guest molecule than on the structure of the water lattice. In particular, the $\nu_{OD}(D_2O)$ band of cyclopropane deuterate I is almost identical in shape to that of oxetane deuterate II. The calculations necessary to interpret these similarities and differences are complex and not certain of success at the present time. The O-D and O-H stretching vibrations of HDO isolated in the H_2O or D_2O lattices indicate the structural differences clearly, and even indicate a structural difference between the structure I hydrate and deuterate of cyclopropane and those of ethylene oxide and oxetane which has not been detected by X-ray powder diffraction studies.

Only the temperature dependence of the water absorption remains to be discussed. The general trends observed with decreasing temperature are a decrease in the frequencies and half-widths of the $\nu_{OD}(HDO)$ and $\nu_{OD}(D_2O)$ bands with very little change in the band shapes. These temperature dependent changes are consistent with those observed for ices II and IX (Section 3.3.1), and must arise from factors discussed previously in Section 3.3.2.

The changes in frequency with temperature are comparable to those observed for oxetane hydrate I (2). The frequencies of the $\nu_{OD}(D_2O)$ and $\nu_{OD}(HDO)$ bands of cyclopropane hydrate I decreased by 6 and 4 cm^{-1}, respectively, between 130 and 65 K, while the frequencies of the corresponding bands of oxetane hydrate I decreased by 12 and 2 cm^{-1}, respectively, between 125 and 62 K (2). No significant differences were observed between the temperature dependence of the water absorption bands of oxetane hydrate I and cyclopropane hydrate I that could be attributed to the ordering transition in oxetane hydrate I below 100 K (81).

5.3 Absorption by the Guest Molecules

5.3.1 General

In the previous chapter, the study of the temperature dependence of the guest absorption revealed some striking differences in the behaviour of the guest bands with temperature. On cooling the samples, some of the guest bands sharpened, some broadened and others split into doublets. The frequencies of the guest bands also exhibited differences in behaviour with temperature. For ethylene oxide hydrate the frequencies of all the guest bands decrease, while the frequencies of some of the guest bands of cyclopropane hydrate I increase, with decreasing temperature. Thus, the factors that determine the temperature dependence of the guest bands appear to be complex. Before discussing the guest absorption in detail, the various factors that can affect the guest absorption will be briefly introduced.

The various factors that are expected to contribute to the breadth of the guest absorption bands have been discussed in references 2 and 141. At 100 K, the guest molecules are rapidly reorienting (76,80,82,84) between a number of nonequivalent potential minima within the cages. The rapid hindered reorientation of the guest molecules between these potential minima can result in a broadening of the guest bands (2). This broadening is dependent on the reorientation rate, and thus, it is temperature dependent and should not contribute to the bandwidths at very low temperatures where the guest molecules have essentially fixed orientations (72).

The vibrational frequencies of the guest must vary depending on which potential minimum within the cage the guest occupies, and thus at high temperatures a broad range of vibrational frequencies may exist. At low temperatures, the guest molecules should occupy only the lower potential minima, and this could result in a decrease in the half-width of the guest absorption bands, or if the potential minima occupied are sufficiently nonequivalent, it could result in a splitting of the guest absorption bands.

The orientational disorder of the water molecules can also contribute to the breadth of the guest absorption bands, since the intermolecular forces between the water and guest molecules occupying similar positions in different cages must differ from cage to cage.

The fluctuations in the intermolecular forces during the vibrations of the guest and water molecules can cause the vibrations of the guest molecules to couple with those of the water molecules and thus broaden the range of vibrational frequencies of the guest molecules. One important interaction of this type is due to transition dipole-transition dipole coupling between the guest and water molecules or between the guest molecules. This type of interaction should become increasingly important as the intensity of the absorption due to the guest or water molecule increases.

Finally, broadening of the guest absorption bands can also result from anharmonic effects within the guest molecules in that hot bands and difference bands can contribute to the temperature dependent absorption by the guest molecules.

The frequencies of the guest bands are expected to reflect the environment of the guest molecules and it has been shown (2) that the differences between the frequencies of the encaged molecules of the clathrate hydrates and the corresponding frequencies in the gas phase can be interpreted in terms of the loose cage - tight cage ideas of Pimentel and Charles (142). The ideas are basically that the interaction energy between a guest molecule is attractive at large guest-cage distances (loose cage environment) and results in vibrational frequencies of the guest being lower than those of the gas, whereas at very short guest-cage distances (tight cage environment) the interaction energy is repulsive and results in the vibrational frequencies of guest being higher than those of the gas (2).

One further effect of the water lattice on the absorption due to the guest is that the disorder of the water molecules results in a lowering of the guest molecule's molecular symmetry, so that those vibrations inactive for the gaseous molecule may become weakly active in the clathrate hydrate.

5.3.2 Discussion of the Absorption by the Guest Molecules in the Structure I Hydrates of Ethylene Oxide and Cyclopropane

The guest absorption bands due to either cyclopropane or ethylene oxide have approximately the same frequencies (Tables 4.3 and 4.6) and bandshapes in the spectra of the structure I hydrates and deuterates, indicating that there is essentially no coupling between the water and guest molecules. An exception is the band due to $\nu_5(A_1)$ of ethylene oxide which appears to interact with the $\nu_R(H_2O)$ vibrations of the hydrate (96). The guest absorption bands of the deuterates are generally better defined than those of the hydrates, so the following discussion will be limited mainly to those of the deuterate.

The assignment of the fundamental absorption due to cyclopropane, given in the previous chapter, was based on the gas phase assignment for cyclopropane (Section 1.7). The frequencies of the fundamental absorption of gaseous and encaged cyclopropane of cyclopropane deuterate I (Table 4.3) are given in Table 5.2, together with their assignment, as given by the symmetrized eigenvector elements determined

TABLE 5.2

Comparison of the Fundamental Frequencies[a] of Cyclopropane in the Spectra of Gaseous Cyclopropane and the Structure I Deuterate of Cyclopropane

Symmetry	No	Description[b]	ν_{gas} [b]	ν_I [c]	$\nu_I - \nu_{gas}$
A_1'	1	C-H stretch	3038.0	3034	-4
A_1'	2	1.3 CH_2 deformation + 0.2 ring breathing	1479.0	-	
A_1'	3	0.4 ring breathing - 0.3 CH_2 deformation	1188.0	-	
A_1''	4	CH_2 twist	1126.0	-	
A_2'	5	CH_2 wag	1070.0	-	
A_2''	6	C-H stretch	3101.7	3104.3	2.6
A_2''	7	CH_2 rock	854.0	859	5
E'	8	C-H stretch	3024.4	3020.5	-3.9
E'	9	CH_2 deformation	1437.7	1433.3	-4.4
E'	10	CH_2 wag	1028.4	1022.8	-5.6
E'	11	ring deformation	868.5	869.2	0.7
E"	12	C-H stretch	3082.0	3088	6
E"	13	0.6 CH_2 rock - 0.6 CH_2 twist	1188.0	-	-
E"	14	0.6 CH_2 twist + 0.5 CH_2 rock	739.0	-	-

a) cm^{-1}.

b) Reference 162.

c) Table 4.3.

from a normal coordinate calculation by Duncan and Burns (162). In the clathrate deuterate, all of the gas phase infrared active vibrations of species A_2'' and E'of point group D_{3h} are observed, and two gas phase infrared inactive vibrations, $\nu_1(A_1'')$ and $\nu_{12}(E'')$, are observed. The vibrational frequencies of encaged cyclopropane are very close to those of gaseous cyclopropane, and the average frequency shift on clathration, defined as the frequency of the encaged molecule minus the frequency in the gas phase, is $-0.5\ \mathrm{cm}^{-1}$.

The frequencies of the fundamental absorption of gaseous ethylene oxide (202) and encaged ethylene oxide at 105 K are given in Table 5.3. In the clathrate deuterate, all of the gas phase infrared active vibrations of species A_1, B_1 and B_2 of point group C_{2v} are observed, but no features are assigned to the gas phase inactive vibrations. The frequencies of the encaged ethylene oxide are generally lower than those of the gas, and the average frequency shift on clathration, as defined above, is $-7.5\ \mathrm{cm}^{-1}$.

The assignment of the bands due to ethylene oxide in ethylene oxide hydrate, given in the previous chapter, was that of Bertie and Othen (96). However,due to two recent studies of the spectra of solid ethylene oxide (203,204), different assignments for some of the features below 900 cm^{-1} are adopted and given in Table 5.3. In the spectra of solid ethylene oxide (203), the absorption and Raman scattering below 900 cm^{-1} has been assigned to four fundamentals:

TABLE 5.3

Comparison of the Fundamental Frequencies[a] of Ethylene Oxide in the Spectra of Gaseous Ethylene Oxide and the Structure I Deuterate of Ethylene Oxide

Symmetry	No	Description[b]	ν_{gas}[b]	ν_I[c]	$\nu_I - \nu_{gas}$
A_1	1	C-H stretch	3018	3006.1	-11.9
A_1	2	CH_2 deformation	1498.4	1490.0	- 8.4
A_1	3	Ring vibration	1270.3	1265.9	- 4.4
A_1	4	CH_2 wag	1148	1120	-28
A_1	5	Ring vibration	876.9	871.0	- 5.9
A_2	6	C-H stretch	-	-	-
A_2	7	CH_2 twist	-	-	-
A_2	8	CH_2 rock	-	-	-
B_1	9	C-H stretch	3005.9	2996.7	- 9.2
B_1	10	CH_2 deformation	1471.9	1465.3	- 6.6
B_1	11	CH_2 wag	1150.6	1149	- 1.6
B_1	12	Ring deformation	821.2	808.5	-12.7
B_2	13	C-H stretch	3065.2	3066.8	+ 1.6
B_2	14	CH_2 twist	1142.0	1145.1	+ 3.1
B_2	15	CH_2 rock	-	805.6	-

a) cm^{-1}

b) Reference 202.

c) Table 4.6.

$\nu_5(A_1)$, a ring vibration, near 860 cm^{-1}; $\nu_8(A_2)$, a CH_2 rock, tentatively near 845 cm^{-1}; $\nu_{12}(B_1)$, the ring deformation, near 820 cm^{-1}; and $\nu_{15}(B_2)$, a CH_2 rock, near 795 cm^{-1}. In the infrared spectrum of gaseous ethylene oxide (202), $\nu_5(A_1)$ is unambiguously assigned at 876.9 cm^{-1}, so the assignment of the band at 871 cm^{-1} in ethylene oxide deuterate is fairly certain. The assignment of the other two infrared active fundamentals of gaseous ethylene oxide, $\nu_{12}(B_1)$ and $\nu_{15}(B_2)$, is uncertain. There is a Q branch at 821.2 cm^{-1} that is due to a vibration of species B_1 or B_2 (202), and in the infrared spectrum of gaseous C_2D_4O, there is a similar Q branch at 809 cm^{-1} (204) and the assignment of these bands to $\nu_{12}(B_1)$, the ring deformation, is preferred to their assignment to $\nu_{15}(B_2)$ given previously (202). Thus the assignment of the feature at 880 cm^{-1} in ethylene oxide deuterate to $\nu_{12}(B_1)$ seems improbable. Further, the infrared and Raman spectra of solid ethylene oxide (203) clearly show that only one fundamental absorbs near 860 cm^{-1}, $\nu_5(A_1)$. Two features are observed at 805.6 and 808.5 cm^{-1} in ethylene oxide deuterate, and three fundamentals, $\nu_8(A_2)$, $\nu_{12}(B_1)$ and $\nu_{15}(B_2)$, are expected to absorb in this region. $\nu_8(A_2)$ is inactive in gaseous ethylene oxide, so the features at 805.6 and 808.5 cm^{-1} are assigned to $\nu_{15}(B_1)$ and $\nu_{12}(B_1)$, respectively. However, in view of the doublet nature of the band due to $\nu_3(A_1)$ (Fig. 4.18), the possibility that both features are components of a doublet due to either $\nu_{12}(B_1)$ or $\nu_{15}(B_2)$ cannot be excluded.

There are only two remaining features in the spectrum of ethylene oxide deuterate that have not been assigned. These are associated with the two strongest absorptions by ethylene oxide and are the shoulder at 880 cm^{-1}, on the high frequency side of $\nu_5(A_1)$ (Fig. 4.17), and the weak satellite band at 1281 cm^{-1} to high frequency of $\nu_3(A_1)$ (Fig. 4.18). These are assigned to absorption by ethylene oxide molecules in the 12-hedral cages. It has been estimated that 10 percent of the guest molecules, in the samples of ethylene oxide hydrate that were used, are in the small cages (96), and the relative intensities of these features to their low frequency counterparts are of this magnitude. The guest molecules in the 12-hedral cages are in a tighter cage environment, and so they would be expected to have higher vibrational frequencies than those molecules in the 14-hedral cages (Section 5.3.1). The frequency shifts are, however, quite large, 9 cm^{-1} for $\nu_5(A_1)$ and 13 cm^{-1} for $\nu_3(A_1)$, especially since the frequency of $\nu_3(A_1)$ varies by only 3 cm^{-1} in the spectra of gaseous, liquid and solid ethylene oxide (96). However, the maximum free diameter of the 12-hedral cage is only 4.86 Å (56), and the largest van der Waals diameter of ethylene oxide is 5.2 Å, so clearly ethylene oxide is in a very tight cage environment in the 12-hedral cages, and large frequency shifts may be expected.

The average frequency shifts on clathration of ethylene oxide, cyclopropane, and oxetane (2) in their structure I deuterates, -7.5, -0.5 and 4.5 cm^{-1}, respectively, correlate well with the loose cage-tight cage ideas of Pimentel and Charles (Section 5.3.1). Thus from the average frequency shifts observed, cyclopropane appears to be in a tighter cage environment than ethylene oxide but in a looser cage environment than oxetane. These trends are completely consistent with the size of the guest molecule relative to that of the cage. The largest van der Waals diameters of ethylene oxide and cyclopropane are 5.2 and 5.4 Å (2), respectively, while the van der Waals diameters of oxetane are 5.5 Å, between the oxygen atom and a β hydrogen atom, and 6.2 Å, between two α hydrogen atoms (2). The mean free diameter of the 14-hedral cages are 5.2 and 6.15 Å for ethylene oxide hydrate (56), while those of cyclopropane and oxetane hydrates should be about 0.05 Å larger, the shortest free diameter being along the $\bar{4}$ axis (Section 1.3). So clearly, cyclopropane is in a tighter cage environment than ethylene oxide but in a looser cage environment than oxetane in their structure I hydrates.

There does also appear to be an approximate correlation between the number of gas phase inactive fundamentals observed in the clathrate deuterates and the relative size of the guest. For ethylene oxide deuterate none of the three gas phase inactive fundamentals are observed, for cyclopropane deuterate I two out of eight are observed, and for oxetane deuterate I four out of four gas phase inactive fundamentals are observed.

In Section 4.6, it was noted that all of the guest bands of ethylene oxide deuterate decrease in frequency with decreasing temperature. This trend is consistent with the guest molecules occupying the lower potential minima within the cages at lower temperatures. In these lower minima the guest molecules presumably experience smaller repulsive forces, and are therefore in a looser cage environment, than in the higher potential minima occupied at the higher temperatures. For cyclopropane deuterate I, all of the guest bands decrease in frequency with decreasing temperature, except for those due to $\nu_7(A_2")$ a CH_2 rock and $\nu_{10}(E')$ a CH_2 wag which increase in frequency with decreasing temperature. Thus, if the interpretation of the frequency shifts of the guest bands of ethylene oxide hydrate is correct, it appears that it is not possible for all of the vibrations of encaged cyclopropane to experience a looser cage environment at the lower temperatures. Three of the four bands due to the vibrations of the β CH_2 groups of oxetane in oxetane deuterate I also increase in frequency with decreasing temperature (2). This has been attributed to the increased occupancy of preferred orientations in which the β CH_2 groups extend into the hexagonal rings formed by the water molecules of the 14-hedral cages (2). A similar effect may explain the temperature dependence of the frequencies of $\nu_7(A_2")$ and $\nu_{10}(E')$ of cyclopropane in its structure I hydrate.

The guest absorption bands of cyclopropane deuterate I, ethylene oxide deuterate and the oxetane deuterates (2) are all fairly sharp with half-widths in the range of 2 to 15 cm^{-1} at about 100 K. The guest absorption bands of cyclopropane deuterate I all have half-widths of 2 to 4 cm^{-1}, except for $\nu_6(A_2'')$ and $\nu_8(E')$ which have half-widths of 8.5 and 7.5 cm^{-1}, respectively. The guest bands of ethylene oxide deuterate all have half-widths of 2 to 5 cm^{-1}, except for $\nu_5(A_1)$ and $\nu_{13}(B_2)$ which have half-widths of 7 and 8 cm^{-1}, respectively. In the oxetane deuterates, the guest absorption bands all have half-widths of 3 to 9 cm^{-1}, except for $\nu_1(A_1)$ and $\nu_{13}(B_2)$ which have half-widths of 11.4 and 14.2 cm^{-1}, respectively (2). Thus, the bands due to oxetane in the oxetane deuterates are generally broader than those of ethylene oxide deuterate and cyclopropane deuterate I. The origin of the breadth of the guest bands in the oxetane deuterates is not clear, but it is believed to be due to the anharmonic effects of the guest molecule, and anharmonic interactions between the intramolecular vibrations of the guest and its rotational and translational vibrations in the cage (2).

The guest bands of oxetane deuterate I are generally stronger than those of ethylene oxide deuterate and cyclopropane deuterate I, so transition dipole-transition dipole coupling should be more important in oxetane deuterate I. This cannot, however, be the dominant cause of the breadth of the guest absorption bands in this deuterate since some of the strong guest bands are quite sharp, and in addition the guest absorption bands of oxetane deuterate II, where the guest-guest distance is greater, are just as broad. This type of interaction can, however, explain the different appearance of the strong guest bands that are superimposed on the $\nu_R(H_2O)$ bands. The relative absorbances of the strongest bands, which are near 870 cm^{-1}, to that of the $\nu_R(D_2O)$ bands in cyclopropane deuterate I, ethylene oxide deuterate and oxetane deuterate I were compared and are in the ratio 1:2.5:3.5. The strong bands at 869 cm^{-1}, $\nu_5(A_1)$, in ethylene oxide deuterate and at 904 cm^{-1}, $\nu_8(A_1)$, in oxetane deuterate I are reduced to shoulders in the corresponding spectra of the hydrates, while the band at 869 cm^{-1}, $\nu_{11}(E')$, in cyclopropane deuterate I, whose relative intensity is much lower than that of the other two bands, is clearly seen in the spectrum of the hydrate (Fig. 4.2).

For ethylene oxide hydrate the half-widths of all of the guest absorption bands, except for that of $\nu_3(A_1)$ which is a doublet, become sharper at the lower temperatures. The contribution to the half-width due to the guest's reorientation can be estimated using the equation $\Delta\nu \approx 2f/c$, where $\Delta\nu$ is the half-width in cm^{-1}, f is the rotational frequency in Hertz and c is the velocity of light in cm/sec (2). The rate of reorientation of ethylene oxide in ethylene oxide hydrate is known from dielectric measurements (76), and its contribution to the half-width of the guest bands at 100 and 50 K (139) is calculated to be about 0.9 and 0.004 cm^{-1}, respectively. Thus, if this is the only contributing factor to the temperature dependence of the half-widths, the half-widths of the guest bands would be expected to decrease by about 0.9 cm^{-1} from 100 to 50 K. The half-widths of all the guest bands due to fundamental absorption whose half-widths could be measured reliably, excluding $\nu_3(A_1)$, decrease by about 1 cm^{-1} over this temperature range. This strongly suggests that the dominant temperature dependent contribution to bandwidth is due to the rate of reorientation of ethylene oxide.

Cyclopropane is nondipolar, so its reorientation rate in the clathrate hydrate cannot be determined by dielectric measurements. Cyclopropane deuterate I has been studied by proton magnetic resonance methods and these studies indicate that cyclopropane reorients at $\geq$ 1 MHz at and above 100 K (82). Cyclopropane is bigger than ethylene oxide, and it is likely that its reorientation rate within the 14-hedral cages is not as great as that of ethylene oxide, so the temperature dependent contribution due to reorientation to the half-widths of the guest bands should be smaller than that of ethylene oxide. For cyclopropane hydrate I the half-widths of the bands due to $\nu_{10}(E')$, $\nu_9(E')$, and $\nu_5+\nu_{10}$ increase by 0.9, 0.3 and 0.6 cm^{-1}, respectively, while that of $\nu_8(E')$ decreases by 3 cm^{-1} from 130 to 45 K and that of $\nu_{10}+\nu_{11}$ is independent of temperature. Thus, the explanation of the changes in half-width of the guest bands of cyclopropane hydrate I is more complex. The contributions to the bandwidth that are temperature dependent are from hot bands and difference bands arising from the low frequency intermolecular vibrations of the guest, from the rate of reorientation of the guest and from different potential minima occupied by the guest at different temperatures. The first two factors would be expected to result in a decrease in the half-widths of the bands at lower temperatures, and thus cannot be the major contributing factors to the temperature dependence of all of the guest bands in cyclopropane hydrate I. In order for the third factor to explain the temperature dependence of the guest bands, the preferred orientations of the guest molecules at lower temperatures must be nonequivalent.

Cyclopropane hydrate I and ethylene oxide hydrate differ from oxetane hydrate I in that some of their guest absorption bands are split into doublets. In cyclopropane deuterate I the bands due to $\nu_7(A_2'')$, a CH_2 rock, and $\nu_{11}(E')$, a ring deformation, split into doublets at about 65 and 85 K, respectively, and in ethylene oxide hydrate the band due to $\nu_3(A_1)$, the ring breathing mode, splits into a doublet at about 130 K. The splitting of the band due to $\nu_{11}(E')$ of cyclopropane could be the result of the lowering of the symmetry of the guest molecule by the cage. However the other two bands that are split, $\nu_7(A_2'')$ of cyclopropane and $\nu_3(A_1)$ of ethylene oxide are nondegenerate. There are two possible explanations for the splitting of these two bands (96). The first is that the guest molecules occupy two sets of preferred orientations in the cages, which are nonequivalent and can result in different frequencies for some of the guest vibrations. The second is that the guest absorption bands are split as a result of intermolecular coupling between guest molecules. If intermolecular coupling is the cause, then it presumably arises from transition dipole-transition dipole coupling and the weakness of the $\nu_7(A_2'')$ band of cyclopropane argues against this. The other possibility of preferred orientations within the cages seems more likely.

If the guest molecules in the structure I hydrates do occupy two sets of nonequivalent orientations in the cages at low temperature, one would expect all of the absorption bands of the guest molecules to be split. This clearly is not the case for ethylene oxide hydrate or cyclopropane hydrate I and none of the guest bands of oxetane hydrate I split (2). The separation of the doublets observed is only 2 to 3 cm^{-1}, so the splitting of guest bands whose half-widths are much greater than this may not be detected. However, some of the guest bands in the spectrum of ethylene oxide deuterate such as $\nu_2(A_1)$ and $\nu_{10}(B_1)$ have half-widths of less than 2 cm^{-1}, yet show no indication of splitting. One can only conclude that the frequencies of only some of the guest vibrations are sufficiently different in the two sets of preferred orientations that doublets are observed. It would be of interest to obtain spectra of cyclopropane hydrate I at temperatures lower than 45 K, since some of the guest bands do broaden at the lower temperatures, and it is possible that they, too, may split at temperatures below 45 K.

The absence of observable splittings in the spectra of oxetane hydrate I may be related to the partial ordering transition observed by Davidson *et al.* (81).

In summary, the relative size of the guest molecules to that of the cage is clearly reflected in the average frequency shifts on clathration and in the number of gas phase infrared-inactive fundamentals observed in the spectra of the clathrate deuterates. The frequency shifts of the guest bands with temperature indicate that the guest molecules generally experience a looser cage environment at the lower temparatures. For ethylene oxide hydrate it appears that the dominant temperature dependent contribution to the bandwidths is due to the reorientation of ethylene oxide, while for cyclopropane hydrate I, this appears to be due to the different potential minima occupied by the guest at different temperatures. Finally, the splitting of some of the guest absorption bands is attributed to guest molecules occupying two nonequivalent sets of preferred orientations within the cages.

References

1. D.A. Othen. Ph.D. thesis, University of Alberta, 1972.
2. P.G. Wright. Ph.D. thesis, University of Alberta, 1976.
3. P.V. Hobbs. Ice Physics. Oxford University Press, London, 1974, Chapt. 1.
4. D. Eisenberg and W. Kauzmann. The Structures and Properties of Water. Oxford University Press, London, 1969, Chapt. 3.
5. B. Kamb. In Water and Aqueous Solutions. Edited by R.A. Horn. Wiley-Interscience, New York, 1972, p. 9.
6. B. Kamb. In Structural Chemistry and Molecular Biology. Edited by A. Rich and N. Davidson. W.H. Freeman Press, San Francisco, 1968, p. 507.
7. F. Franks. In Water. A Comprehensive Treatise. Vol. 1. Edited by F. Franks. Plenum Press, New York, 1972, Chapt. 4.
8. N.H. Fletcher. The Chemical Physics of Ice. Cambridge University Press, London, 1970.
9. E. Whalley. In Physics of Ice. Edited by E. Whalley, N. Riehl, B. Bullemer and H. Engelhardt. Plenum Press, New York, 1969, p. 19.
10. B. Kamb. In Physics and Chemistry of Ice. Edited by E. Whalley, S.J. Jones and L.W. Gold. Royal Society of Canada, Ottawa, 1973, p. 28.

11. B. Kamb. Trans. Am. Crystallogr. Ass. 5, 61 (1969).

12. E. Whalley and D.W. Davidson. J. Chem. Phys. 43, 2148 (1965).

13. W.C. Hamilton, B. Kamb, S.J. LaPlaca and A. Prakash. In Physics of Ice. Edited by N. Riehl, B. Bullemer and H. Englehardt. Plenum Press, New York. 1969, p. 44.

14. S.W. Rabideau and E.D. Finch. In Physics of Ice. Edited by N. Riehl, B. Bullemer and H. Engelhardt. Plenum Press, New York, 1969, p. 59.

15. S.J. LaPlaca, W.C. Hamilton, B. Kamb and A. Prakash. J. Chem. Phys. 58, 567 (1973).

16. B. Kamb, W.C. Hamilton, S.J. LaPlaca and A. Prakash. J. Chem. Phys. 55, 1934 (1971).

17. E.D. Finch, S.W. Rabideau, R.G. Wenzel and N.G. Nereson. J. Chem. Phys. 49, 4361 (1968).

18. S.W. Rabideau, E.D. Finch, G.P. Arnold and A.L. Bowman. J. Chem. Phys. 49, 2514 (1968).

19. Reference 3. pp. 82-169.

20. G.J. Wilson, R.K. Chan, D.W. Davidson and E. Whalley. J. Chem. Phys. 43, 2384 (1965).

21. G.P. Johari and E. Whalley. In Physics and Chemistry of Ice. Edited by E. Whalley, S.J. Jones and L.W. Gold. Royal Society of Canada, Ottawa, 1973, p. 278.

22. G.P. Johari, A. Lavergne and E. Whalley. J. Chem. Phys. 61, 4292 (1974).

23. E. Whalley, D.W. Davidson and J.B.R. Heath. J. Chem. Phys. 45, 3976 (1966).

24. E. Whalley, J.B.R. Heath and D.W. Davidson. J. Chem. Phys. 48, 2362 (1968).

25. L.C. Allen. In Physics and Chemistry of Ice. Edited by E. Whalley, S.J. Jones and L.W. Gold. Royal Society of Canada, Ottawa, 1973, p. 13.

26. K. Lonsdale. Proc. Roy. Soc. (London) A 247, 424 (1958).

27. S.W. Peterson and H.A. Levy. Acta Cryst. 10, 70 (1957).

28. K. Shimaoka. J. Phys. Soc. Japan 15, 106 (1960).

29. G. Honjo and K. Shimaoka. Acta Cryst. 10, 710 (1957).

30. G. Tammann. Ann. Phys. 2, 1 (1900).

31. P.W. Bridgman. Proc. Am. Acad. Arts Sci. 47, 441 (1912).

32. P.W. Bridgman. J. Chem. Phys. 3, 597 (1935).

33. P.W. Bridgman. J. Chem. Phys. 5, 964 (1937).

34. R.L. McFarlan. J. Chem. Phys. 4, 60 (1936).

35. R.L. McFarlan. J. Chem. Phys. 4, 253 (1936).

36. J.E. Bertie, L.D. Calvert and E. Whalley. J. Chem. Phys. 38, 840 (1963).

37. J.E. Bertie and E. Whalley. J. Chem. Phys. 40, 1646 (1964).

38. B. Kamb. Acta Cryst. 17, 1437 (1964).

39. G.P. Arnold, R.G. Wenzel, S.W. Rabideau, N.G. Nereson and A.L. Bowman. J. Chem. Phys. 55, 589 (1971).

40. H. Englehardt and E. Whalley. J. Chem. Phys. 56, 2678 (1972).

41. B. Kamb and H. Engelhardt. Symposium on Physics and Chemistry of Ice. Cambridge, England, 1977.

42. W.B. Kamb and S.K. Datta. Nature 187, 140 (1960).

43. B. Kamb and A. Prakash. Acta Cryst. B 24, 1317 (1968).

44. K. Nishibata and E. Whalley. J. Chem. Phys. 60, 3189 (1974).

45. S.W. Rabideau, E.D. Finch and A.B. Denison. J. Chem. Phys. 49, 4660 (1968).

46. A.J. Brown and E. Whalley. J. Chem. Phys. 45, 4360 (1966).

47. B. Kamb and A. Prakash, unpublished data, cited in reference 48.

48. P.T.T. Wong and E. Whalley. J. Chem. Phys. 64, 2359 (1976).

49. S. Block, C.W. Weir and G.J. Piermarini. Science 148, 947 (1965).

50. B. Kamb. Science 150, 205 (1965).

51. B. Kamb, A. Prakash, W.C. Hamilton and S.J. LaPlaca, unpublished data, cited in reference 10.

52. D.W. Davidson. In Water. A Comprehensive Treatise. Vol. 2. Edited by F. Franks. Plenum Press, New York, 1973, p. 115.

53. G.A. Jeffrey and R.K. McMullan. In Progress in Inorganic Chemistry. Vol. 8. Edited by F.A. Cotton, Academic Press, New York, 1967, p. 43.

54. H.M. Powell. In Non-Stoichiometric Compounds. Edited by L. Mandelcorn. Academic Press, New York, 1964, Chapt. 7.

55. R.K. McMullan and G.A. Jeffrey. J. Chem. Phys. 42, 2725 (1965).

56. F. Hollander and G.A. Jeffrey. J. Chem. Phys. 66, 4699 (1977).

57. T.C.W. Mak and R.K. McMullan. J. Chem. Phys. 42, 2732 (1964).

58. Reference 52, p. 132.

59. Reference 52, p. 129.

60. Reference 52, p. 130.

61. Reference 52, p. 131.

62. D.W. Glew and N.S. Rath. J. Chem. Phys. 44, 1710 (1966).

63. D.F. Sargent and L.D. Calvert. J. Phys. Chem. 70, 2689 (1966).

64. J.C. Rosso and L. Carbonnel. C.R. Acad. Sci. Paris, Ser. C. 274, 1108 (1972).

65. D.R. Hafemann and S.L. Miller. J. Phys. Chem. 73, 1392 (1969); 73, 1398 (1969).

66. S.L. Miller. Proc. Nat. Acad. Sci. U.S. 47, 1515 (1961).

67. A.J. Barduhn, H.E. Towlson and Y.C. Hu. A.I. Ch. E.J. 8, 176 (1962).

68. Y.A. Majid, S.K. Garg and D.W. Davidson. Can. J. Chem. 47, 4697 (1969).

69. S.R. Gough and D.W. Davidson. In Physics and Chemistry of Ice. Edited by E. Whalley, S.J. Jones and L.W. Gold. Royal Society of Canada, Ottawa, 1973, p. 51.

70. Reference 52, pp. 173-190.

71. Reference 52, pp. 201-216.

72. S.K. Garg and D.W. Davidson. In Physics and Chemistry of Ice. Edited by E. Whalley, S.J. Jones and L.W. Gold. Royal Society of Canada, Ottawa, 1973, p. 56.

73. Reference 52, pp. 195-200.

74. Reference 52, pp. 218-226.

75. N.E. Hill, W.E. Vaughan, A.H. Price and M. Davies. Dielectric Properties and Molecular Behaviour. Van Nostrand Reinhold, London, 1969, p. 297.

76. S.K. Garg, B. Morris and D.W. Davidson. J. Chem. Soc. Faraday Trans. II 68, 481 (1972).

77. R.E. Hawkins and D.W. Davidson. J. Phys. Chem. 70, 1889 (1966).

78. S. Brownstein, D.W. Davidson and D. Fiat. J. Chem. Phys. 46, 1454 (1967).

79. S.K. Garg, Y.A. Majid, J.A. Ripmeester and D.W. Davidson. Mol. Phys. 33, 729 (1977).

80. M. Davies and K. Williams. Trans. Faraday Soc. 64, 529 (1968).

81 S.R. Gough, S.K. Garg and D.W. Davidson. Chem. Phys. 3, 239 (1974).

82. A.W.K. Khanzada and C.A. McDowell. J. Mol. Struct. 16, 1 (1973).

83. R.J. Hayward and K.J. Packer. Mol. Phys. 25, 1443 (1973).

84. J.A. Ripmeester. Can. J. Chem. 54, 3677 (1976).

85. D.W. Davidson. Can. J. Chem. 49, 1224 (1971).

86. W. Vedder and D.F. Hornig. In Advances in Spectroscopy. Vol. 2. Edited by H.W. Thomson. Interscience, New York, 1961, p. 189.

87. C. Kittel. Introduction to Solid State Physics, 3rd edition. Wiley, New York, 1967, Chapters 1 and 5.

88. L. Brillouin. Wave Propagation in Periodic Structures, 2nd edition. Dover, London, 1953.

89. P.M.A. Sherwood. Vibrational Spectroscopy of Solids. Cambridge University Press, London, 1972.

90. G. Turrell. Infrared and Raman Spectra of Crystals. Academic Press, London, 1972.

91. R.S. Halford. J. Chem. Phys. 14, 8 (1946).

92. D.F. Hornig. J. Chem. Phys. 16, 1063 (1948).

93. H. Winston and R.S. Halford. J. Chem. Phys. 17, 607 (1949).

94. S.S. Mitra. In Optical Properties of Solids. Edited by S.S. Mitra. Plenum Press, New York, 1969, Chapt. 14.

95. A.S. Davydov. Theory of Molecular Excitons. McGraw-Hill, New York, 1962.

96. J.E. Bertie and D.A. Othen. Can. J. Chem. 51, 1159 (1973).

97. E. Whalley and J.E. Bertie. J. Chem. Phys. 46, 1264 (1967).

98. J.E. Bertie and E. Whalley. J. Chem. Phys. 46, 1271 (1967).

99. J.E. Bertie and J.W. Bell. J. Chem. Phys. 54, 160 (1971).

100. E.B. Wilson Jr., J.C. Decius and P.C. Cross. Molecular Vibrations. McGraw-Hill, New York, 1955.

101. E. Whalley. In Developments in Applied Spectroscopy. Edited by W.K. Baer, A.J. Perkins and E.L. Grove. Plenum Press, New York, 1968, 6, 277 (1967).

102. J.E. Bertie. Appl. Spect. 22, 634 (1968).

103. Reference 3, pp. 231-246.

104. E. Whalley. In Physics and Chemistry of Ice. Edited by E. Whalley, S.J. Jones and L.W. Gold. Royal Society of Canada, Ottawa. 1973, p. 73.

105. J.E. Bertie, H.J. Labbé and E. Whalley. J. Chem. Phys. 50, 4501 (1969).

106. R. Zimmerman, G.C. Pimentel. Proc. Intern. Meeting Spectrosc. 4th Bologna 2, 726 (1959).

107. C. Haas and D.F. Hornig. J. Chem. Phys. 32, 1763 (1960).

108. D.F. Hornig, H.F. White and F.P. Reding. Spectrochim. Acta 12, 338 (1958).

109. T.A. Ford and M. Falk. Can. J. Chem. 46, 3579 (1968).

110. J.E. Bertie and E. Whalley. J. Chem. Phys. 40, 1637 (1964).

111. M.J. Taylor and E. Whalley. J. Chem. Phys. 40, 1660 (1964).

112. P.T.T. Wong and E. Whalley. J. Chem. Phys. 62, 2418 (1975).

113. P.T.T. Wong and E. Whalley. J. Chem. Phys. 65, 829 (1976).

114. N. Ockman. Advan. Phys. 7, 199 (1958).

115. J.E. Bertie and S.M. Jacobs. J. Chem. Phys. 67, 2445 (1977).

116. T.C. Sivakumar, D. Schuh, M.G. Sceats and S.A. Rice. Chem. Phys. Lett. 48, 212 (1977).

117. E.R. Lippincott, C.E. Weir and A. Van Valkenburg. J. Chem. Phys. 32, 612 (1960).

118. J.E. Bertie, H.J. Labbé and E. Whalley. J. Chem. Phys. 49, 2141 (1968).

119. J.E. Bertie, H.J. Labbé and E. Whalley. J. Chem. Phys. 49, 775 (1968).

120. J.P. Marckman and E. Whalley. J. Chem. Phys. 41, 1450 (1964).

121. R.S. Hawke, K. Syassen, W.B. Holzapfel. Rev. Sci. Instruments 45, 1598 (1974).

122. A.H. Hardin and K.B. Harvey. Spectrochim. Acta 29A, 1139 (1973).

123. R.A. Fifer and J. Schiffer. J. Chem. Phys. 52, 2664 (1970).

124. J. Schiffer, M. Intenzo, P. Hayward and C. Calabrese. J. Chem. Phys. 64, 3014 (1976).

125. R. McGraw, W.G. Madden, S.A. Rice and M.G. Sceats. Chem. Phys. Lett. 48, 219 (1977).

126. G. Herzberg. Molecular Spectra and Molecular Structure II. Infrared and Raman Spectra of Polyatomic Molecules. D. Van Nostrand Co. Inc., Princeton, N.J. Chapt. III. Section 2.

127. A.J. Leadbetter. Proc. Roy. Soc. (London) A 287, 403 (1965).

128. B. Renker. In Physics and Chemistry of Ice. Edited by E. Whalley, S.J. Jones and L.W. Gold. Royal Society of Canada, Ottawa, 1973, p. 82.

129. J.E. Bertie and M. Solinas. Can. J. Chem. 53, 2642 (1975).

130. A.W. Naumann and G.J. Safford. J. Chem. Phys. 47, 867 (1967).

131. K.B. Harvey, F.R. McCourt and H.F. Shurvell. Can. J. Chem. 42, 960 (1964).

132. A.H. Hardin and K.B. Harvey. Can. J. Chem. 49, 4114 (1971).

133. W.A.P. Luck and W. Ditter. J. Phys. Chem. 74, 3687 (1970).

134. J.W. Anthonsen. Acta Chem. Scand. A 29, 175 (1975).

135. K.W. Allen and G.A. Jeffrey. J. Chem. Phys. 38, 2304 (1963).

136. M.M.X. Gerbaux, C. Barthel and A. Hadni. Spectrochim. Acta 31A, 1901 (1975).

137. J.E. Bertie and M. Solinas. Can. J. Chem. 53, 2624 (1975).

138. J.E. Bertie, F.E. Bates and D.K. Hendricksen. Can. J. Chem. 53, 71 (1975).

139. J.E. Bertie and S.M. Jacobs. Can. J. Chem. 55, 1777 (1977).

140. J.E. Bertie and D.A. Othen. Can. J. Chem. 50, 3443 (1972).

141. D.D. Klug and E. Whalley. Can. J. Chem. 51, 4062 (1973).

142. G.C. Pimentel and S.W. Charles. Pure Appl. Chem. 7, 111 (1963).

143. A.W. Baker and R.C. Lord. J. Chem. Phys. 23, 1636 (1955).

144. H.H. Gunthard, R.C. Lord and T.K. McCubbin, Jr. J. Chem. Phys. 25, 768 (1956).

145. J.L. Duncan. J. Mol. Spectrosc. 25, 451 (1968).

146. J.L. Duncan and D.C. McKean. J. Mol. Spectrosc. 27, 117 (1968).

147. J.L. Duncan and D. Ellis. J. Mol. Spectrosc. 28, 540 (1968).

148. T.K. McCubbin, Jr., V. Withstandley and S.R. Polo. J. Mol. Spectrosc. 31, 95 (1969).

149. R. Wyatt, J.T. Roberts, R.E. Wentz and P.M. Wilt. J. Chem. Phys. 50, 2552 (1969).

150. G.J. Cartwright and I.M. Mills. J. Mol. Spectrosc. 34, 415 (1970).

151. F.N. Masri and W.E. Blass. J. Mol. Spectrosc. 39, 21 (1971).

152. V. Withstandley, T.K. McCubbin, Jr. and S.R. Polo. J. Mol. Spectrosc. 47, 297 (1973).

153. P.M. Mathai, G.G. Shepherd and H.L. Welsh. Can. J. Phys. 34, 1448 (1956).

154. R.J. Butcher and W.J. Jones. J. Mol. Spectrosc. 47, 64 (1973).

155. A.M. Pyndyk and V.B. Podobedov. Opt Spectrosc. 35, 31 (1973).

156. S.J. Daunt and H.F. Shurvell. J. Raman Spectrosc. 2, 481 (1974).

157. C. Brecher, E. Krikorian, J. Blanc and R.S. Halford. J. Chem. Phys. 35, 1097 (1961).

158. J.B. Bates. J. Chem. Phys., 58, 4236 (1973).

159. J.B. Bates, D.E. Sands and W.H. Smith. J. Chem. Phys. 51, 105 (1969).

160. J. LeBrumant. Compt. Rend. Acad. Sci. Paris 274B, 637 (1972).

161. H.F. Shurvell, S.J. Daunt and D.W. James. J. Mol. Spectrosc. 53, 77 (1974).

162. J.L. Duncan and G.R. Burns. J. Mol. Spectrosc. 30, 253 (1969).

163. T. Hirokawa, M. Hayashi and H. Murata. J. Sci. Hiroshima Univ. Ser. A 37, 271 (1973).

164. T. Hirokawa. J. Sci. Hiroshima Univ. Ser. A 39, 161 (1975).

165. J.C. Evans and G. Y-S. Lo. J. Phys. Chem. 71, 3942 (1967); 73, 445 (1969).

166. J.E. Bertie and E. Whalley. Spectrochim. Acta 20, 1349 (1964).

167. K. Simpson. Ph.D. thesis, University of Alberta, 1973.

168. R. Brill and A. Tippe. Acta Cryst. 23, 343 (1967).

169. B. Meyer. Low Temperature Spectroscopy. American Elsevier, New York, 1971, p. 192.

170. L.R. Blaine, E.K. Plyler and W.S. Benedict. J. Res. Natl. Bur. Std. 66A, (1962).

171. I.U.P.A.C. Tables of Wavenumbers for the Calibration of Infrared Spectrophotometers. Butterworths, London, 1961.

172. E.W. Nuffield. X-ray Diffraction Methods. J. Wiley and Sons Inc., New York, 1966, p. 107.

173. M. Falk and O. Knop. In Water. A Comprehensive Treatise. Vol. 2. Edited by F. Frank. Plenum Press, New York, Chapt. 2.

174. B. Srivastava, D.P. Khandelwal and H.D. Bist. Chem. Phys. Lett. 39, 366 (1976).

175. L.A. Woodward. Introduction to the Theory of Molecular Vibrations and Vibrational Spectroscopy. Oxford University Press, London, 1972.

176. I.M. Mills. In Infrared Spectroscopy and Molecular Structure. Edited by M. Davies. Elsevier, Amsterdam, 1963, Chapt. V.

177. Reference, 126, Chapt. II, Section 5.

178. F.A. Cotton. Chemical Applications of Group Theory, 2nd edition. Wiley-Interscience, New York, 1971, Chapt. 6.

179. J.H. Schachtschneider. Project No. 31450. Tech. Rep. No. 57-65, Shell Development Comp. Emeryville, CA, 1965.

180. D.F. Hornig and D.C. McKean. J. Chem. Phys. 59, 1133 (1955).

181. J. Overend. In Infrared Spectroscopy and Molecular Structure, Edited by M. Davies, Elsevier, Amsterdam, 1963, Chapt. X.

182. S.-I. Ikawa and S. Maeda. Spectrochim. Acta 24A, 655 (1968).

183. International Tables for X-ray Crystallography, 2nd edition. Vol. 1. Edited by F. Henry and K. Lonsdale, T. Kynoch Press, Birmingham, 1965.

184. S.D. Colson and P.B. Klein. Chem. Phys. Lett. 34, 17 (1975).

185. J. Overend. J. Chem. Phys. 64, 2878 (1976).

186. S.M. Jacobs, Private communication.

187. J.C. Evans and N. Wright. Spectrochim. Acta 16, 352 (1960).

188. J.C. Evans. Spectrochim. Acta 16, 994 (1960).

189. J.C. Evans. Spectrochim. Acta 18, 507 (1961).

190. D.A. Othen, O. Knop and M. Falk. Can. J. Chem. 53, 3837 (1975).

191. M.P. Marzocchi, L. Angeloni and G. Sbrana. Chem. Phys. 12, 349 (1976).

192. J. de Villepin and A. Novak. J. Mol. Struct. 30, 255 (1970).

193. M.F. Claydon and N. Sheppard. Chem. Comm. 1431 (1969).

194. B. Orel, D. Hadzi and F. Cabassi. Spectrochim. Acta 31A, 169 (1975).

195. W.C. Price and K.S. Tetlow. J. Chem. Phys. 16, 1157 (1948).

196. Handbook of Chemistry and Physics, 51st edition. Edited by R.C. Weast. The Chemical Rubber Co., 1970.

197. F.A. Jenkins and H.E. White. Fundamentals of Optics, 3rd edition. McGraw-Hill Book Company Inc., 1957, p. 469.

198. S.I. Chan, J. Zinn, J. Fernandez and W.D. Gwinn. J. Chem. Phys. 33, 1643 (1960).

199. G.L. Cunningham, Jr., A.W. Boyd, R.J. Myers, W.D. Gwinn and W.I. Levan. J. Chem. Phys. 19, 676 (1951).

200. E. Whalley. Private communication.

201. J.D. Bernal and R.H. Fowler. J. Chem. Phys. 1, 515 (1933).

202. J.E. Bertie and D.A. Othen. Can. J. Chem. 51, 1155 (1973).

203. J.E. Bertie and S.M. Jacobs. J. Chem. Phys., in press.

204. N.W. Cant and W.J. Armstead. Spectrochim. Acta 21A, 839 (1974).

205. W.B. Kamb, A. Prakash and C. Knobler. Acta Cryst. 22, 706 (1967).

Appendix

Symmetrized Eigenvectors^{a,b} for Ice II and IX

Ice II

```
PREQUENCY =2534.5 CM-1
  0.2363 -0.5814 -0.1457  0.3955  0.0     0.0     0.0     0.0     0.0     0.0
  0.0     0.0     0.0     0.0     0.0     0.0     0.0     0.0     0.0     0.0
  0.0     0.0     0.0     0.0
FREQUENCY =2487.3 CM-1
 -0.0300  0.4141  0.0276  0.6336  0.0     0.0     0.0     0.0     0.0     0.0
  0.0     0.0     0.0     0.0     0.0     0.0     0.0     0.0     0.0     0.0
  0.0     0.0     0.0     0.0
FREQUENCY =2398.5 CM-1
 -0.4993 -0.2580  0.4655  0.1209  0.0     0.0     0.0     0.0     0.0     0.0
  0.0     0.0     0.0     0.0     0.0     0.0     0.0     0.0     0.0     0.0
  0.0     0.0     0.0     0.0
FREQUENCY =2360.2 CM-1
 -0.4838 -0.0433 -0.5532  0.0291  0.0     0.0     0.0     0.0     0.0     0.0
  0.0     0.0     0.0     0.0     0.0     0.0     0.0     0.0     0.0     0.0
  0.0     0.0     0.0     0.0
FREQUENCY =2543.8 CM-1
  0.0     0.0     0.0     0.0     0.2324 -0.3789  0.4586  0.3901  0.0     0.0
  0.0     0.0     0.0     0.0     0.0     0.0     0.0     0.0     0.0     0.0
  0.0     0.0     0.0     0.0
FREQUENCY =2522.4 CM-1
  0.0     0.0     0.0     0.0     0.5236  0.2843  0.2515 -0.3678  0.0     0.0
  0.0     0.0     0.0     0.0     0.0     0.0     0.0     0.0     0.0     0.0
  0.0     0.0     0.0     0.0
FREQUENCY =2487.3 CM-1
  0.0     0.0     0.0     0.0    -0.0575  0.5914  0.1220  0.4552  0.0     0.0
  0.0     0.0     0.0     0.0     0.0     0.0     0.0     0.0     0.0     0.0
  0.0     0.0     0.0     0.0
```

```
FREQUENCY =2397.3 CM-1
   0.0      0.0      0.0      0.0      0.4568  -0.0592  -0.5062   0.2804   0.0      0.0
   0.0      0.0      0.0      0.0      0.0      0.0      0.0      0.0      0.0      0.0
   0.0      0.0      0.0      0.0
FREQUENCY =2545.6 CM-1
   0.0      0.0      0.0      0.0      0.0      0.0      0.0      0.0      0.1649  -0.0671
  -0.2848   0.4355  -0.2350  -0.4437   0.1015  -0.0151   0.0      0.0      0.0      0.0
   0.0      0.0      0.0      0.0
FREQUENCY =2545.6 CM-1
   0.0      0.0      0.0      0.0      0.0      0.0      0.0      0.0     -0.2350   0.4437
   0.1015   0.0151  -0.1649  -0.0671   0.2848   0.4355   0.0      0.0      0.0      0.0
   0.0      0.0      0.0      0.0
FREQUENCY =2504.2 CM-1
   0.0      0.0      0.0      0.0      0.0      0.0      0.0      0.0      0.1516  -0.0024
   0.1295   0.4976  -0.0479   0.5189   0.1139   0.0219   0.0      0.0      0.0      0.0
   0.0      0.0      0.0      0.0
FREQUENCY =2504.2 CM-1
   0.0      0.0      0.0      0.0      0.0      0.0      0.0      0.0     -0.0479  -0.5188
   0.1139  -0.0219  -0.1516  -0.0024  -0.1295   0.4976   0.0      0.0      0.0      0.0
   0.0      0.0      0.0      0.0
FREQUENCY =2444.6 CM-1
   0.0      0.0      0.0      0.0      0.0      0.0      0.0      0.0     -0.5576  -0.1637
  -0.3629   0.0569  -0.0978   0.1893   0.0935  -0.1415   0.0      0.0      0.0      0.0
   0.0      0.0      0.0      0.0
FREQUENCY =2444.6 CM-1
   0.0      0.0      0.0      0.0      0.0      0.0      0.0      0.0      0.0978   0.1893
  -0.0935  -0.1415  -0.5576   0.1637  -0.3629  -0.0569   0.0      0.0      0.0      0.0
   0.0      0.0      0.0      0.0
FREQUENCY =2414.9 CM-1
   0.0      0.0      0.0      0.0      0.0      0.0      0.0      0.0      0.3252  -0.0071
  -0.4770  -0.2516   0.0788   0.2113   0.2359   0.2208   0.0      0.0      0.0      0.0
   0.0      0.0      0.0      0.0
FREQUENCY =2414.9 CM-1
   0.0      0.0      0.0      0.0      0.0      0.0      0.0      0.0     -0.0788   0.2113
  -0.2359   0.2208   0.3252   0.0071  -0.4770   0.2516   0.0      0.0      0.0      0.0
   0.0      0.0      0.0      0.0
```

```
FREQUENCY =2520.0 CM-1
   0.0      0.0      0.0      0.0      0.0      0.0      0.0      0.0      0.0      0.0
   0.0      0.0      0.0      0.0      0.0      0.0     -0.0888  -0.6596  -0.0371   0.2078
   0.1793  -0.1104   0.0925  -0.1831
FREQUENCY =2520.0 CM-1
   0.0      0.0      0.0      0.0      0.0      0.0      0.0      0.0      0.0      0.0
   0.0      0.0      0.0      0.0      0.0      0.0      0.1793   0.1104   0.0925   0.1831
   0.0888  -0.6596   0.0371   0.2078
FREQUENCY =2501.6 CM-1
   0.0      0.0      0.0      0.0      0.0      0.0      0.0      0.0      0.0      0.0
   0.0      0.0      0.0      0.0      0.0      0.0     -0.1190   0.1532   0.1440   0.6775
  -0.1406   0.1691  -0.0623  -0.0282
FREQUENCY =2501.5 CM-1
   0.0      0.0      0.0      0.0      0.0      0.0      0.0      0.0      0.0      0.0
   0.0      0.0      0.0      0.0      0.0      0.0     -0.1406  -0.1691  -0.0623   0.0282
   0.1190   0.1532  -0.1440   0.6775
FREQUENCY =2428.2 CM-1
   0.0      0.0      0.0      0.0      0.0      0.0      0.0      0.0      0.0      0.0
   0.0      0.0      0.0      0.0      0.0      0.0      0.2486   0.1627  -0.2360   0.1455
   0.4148   0.2008   0.4109   0.0356
FREQUENCY =2428.2 CM-1
   0.0      0.0      0.0      0.0      0.0      0.0      0.0      0.0      0.0      0.0
   0.0      0.0      0.0      0.0      0.0      0.0     -0.4148   0.2008  -0.4109   0.0357
   0.2486  -0.1627  -0.2360  -0.1455
FREQUENCY =2374.4 CM-1
   0.0      0.0      0.0      0.0      0.0      0.0      0.0      0.0      0.0      0.0
   0.0      0.0      0.0      0.0      0.0      0.0     -0.4604   0.0613   0.1055  -0.0778
  -0.1425  -0.0901   0.5239   0.0912
FREQUENCY =2374.4 CM-1
   0.0      0.0      0.0      0.0      0.0      0.0      0.0      0.0      0.0      0.0
   0.0      0.0      0.0      0.0      0.0      0.0      0.1426  -0.0901  -0.5239   0.0912
  -0.4604  -0.0613   0.1055   0.0778
```

Ice IX

```
FREQUENCY =2530.5 CM-1
  0.2443 -0.6132 -0.3587  0.0     0.0     0.0     0.0     0.0     0.0     0.0
  0.0     0.0     0.0     0.0     0.0     0.0     0.0     0.0     0.0     0.0
  0.0     0.0     0.0     0.0
FREQUENCY =2412.0 CM-1
  0.3119  0.4471 -0.5071  0.0     0.0     0.0     0.0     0.0     0.0     0.0
  0.0     0.0     0.0     0.0     0.0     0.0     0.0     0.0     0.0     0.0
  0.0     0.0     0.0     0.0
FREQUENCY =2334.3 CM-1
  0.6201  0.0171  0.3966  0.0     0.0     0.0     0.0     0.0     0.0     0.0
  0.0     0.0     0.0     0.0     0.0     0.0     0.0     0.0     0.0     0.0
  0.0     0.0     0.0     0.0
FREQUENCY =2502.7 CM-1
  0.0     0.0     0.0     0.1289 -0.3409 -0.6643  0.0     0.0     0.0     0.0
  0.0     0.0     0.0     0.0     0.0     0.0     0.0     0.0     0.0     0.0
  0.0     0.0     0.0     0.0
FREQUENCY =2466.3 CM-1
  0.0     0.0     0.0    -0.0292  0.6726 -0.3503  0.0     0.0     0.0     0.0
  0.0     0.0     0.0     0.0     0.0     0.0     0.0     0.0     0.0     0.0
  0.0     0.0     0.0     0.0
FREQUENCY =2348.2 CM-1
  0.0     0.0     0.0     0.7241  0.0878  0.1041  0.0     0.0     0.0     0.0
  0.0     0.0     0.0     0.0     0.0     0.0     0.0     0.0     0.0     0.0
  0.0     0.0     0.0     0.0
FREQUENCY =2532.7 CM-1
  0.0     0.0     0.0     0.0     0.0     0.0     0.3978  0.3222 -0.5508  0.0
  0.0     0.0     0.0     0.0     0.0     0.0     0.0     0.0     0.0     0.0
  0.0     0.0     0.0     0.0
FREQUENCY =2466.7 CM-1
  0.0     0.0     0.0     0.0     0.0     0.0     0.0541  0.6349  0.4119  0.0
  0.0     0.0     0.0     0.0     0.0     0.0     0.0     0.0     0.0     0.0
  0.0     0.0     0.0     0.0
```

```
FREQUENCY =2411.2 CM-1
  0.0      0.0      0.0      0.0      0.0      0.0      0.6169 -0.2634   0.3191   0.0
  0.0      0.0      0.0      0.0      0.0      0.0      0.0      0.0      0.0      0.0
  0.0      0.0      0.0      0.0
FREQUENCY =2517.8 CM-1
  0.0      0.0      0.0      0.0      0.0      0.0      0.0      0.0      0.0      0.2317
  0.6431 -0.3155    0.0      0.0      0.0      0.0      0.0      0.0      0.0      0.0
  0.0      0.0      0.0      0.0
FREQUENCY =2458.8 CM-1
  0.0      0.0      0.0      0.0      0.0      0.0      0.0      0.0      0.0     -0.6968
  0.2375 -0.0567    0.0      0.0      0.0      0.0      0.0      0.0      0.0      0.0
  0.0      0.0      0.0      0.0
FREQUENCY =2395.3 CM-1
  0.0      0.0      0.0      0.0      0.0      0.0      0.0      0.0      0.0      0.0506
  0.3261   0.6636   0.0      0.0      0.0      0.0      0.0      0.0      0.0      0.0
  0.0      0.0      0.0      0.0
FREQUENCY =2522.1 CM-1
  0.0      0.0      0.0      0.0      0.0      0.0      0.0      0.0      0.0      0.0
  0.0      0.0      0.1679 -0.5194   0.2810 -0.1753   0.0218 -0.3984   0.0      0.0
  0.0      0.0      0.0      0.0
FREQUENCY =2496.7 CM-1
  0.0      0.0      0.0      0.0      0.0      0.0      0.0      0.0      0.0      0.0
  0.0      0.0      0.1443   0.3062   0.0360   0.0491 -0.5697 -0.3628   0.0      0.0
  0.0      0.0      0.0      0.0
FREQUENCY =2467.2 CM-1
  0.0      0.0      0.0      0.0      0.0      0.0      0.0      0.0      0.0      0.0
  0.0      0.0     -0.1750 -0.4116 -0.0067   0.1881 -0.4691   0.3409   0.0      0.0
  0.0      0.0      0.0      0.0
FREQUENCY =2461.8 CM-1
  0.0      0.0      0.0      0.0      0.0      0.0      0.0      0.0      0.0      0.0
  0.0      0.0      0.4696   0.0110 -0.0654 -0.4363 -0.1310   0.3435   0.0      0.0
  0.0      0.0      0.0      0.0
FREQUENCY =2388.8 CM-1
  0.0      0.0      0.0      0.0      0.0      0.0      0.0      0.0      0.0      0.0
  0.0      0.0      0.0397 -0.1972 -0.6761 -0.0235 -0.0025 -0.2208   0.0      0.0
  0.0      0.0      0.0      0.0
```

```
FREQUENCY =2352.6 CM-1
  0.0       0.0       0.0       0.0       0.0       0.0       0.0       0.0       0.0       0.0
  0.0       0.0       0.4913   -0.0537    0.0082    0.5314    0.1182    0.0537    0.0       0.0
  0.0       0.0       0.0       0.0
FREQUENCY =2522.1 CM-1
  0.0       0.0       0.0       0.0       0.0       0.0       0.0       0.0       0.0       0.0
  0.0       0.0       0.0       0.0       0.0       0.0       0.0       0.0       0.1679   -0.5194
  0.2810   -0.1753    0.0218   -0.3984
FREQUENCY =2496.7 CM-1
  0.0       0.0       0.0       0.0       0.0       0.0       0.0       0.0       0.0       0.0
  0.0       0.0       0.0       0.0       0.0       0.0       0.0       0.0       0.1443    0.3062
  0.0360    0.0491   -0.5697   -0.3629
FREQUENCY =2467.2 CM-1
  0.0       0.0       0.0       0.0       0.0       0.0       0.0       0.0       0.0       0.0
  0.0       0.0       0.0       0.0       0.0       0.0       0.0       0.0      -0.1749   -0.4116
 -0.0067    0.1879   -0.4692    0.3410
FREQUENCY =2461.8 CM-1
  0.0       0.0       0.0       0.0       0.0       0.0       0.0       0.0       0.0       0.0
  0.0       0.0       0.0       0.0       0.0       0.0       0.0       0.0       0.4697    0.0111
 -0.0654   -0.4364   -0.1309    0.3434
FREQUENCY =2388.8 CM-1
  0.0       0.0       0.0       0.0       0.0       0.0       0.0       0.0       0.0       0.0
  0.0       0.0       0.0       0.0       0.0       0.0       0.0       0.0       0.0397   -0.1972
 -0.6761   -0.0235   -0.0025   -0.2209
FREQUENCY =2352.6 CM-1
  0.0       0.0       0.0       0.0       0.0       0.0       0.0       0.0       0.0       0.0
  0.0       0.0       0.0       0.0       0.0       0.0       0.0       0.0       0.4913   -0.0537
  0.0082    0.5314    0.1182    0.0537
```

a) Obtained from force field II of Table 3.16 for Ice II and from force field III of Table 3.10 for ice IX.

b) Entries under each frequency are listed in the order of the symmetry coordinates of Table 3.13 for ice II and of Table 3.16 for ice IX.